J.K. Wight

ORIGINAL AND REPAIRED REINFORCED CONCRETE BEAM-COLUMN SUBASSEMBLAGES SUBJECTED TO EARTHQUAKE TYPE LOADING

by

Duane L. N. Lee

James K. Wight

Robert D. Hanson

Report on Research Conducted under Grant No. GI-39123 from the National Science Foundation

Report UMEE 76S4

Department of Civil Engineering
The University of Michigan
Ann Arbor, MI 48109

April 1976

engn
UHR 0358

ABSTRACT

Eight reinforced concrete exterior beam-column sub-assemblages were designed using the most recent building code recommendations for either seismic or nonseismic areas in order to represent both types of existing structures. The only difference between the two designs was the amount of transverse reinforcement. The specimens were cast and tested to determine their behavior with special attention being focused on the beam-to-column joint. During testing, the specimens were subjected to a loading which simulated the type of motions that could be expected during either a moderate or a severe earthquake to obtain different degrees of damage.

The damaged specimens were repaired using either of two repair techniques depending on the degree of damage. For the moderately damaged specimens, the pressure injection of epoxy was used. The removal of the damaged material and replacement with various high early strength materials was used to repair more severely damaged specimens. The specimens were retested in the same manner as the original test to determine the behavior of the repaired specimens and to compare this behavior with the original behavior.

Based on this investigation, two principal conclusions were made. They are (1) epoxy injection and removal and replacement techniques of repair can effectively restore structural integrity to damaged members, and (2) the original specimens showed that the concrete in the beam-to-column joint can resist twice the shear force recommended by ASCE/ACI Committee 352.

ACKNOWLEDGMENTS

This report was submitted by Dr. Lee to The University of Michigan in partial fulfillment of the requirements for the degree Doctor of Philosophy (Civil Engineering). Professors Wight and Hanson provided guidance and assistance throughout this investigation as co-chairmen of the doctoral committee. The authors would like to thank Professors William J. Anderson, Glen V. Berg and Subhash C. Goel (members of his doctoral committee) for reviewing the report and offering helpful suggestions.

The investigation was supported by the National Science Foundation through Grant GI-39123. Repair material and technical assistance were furnished by Messrs. A. Rossi and R. Schutz of Sika Chemical Corporation, R. Best of Republic Steel Corporation and W. Bleecher of United States Gypsum Company. The authors would like to thank Dr. Lee's parents for their encouragement and financial assistance and the Department of Civil Engineering for fellowships and computer support of Dr. Lee during this investigation. However, any opinions, findings, conclusions or recommendations expressed herein are those of the authors and do not necessarily reflect the views of these sponsors.

Fellow graduate student, Frank Somogyi, assisted in testing the concrete cylinders.

TABLE OF CONTENTS

TABLE OF CONTENTS (continued)

LIST OF TABLES

LIST OF FIGURES

LIST OF APPENDICES

NOTATION

A_b = area of reinforcing bar, sq. in.

A_{cv} = effective area of cross section, sq. in.

A_g = gross area of cross section, sq. in.

A_v = area of transverse reinforcement within a distance s, sq. in.

b = horizontal projection of inclined distance between points measured by LVDT for joint distortion, in.

b_w = width of cross section, in.

d = distance from extreme compression fiber to tension reinforcement, in.

= distance between points measured by LVDT for joint distortion, in.

d_b = nominal diameter of reinforcing bar, in.

E_c = modulus of elasticity for concrete, psi

f'_c = compressive strength of concrete, psi

f_h = tensile stress developed by standard hook reinforcement, psi

f_s = stress in reinforcement, psi

f_{si} = reinforcement stress at location i, psi

f_{sj} = reinforcement stress at location j, psi

f_y = yield strength of reinforcement, psi

G = shear modulus for concrete, psi

h = vertical projection of inclined distance between points measured by LVDT for joint distortion, in.

l_d = straight development length, in.

l_e = equivalent straight embedment length provided by standard hook, in.

l_{ij} = distance between i and j, in.

l_s = straight embedment length before standard hook, in.

NOTATION (continued)

M_b = balanced moment capacity of column

n = number of transverse reinforcement in joint

N = applied axial load on column

N_b = balanced axial load capacity of column

N_u = axial load in column occurring simultaneously with V_u or V_t, lbs.

p_b = perimeter of reinforcing bar, in.

P = applied beam-tip force

s = spacing of stirrup-ties or hoops, in.

u_{avg} = average bond stress, psi

v_c = shear stress resisted by concrete, psi

v_s = shear stress resisted by transverse reinforcement, psi

v_u = total design shear stress, psi

V = reaction force in column

V_c = shear force attributed to concrete, lbs.

V_{col} = shear force in column, lbs.

V_s = shear force attributed to transverse reinforcement, lbs.

V_t = total shear force across section, lbs.

V_u = total design shear force across section, lbs.

α, β = constants dependent upon whether ductility and strength or just strength is desired

γ = constant dependent upon confinement provided by other members framing into joint

= distortion in joint, rad.

= shear distortion in beam, rad.

δ_1, δ_2 = deflections measured by LVDT 1 and 2 for joint distortion, in.

Δ = applied beam-tip deflection, in.

Δ_t = total calculated beam-tip deflection, in.

Δ_y = beam-tip deflection at time of first yield of beam top bar, in.

Δ_1 = beam-tip deflection due to rotation of column at beam-column joint, in.

Δ_2 = beam-tip deflection due to shear distortion in joint, in.

Δ_3 = beam-tip deflection due to shear distortion in beam, in.

Δ_4 = beam-tip deflection due to rotation of beam over 10 in. length beginning from inside column face, in.

Δ_5 = beam-tip deflection due to flexure of beam 10 in. from inside column face relative to column, in.

Δ_6 = beam-tip deflection due to flexure of beam between section 10 in. from inside column face and point of load application, in.

ε = strain in top beam reinforcement, in./in.

ε_y = strain in top beam reinforcement at first yield of beam top bar, in./in.

θ = relative rotation of beam, rad.

θ_y = relative rotation of beam at first yield of beam top bar, rad.

ξ = constant for standard hook

τ = shear stress in beam, psi

ϕ = capacity reduction factor

ψ = constant dependent upon straight embedment length, concrete cover normal to plane of hook and over tail extension, and confinement provided by transverse reinforcement in joint

CHAPTER 1

INTRODUCTION

1.1 Statement of the Problem

During an earthquake, a structure is deflected both horizontally and vertically while the structural and non-structural members are called upon to dissipate the input energy. For large earthquake motions, most of this energy dissipation is through inelastic deformations. To utilize the energy dissipation capability of the structural members, the joint connecting the beams and columns must continue to function. Recent earthquakes in Caracas (33) Tokachi-Oki (57), San Fernando (27), and Managua (48) have shown damage to occur in the beam-to-column joint. To insure satisfactory response of the structure, a better understanding of the behavior of the joint and the members framing into it is needed.

After an earthquake, structural members which have sustained significant inelastic deformations will require repair. In practice, when the damaged region is repaired with high strength materials, the repair is assumed to be sufficient to carry gravity loads. However, it is unknown if the capability of the structure to resist seismic loads has been restored. Poor behavior of the repaired members during subsequent earthquakes may result in a catastrophic collapse of the structure. Thus, there is a need to investigate the behavior of repaired structural members.

1.2 Objectives and Scope

The principal objectives of this study were: 1) to investigate the behavior of beam-column subassemblages designed according to the most recent recommendations to resist seismic loading, 2) to use these test results to suggest improved recommendations for design of the subassemblages, 3) to evaluate two repair techniques currently used in practice, 4) to investigate the short and long term loading of different materials which may be used for structural repairs, and 5) to investigate the behavior of repaired beam-column subassemblages.

The specimens used to investigate the original and repaired cyclic behavior were exterior beam-column subassemblages. Standard 4 in. by 8 in. test cylinders were used to investigate the short and long term loading properties of the repair materials.

The study is divided into three sections: behavior of original subassemblages; repair techniques and repair materials; and behavior of repaired subassemblages.

The subassemblages were designed using two different procedures. The first represented structures not subjected to earthquake conditions and the second represented structures designed according to current seismic provisions. The subassemblages were subjected to displacement patterns representing the effect of either a moderate or a severe earthquake loading to study the behavior of

the original specimens. It was expected that these two loading patterns would produce different degrees of damage. The materials to be used in the repairs were investigated for short term stiffness and strength, and long term creep properties. The damaged specimens were repaired using two different repair techniques currently used in practice. For moderate damage, the subassemblages were repaired by epoxy injection of the major cracks in the concrete. For more extensive damage, the subassemblages were repaired by removing and replacing the damaged concrete. After repair, the subassemblages were retested to determine their behavior.

1.3 Review of Previous Investigations

The amount of research on the behavior of reinforced concrete structural components subjected to repeated and reversal loading in the inelastic range is quite abundant. However, amount of research conducted on the cyclic behavior of repaired structural components is limited. A brief review of some of these investigations on structural components will be presented below. Also, a brief review of research conducted on reinforcing steel and concrete will be given.

Behavior of Materials

A previous investigation (79) has shown that steel, after initial yielding in tension, will not exhibit a

definite yield point during stress reversal. This dependence on the previous stress history has been defined to be the Bauschinger effect. Additional cycles of stress reversals, as investigated by Singh, Gerstle, and Tulin (68), Kent (41), and Aktan, Karlsson and Sozen (2), resulted in a smooth stress-strain curve. The primary parameters influencing the cyclic behavior of the reinforcing steel (68) were a) the virgin properties of the material, b) the previous loading history, c) the rate of straining, d) the elapsed time between cycles, and e) the temperature. The Ramberg-Osgood curvilinear cyclic characteristic relationship has been used (2,41) to represent the cyclic behavior of the reinforcing steel.

The behavior of concrete under repeated loading was investigated by Sinha, Gerstle, and Tulin (70), Karsan and Jirsa (39,40) and Kent and Park (42) and can be reasonably assumed to be bounded by the stress-strain curve based on monotonic loading. Kent and Park presented a relationship to calculate the monotonically loaded stress-strain curve based on the concrete strength and confinement.

Behavior of Members

Bertero (6) emphasized the importance of the loading history to determine the hysteretic behavior of a reinforced concrete member. Gradual increases in deflection with each cycle of loading may increase the energy

dissipation capacity and the maximum strength of the member when compared with the results obtained by cycling to deflections which correspond to the maximum load resistance of the member during the first cycle. The latter loading scheme for testing member behavior may represent the worst possible condition.

Brown and Jirsa (16) investigated the hysteretic behavior of reinforced concrete cantilever beams. Their results indicated that after the first quarter cycle of loading, the behavior was nonlinear due to a combination of a) Bauschinger effect in the reinforcement, b) shear deformations, c) closure of residual cracks, and d) slippage of the anchored longitudinal reinforcement.

Bertero and Popov (7) investigated the hysteretic behavior of reinforced concrete flexural members subjected to high and low shear stresses. They suggested that the hysteretic behavior can be improved by reducing the spacing of the transverse reinforcement and by increasing the area of compression reinforcement.

Wight and Sozen (85) investigated the hysteretic behavior of reinforced concrete columns subjected to shear reversals. The parameters varied were the column axial load, the spacing of the transverse reinforcement, and the severity of loading. Their results indicated that the specimens had less stiffness and strength degradation with more closely spaced transverse reinforcement.

Park, Kent, and Sampson (59) calculated the moment-curvature response of reinforced concrete members subjected to cyclic loading. Their analytical results, which were derived from the stress-strain curves for concrete and steel, compared well with their experimental data. However, because of the computer time involved, they suggested that the Ramberg-Osgood relationship or Clough's (24) degrading stiffness model should be used to determine member behavior.

Behavior of Joints

Marques and Jirsa (50), investigated the behavior of 90 deg. hooks anchored in concrete which were intended to simulate conditions at an exterior beam-column joint. The parameters which were varied in that investigation were column size, column axial load, longitudinal column reinforcement, side cover, and transverse reinforcement through the joint. Their results indicated that the strength capacity of the hooked anchorage could be increased if both the confinement of the hook in the form of cover or ties, and the straight lead embedment length before the hook were increased. Tests by Townsend (80) on exterior beam-column joints indicated that insufficient straight lead embedment length before the hook will result in a poor hysteretic response.

Hanson and Connor (32) investigated exterior beam-column subassemblages reinforced with Grade 40 steel.

Their results indicated that properly designed and detailed joints can resist moderate earthquakes without loss of strength. A further investigation by Hanson (31) indicated Grade 60 reinforcement can be used in subassemblages that are designed to develop ductile behavior.

Park and Paulay (60) investigated the behavior of beam-column subassemblages. The parameters varied were the amount and arrangement of the transverse reinforcement in the joint and the method of anchoring the beam bars. Their results indicated that for inelastic cyclic load conditions the shear resistance contributed by the concrete should be neglected in the design of joints. Also, the use of beam stub protruding beyond the far face of the column can be used to anchor the beam bars effectively.

Megget (54) tested reinforced concrete beam-column subassemblages to determine the effect of transverse beam stubs on the joint. His results indicated that the specimen with the transverse beam stubs behaved better than the specimen without the stub. This better behavior was attributed to the fact that the damage formed in the main beam for the stubbed specimen rather than in the joint as was the case for the plain specimen.

Uzumuri and Seckin (82) investigated the behavior of unreinforced and reinforced beam-column joints. For the unreinforced joint, their results showed that the concrete shear capacity was 27 percent higher than the

maximum value specified by ACI 318-71. For the reinforced joints, the shear stress resisted by the concrete decreased with increases in the amount of transverse reinforcement which is not in agreement with truss analogy predictions.

Behavior of Repaired Members

Mahin, Bertero, Atalay and Rea (49), Celebi and Penzien (22), and Hidalgo and Clough (34) used the epoxy injection technique to repair structural members and frames. Celebi, et al, found that the beam stiffness, strength, and energy dissipation capabilities were restored. However, Mahin, et al, found that the stiffness and strength were restored, but the energy dissipation capability was not restored. Also, Mahin, et al, and Hidalgo, et al, expressed doubt as to the effectiveness of the epoxy injection technique for restoring the bond between the reinforcement and concrete.

Lee and Hanson (45) used the removal and replacement technique to repair beam-column joints. Their results indicated that the repair of joints with a high strength material can shift the damage from the joint into the beam and/or column during retest.

CHAPTER 2

EXPERIMENTAL INVESTIGATION

2.1 Design of Specimens

The beam-column subassemblages were designed using two criteria. For the first design, referred to here as "Type I Design", the American Concrete Institute Building Code (ACI 318-71) (17) for nonseismic areas (Appendix A excluded) was used. This design was assumed to represent existing structures which were designed without considering seismic loading. For the second design, referred to as "Type II Design", ACI 318-71 including Appendix A (special provisions for the design of ductile moment-resisting space frames) and Recommendations for Design of Beam-Column Joints in Monolithic Reinforced Concrete Structures (63) were used. A detailed discussion of both criteria used in designing the specimens is given in Appendix A. Overall dimensions of the specimens and the details of the reinforcing steel for Type I and Type II designs are shown in Figs. 2.1(a) and 2.1(b), respectively. The primary difference between the subassemblages resulting from the two design criteria was the amount of transverse reinforcement.

The nominal yield stress for the longitudinal reinforcement in the column was 60,000 psi and that for the longitudinal reinforcement in the beam was 40,000 psi. All the transverse reinforcement had a nominal yield

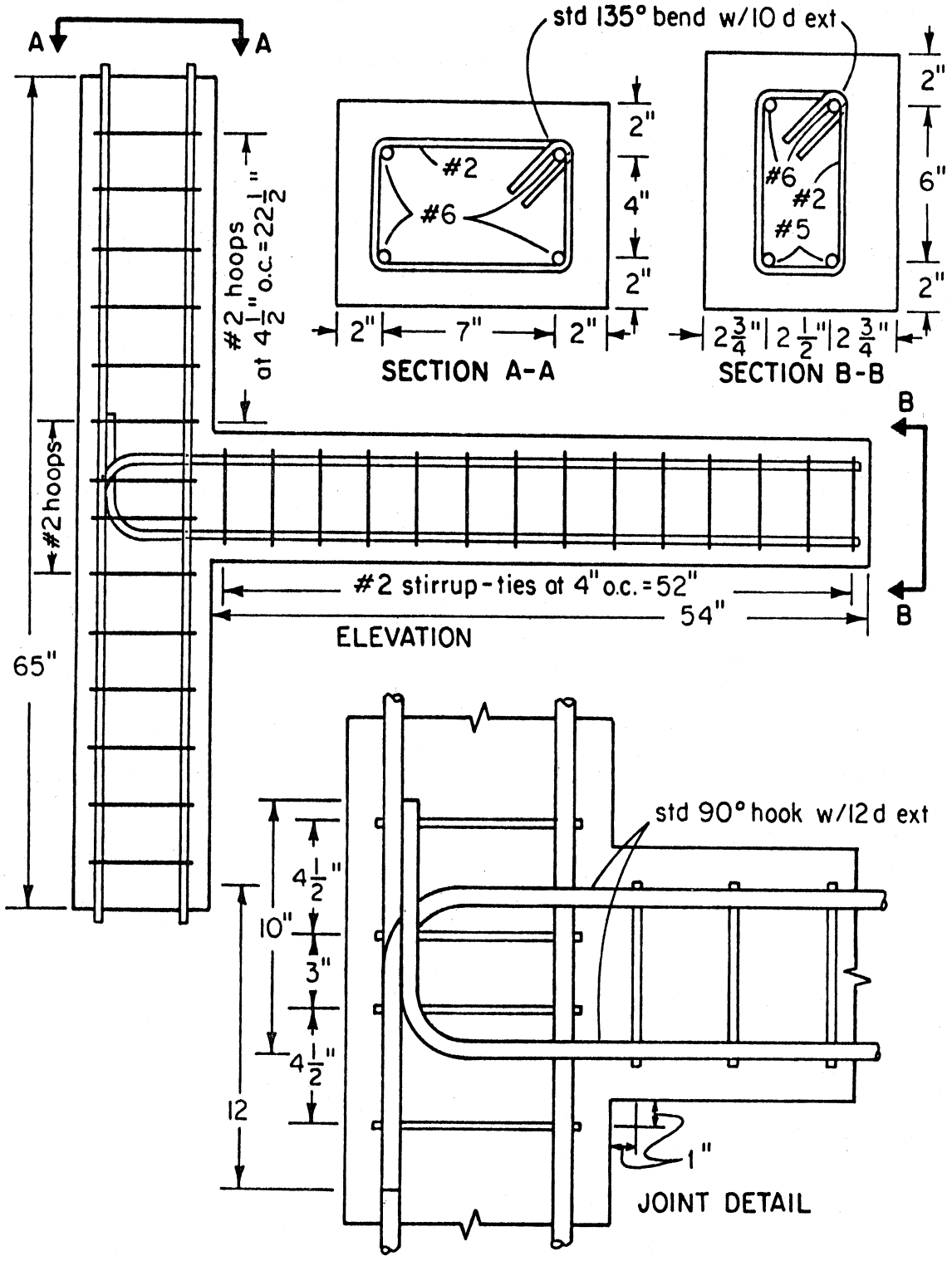

Fig. 2.1(a) Details of Beam-Column Subassemblage for Type I Design

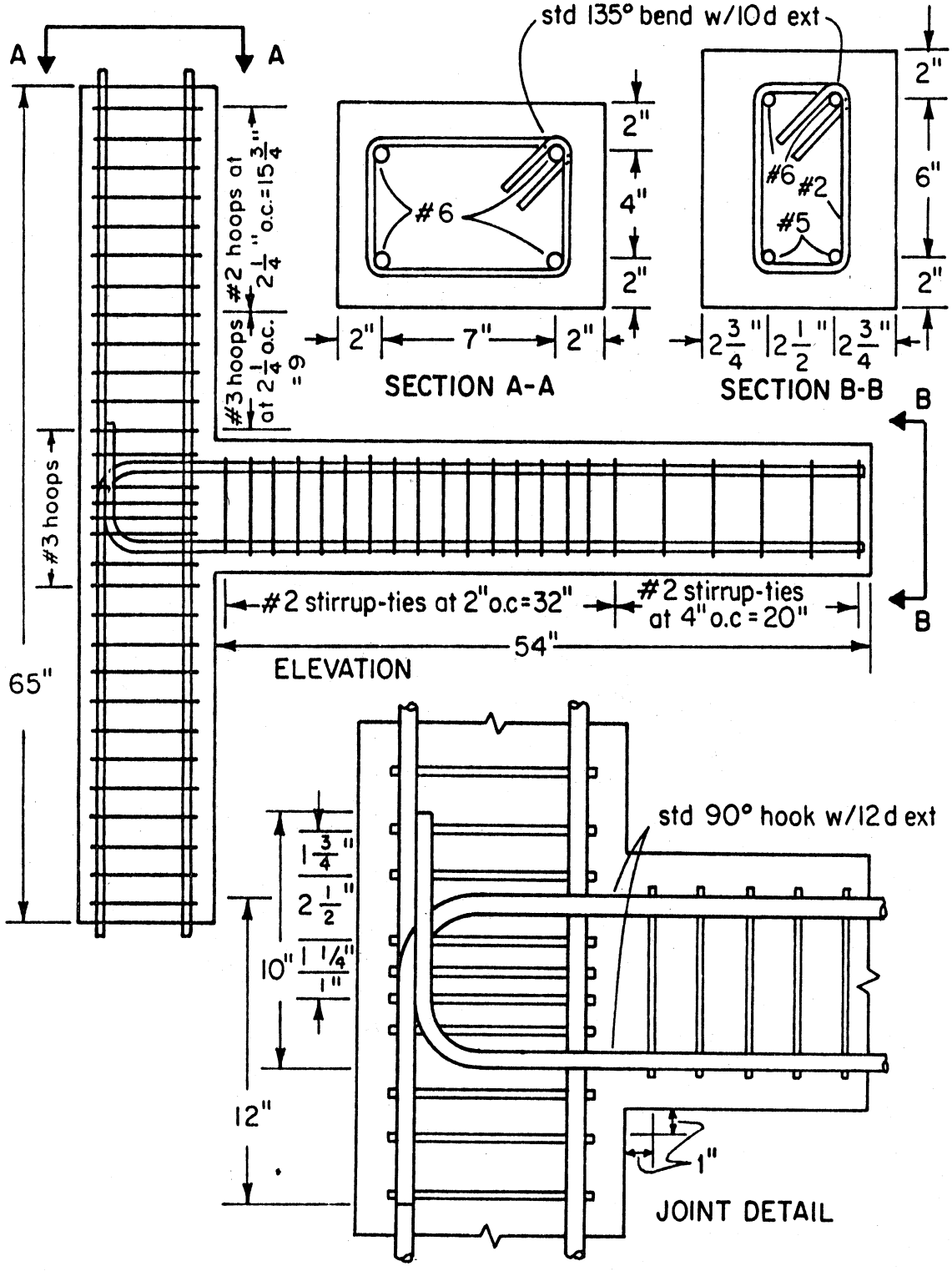

Fig. 2.1(b) Details of Beam-Column Subassemblage for Type II Design

stress of 40,000 psi. The average yield stress for the No. 6 longitudinal reinforcement in the column based upon six tests was 77,900 psi, and that for the longitudinal reinforcement in the beam was 49,600 psi (eight tests) and 50,500 psi (eight tests) for the No. 6 top and the No. 5 bottom bars respectively. For the transverse reinforcement, the plain No. 2 bars and the No. 3 bars had an average yield strength of 39,600 psi (three tests) and 56,400 psi (three tests) respectively.

The specified concrete strength for the beam-column subassemblages was 4,000 psi. See Appendix C for the composition of the concrete mix using 3/8 in. maximum size aggregate. The average 28 day concrete strength as determined by standard 4 x 8 in. test cylinders was 3,700 psi (three tests) and 4,200 psi (three tests) for the two different casting.

The measured material properties of the reinforcing steel and concrete for each specimen at the time of original testing are summarized in Appendix B.

The two criteria used in designing the beam-column subassemblages provided a means to determine the effectiveness of repair for structures designed either with or without seismic considerations of the current code. Also the effectiveness of the added transverse reinforcement for seismic resistance can be evaluated from the original tests of the different designed specimens.

See Appendix C for a discussion of the fabrication of the beam-column subassemblages.

2.2 Testing of Specimens

The original and repaired specimens were tested in a horizontal position as shown in Fig. 2.2. Rollers

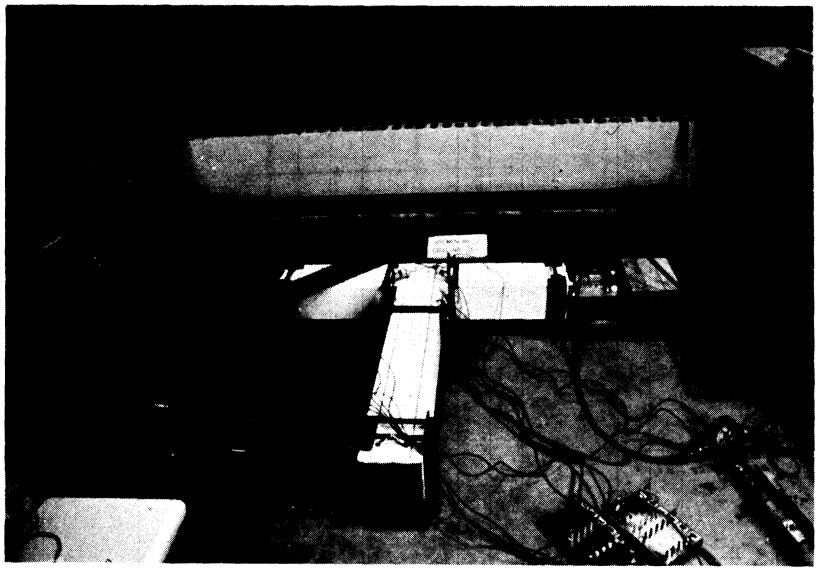

Fig. 2.2 Specimen in Horizontal Position During Testing

were placed on each side of the column near its end to represent inflection points. After a constant axial force was applied to the column, the beam tip was slowly deflected by a hydraulic actuator. Figure 2.3 shows the location of the applied deflection and reaction forces. A detailed description of the loading system is given in Appendix D.

Two displacement patterns (Fig. 2.4) were used to obtain different degrees of damage during original

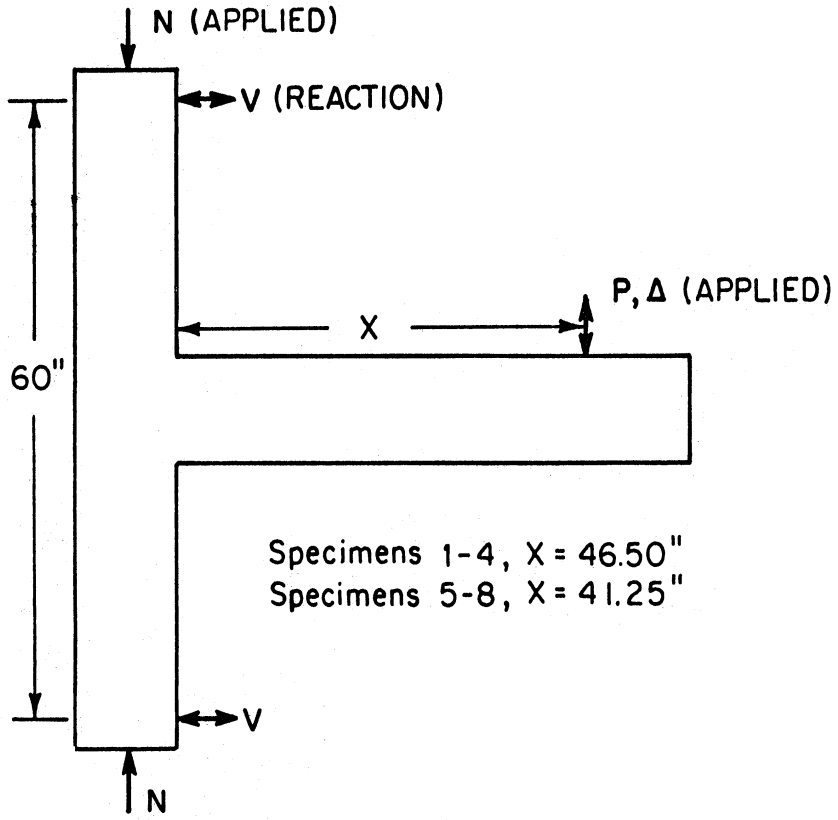

Fig. 2.3 Location of Applied and Reaction Forces

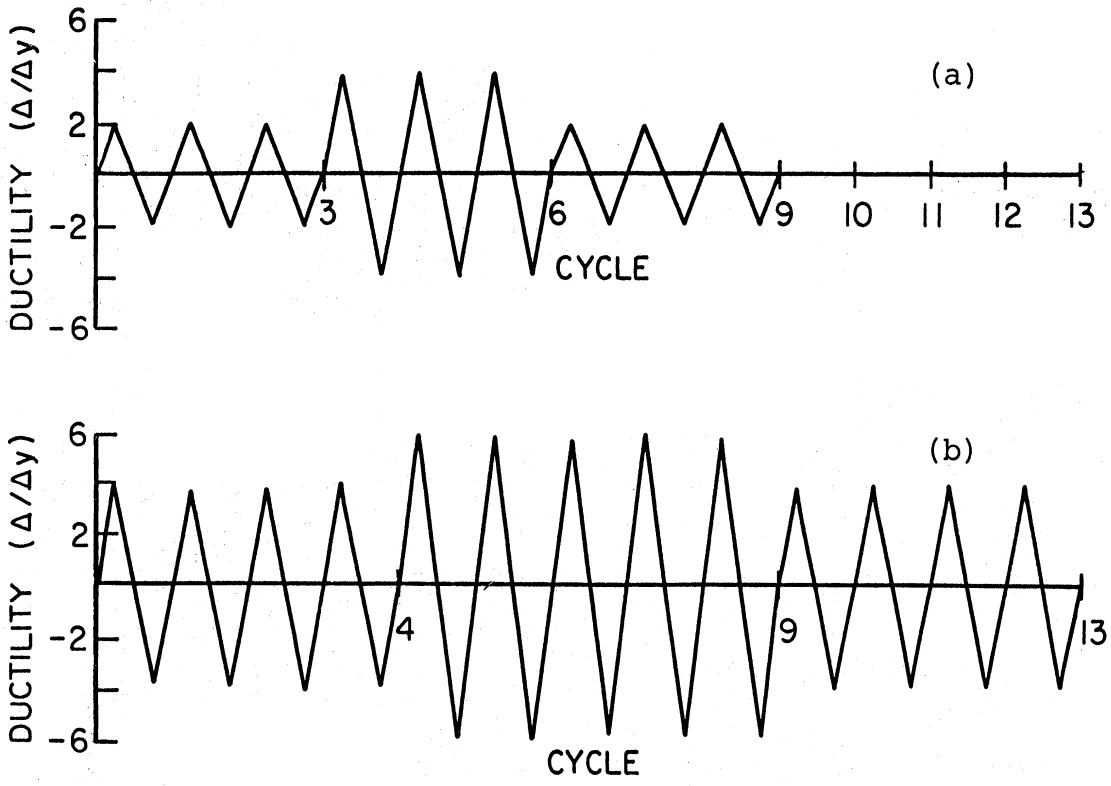

Fig. 2.4 Displacement Pattern representing (a) Moderate and (b) Severe Earthquake Loading

testing. The displacement patterns were meant to simulate the type of displacements the subassembly may be subjected to during a moderate earthquake and a severe earthquake respectively. These displacement patterns represent what the writer believes the subassemblage should be able to resist in order to survive either a moderate or severe earthquake. In addition to having four more cycles of loading, the amplitude of the displacement pattern representing a severe earthquake was selected to produce crushing in the beam compression zone during the first quarter cycle of loading, thus producing a more severe type of damage as compared to the moderate earthquake loading. The term ductility as used in this dissertation and shown in Fig. 2.4 was defined as the beam-tip displacement divided by the displacement at time of first yielding of the beam top bars. The loading sequence always started with the beam top reinforcement acting in tension. The uniform patterns illustrated in Fig. 2.4 were utilized to permit studies of the degrading hysteretic characteristics of the specimens. For retesting, each repaired specimen was subjected to the same displacement history as used during original testing in order that direct comparisons of the results could be made.

For each specimen, the type of design, column loading, and displacement pattern used are summarized in Table 2.1. The 40 kip column compression load for Specimens 1 through

Table 2.1 Design and Loading Parameters

Specimen	Type of Design	Type of Loading	Column Load (kips)
1	II	Moderate	40
2	II	Severe	40
3	I	Moderate	40
4	I	Severe	40
5	II	Severe	0
6	I	Severe	0
7	I	Severe	0
8	I	Severe	0

4 represented about 35 percent of the design balanced axial load. For Specimens 2 and 4, a ductility of about five (instead of six) was attained during cycles 5 through 9 [Fig. 2.4(b)] due to a limitation of the actuator stroke. The beam shear span was decreased by moving the actuator 5 1/4 in. closer to the column for Specimens 5 through 8 as shown in Fig. 2.3 to obtain a ductility of six during cycles 5 through 9 as given in Fig. 2.4(b). Specimens 6 through 8 used the same design and loading parameters so that the behavior of different repair materials could be compared by retesting.

Data Acquisition. During original testing and retesting, the force and deflection at the beam loading

point were continuously recorded and used to monitor the progress of the test. This data were later used to analyze the stiffness and load degradation, and energy dissipation capacity of the specimen. For the original testing, high elongation electrical resistance strain gages, applied to the reinforcing steel in the joint and the beam, were used to indicate steel strains. A detailed description of the techniques for application of the gages is given in Appendix E. The location and identification of the gages in the subassemblage for both the Type I and Type II Designs are given in Fig. 2.5.

Shear distortion in the joint and the beam rotation at a section 10 in. from and relative to the inside column face were both measured with Linear Variable Differential Transformers (LVDT). The location of the LVDTs to measure shear distortion in the joint and relative beam rotation can be seen in Figs. 2.6 and 2.7 respectively. See Appendix D for a description of the LVDTs and the recording devices.

2.3 Repair of Specimens

After original testing, the specimens were repaired in an upright position using either of two repair techniques. The first technique, referred to as the epoxy injection technique, uses low viscosity epoxy which is injected into cracks for the purposes of restoring bond between the reinforcing steel and concrete, and continuity

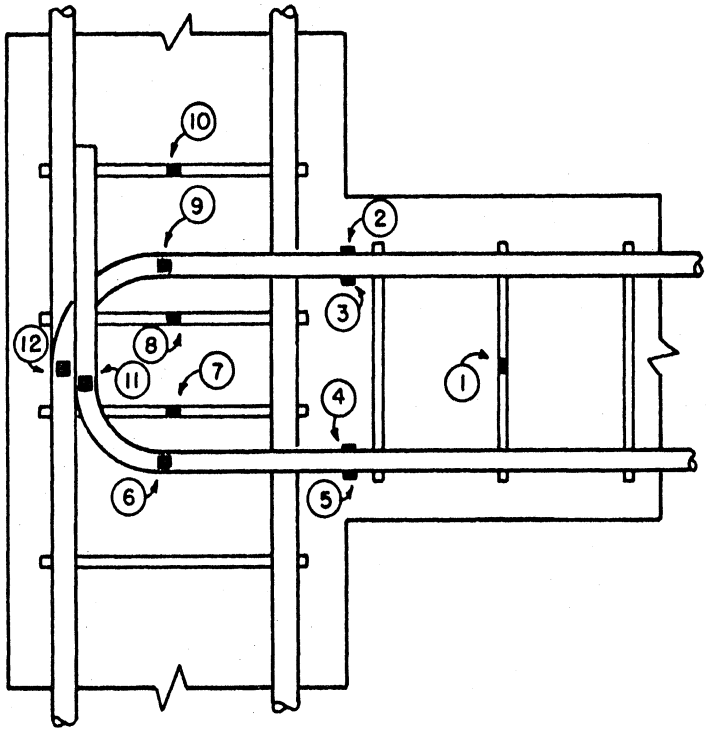

Fig. 2.5(a) Location and Identification of Strain Gages for Type I Design, Specimens 3 and 6

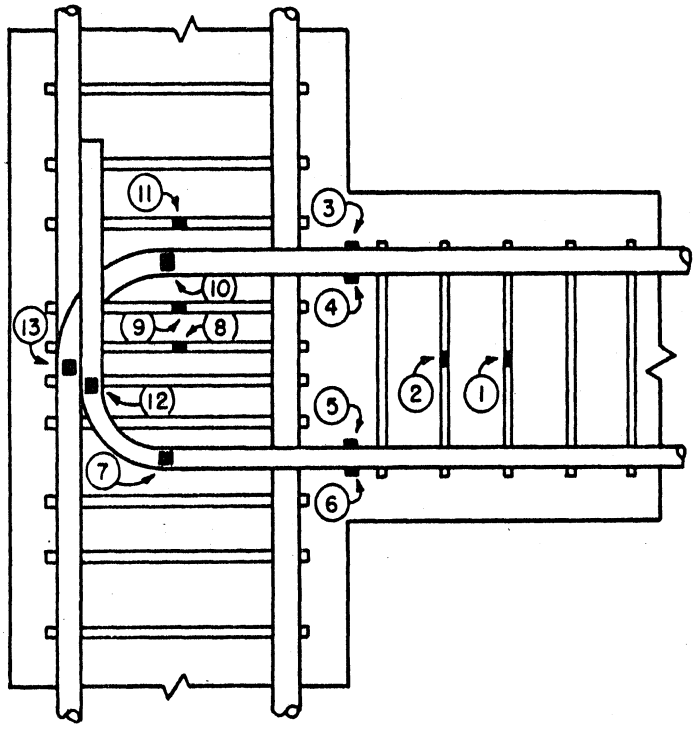

Fig. 2.5(b) Location and Identification of Strain Gages for Type II Design, Specimens 1, 2, and 5

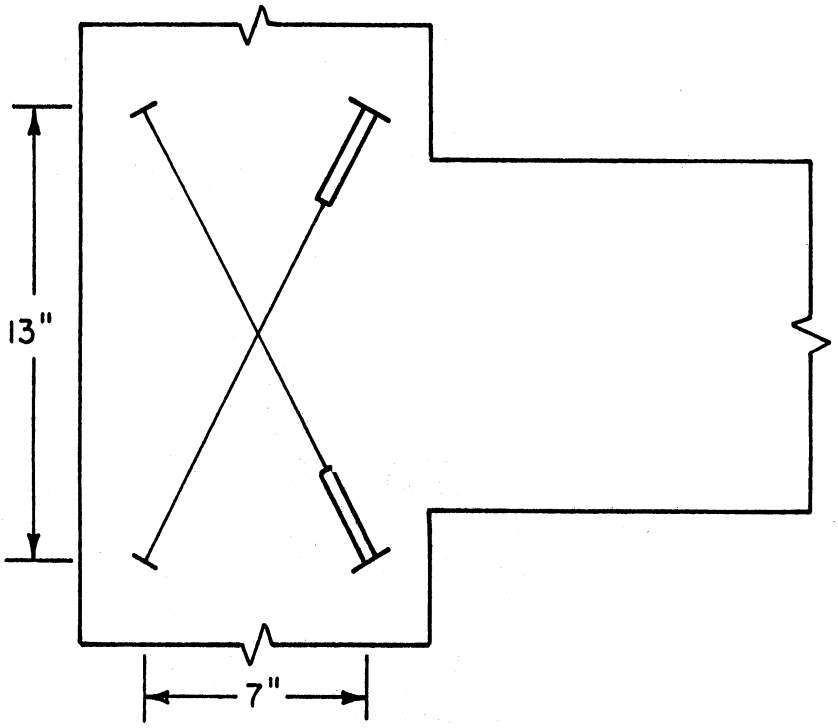

Fig. 2.6 Location of LVDTs to Measure Joint Distortion

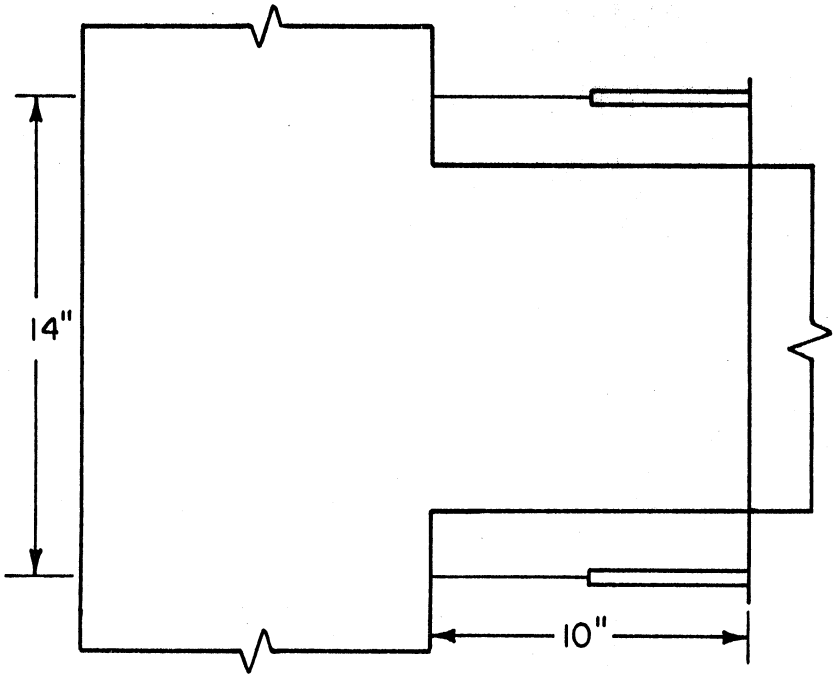

Fig. 2.7 Location of LVDTs to Measure Relative Beam Rotation

in the concrete. The epoxy injection type of repair is more applicable for moderately damaged members where the concrete on both sides of the crack is intact. For more severely damaged members, the second technique, referred to as the removal and replacement technique was used. The removal and replacement type of repair consisted of removing the damaged concrete and replacing it with high early strength material of equal or higher strength than the original concrete. High early strength materials enable the structure to be returned to full use earlier after repairs. The replacement materials considered in this investigation were epoxy-sand mortar, Duracal cement concrete, high strength quick setting concrete, and high early strength (Type III) concrete. A brief description of the repair materials as well as their short and long term loading properties are given in Chapter 4.

A detailed description of the repair procedure for both the epoxy injection, and removal and replacement techniques used in this investigation also is given in Chapter 4.

CHAPTER 3

ORIGINAL BEHAVIOR OF SPECIMENS

The type of design, column load, and displacement pattern used to determine the original behavior for each beam-column subassemblage are summarized in Table 2.1.

3.1 Visual Observations

For all the specimens, the primary damage during original testing occurred in the portion of the beam adjacent to the beam-to-column interface. Most of this damage can be attributed to flexural action. As the beam was displaced downward during the first quarter cycle of loading, flexural cracks propagating about two-thirds the depth of the beam were observed first at the beam-to-column interface and in the portion of the beam near the interface. Additional downward displacement of the beam resulted in inclined cracks forming at the end of the flexural cracks and continuing to the level of the bottom reinforcement. For the specimens subjected to the displacement pattern representing severe earthquake loading, minor spalling was observed in the compression zone of the beam near the inside column face during the first quarter cycle of loading as shown in Fig. 3.1.

Unloading of the beam during the second quarter cycle of loading resulted in the flexural cracks narrowing but at zero beam load, the cracks still remained open due to the elongation of the top reinforcement.

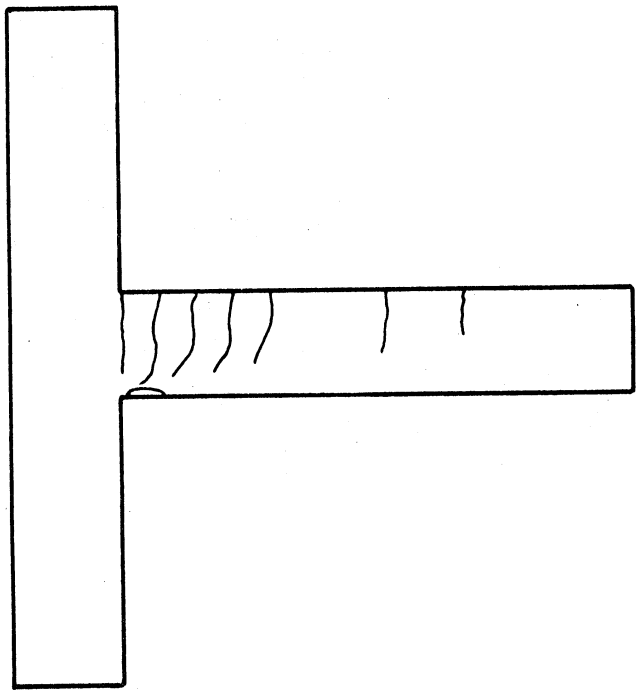

Fig. 3.1 Cracking and Spalling in Beam after First Quarter Cycle of Severe Earthquake Loading

Application of a negative (upward) beam force resulted in observed behavior similar to that described above. Vertical and inclined cracks formed and propagated upward from the bottom of the beam. No spalling was observed in the compression zone when the bottom reinforcement was in tension during the second half cycle of loading.

The second and subsequent cycles of loading at the same displacement level produced little additional cracking. Flexural cracks opened and narrowed during cyclic beam action.

For the specimens subjected to the displacement pattern representing a moderate earthquake loading, the first cycle at the higher displacement level produced little additional cracking. Instead, the existing cracks became

wider. During subsequent cycles at the higher displacement level, the cracks remained stable; opening and narrowing within each cycle of loading. No spalling was observed in the compression zone.

For the specimens subjected to the displacement pattern representing severe earthquake loading, the first cycle at the higher displacement level produced additional deterioration in the beam. Spalling in the compression zone increased and the flexural cracks became wider. For subsequent cycles at the higher displacement level, a relative transverse movement along the vertical cracks in the beam was observed. This movement was especially noticeable near the zero load position and was more severe for specimens with Type I Design. Due to the movement along the crack, additional concrete cover was spalled off caused by the dowel action in the longitudinal reinforcement. After the cover spalled off, outward buckling of the top and bottom longitudinal bars was observed. The buckling of these bars was more severe for specimens with Type I Design. Most of the damage occurred in a region five inches from the inside column face and the beam appeared to pivot about that location during cyclic beam action.

For the remaining cycles of loading at the lower displacement level, there was no additional deterioration in the beam for specimens subjected to the displacement pattern representing a moderate earthquake loading. For

the specimens subjected to the displacement pattern representing a severe earthquake loading little additional spalling and cracking occurred in the beam with Type II Design. However, spalling continued in the beams with Type I Design during the cycles of loading at the lower displacement level.

Specimens with Type II Design held together better during original testing than those of Type I Design as seen by comparing Specimens 5 and 7 in Figs. 3.2(a) and 3.2(b) respectively. Both specimens were subjected to the displacement pattern representing a severe earthquake loading.

Specimens subjected to a displacement pattern representing a severe earthquake loading sustained more damage than those subjected to the moderate earthquake loading as seen by comparing Specimens 4 and 3 in Figs. 3.3(a) and 3.3(b) respectively. Both specimens had Type I Design.

The joint behaved well for all the specimens during original testing. (Joint used in this context implies the column region throughout the beam depth.) Most of the cracking in the joint occurred during the first cycle of loading. Subsequent cycles at the same displacement level and at higher displacement level produced little additional cracking. At the completion of the test, the cracks remained narrow and the concrete in the joint remained intact.

The primary cracking pattern in the joint for specimens with a 40 kip column axial load was the X-type

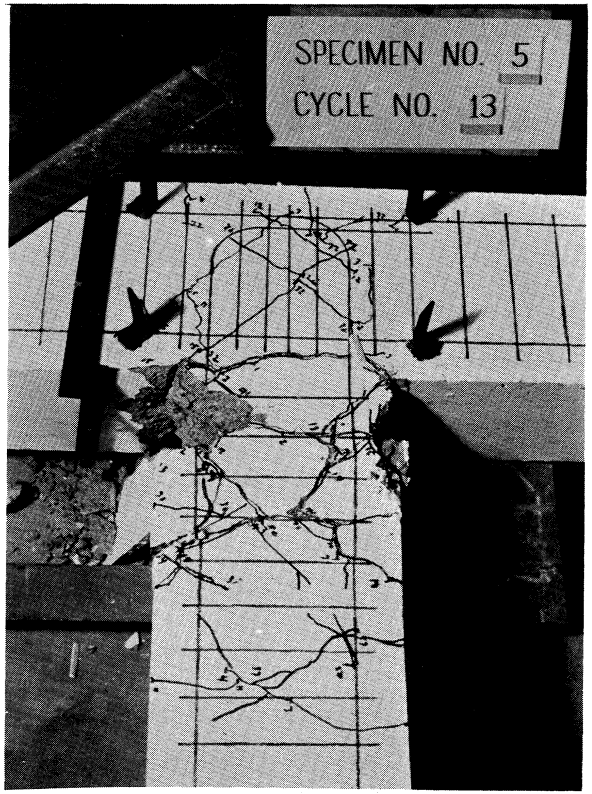

(a) Specimen 5 of Type II Design

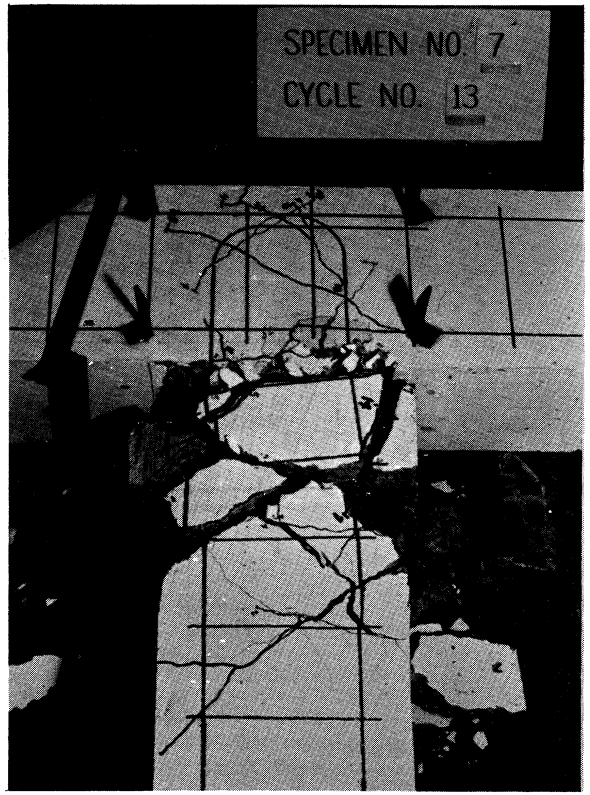

(b) Specimen 7 of Type I Design

Fig. 3.2 Comparison of Damage after Severe Earthquake Loading

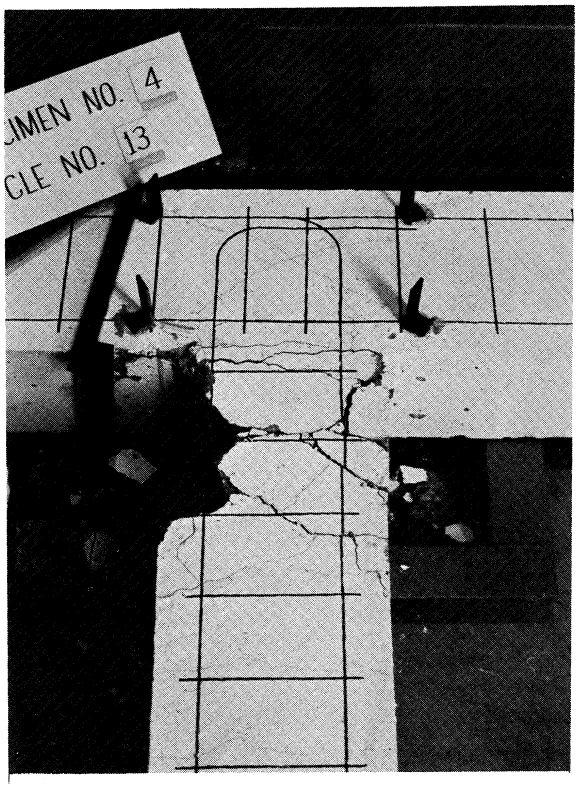

(a) Specimen 4 after Severe Earthquake Loading

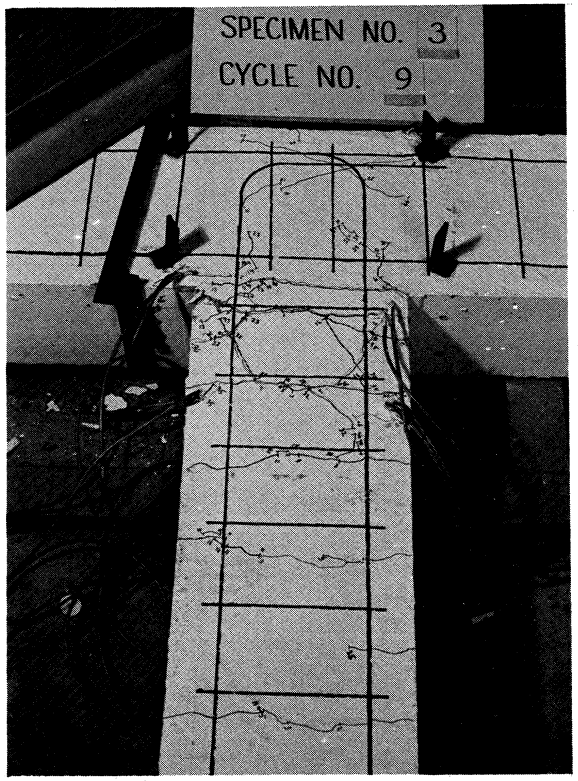

(b) Specimen 3 after Moderate Earthquake Loading

Fig. 3.3 Comparison of Damage for Different Levels of Loading with Type I Design

diagonal crack. In fact, these were the only joint cracks observed in Specimens 2 and 4 with Type II and Type I designs respectively. For the specimens with the zero column axial load, splitting cracks followed the straight portion and around the hook of the beam longitudinal reinforcement anchored in the column. In addition to the splitting cracks, diagonal cracks also were observed in the joint. The effect of the column axial load on cracking in the joint can be seen by comparing Fig. 3.4

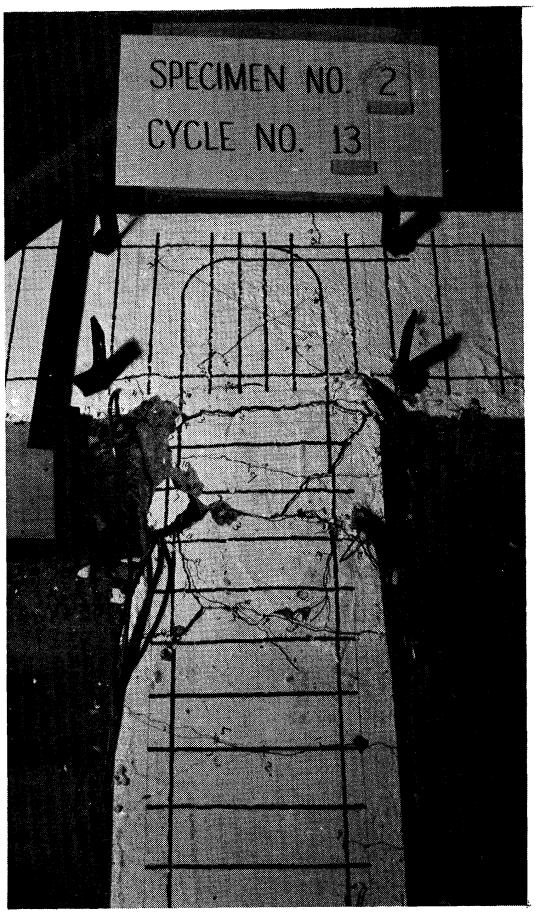

Fig. 3.4 Cracking in Joint for Specimen 2 with 40 kip Column Axial Load after Severe Earthquake Loading

for Specimen 2 (40 kip column axial load) with Fig. 3.2(a) for Specimen 5 (zero column axial load). Both specimens had Type II Design and were subjected to the displacement pattern representing severe earthquake loading.

No cracking of the column was observed during original testing for any of the specimens. Also, none of the longitudinal or transverse reinforcement fractured during testing.

3.2 Measured Force and Deflection

The beam-tip force vs deflection curves are shown in Figs. 3.5(a) through 3.5(h) for Specimens 1 through 8 respectively. Most of these curves represent typical flexural type behavior. Positive load and displacement correspond to the downward movement of the beam. For all the specimens, the first quarter cycle of the force-deflection curve was unique. The curve was almost linear before yielding of the beam top reinforcement. After yielding the force-deflection curve deviated from the linear behavior and the stiffness became much less. Although minor spalling was observed in the beam compression zone for the specimens subjected to the displacement pattern representing severe earthquake loading, almost no drop in load was observed during the first quarter cycle of loading. The unloading portion of the force-deflection curve had approximately the same average slope as the

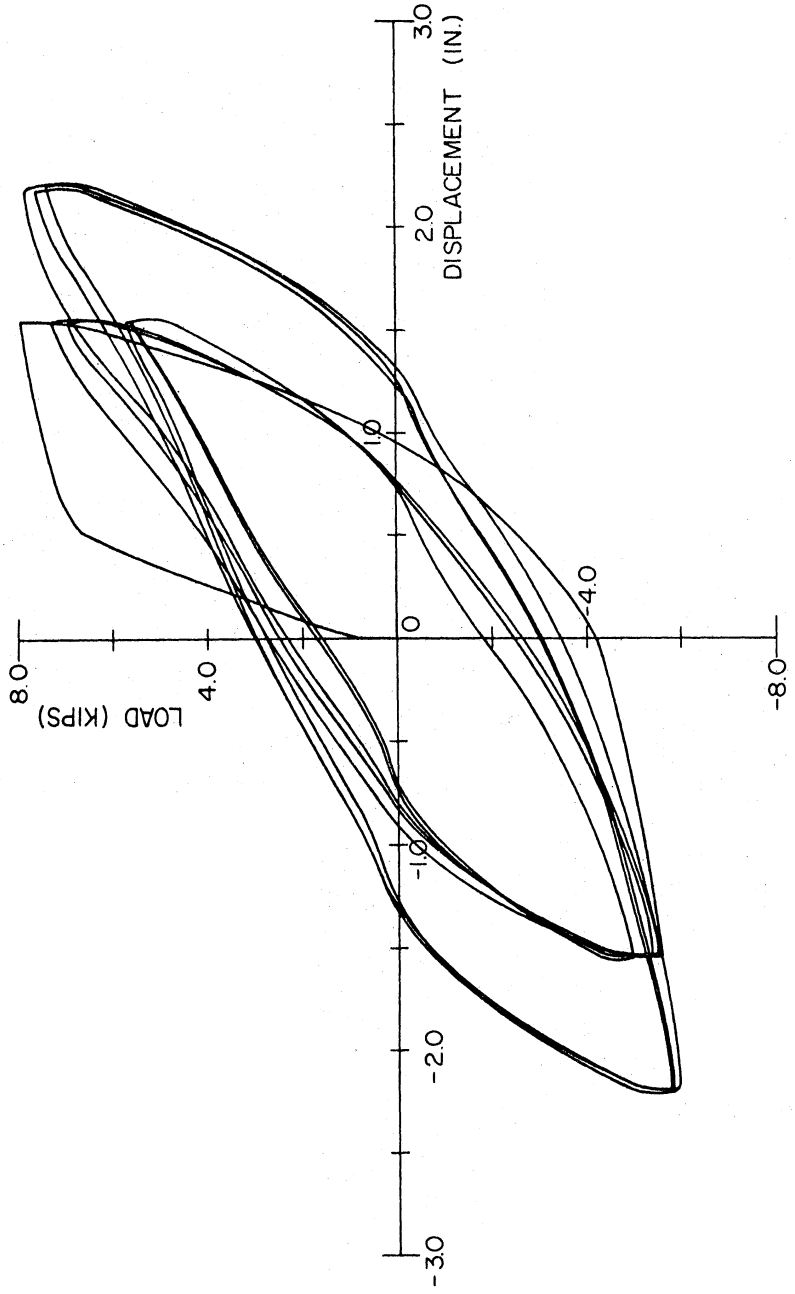

Fig. 3.5(a) Beam-Tip Force-Deflection Curves, Specimen 1

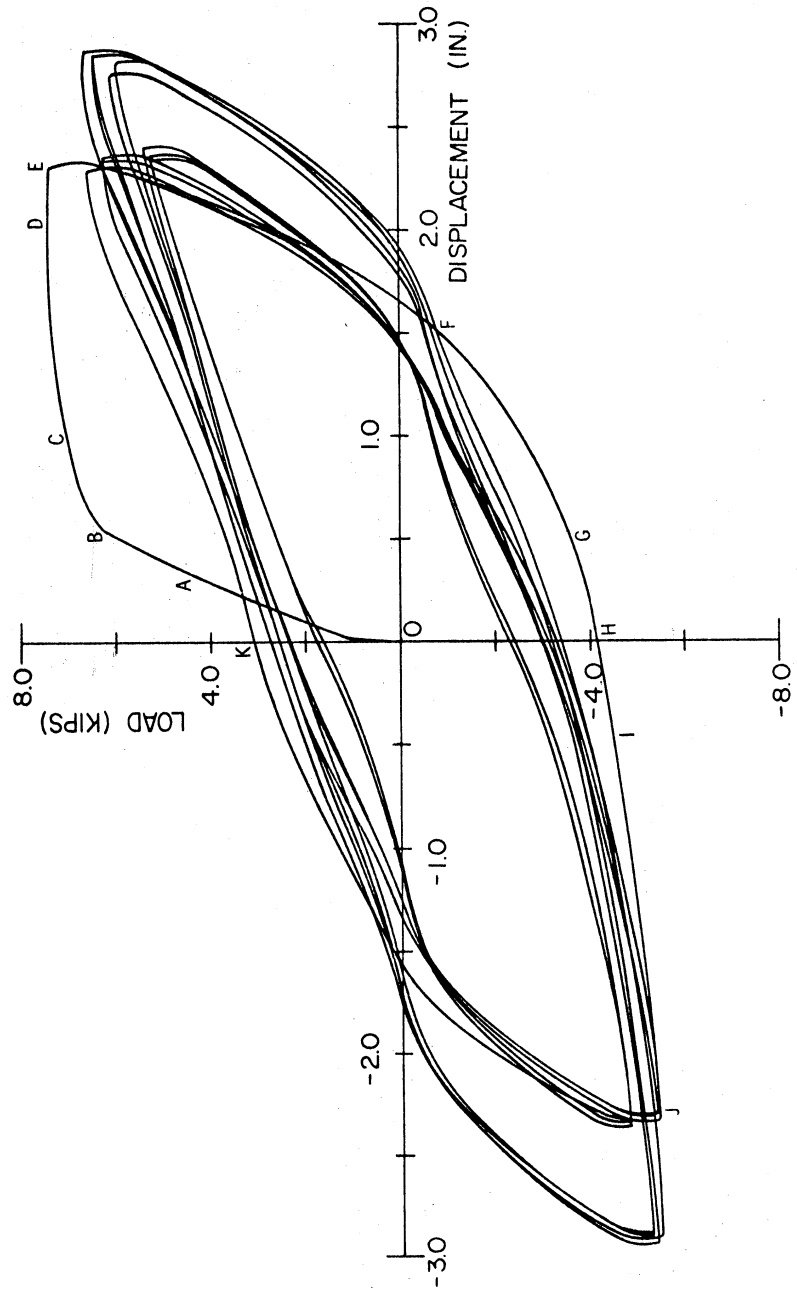

Fig. 3.5(b) Beam-Tip Force-Deflection Curves, Specimen 2

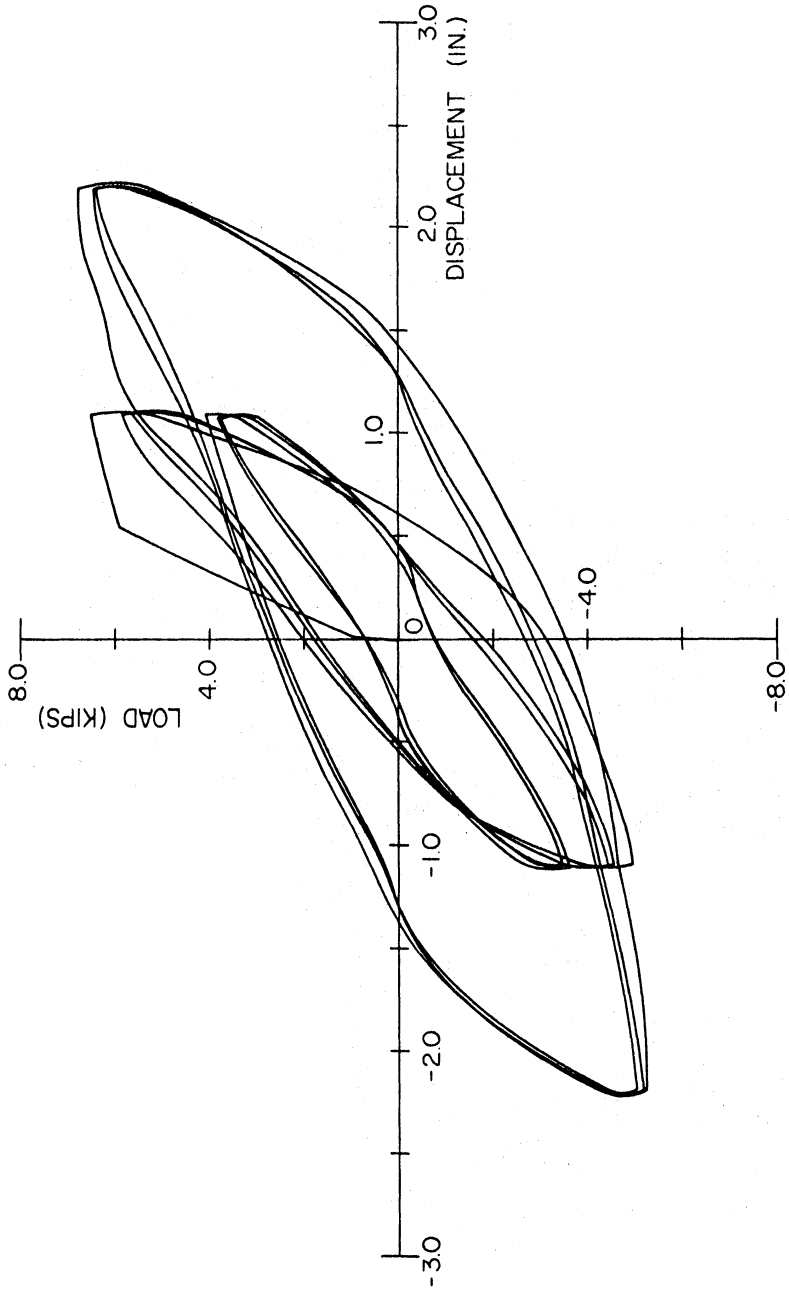

Fig. 3.5(c) Beam-Tip Force-Deflection Curves, Specimen 3

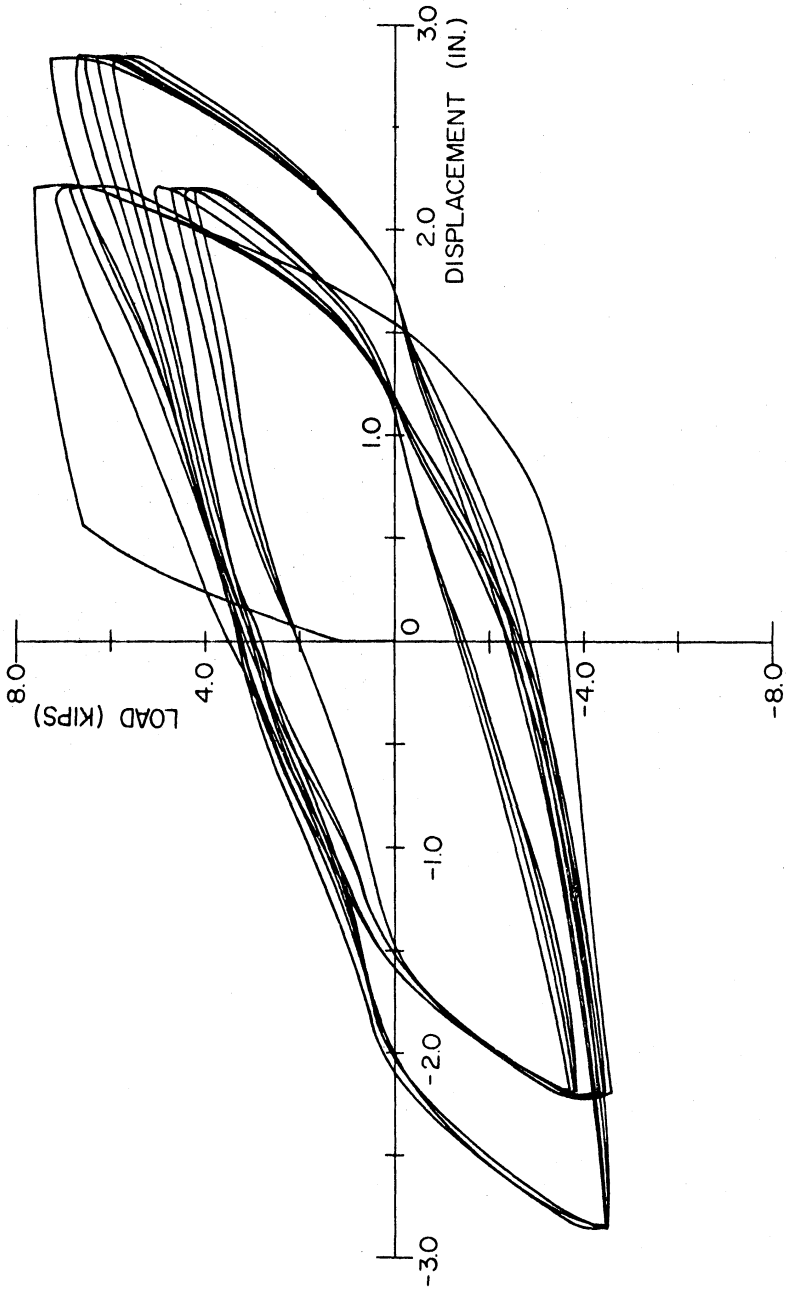

Fig. 3.5(d) Beam-Tip Force-Deflection Curves, Specimen 4

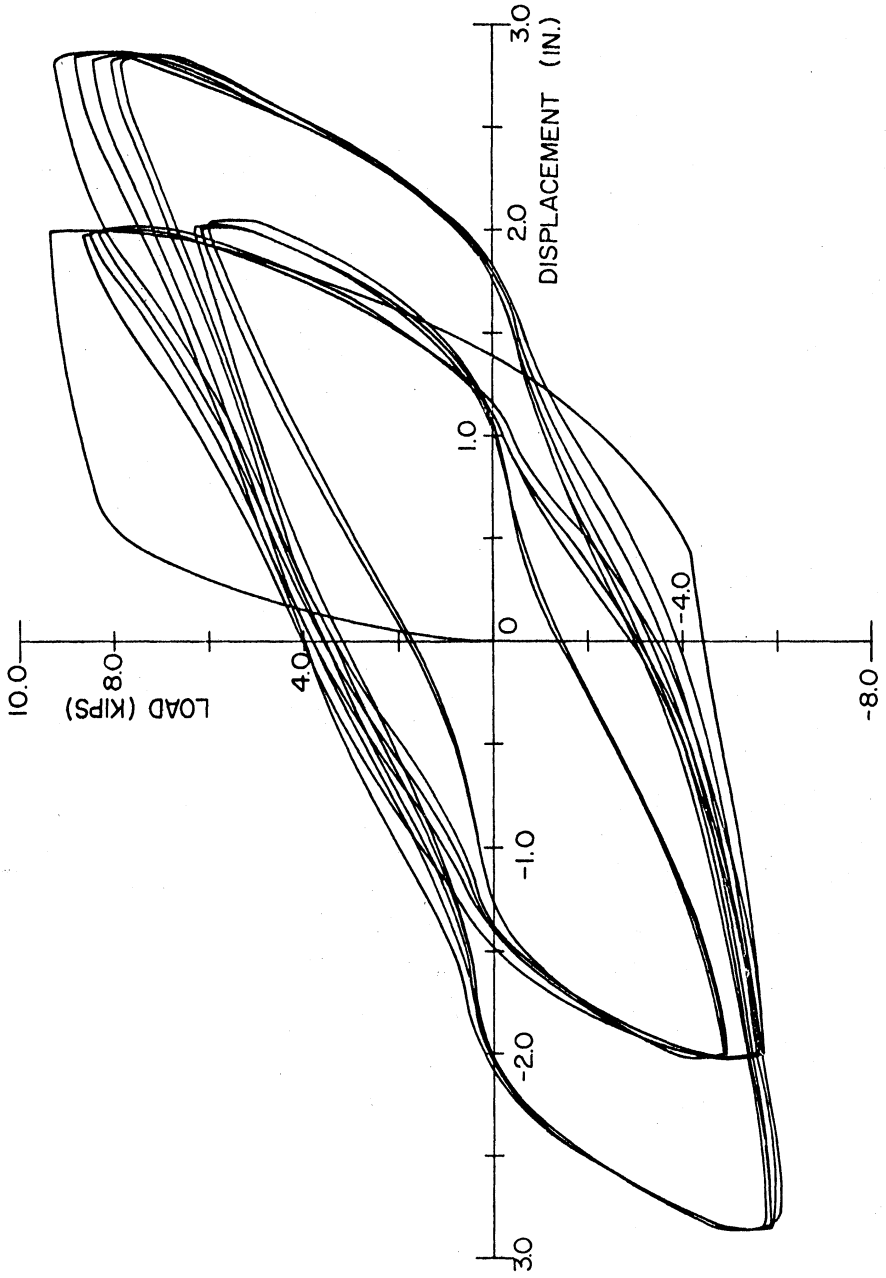

Fig. 3.5(e) Beam-Tip Force-Deflection Curves, Specimen 5

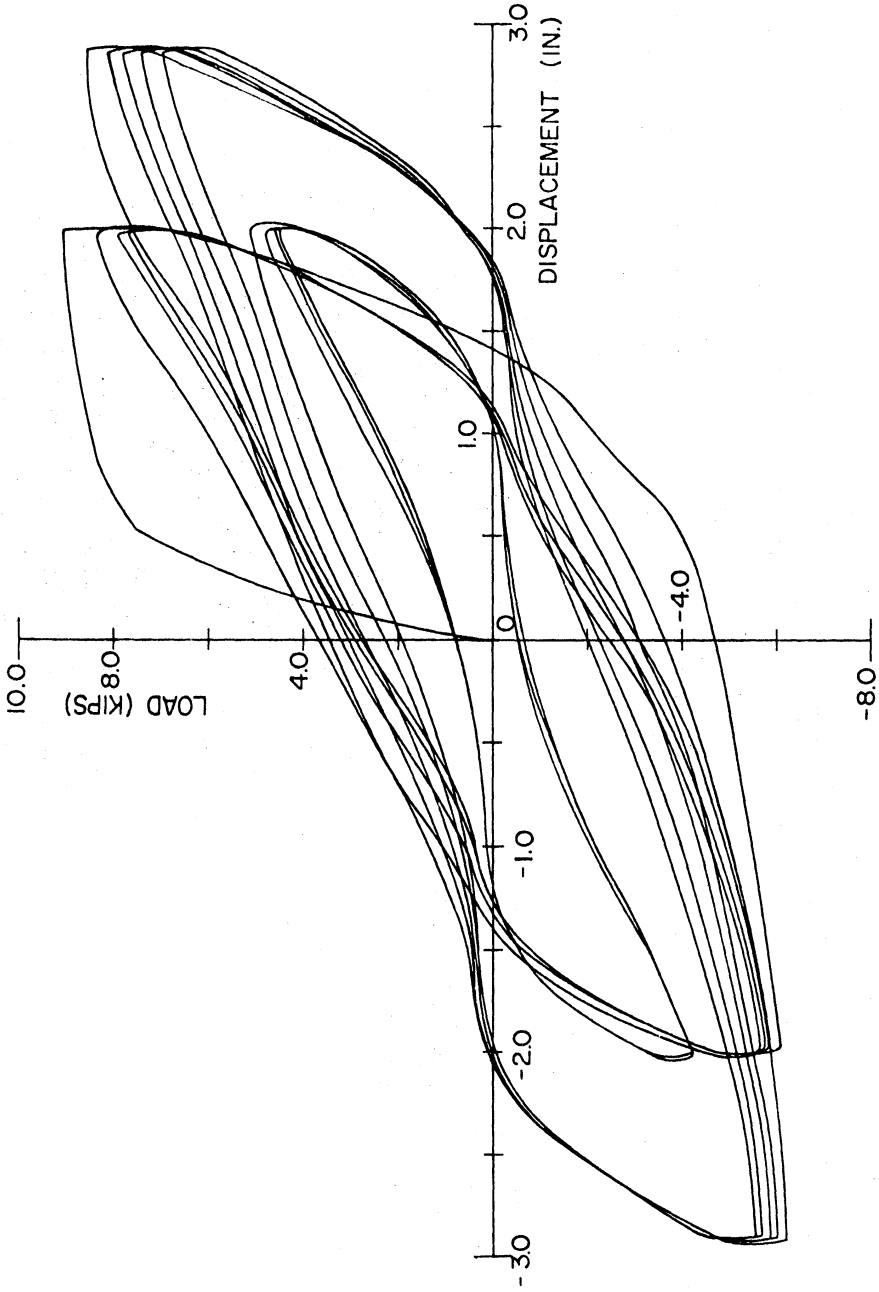

Fig. 3.5(f) Beam-Tip Force-Deflection Curves, Specimen 6

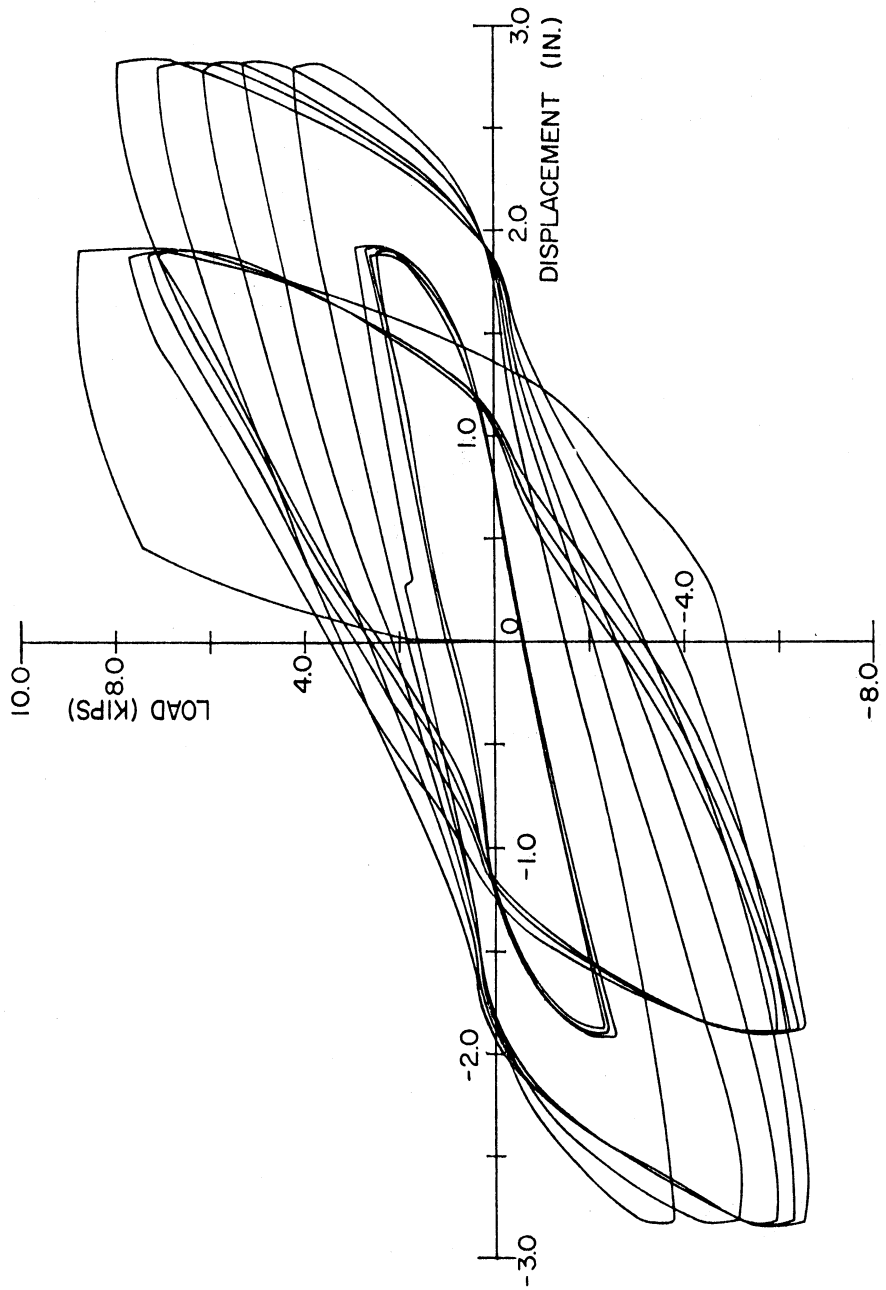

Fig. 3.5(g) Beam-Tip Force-Deflection Curves, Specimen 7

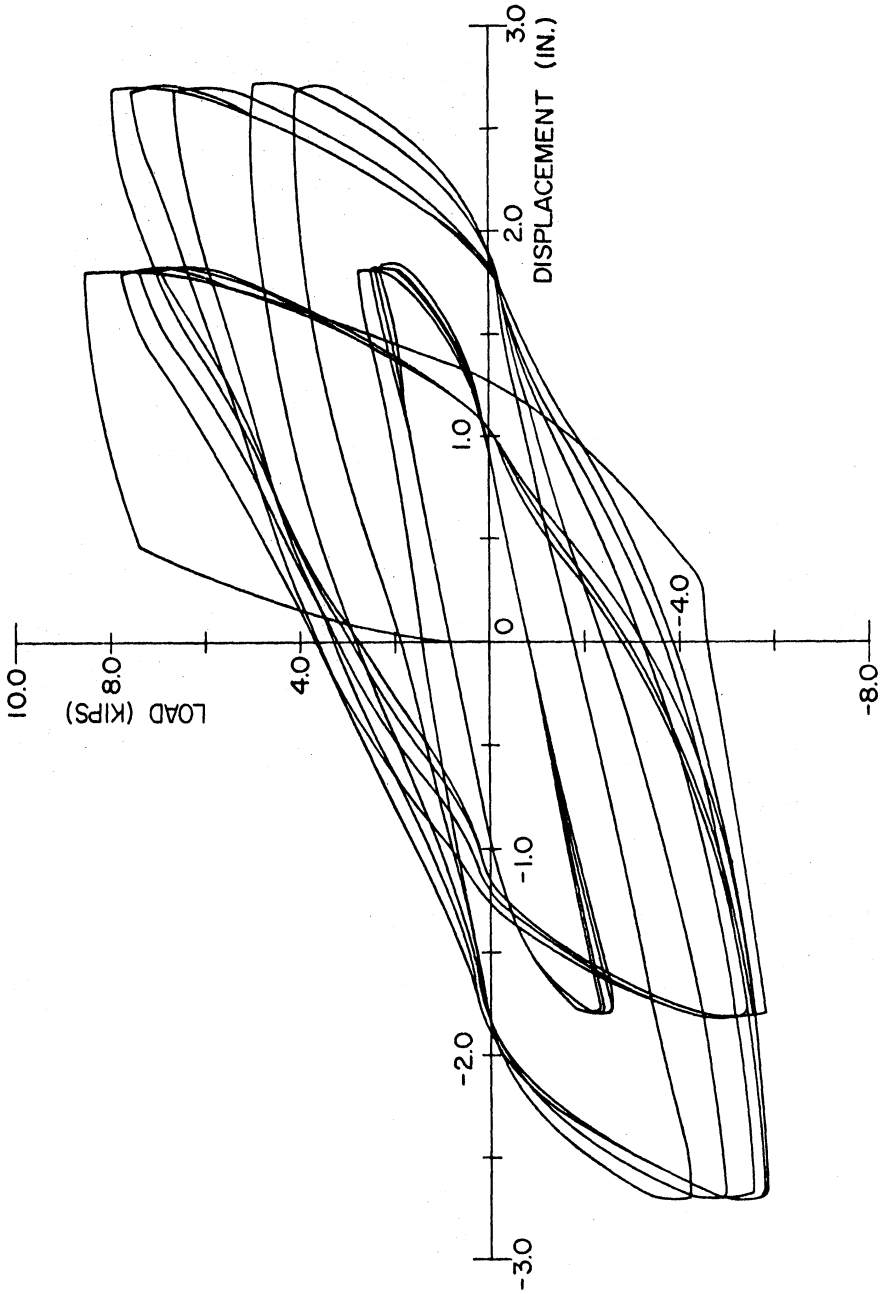

Fig. 3.5(h) Beam-Tip Force-Deflection Curves, Specimen 8

initial loading portion. For negative forces, the force-deflection curve was smooth with the negative yield load being less obvious. The unloading portion from the maximum negative force had a smaller slope than for initial loading. For the second and subsequent cycles of loading, the force-deflection curves were smooth.

The curvilinearity of the force-deflection hysteretic curves was influenced by a combination of: a) the curvilinear behavior of the beam tension and compression reinforcement due to the "Bauschinger Effect", b) the opening and closing of residual cracks, and c) the slippage between the concrete and reinforcement.

The force-deflection curves had a reverse curvature near zero beam load at both positive and negative beam displacements for the second and subsequent cycles. The reverse curvature was primarily due to transverse movement along the vertical cracks in the beam. This movement will be referred to as a "shear slippage". The figures indicate that the reverse curvature was more pronounced with each additional cycle of loading. The severity of shear slippage can be judged indirectly by measuring the energy dissipated (the area enclosed by the force-deflection curves).

The peak-to-peak load at maximum beam deflection, energy dissipated, and cumulative energy dissipated, obtained from the force-deflection curves, are plotted for

each cycle of loading for all of the specimens in Figs. 3.6(a) through 3.6(h). The peak-to-peak load and energy dissipation degrades after each cycle at constant beam displacement. This degradation was due to the reduction in stiffness in the subassemblage caused primarily by additional cracking and spalling of the concrete in the beam, shear slippage in the beam, and bond deterioration between the concrete and beam longitudinal reinforcement in the beam and joint.

Specimens with Type II Design had less load degradation than specimens with Type I Design as seen by the comparison in Fig. 3.7(a) for Specimens 5 and 7. Both specimens were subjected to the severe earthquake loading and had zero column load. This normalized peak-to-peak load was obtained by dividing the peak-to-peak load for each cycle given in Fig. 3.6 by that of the corresponding first cycle. Specimens with Type II Design also dissipated more energy as shown by the comparison in Fig. 3.7(b) for Specimens 5 and 7.

3.3 Measured Strains in Reinforcement

High elongation electrical resistance strain gages were attached to the reinforcing steel for some of the beam-column subassemblages. The identification and locations of the gages are shown in Fig. 2.5(a) for Specimens 3 and 6 and Fig. 2.5(b) for Specimens 1, 2, and 5.

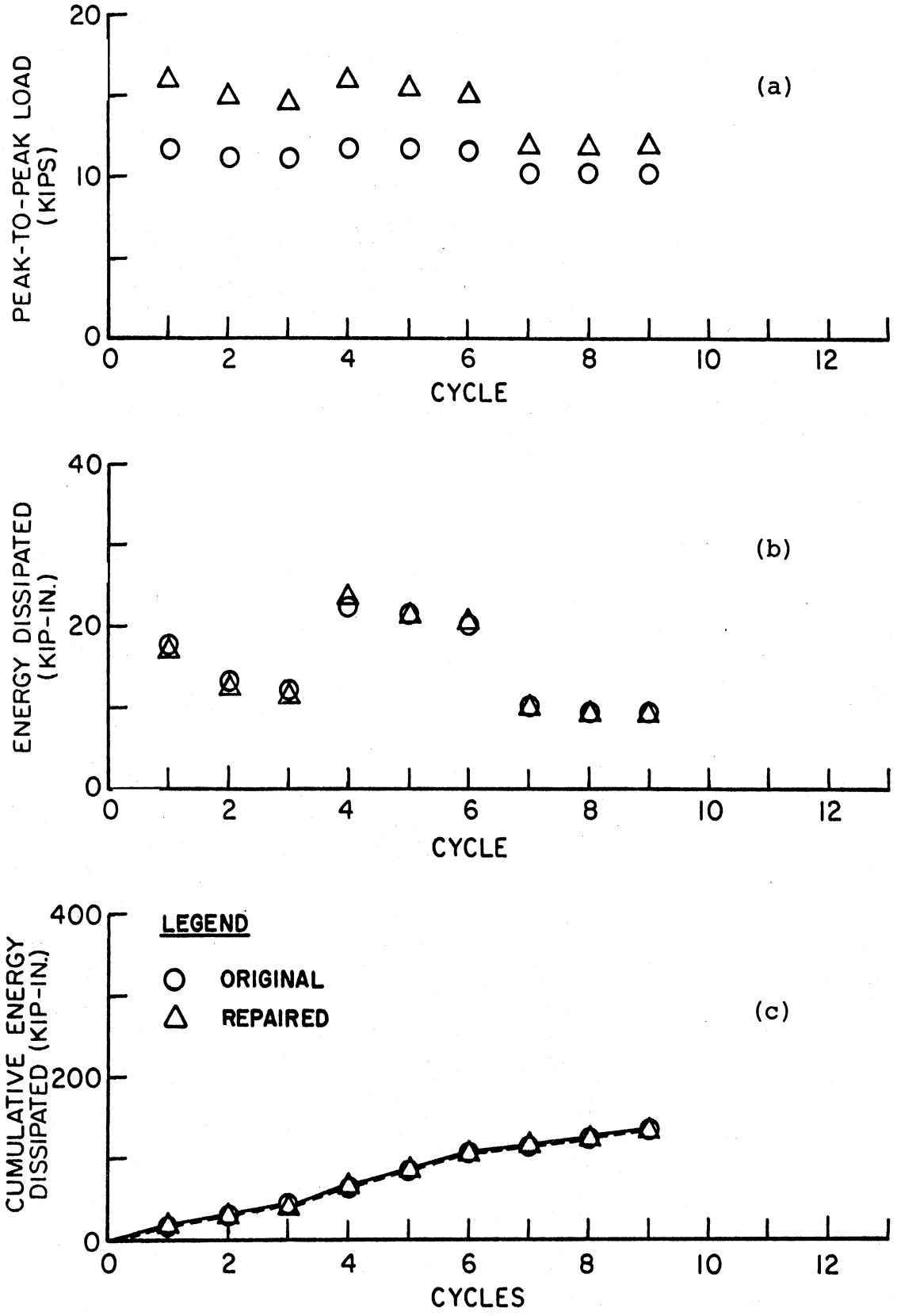

Fig. 3.6(a) Cyclic Behavior of Specimen 1 (a) Peak-to-Peak Load, (b) Energy Dissipated, and (c) Cumulative Energy Dissipated

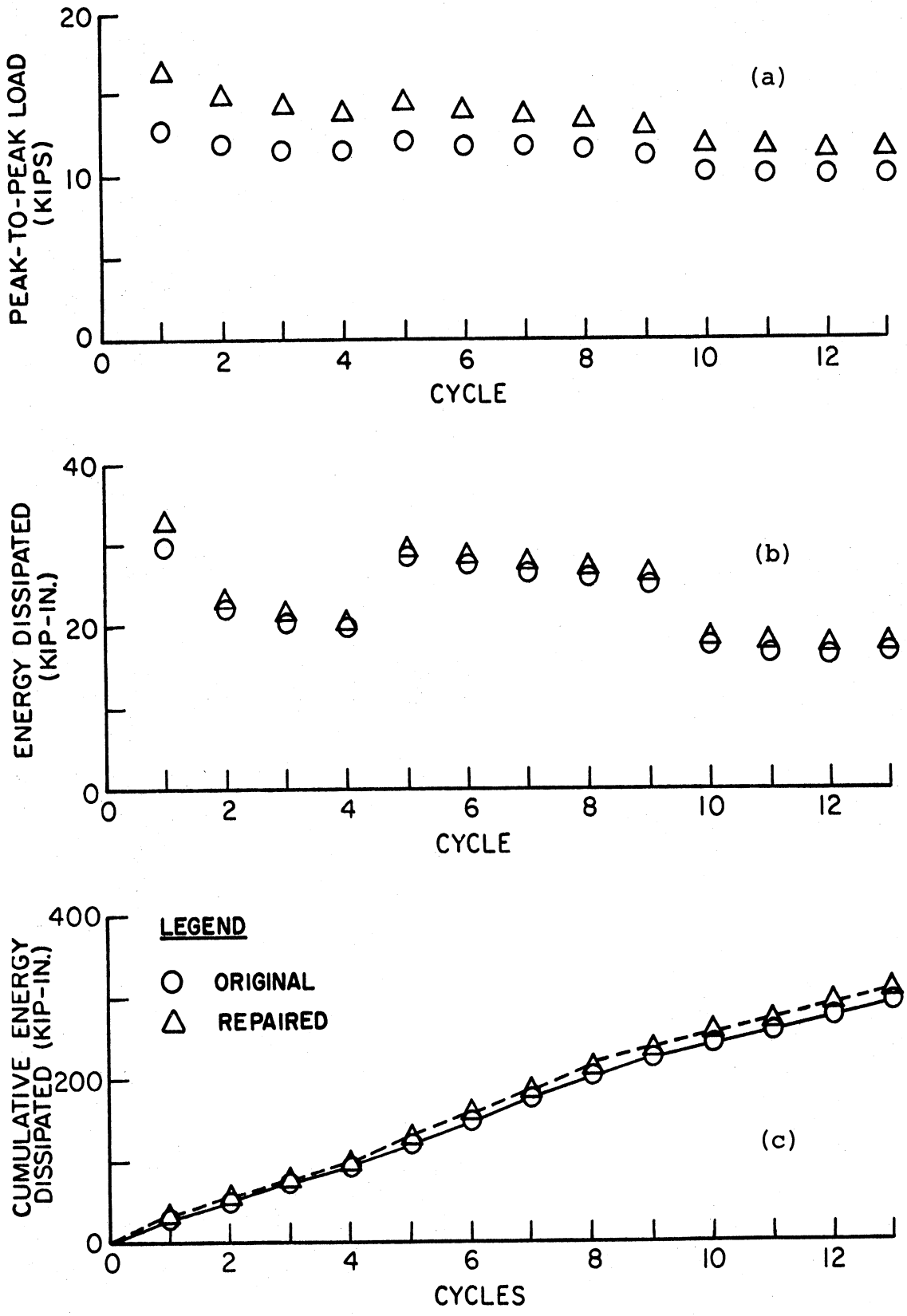

Fig. 3.6(b) Cyclic Behavior of Specimen 2 (a) Peak-to-Peak Load, (b) Energy Dissipated, and (c) Cumulative Energy Dissipated

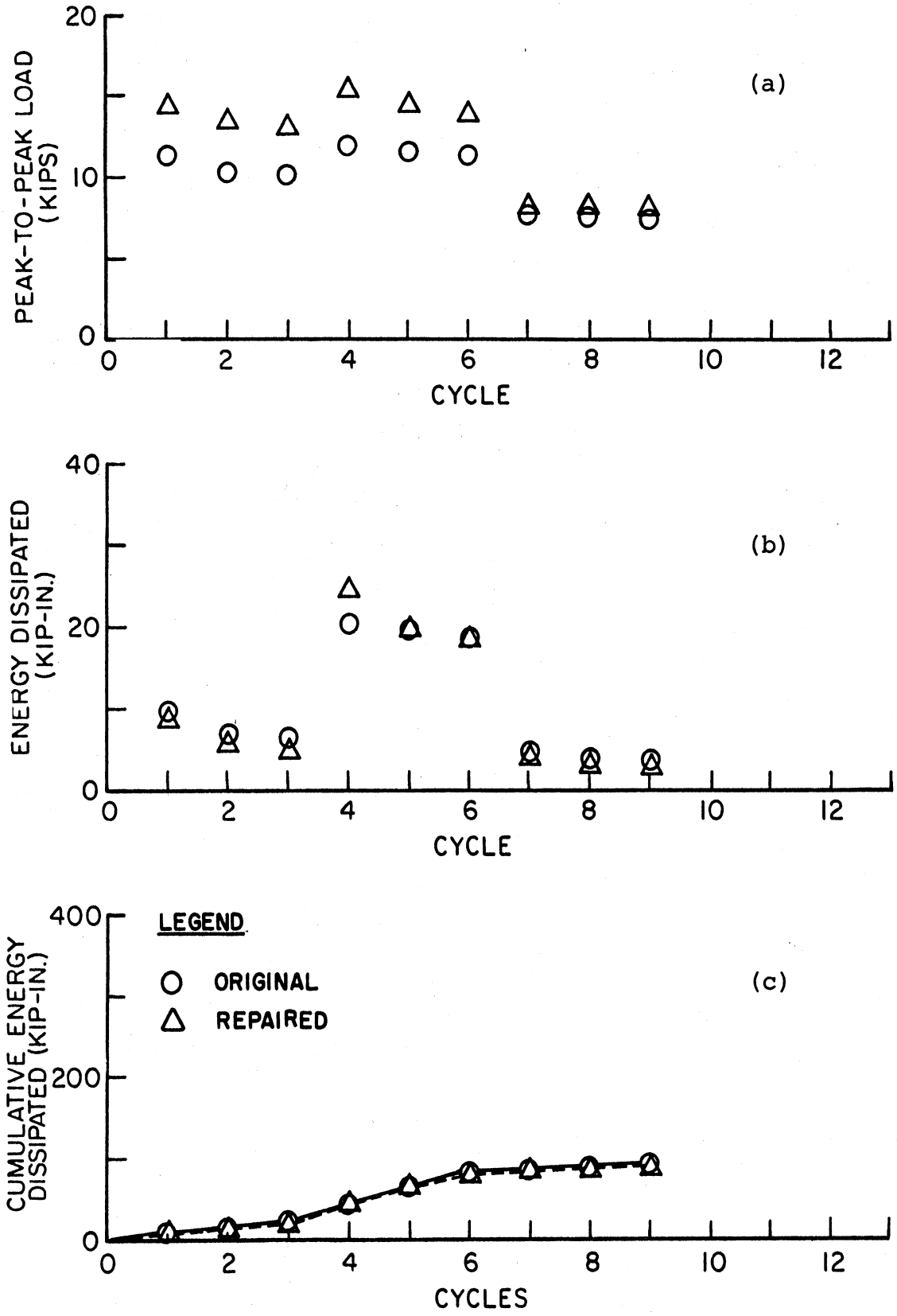

Fig. 3.6(c) Cyclic Behavior of Specimen 3 (a) Peak-to-Peak Load, (b) Energy Dissipated, and (c) Cumulative Energy Dissipated

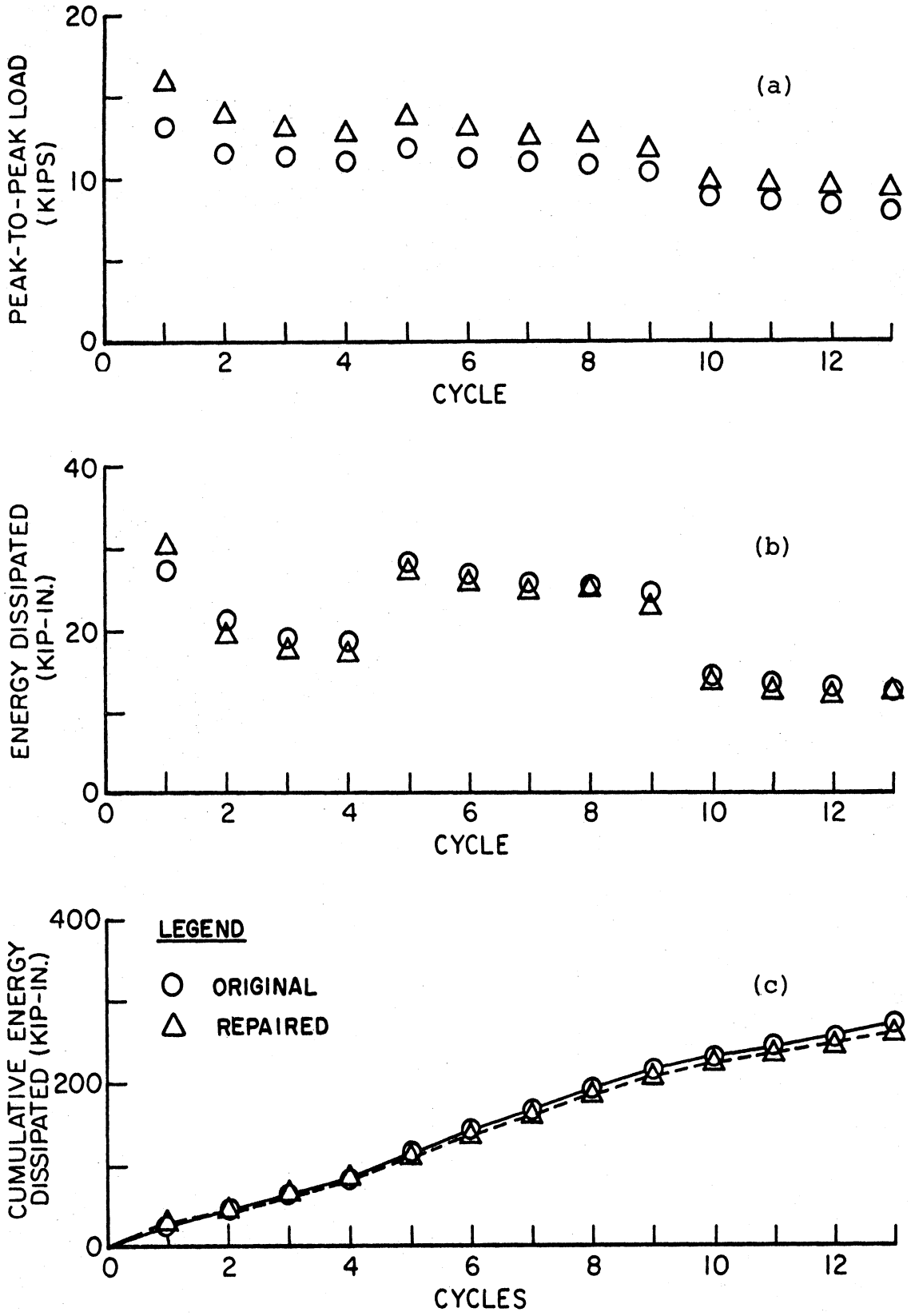

Fig. 3.6(d) Cyclic Behavior of Specimen 4 (a) Peak-to-Peak Load, (b) Energy Dissipated, and (c) Cumulative Energy Dissipated

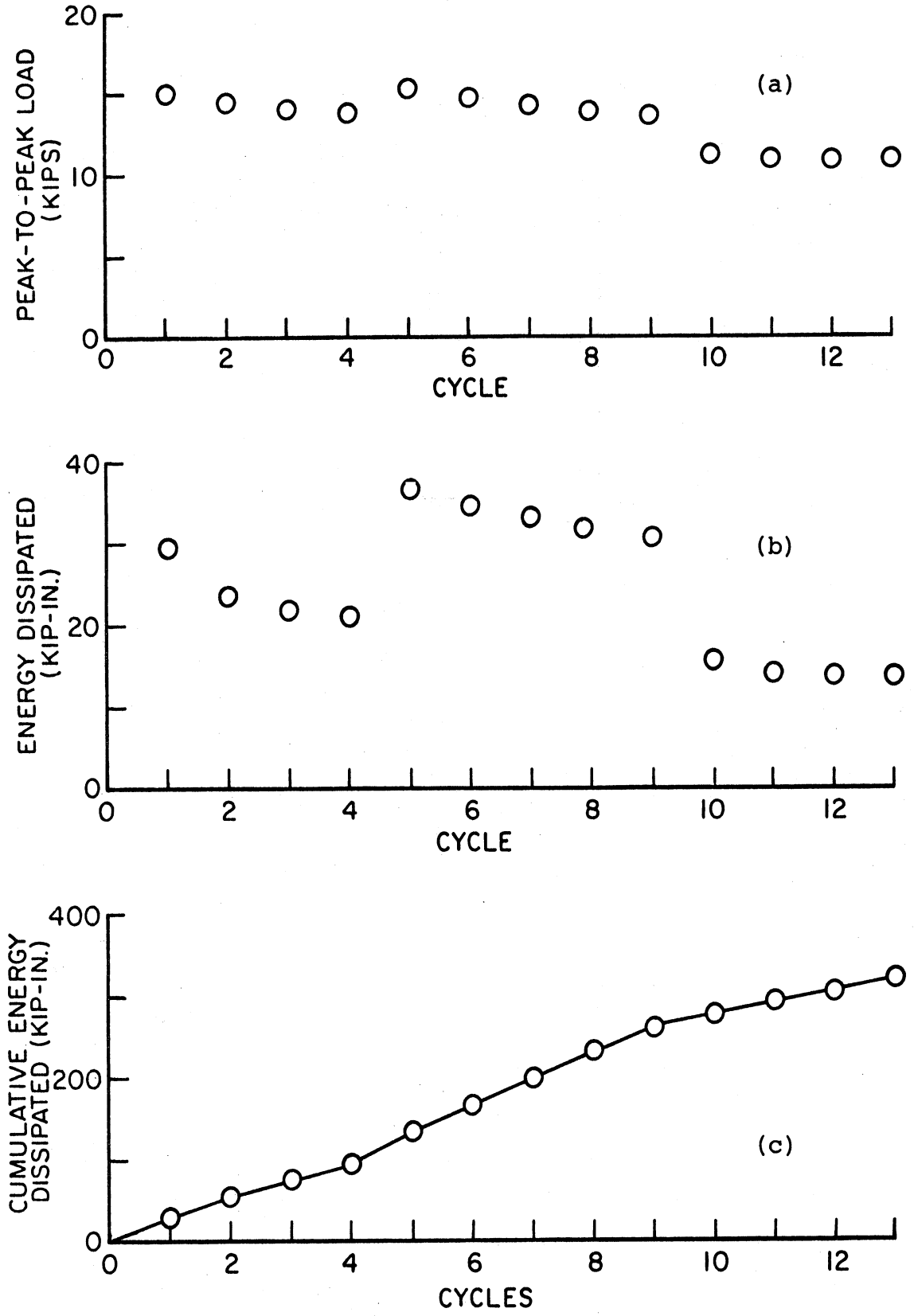

Fig. 3.6(e) Cyclic Behavior of Specimen 5 (a) Peak-to-Peak Load, (b) Energy Dissipated, and (c) Cumulative Energy Dissipated

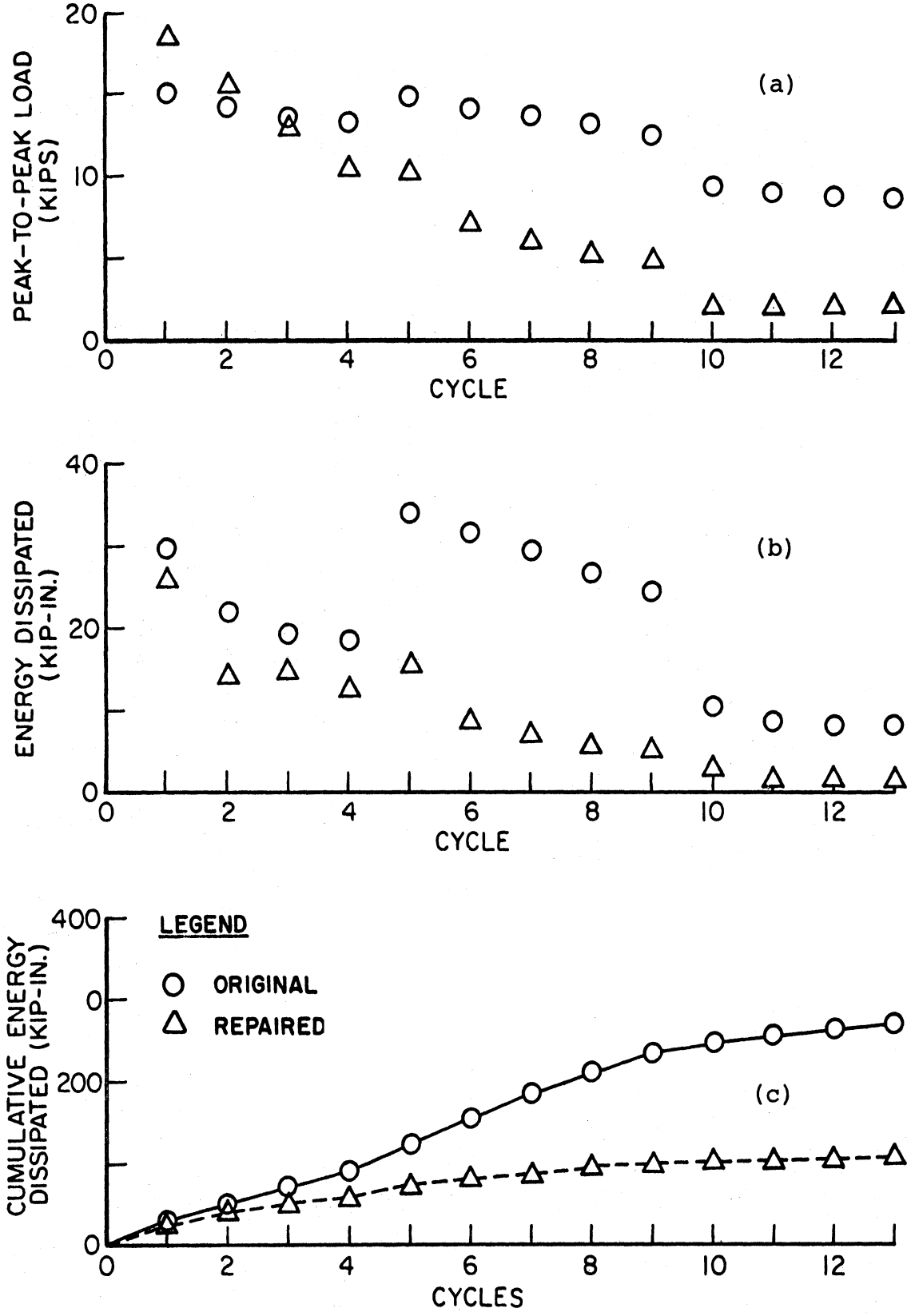

Fig. 3.6(f) Cyclic Behavior of Specimen 6 (a) Peak-to-Peak Load, (b) Energy Dissipated, and (c) Cumulative Energy Dissipated

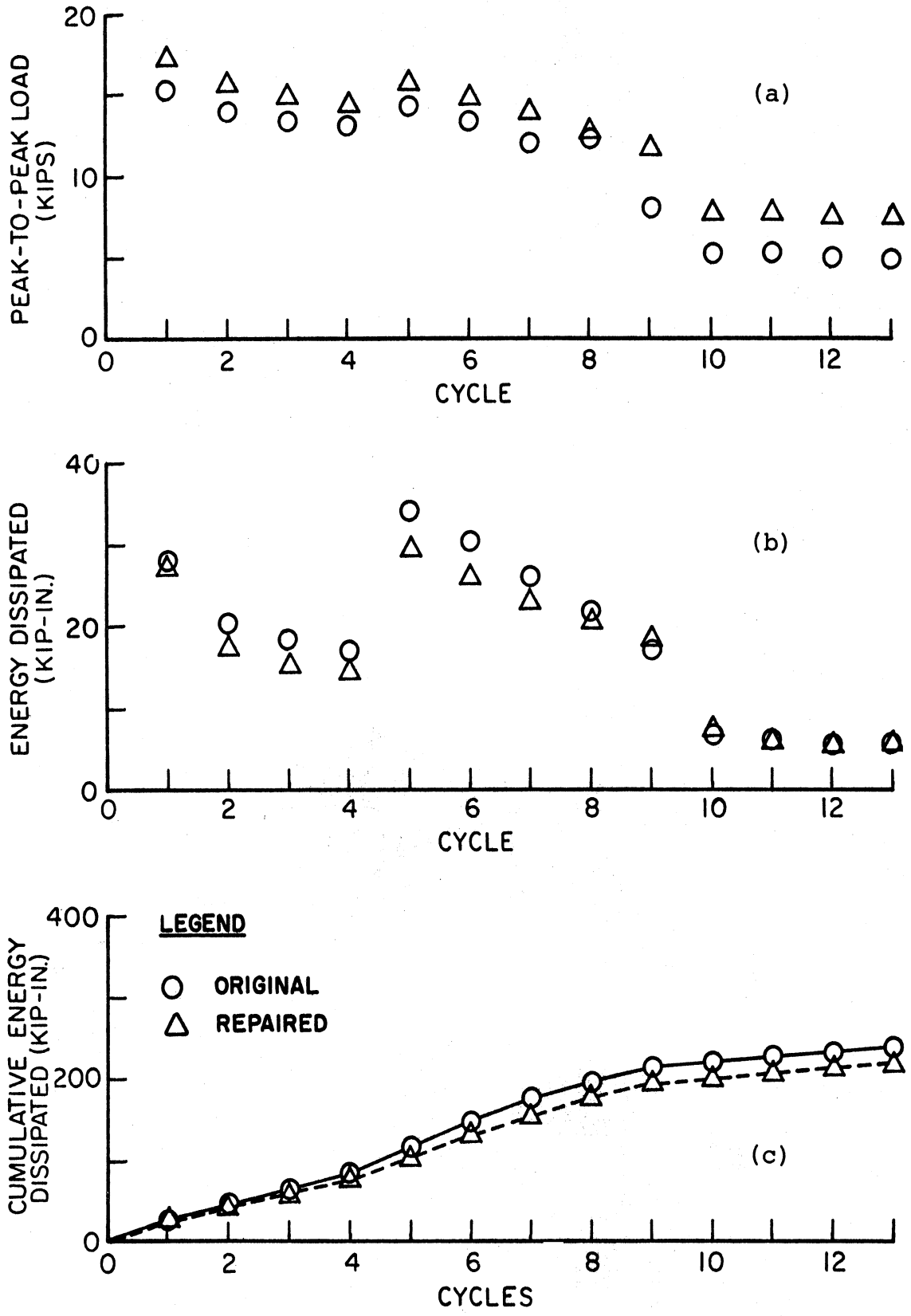

Fig. 3.6(g) Cyclic Behavior of Specimen 7 (a) Peak-to-Peak Load, (b) Energy Dissipated, and (c) Cumulative Energy Dissipated

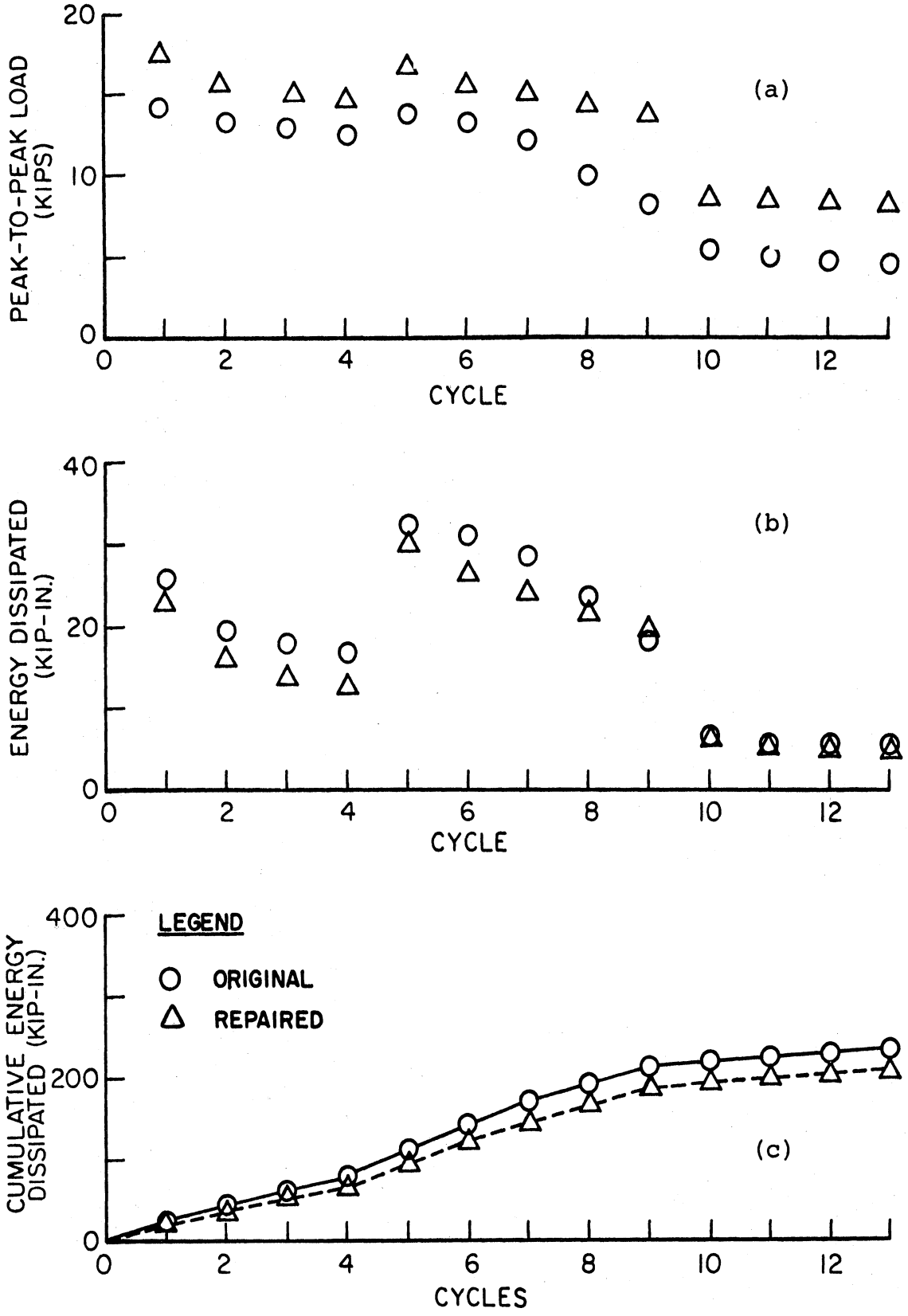

Fig. 3.6(h) Cyclic Behavior of Specimen 8 (a) Peak-to-Peak Load, (b) Energy Dissipated, and (c) Cumulative Energy Dissipated

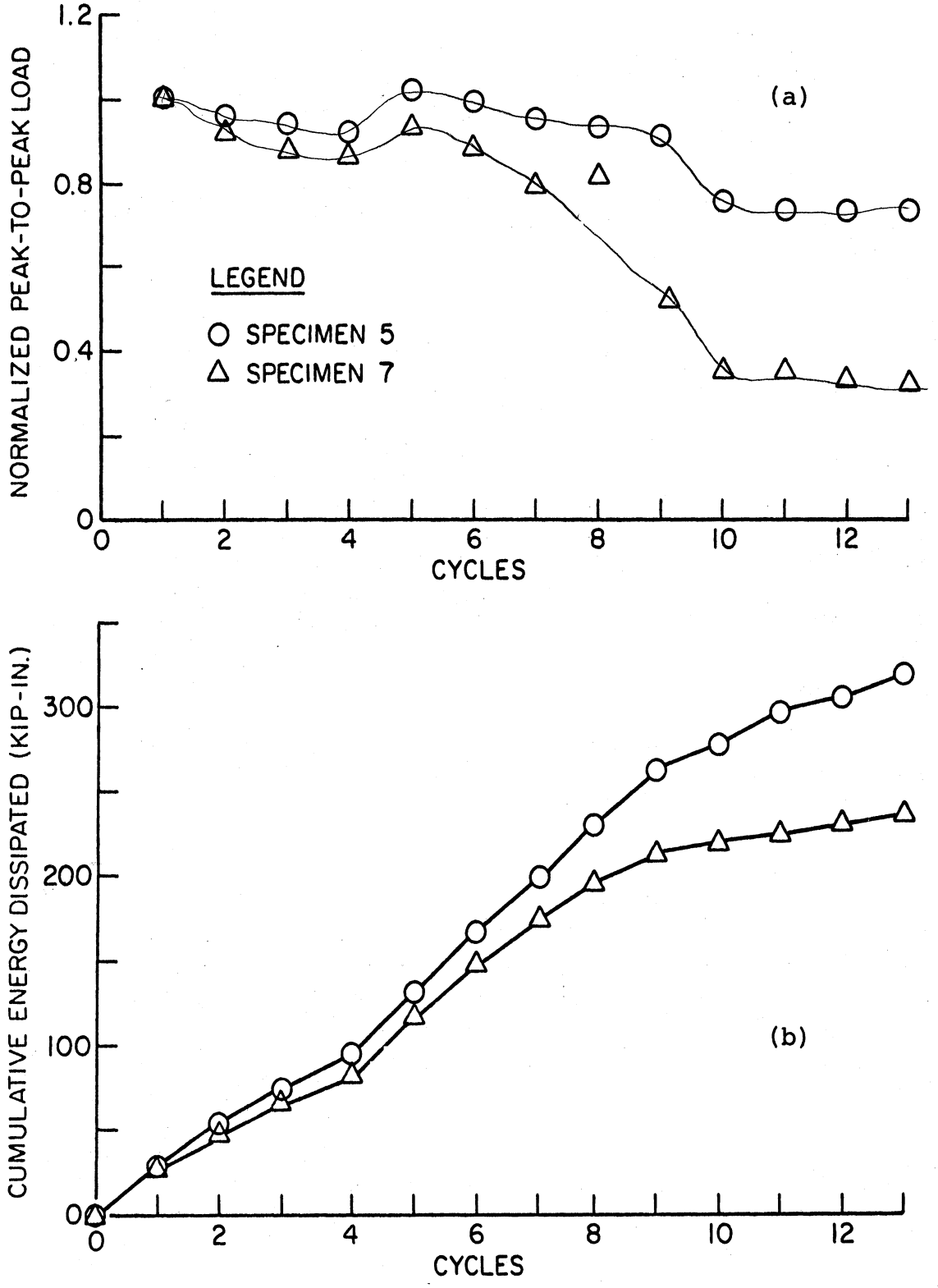

Fig. 3.7 Comparison of (a) Normalized Peak-to-Peak Load and (b) Cumulative Energy Dissipated for Specimen 5 of Type II Design and Specimen 7 of Type I Design

(Specimens 1 and 2 contained only gages 1 through 11 and Specimen 3 only gages 1 through 10.) For all the gages, positive strain indicated the elongation of the reinforcement.

Stress-strain curves for the reinforcement used in the beam-column subassemblages are given in Appendix B, Figs. B.1(a) through B.1(e). These curves were used to obtain the modulus of elasticity, yield stress, and strain at the commencement of strain hardening in the reinforcement.

3.3.1 Transverse Reinforcement in Beam

The strains in the transverse reinforcement at the location of Gage 1 for Specimen 2 are plotted with beam shear and beam-tip deflection for the first cycle of severe earthquake loading in Figs. 3.8(a) and 3.8(b) respectively. The increase in beam shear and deflection resulted in a relatively small change in reinforcement strain from points 0 to B (the commencement of yielding of the beam top reinforcement occurred at point B). Further increase in beam deflection from point B resulted in a larger change in reinforcement strain, indicating the formation of an inclined crack. Between points D and E, minor spalling occurred in the beam compression zone. There was a small decrease in shear and a slight reduction in reinforcement strain. Unloading of the beam resulted in the reduction of reinforcement strain from points E to F.

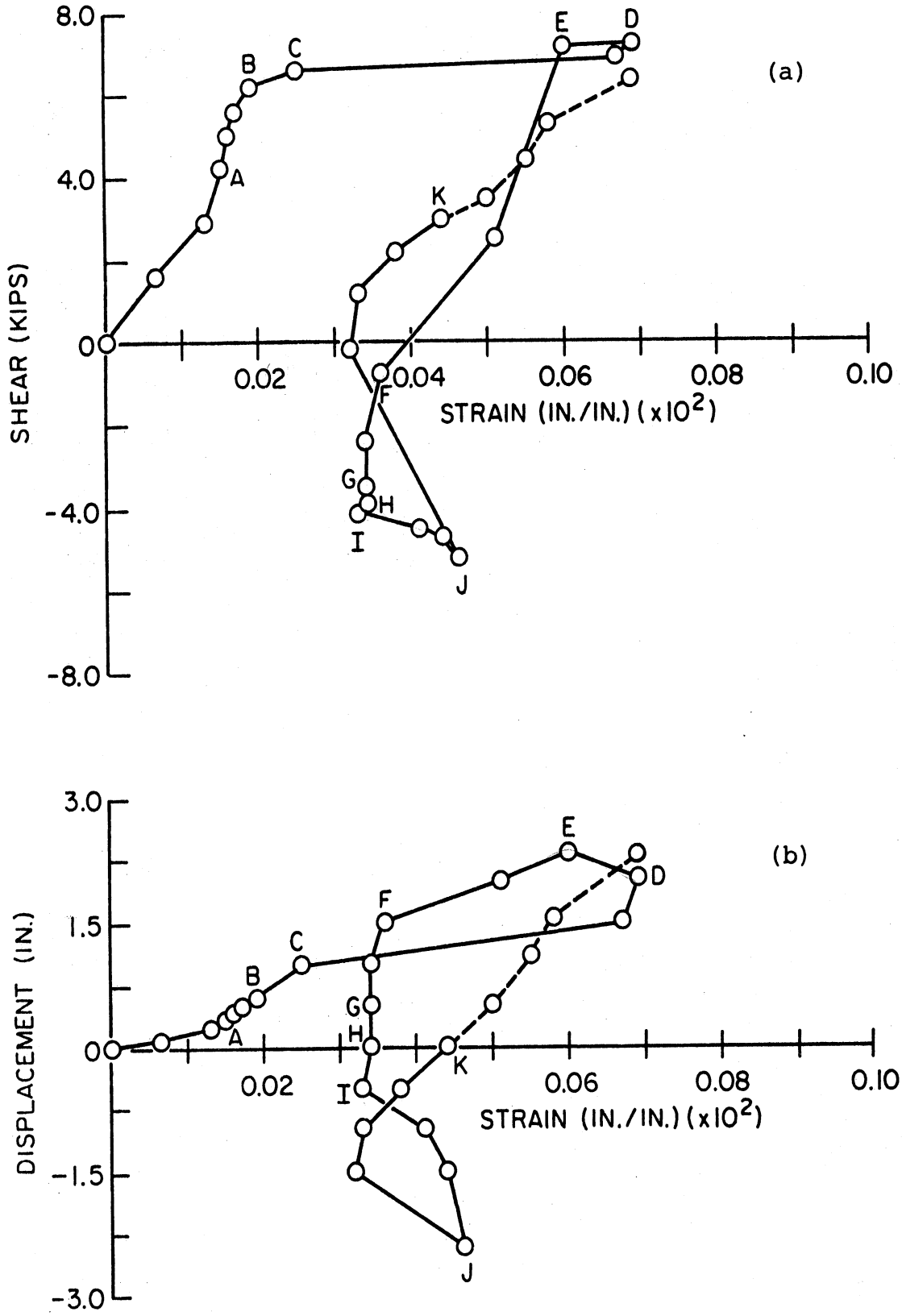

Fig. 3.8 Plot of Stirrup-Tie Strain at Gage 1 with (a) Beam Shear and (b) Beam-Tip Deflection during First Cycle of Loading, Specimen 2

Applying a negative shear resulted in a small change in reinforcement strain from points F to I which implied the stirrup-tie was resisting little additional shear. The negative force caused the flexural cracks from the first quarter cycle of loading to close and most of the shear was resisted by the cracked concrete through friction and aggregate interlock. Further increase in negative shear from points I to J resulted in a larger increase in reinforcement strain indicating the formation of an inclined crack. The unloading of the beam from point J resulted in a reduction in reinforcement strain.

The strains measured by Gage 1 for the second and subsequent cycles of loading are plotted with the first cycle for Specimen 2 in Figs. 3.9(a) and 3.9(b). These figures indicate the reinforcement strains remained below the yield strain and showed relatively stable behavior at the same displacement level. As seen in Fig. 3.9(a), a strain and therefore a stress still existed in the stirrup-tie at zero beam shear. This residual stress is due to the enlargement of the beam core caused by cracking in the concrete.

The measured strains in the transverse reinforcement for specimens with Type II Design were less and had more stable behavior than those for specimens with Type I Design as seen by comparing Fig. 3.9(b) and Fig. 3.10 for

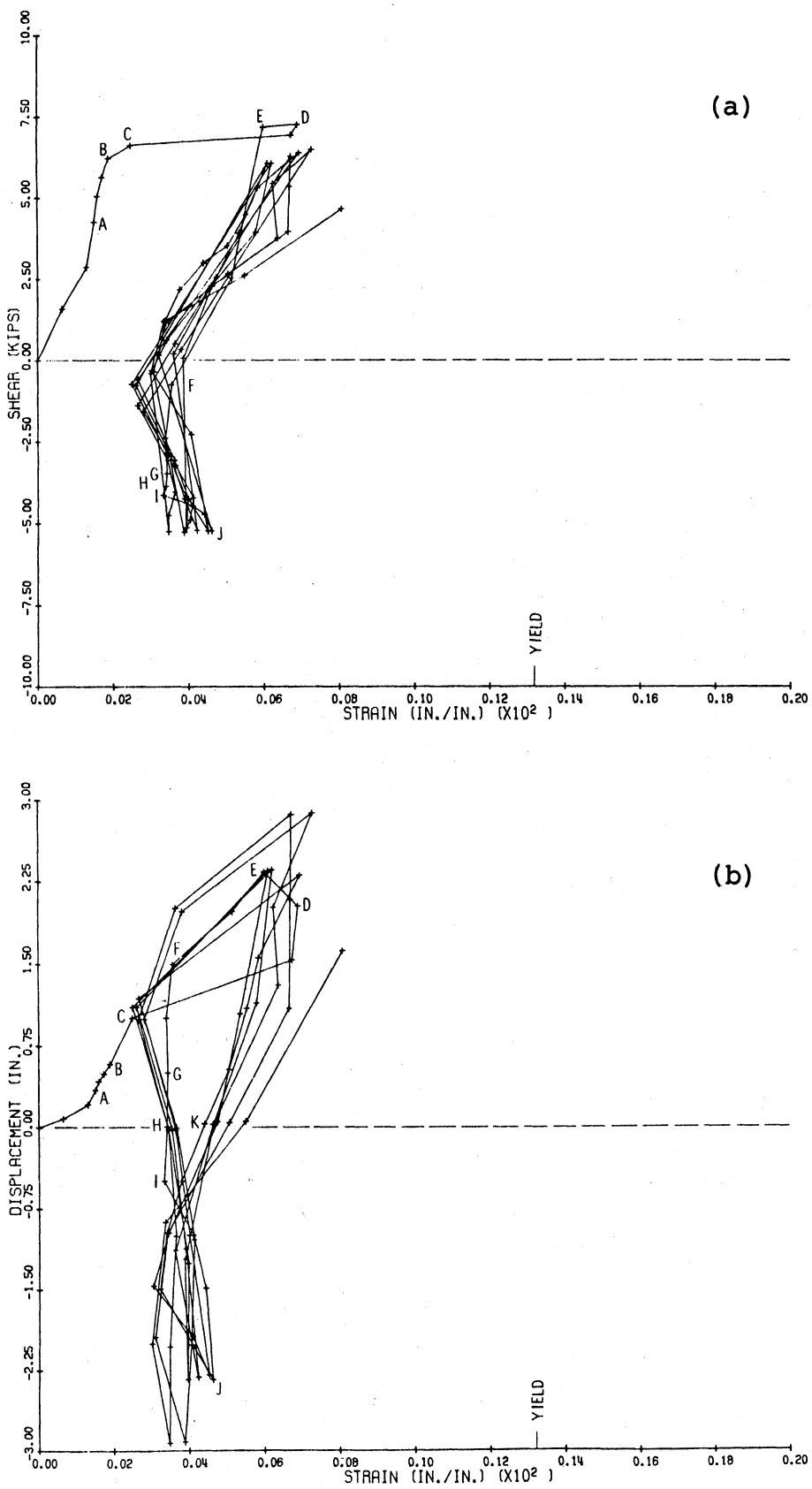

Fig. 3.9 Plot of Stirrup-Tie Strain at Gage 1 with (a) Beam Shear and (b) Beam-Tip Deflection, Specimen 2

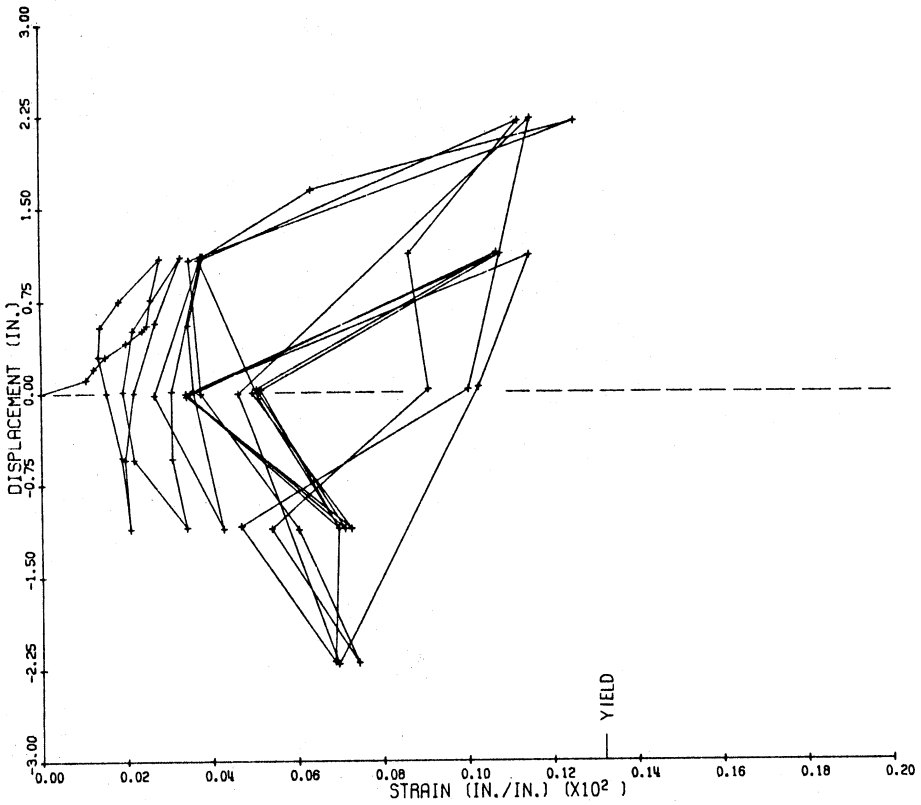

Fig. 3.10 Plot of Stirrup-Tie Strain at Gage 1 with Beam-Tip Deflection, Specimen 3 of Type I Design

Specimens 2 and 3 respectively. The strains (measured by Gage 1) indicate the stirrup-tie was close to yielding when Specimen 3 was subjected to a moderate earthquake loading. Specimen 2 was subjected to the severe earthquake loading and the transverse reinforcement never approached yield.

3.3.2 Longitudinal Beam Reinforcement

Strains in the top reinforcement, as measured at the beam-to-column interface by Gages 3 and 4 for Specimen 2, are plotted with beam-tip force and deflection for the first cycle of severe earthquake loading in Figs. 3.11(a) and 3.11(b) respectively. It can be seen that the strains

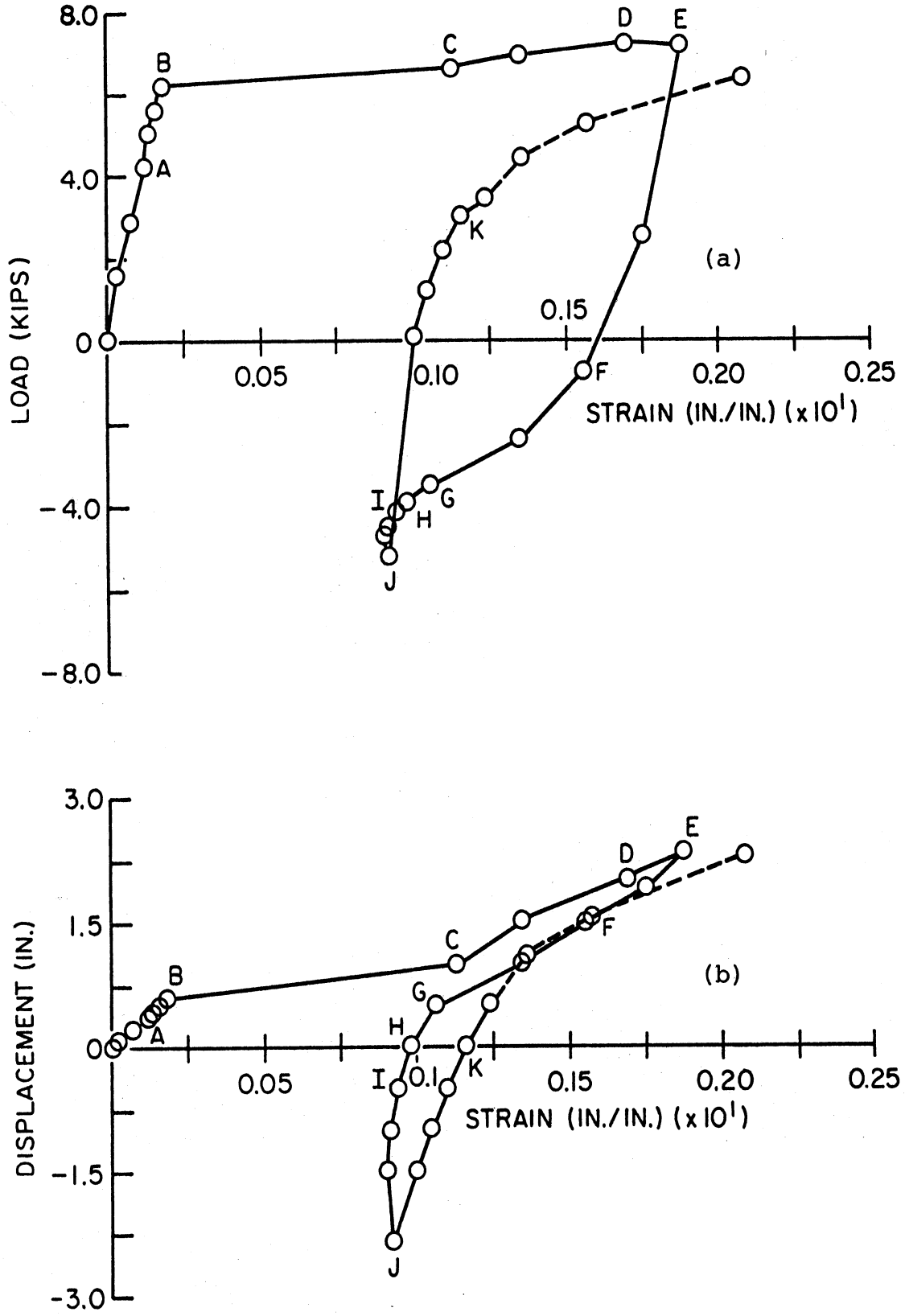

Fig. 3.11 Plot of Top Bar Strain at Gages 3 and 4 with (a) Beam-Tip Force and (b) Beam-Tip Deflection during First Cycle of Loading, Specimen 2

indicate that the reinforcement has yielded, points B to C, and has passed into the strain hardening region, points C to E. Unloading the beam resulted in the strains decreasing almost linearly from point E toward F with the same slope as from point 0 to B. Applying a negative beam force resulted in a further reduction in strain from points F to H. This implied that the top reinforcement resisted some of the compressive force during negative loading. Further increase in negative force and beam deflection resulted in a small change in strains from points H to J. This is due to concrete resisting the additional compressive stress after the cracks have closed. Unloading the negative force and applying a positive beam force caused the strains to increase from points J to K.

The strains measured at the beam-column interface for the second and subsequent cycles, along with the first cycle of loading, are plotted with beam-tip force and deflection for Specimen 2 in Figs. 3.12(a) and 3.12(b) respectively. The strains from the second and subsequent cycles of loading showed relatively stable behavior at the same displacement level.

During the first quarter cycle of loading, the beam-tip deflection ductility was compared to the strain ductility of the reinforcement at the beam-to-column interface. This comparison is made for Specimen 2 and is shown in Fig. 3.13. The deflection ductility was obtained by

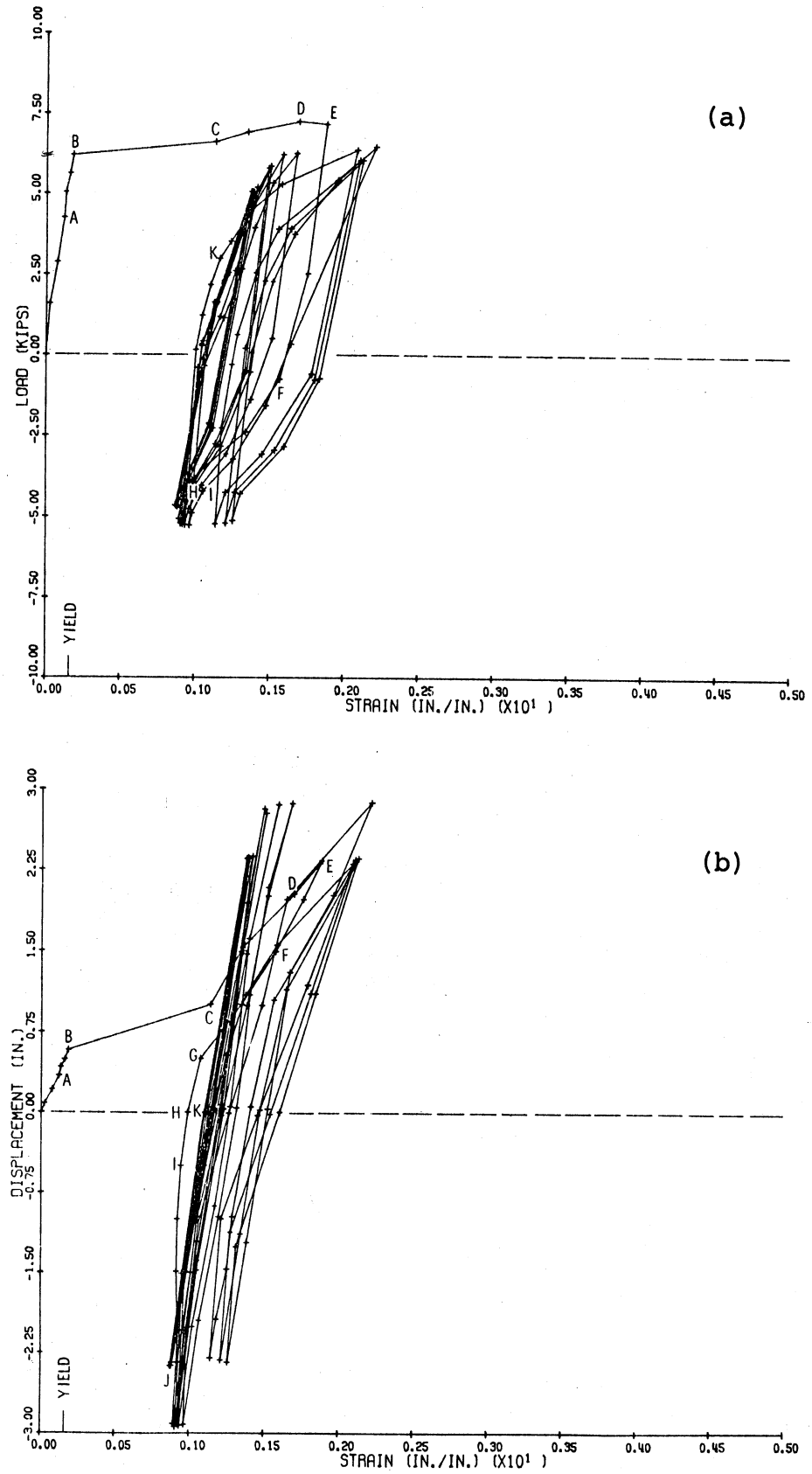

Fig. 3.12 Plot of Top Bar Strain at Gages 3 and 4 with (a) Beam-Tip Force and (b) Beam-Tip Deflection, Specimen 2

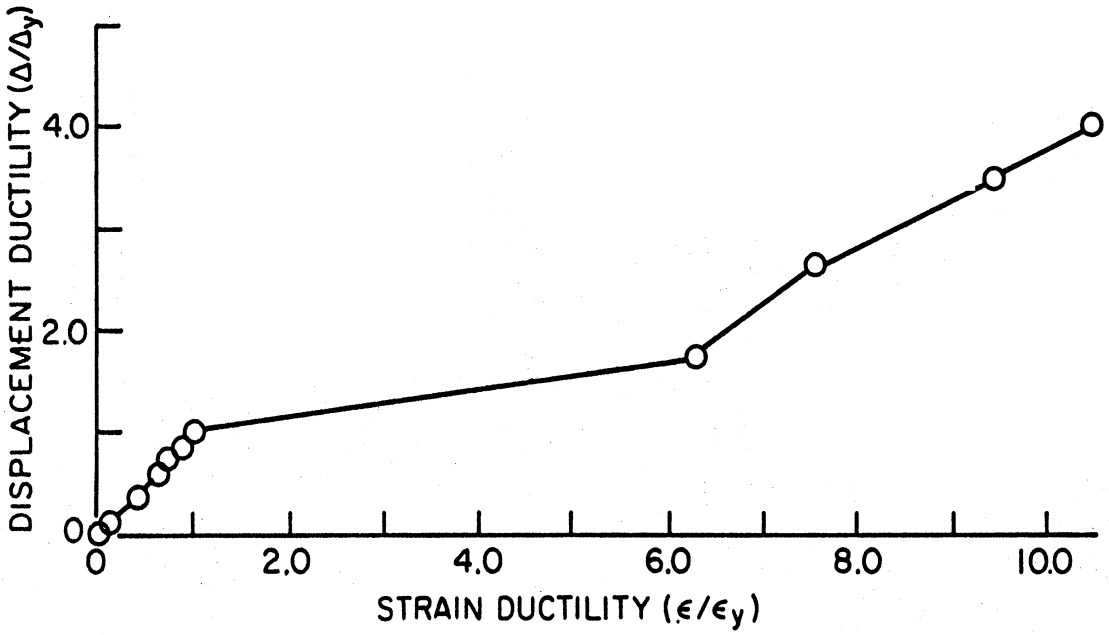

Fig. 3.13 Comparison between Reinforcement Strain Ductility and Beam-Tip Deflection Ductility, Specimen 2

dividing the beam deflection by the deflection at first yield of the top reinforcement. The strain ductility was obtained by dividing the reinforcement strain by the yield strain for the steel. The yield displacement and yield strain were taken to be that shown at point B in Fig. 3.11(b). Figure 3.13 indicates beam displacement ductilities of 2 and 4 corresponds to reinforcement strain ductilities 6.7 and 10.5 respectively.

The strains in the top reinforcement measured just before the hook by Gage 10 for Specimen 2 are plotted with the beam-tip deflection in Fig. 3.14. The strains showed a relatively stable behavior at the same displacement level and indicated that the steel just before the hook

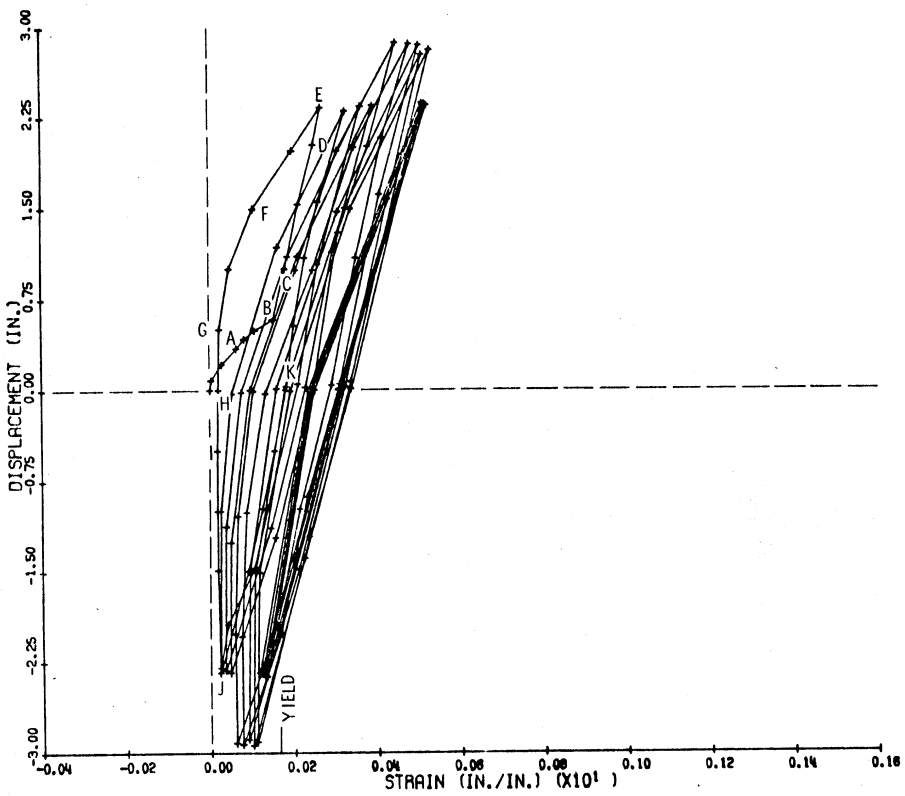

Fig. 3.14 Plot of Top Bar Strain before Hook at Gage 10 with Beam-Tip Deflection, Specimen 2

yielded during the first quarter cycle of severe earthquake loading.

The strains in the top reinforcement measured just past the hook by Gage 13 for Specimen 5 are shown with the beam-tip deflection in Fig. 3.15. The strains showed relative stable behavior at the same displacement level and indicated the steel remained elastic at that location during the first four cycles of severe earthquake loading. At the higher displacement level, the steel after the hook came very close to yielding.

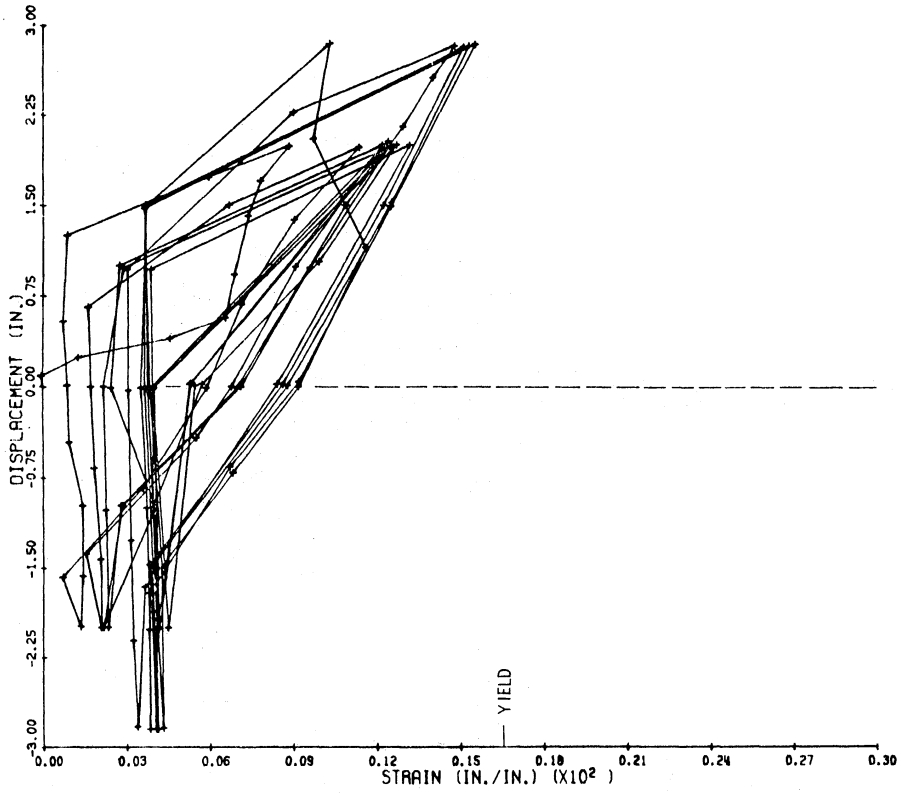

Fig. 3.15 Plot of Top Bar Strain after Hook at Gage 13 with Beam-Tip Deflection, Specimen 5

For the bottom reinforcement the strains measured at the beam-to-column interface by Gages 5 and 6 for Specimen 2 are plotted with the beam-tip force and deflection in Figs. 3.16(a) and 3.16(b) respectively. By observing the results shown in Figs. 3.16 and 3.12 during the first quarter cycle of loading, it is apparent that compressive strains existed in the bottom reinforcement before the top reinforcement yielded (point B). This indicated that the concrete and bottom reinforcement resisted the compressive stresses during bending. After the top reinforcement yielded, small tensile strains were measured in the bottom

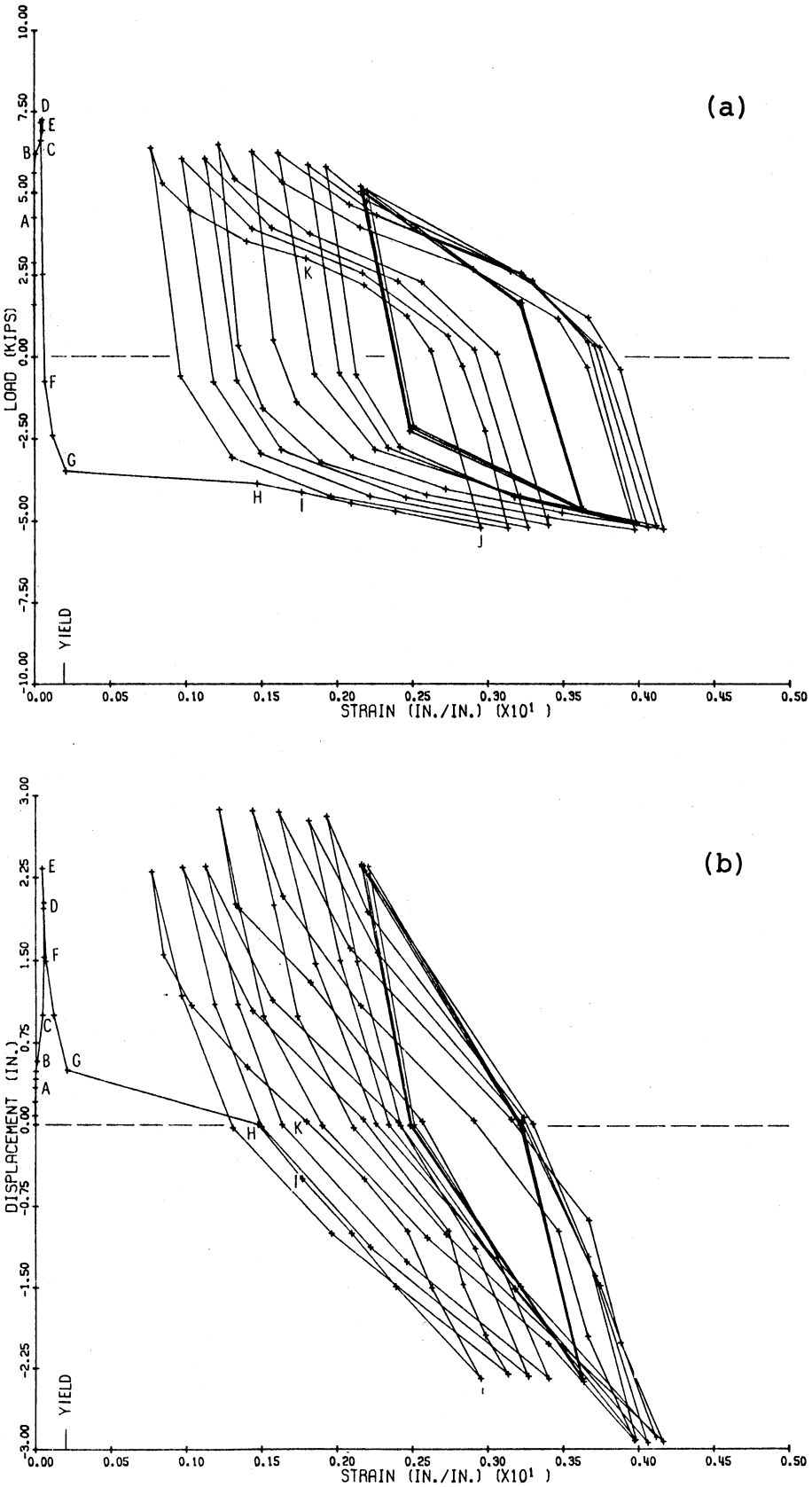

Fig. 3.16 Plot of Bottom Bar Strain at Gages 5 and 6 with (a) Beam-Tip Force and (b) Beam-Tip Deflection, Specimen 2

reinforcement. This is due to the shift in the neutral axis to a level below the bottom reinforcement. Unloading of the beam at the end of the first quarter cycle of loading (point E) and application of a negative force resulted in a increase in strain in the bottom reinforcement until the commencement of tensile yielding as indicated by point G in Fig. 3.16. Further increases in beam displacement caused the bottom reinforcement to pass through the yield plateau and into the strain hardening region, points H to J in Fig. 3.16(a). To complete the first cycle of loading, the strains were reduced as the negative beam force and deflection were reduced from points J to K as shown in Figs. 3.16. For the second and subsequent cycles of loading, the strains indicated that the bottom reinforcement elongated cumulatively after each cycle. This behavior may eventually lead to low cycle fatigue fracture of the reinforcement.

For the bottom reinforcement, the strains measured just before the hook by Gage 7 for Specimen 2, indicated that the steel yielded during the first cycle of loading as shown in Fig. 3.17. The strains measured just after the hook by Gage 12 for Specimen 5 indicated that the steel was elastic during the first cycle of loading as shown in Fig. 3.18. However, for subsequent cycles at the higher displacement level, the strains indicated that the steel yielded at this location.

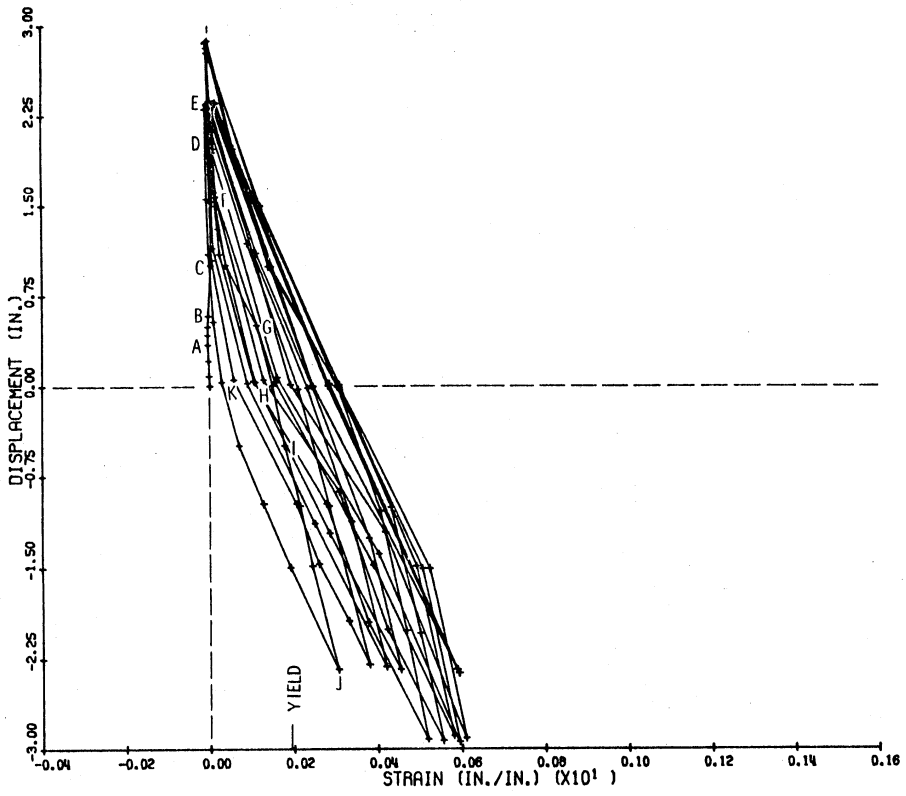

Fig. 3.17 Plot of Bottom Bar Strain before Hook at Gage 7 with Beam-Tip Deflection, Specimen 2

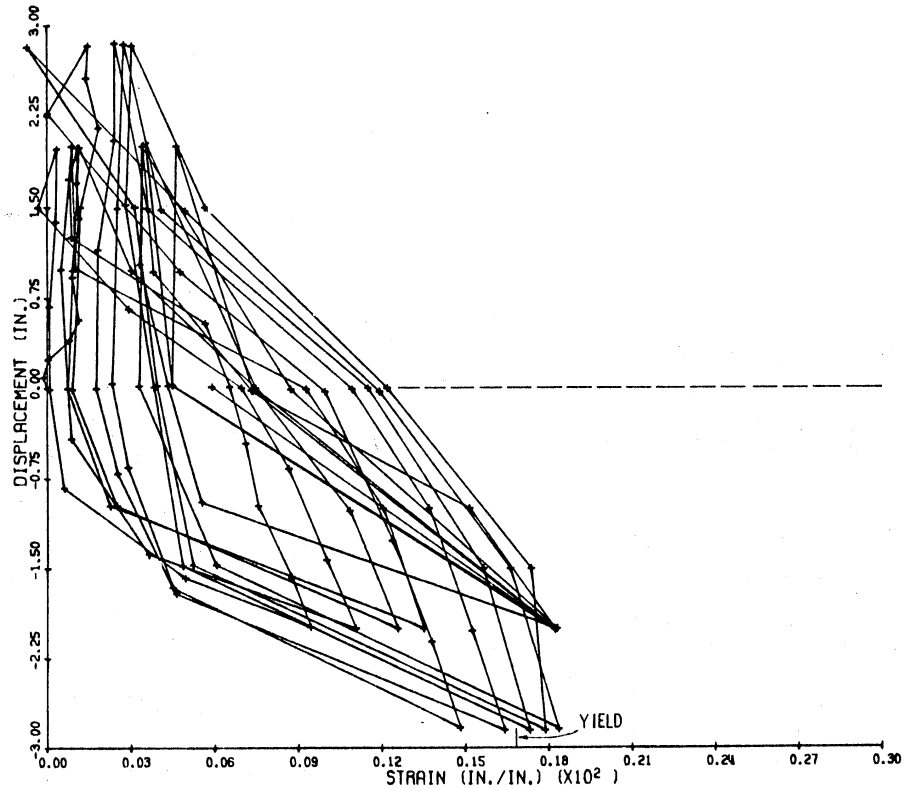

Fig. 3.18 Plot of Bottom Bar Strain after Hook at Gage 12 with Beam-Tip Deflection, Specimen 5

3.3.3 Transverse Reinforcement in Joint and Column

The strains measured by Gage 8 on a hoop in the joint of Specimen 2 are plotted with beam-tip deflection for the first cycle of severe earthquake loading in Fig. 3.19. For initial loading, only small strains were

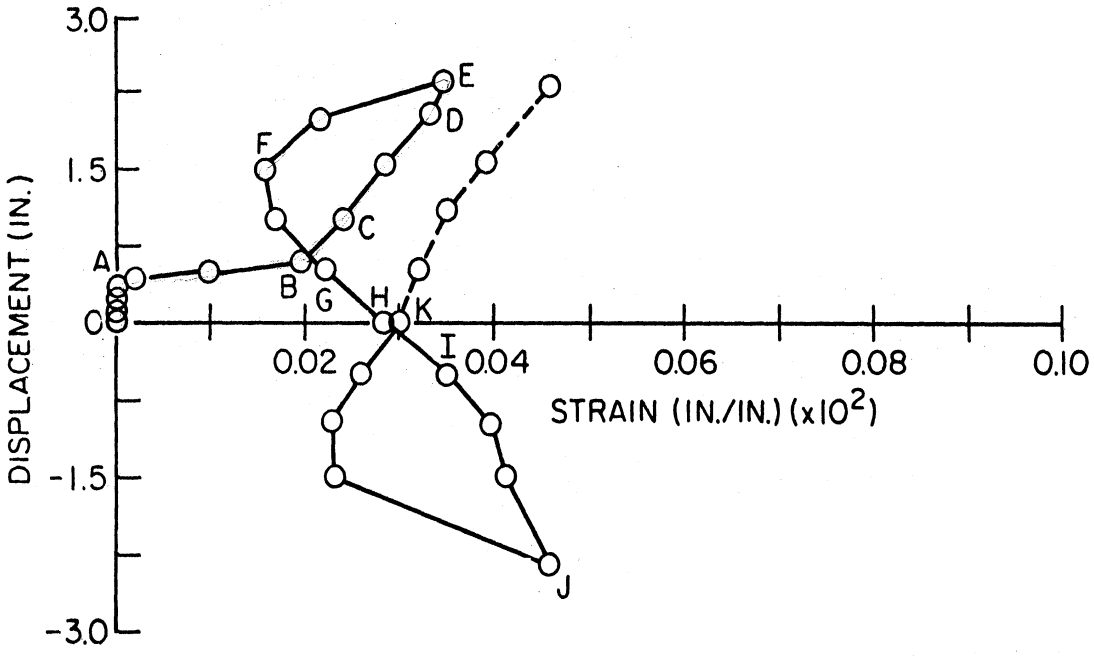

Fig. 3.19 Plot of Strain at Gage 8 for Hoop in Joint with Beam-Tip Deflection during First Cycle of Loading, Specimen 2

measured in the hoop. Increase in beam deflection from point A resulted in a sharp increase in hoop strains, which indicated a diagonal crack may have formed in the joint. Continued increase in beam deflection from point B toward E resulted in a increase in strain which indicated the hoop resisted more shear. After the first quarter cycle of loading, a decrease in beam deflection resulted

in a reduction in strains (points E to F) until the beam load reversed when the strains increased (points F to J). After peak negative deflection, a decrease in beam deflection resulted in a reduction in strains until the load reversed again to complete the first cycle of loading. Strains measured during the second and subsequent cycles of loading, along with the first cycle, are shown in Fig. 3.20. The results indicate that the hoop remained

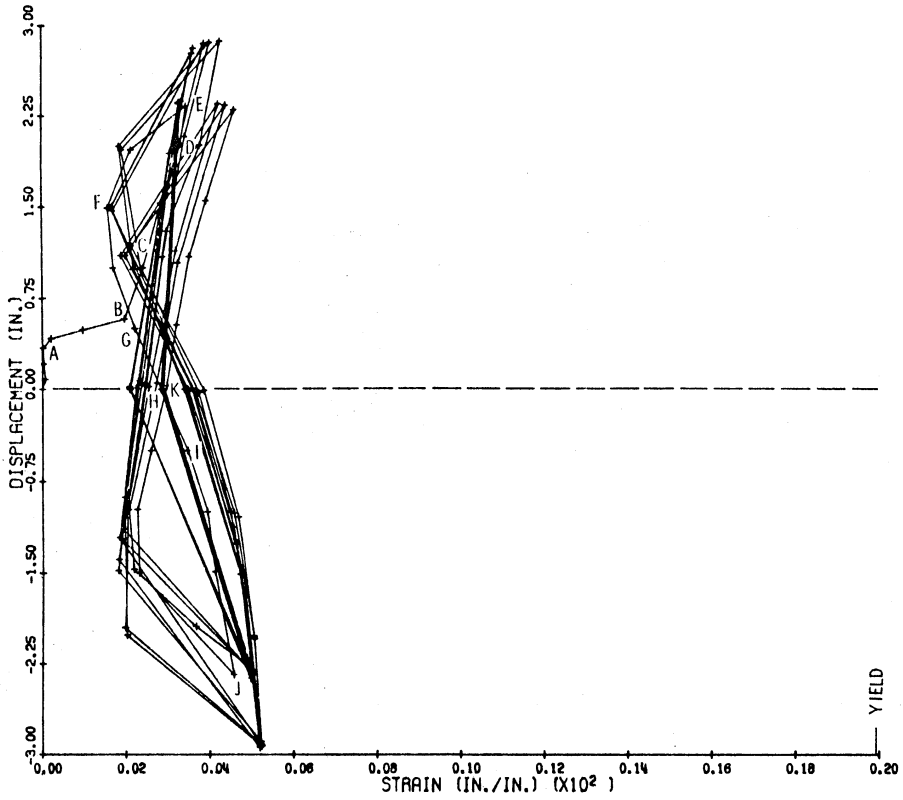

Fig. 3.20 Plot of Strain at Gage 8 for Hoop in Joint with Beam-Tip Deflection, Specimen 2

elastic and showed relative stable behavior for the same displacement level. At the points of zero beam force,

strains and therefore stresses still existed in the hoop. This is due to the enlargement of the column core caused by cracking in the concrete.

The strains measured on the hoops directly above and below the beam top longitudinal reinforcement are plotted with beam-tip deflection during the first quarter cycle of severe earthquake loading for Specimens 2, 5, and 6 in Fig. 3.21(a) through 3.21(c) respectively. Specimens 5 and 6 had zero column axial load. The strains were measured by Gages 9 and 11 for Specimens 2 and 5 with Type II Design and Gages 8 and 10 for Specimen 6 with Type I Design. Except for Specimen 6, the hoop directly above the top reinforcement was strained the same or higher than the hoop directly below the top reinforcement. This is attributed to the localized behavior for the hoops near the top reinforcement. For Specimen 6, the hoop in the joint directly below the top reinforcement was strained to a higher level than the hoop in the column directly above the top reinforcement. The localized effect was not as significant for Specimen 6 because the top hoop was spaced further into the column [see Fig. 2.1(a)].

The strains measured by Gage 10 on a hoop in the column for Specimen 6 are plotted with beam-tip deflection in Fig. 3.22. The overall shape of the curves resembles those presented earlier for the transverse reinforcement in the beam and joint. The strains indicated the hoop

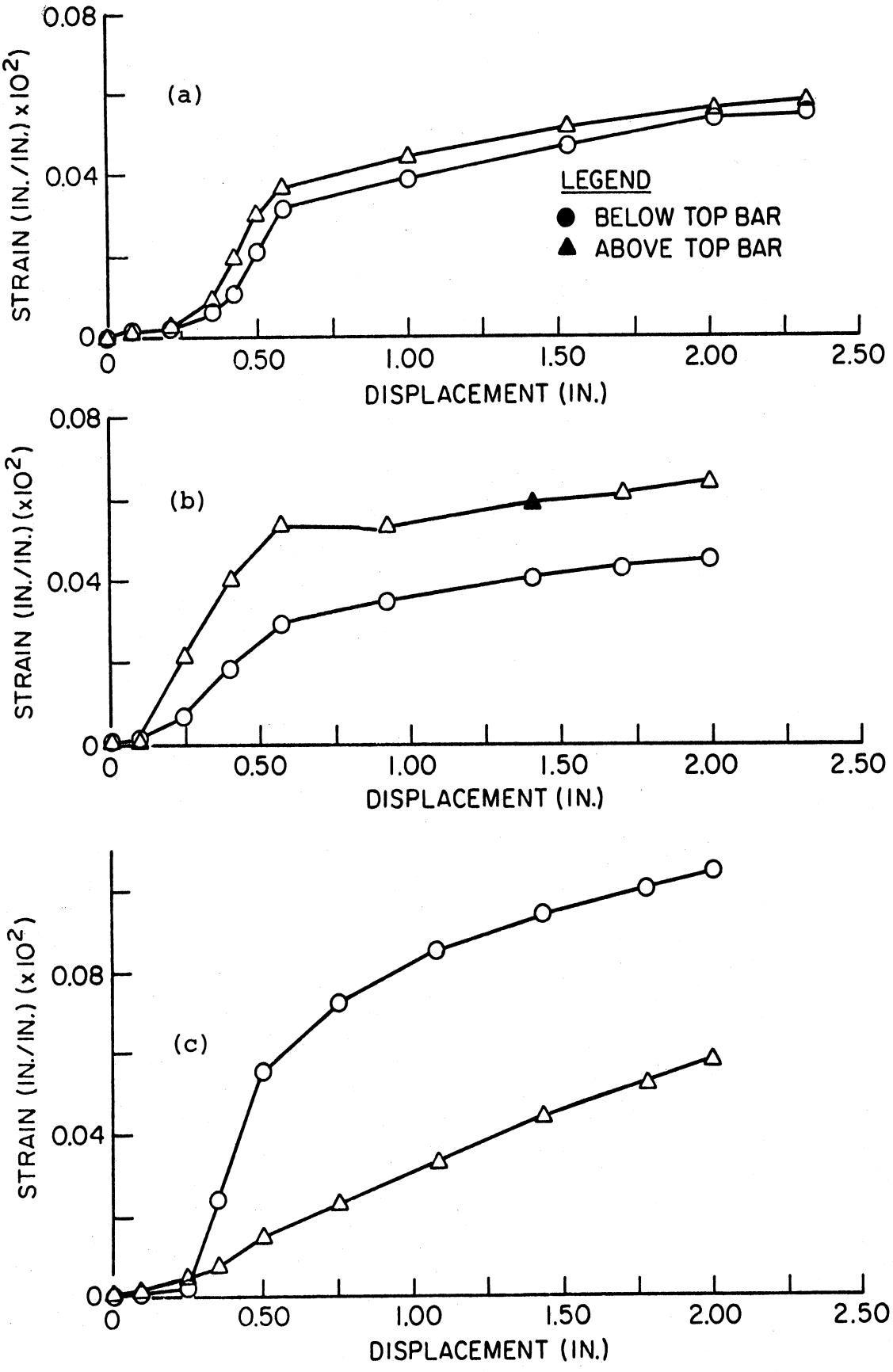

Fig. 3.21 Comparison of Strain for Hoops above and below Top Bars for (a) Specimen 2 (b) Specimen 5, and (c) Specimen 6

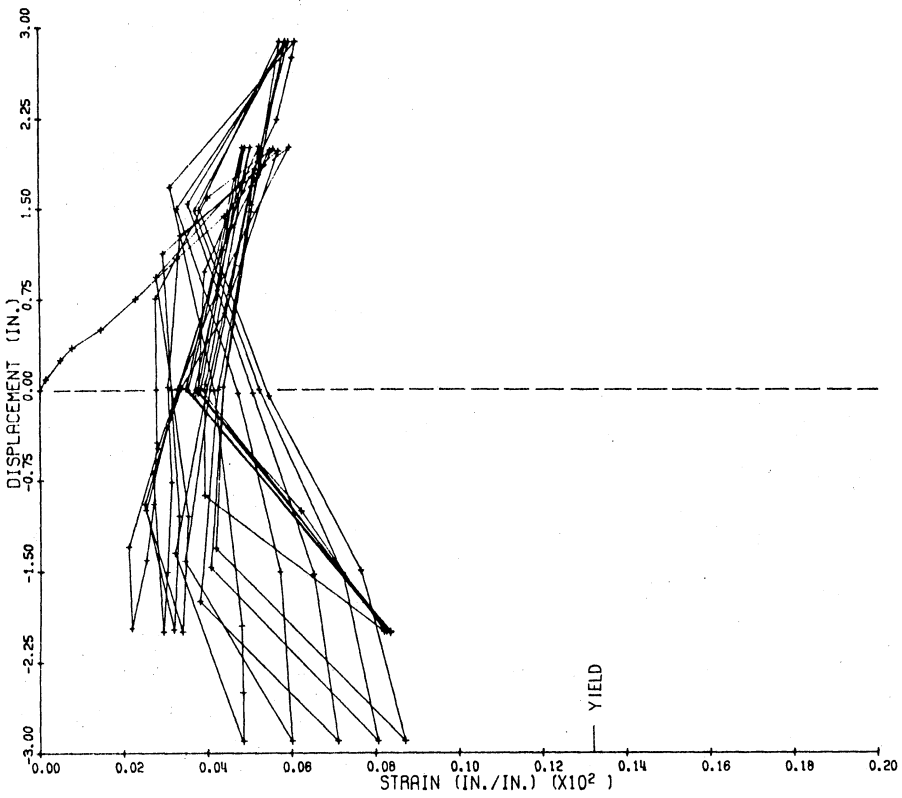

Fig. 3.22 Plot of Strain at Gage 10 for Hoop in Column with Beam-Tip Deflection, Specimen 6

remained elastic and the behavior was stable except at peak negative beam deflections where the strains increased after every cycle of loading. The increase in strains implied the hoop resisted a larger percentage of the shear after each cycle of loading. This increase in shear resistance provided by the hoop was attributed to the decrease in stiffness in the concrete caused primarily by internal cracking.

3.4 Measured Distortion in Joint

The distortion in the joint is plotted with beam-tip deflection for Specimens 2, 5 and 6 with severe earthquake loading in Figs. 3.23(a) through 3.23(c) respectively.

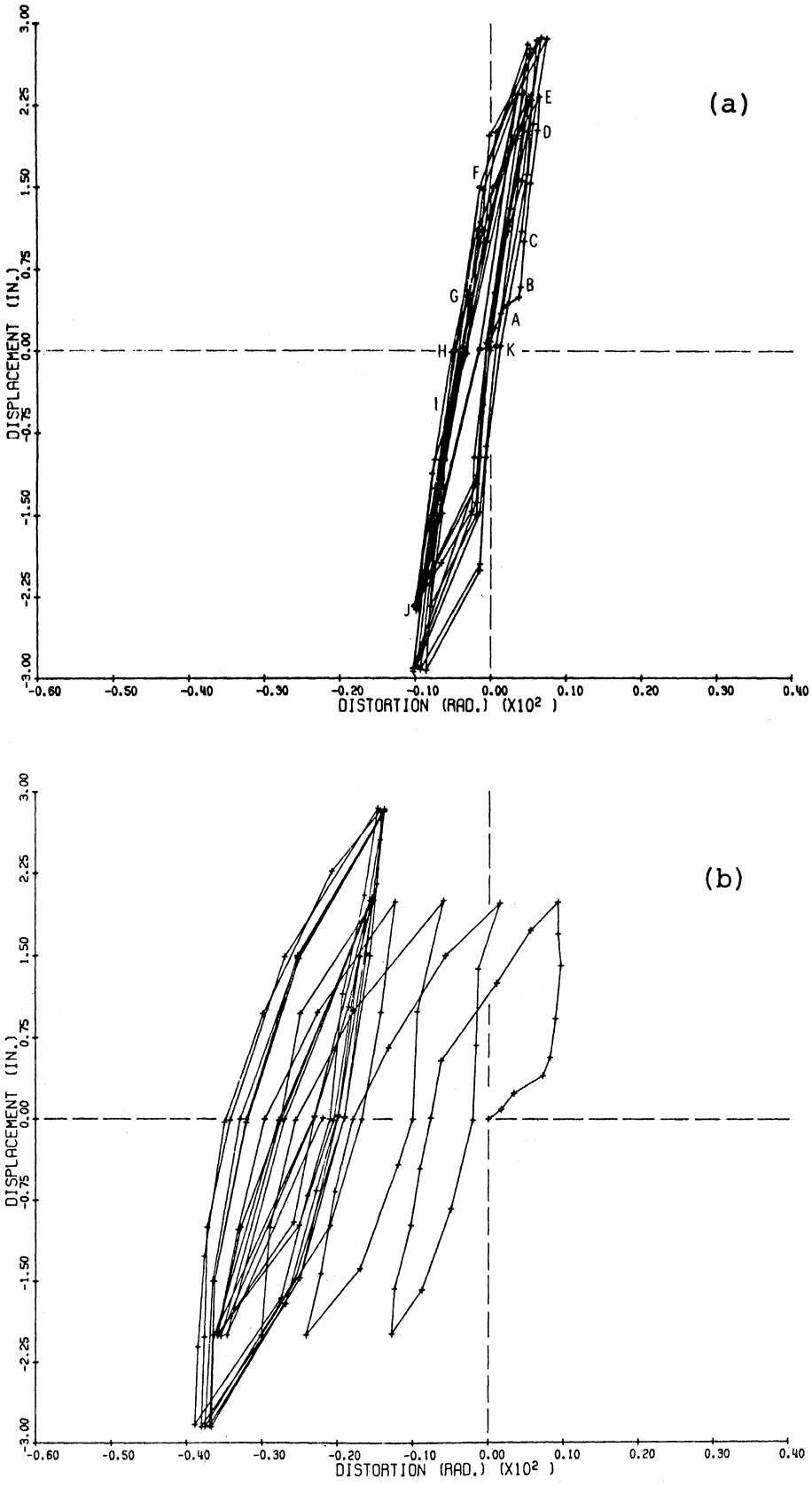

Fig. 3.23 Plot of Joint Distortion with Beam-Tip Deflection for (a) Specimen 2 and (b) Specimen 5

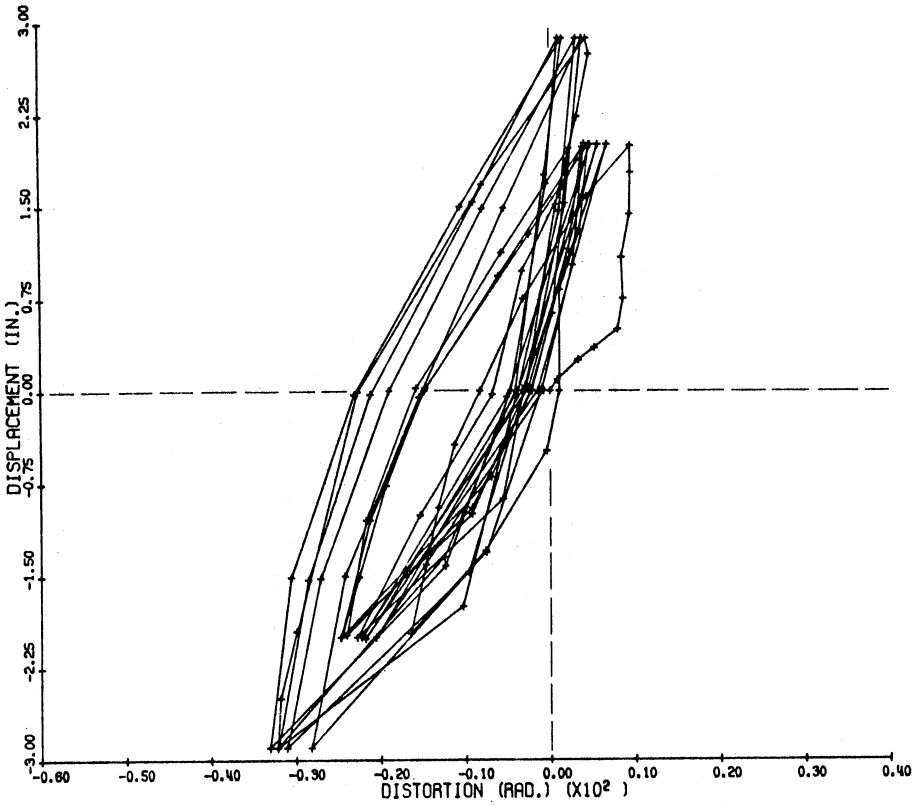

Fig. 3.23(c) Plot of Joint Distortion with Beam-Tip Deflection, Specimen 6

The distortion values γ were based on the average of LVDT measurements (Fig. 3.24), as indicated by the expression

$$\gamma = \frac{\delta_1 + \delta_2}{2} \left(\frac{d}{h\ b}\right) \qquad (3.1)$$

where δ_1, δ_2 = measurements made by LVDT 1 and 2 respectively,

b = horizontal projection of inclined distance between points measured by LVDT,

h = vertical projection of inclined distance between points measured by LVDT,

and d = distance between points measured by LVDT.

The values of b, h, and d were 7.0, 13.0 and 14.8 in. respectively, as indicated by Fig. 2.6. Specimen 2, with a 40 kip column axial load, showed a more stable

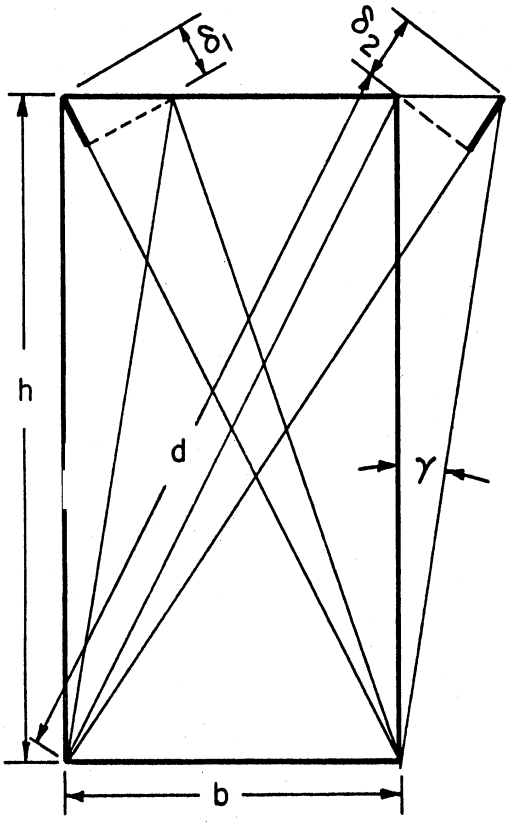

Fig. 3.24 Schematic Diagram to Measure Joint Distortion [From Bertero (8)]

joint distortion behavior than Specimens 5 and 6 with zero column axial load. Also, the column axial load tended to make the joint stiffer as can be seen by comparing the distortions from Specimen 2 and Specimens 5 and 6 during the first quarter cycle of loading in Fig. 3.25. The amount of transverse reinforcement in the joint did not noticeably affect the stiffness as seen by comparing the results in Fig. 3.25 for Specimen 5 with Type II Design and Specimen 6 with Type I Design.

3.5 Measured Rotation in Beam

The beam rotation at a section 10 in. from the inside column face, measured relative to the column face is

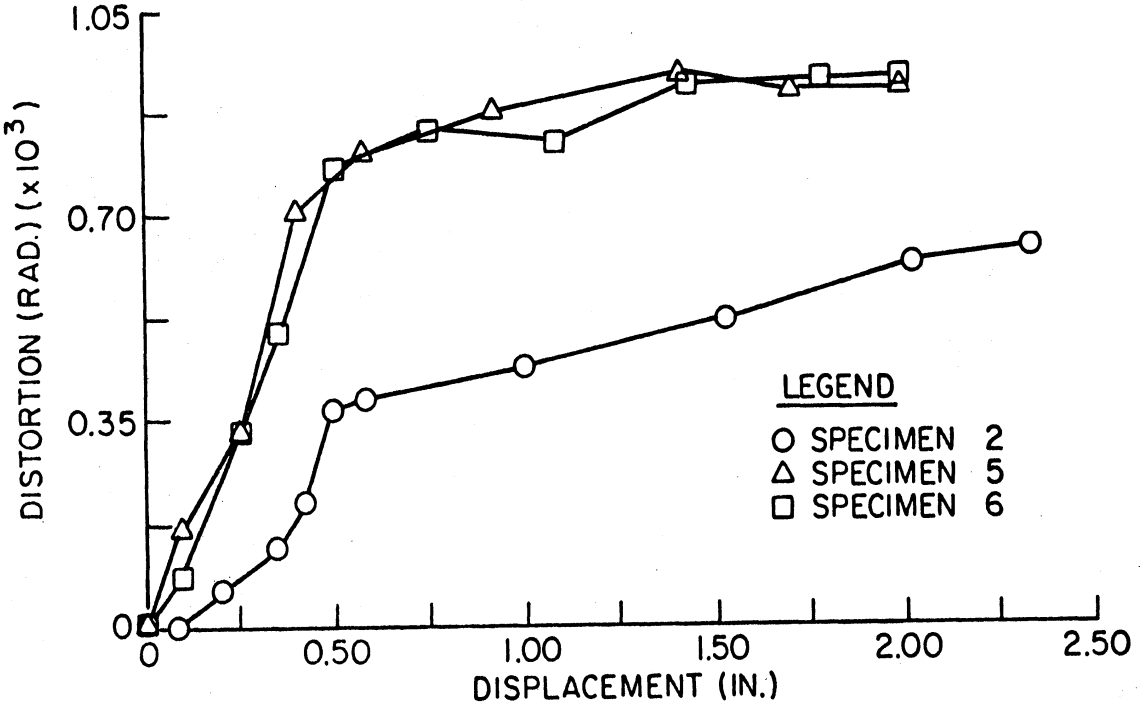

Fig. 3.25 Comparison of Joint Distortion for Specimen 2 with 40 kip Column Axial Load and Specimens 5 and 6 with Zero Column Axial Load

plotted with beam-tip force and deflection for Specimen 2 in Figs. 3.26(a) and 3.26(b) respectively. (For the location of the LVDTs used to measure the rotation, see Fig. 2.7.) The measured rotation values include contributions from the rotation of the joint and anchorage slippage in the joint in addition to the rotation of the beam over a measured length of 10 in. The beam force-rotation curves in Fig. 3.26(a) are similar in shape to those of beam force-deflection presented earlier in Sec. 3.2.

For the first quarter cycle of severe earthquake loading, a comparison can be made between the beam-tip deflection ductility and the relative beam rotation ductility as shown for Specimen 2 in Fig. 3.27. The yield rotation was taken to be the value at which deviation from linear

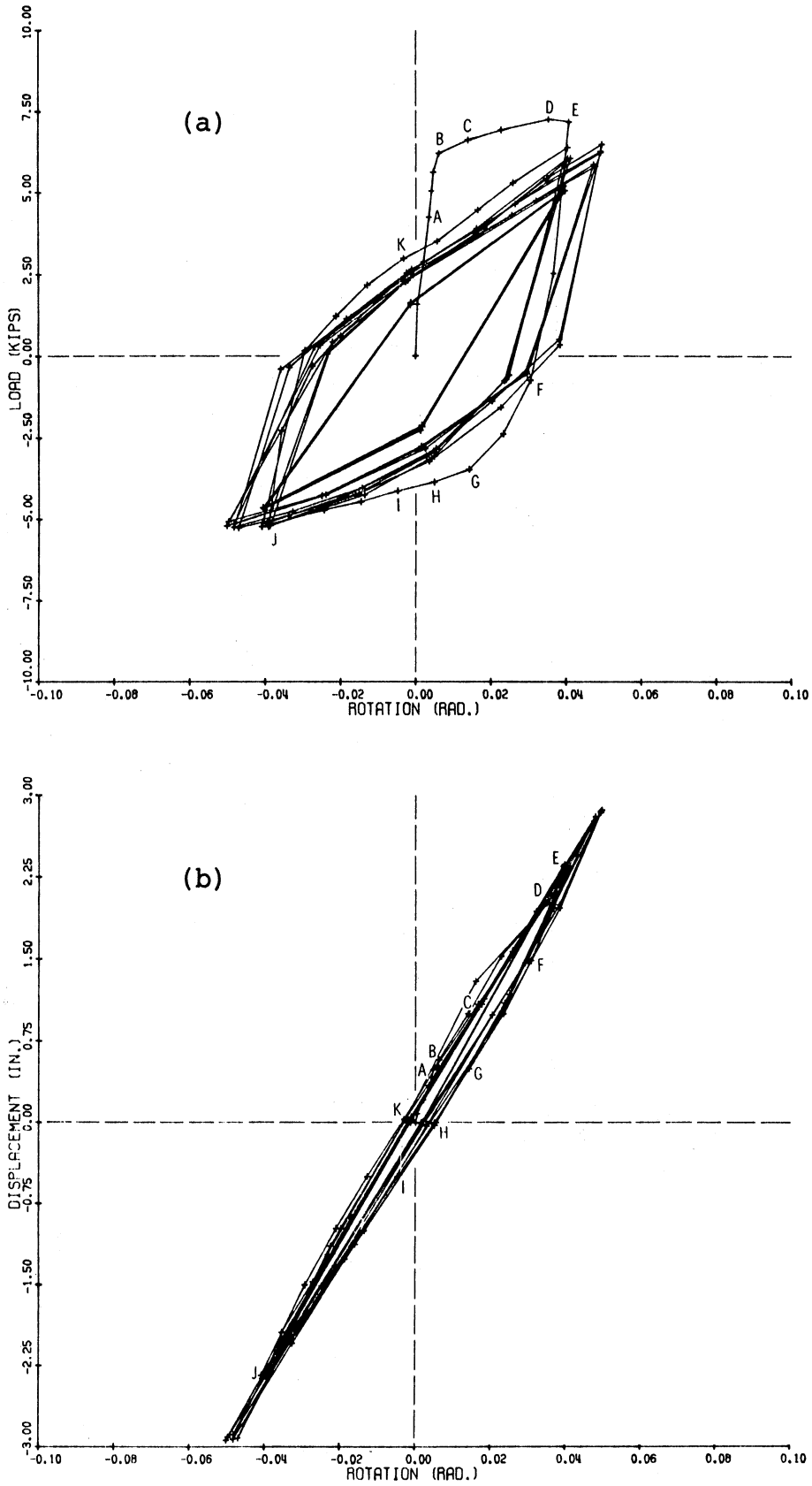

Fig. 3.26 Plot of Relative Beam Rotation with (a) Beam-Tip Force and (b) Beam-Tip Deflection, Specimen 2

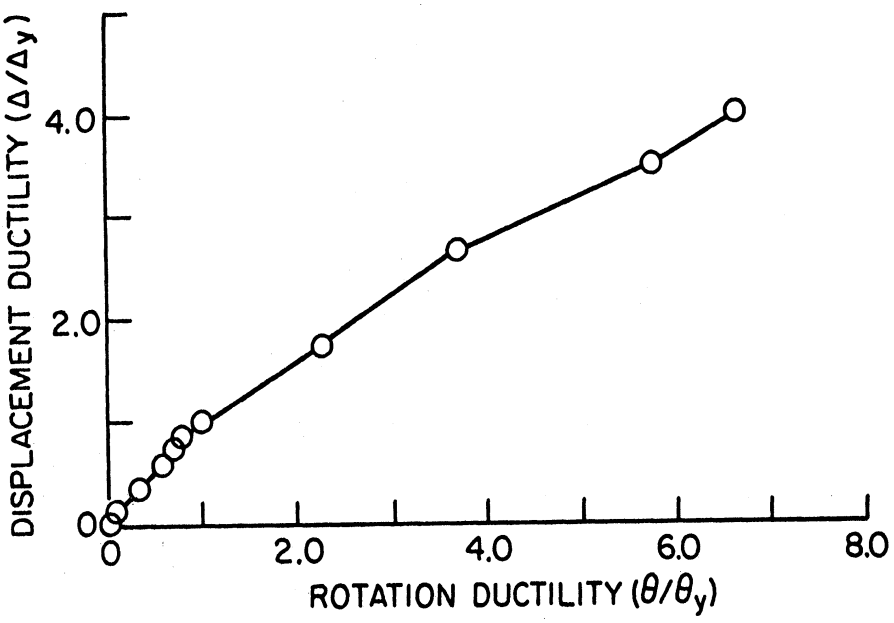

Fig. 3.27 Comparison between Relative Beam Rotation Ductility and Beam-Tip Deflection Ductility, Specimen 2

behavior occurred (point B) as see in Fig. 3.26(a). For Fig. 3.27, displacement ductilities of 2.0 and 4.0 correspond to rotation ductilities of 2.7 and 6.6 respectively.

3.6 Analysis and Discussion

An analysis of the data obtained during this investigation and a discussion of these results will now be presented.

3.6.1 Yield Moment

The experimental yield moments were obtained by multiplying the yield load from the first quarter cycle of the force-deflection curve (Fig. 3.5) by the moment arm to the critical section located at the inside column face to be as given in column 4 of Table 3.1 for all the specimens. The theoretical yield moments were calculated by assuming a linear stress distribution in the concrete

Table 3.1 Comparison of Beam Yield Moment

Specimen	Moments		
	Design (kip-in.)	Calculated (kip-in.)	Experimental (kip-in.)
(1)	(2)	(3)	(4)
1	244	316	316
2	244	296	298
3	244	297	279
4	244	297	307
5	244	308	326
6	244	312	309
7	244	288	309
8	244	293	305

and were based on nominal and measured steel and concrete strengths. The measured steel and concrete strengths are summarized in Appendix B, Tables B.1 and B.2 respectively. The moments obtained using nominal stresses are called the design moments and are given in column 2 of Table 3.1. For measured material properties the calculated moments are given in column 3 of Table 3.1. The moments calculated with measured material properties show good agreement with the experimental results.

3.6.2 Shear in Beam

The shear in the beam was assumed to be resisted by the concrete and the transverse reinforcement as indicated by the expression

$$V_t = V_c + V_s \qquad (3.2)$$

where V_t = total shear force in the beam,

V_c = shear force attributed to the concrete,

and V_s = shear force attributed to the transverse reinforcement.

Using the truss analogy, the shear resistance provided by the transverse reinforcement can be expressed as

$$V_s = \frac{A_v f_s d}{s} \tag{3.3}$$

where A_v = area of transverse reinforcement over a distance s,

f_s = stress in transverse reinforcement,

d = distance from extreme compression fiber to tension reinforcement,

and s = spacing of transverse reinforcement.

For this investigation, the strains measured in stirrupties were multiplied by the modulus of elasticity for the reinforcement to obtain stresses. The stresses were then used with Eq. 3.3 to calculate the shear resistance attributed to the transverse reinforcement. For Specimen 2 the term f_s in Eq. 3.3 was based on an average strain obtained from Gages 1 and 2. Strains measured by Gage 1 were presented earlier in Fig. 3.8.

The results are summarized for the first quarter cycle of loading in Figs. 3.28(a) and 3.28(b) for Specimen 2 with Type II Design and Specimen 6 with Type I Design respectively. The total shear force in the beam obtained from Figs. 3.5(b) and 3.5(f) minus the shear resisted by

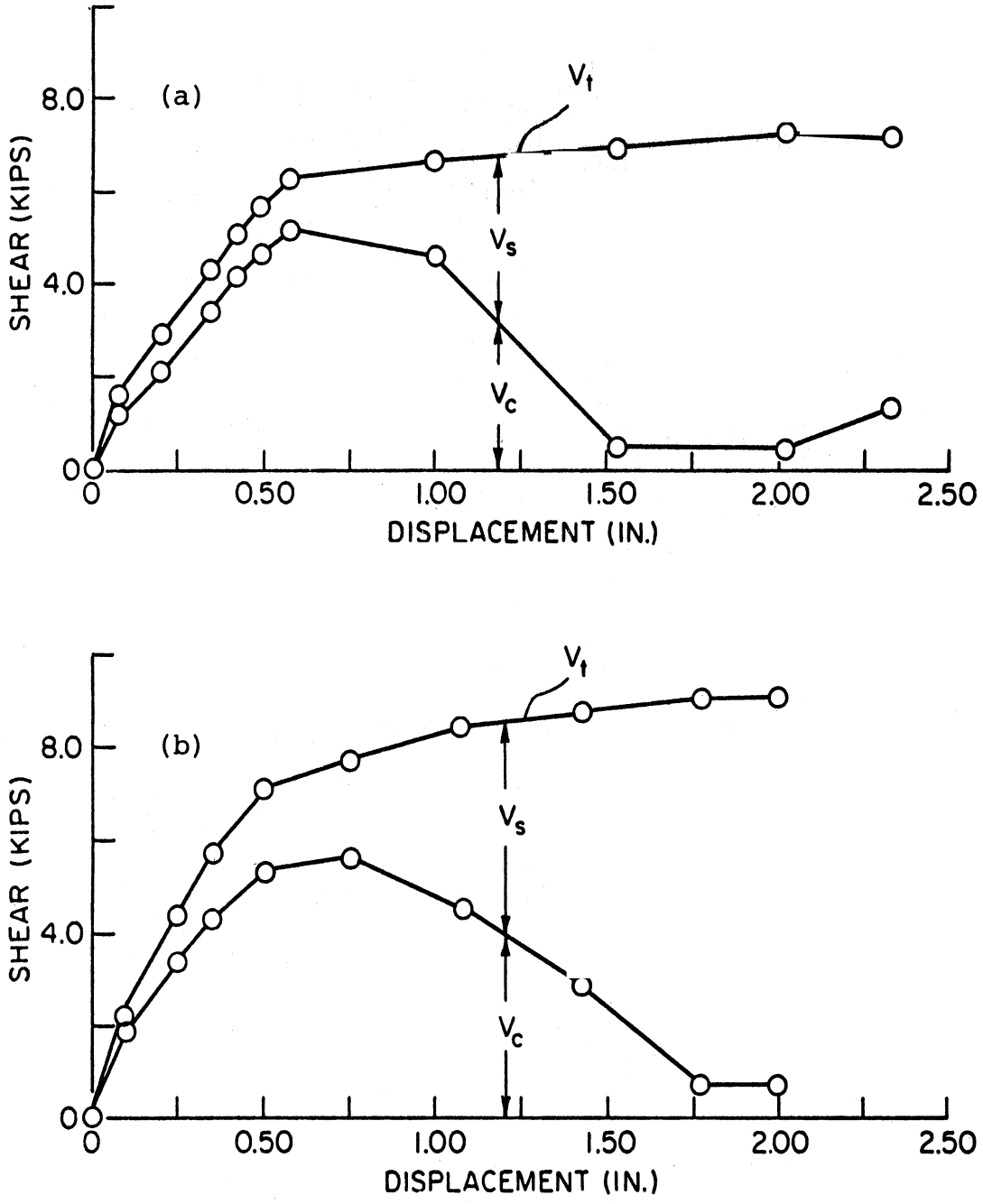

Fig. 3.28 Plot of Beam Shear Resisted by Concrete and Transverse Reinforcement with Beam-Tip Deflection for (a) Specimen 2 and (b) Specimen 6

the transverse reinforcement equals the shear resisted by the concrete as plotted in Fig. 3.28. This figure shows the transverse reinforcement resisted almost all the shear near the end of the first quarter cycle of severe earthquake loading. Also, the figure indicates that the largest shear resisted by the concrete was 5.1 kips and 5.9 kips for Specimens 2 and 6 respectively. An approximation of the shear stress resisted by the concrete was found by dividing these maximum values by $b_w d$ to be $1.23\sqrt{f'_c}$ and $1.54\sqrt{f'_c}$ for Specimens 2 and 6 respectively. The actual compressive strength of the concrete, f'_c, was used in this calculation.

For each subsequent cycle of loading at the same displacement level, the transverse reinforcement will resist a greater percentage of the shear. This can be seen by studying Figs. 3.5(b) and 3.9 for Specimen 2. The total beam shear decreased after each cycle of loading and the strains in the stirrup-tie remained relatively stable indicating a greater percentage of shear was resisted by the reinforcement after each cycle of loading.

3.6.3 Anchorage

The strains in the beam top longitudinal reinforcement at the beam-to-column interface and those just before the hook for Specimen 2 are plotted for the first quarter cycle of severe earthquake loading in Fig. 3.29(a). The

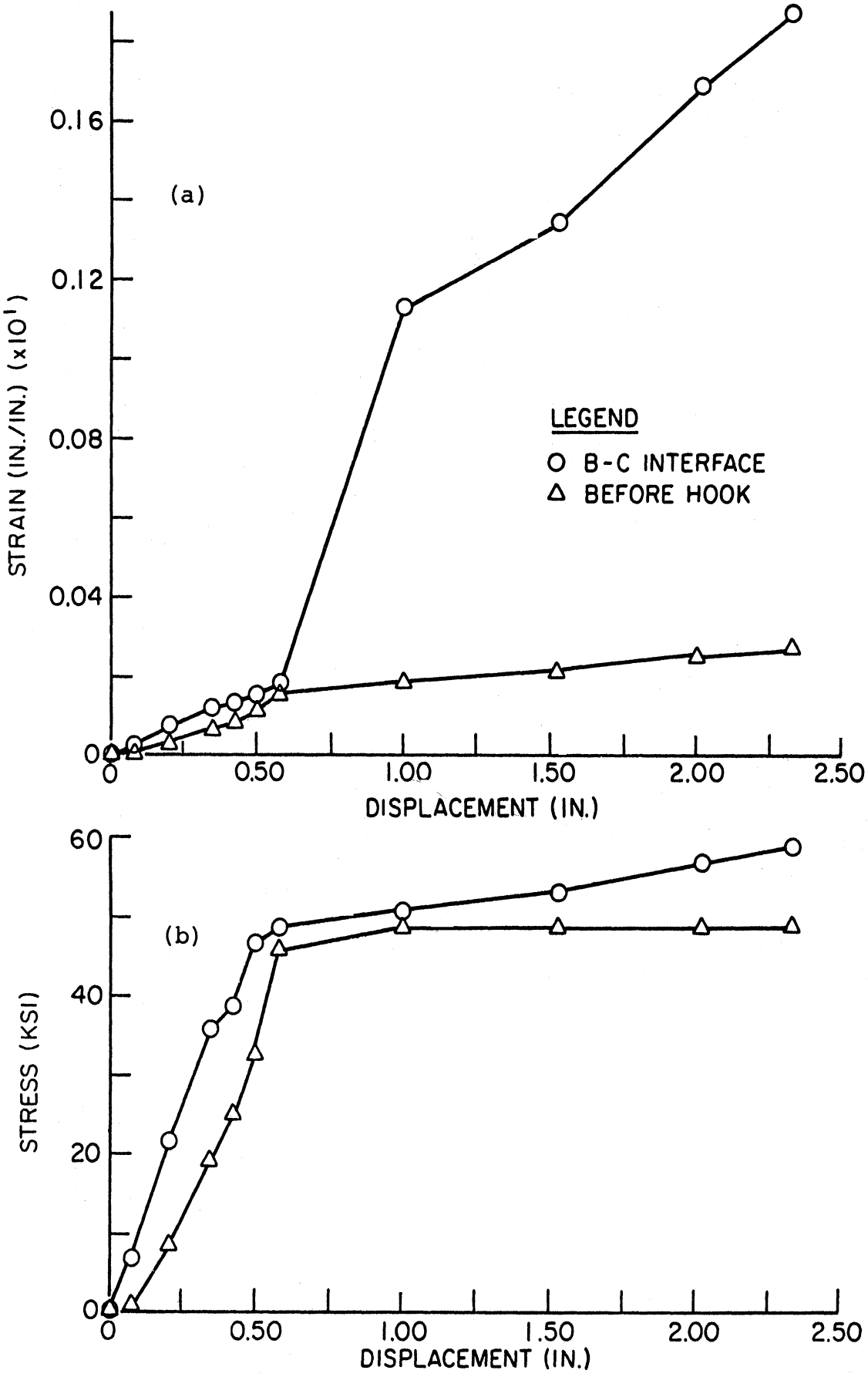

Fig. 3.29 First Quarter Cycle of Loading for Specimen 2 (a) Strain and (b) Stress along Beam Top Bar Anchored in Joint

strains were shown earlier in Figs. 3.11 and 3.14. The stresses obtained from these strains are shown in Fig. 3.29(b). Although a large difference in strain existed after the yielding of the top reinforcement at the beam-column interface, there was only a small difference in stress due to the yielding plateau and the lower stiffness of the reinforcement in the strain hardening region. The average bond stress u_{avg} between the hook and beam-column interface was calculated by the expression

$$u_{avg} = \frac{(f_{si} - f_{sj})\ A_b}{p_b\ l_{ij}} \qquad (3.4)$$

where f_{si} = reinforcement stress at location i, the beam-column interface,

f_{sj} = reinforcement stress at location j, just before the hook

A_b = area of reinforcing bar,

p_b = perimeter of reinforcing bar,

and l_{ij} = distance between i and j.

Values for u_{avg} for Specimen 2 during the first quarter cycle of loading are plotted in Fig. 3.30(a). The average bond stress increases up to 500 psi, decreases to 50 psi and then increases to 300 psi. This fluctuation in average bond stress may correspond to a change in bond mechanism from adhesion, to friction and bearing. The average bond stress was also calculated in a similar manner for Specimens 5 and 6 with zero column axial load and the results are shown in Figs. 3.30(b) and 3.30(c)

repaired region for all the specimens. Few new cracks were observed in the joint and no cracks were observed in the column for specimens with the 40 kip column axial load. For the specimens with zero column axial load, new cracks were observed in the joint. Also, cracks were observed in the column for Specimens 6 and 8 during retest.

The measured beam-tip force and deflection indicated that the strength capacity was higher for the repaired specimens. This increase in strength can be attributed to the stressing of the beam longitudinal reinforcement further into the strain hardening range during retest.

The measured joint distortions were greater for the repaired specimens. This was due to the increase in shear in the joint resulting from the higher beam strength. The measured relative beam rotation over the first 10 in. of the beam was less for the repaired specimens. This reduction was due to the absence of the yielding plateau on the stress-strain curve for the tensioned reinforcement after original testing.

6.6 Conclusions

Based on this investigation, the following conclusions are made.

(1) Epoxy injection, and removal and replacement techniques of repair can effectively restore the stiffness, strength and energy dissipation

respectively. The maximum average bond stress for Specimens 5 and 6 was 230 psi and 330 psi respectively before a decrease to zero. The zero bond stress indicated slippage of reinforcement. The average bond stresses were higher for specimens with the 40 kip column axial load as seen by comparing the results for Specimen 2, with those for Specimens 5 and 6. The column axial load improved the confinement around the reinforcement and improved the frictional and bearing resistance. For subsequent cycles of loading, it is expected that the average bond stress would decrease due to deterioration in the concrete around the perimeter of the bar. The deterioration is caused by the shearing action of the reinforcing bar ridges against the concrete.

To determine the resistant capacity of the hook during the first quarter cycle of loading the strains measured just before the hook and those just after the hook are converted to stresses and plotted in Fig. 3.31(a) for Specimen 5 with Type II Design. These results show that the 90 deg. hook was capable of resisting 60 percent of the total stress at yielding of the steel just before the hook. A similar comparison also was made for Specimen 6 with Type I Design as shown in Fig. 3.31(b) and the hook was found to resist 70 percent of the stress at yield. For subsequent cycles of loading, the hook will resist less stress due to cracking and crushing of the concrete

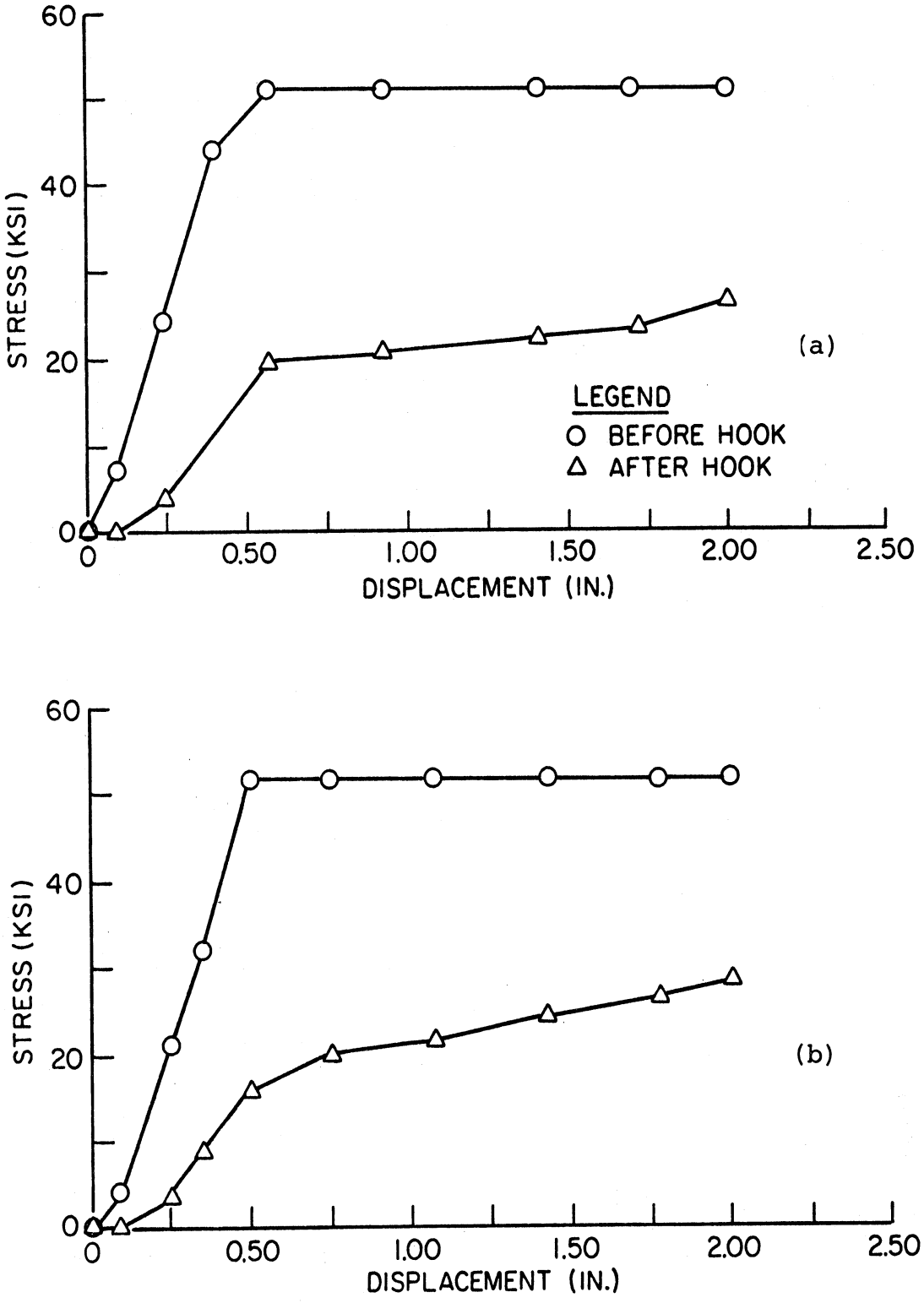

Fig. 3.31 Plot of Stress along Hook with Beam-Tip Deflection for (a) Specimen 5 and (b) Specimen 6

under the hook. Therefore it is essential that an extension length of bar beyond the hook is provided to avoid pullout of the bar.

3.6.4 Shear in Joint

The shear force in the joint was assumed to be resisted by the concrete and the transverse reinforcement. To determine the shear force in the joint during the first quarter cycle of loading, the following expression was used.

$$V_t = A_s f_s - V_{col} \tag{3.5}$$

where V_t = total shear force in the joint,

A_s = area of beam top reinforcement anchored in the column,

f_s = stress in the top reinforcement at the beam-to-column interface,

and V_{col} = shear force in the column.

The shear force in the column can be obtained by static equilibrium using the measured beam force. The total shear force in the joint is plotted with beam-tip deflection during the first quarter cycle of loading in Fig. 3.32(a) for Specimen 2 (Type II Design, 40 kip column axial load). The stress in the top reinforcement at the beam-column interface was presented earlier in Fig. 3.29(b). The shear force resisted by the transverse reinforcement was calculated by Eq. 3.3 using averaged strains measured by Gages 8 [Fig. 3.19(a)] and 9. These results given in

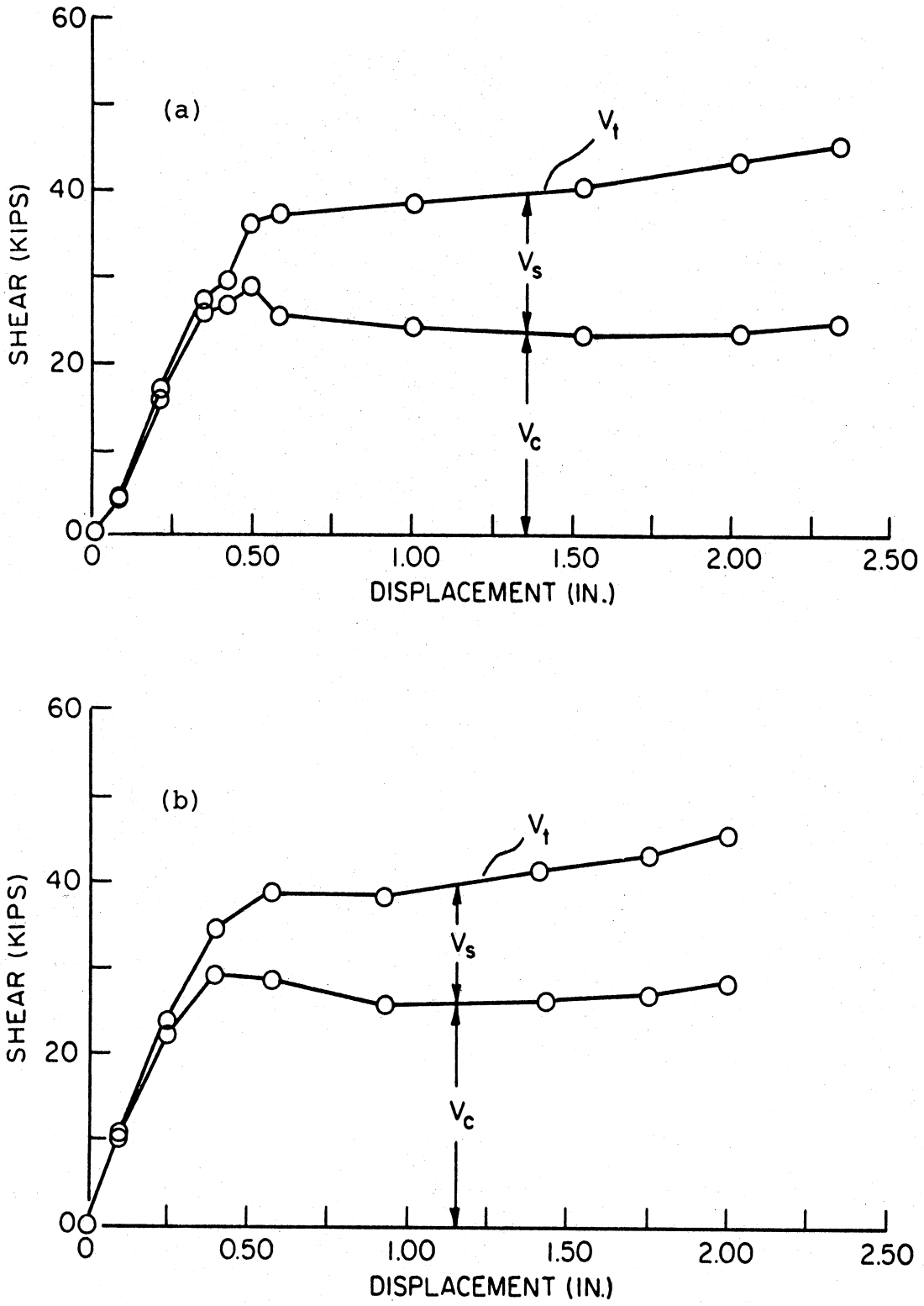

Fig. 3.32 Plot of Joint Shear Resisted by Concrete and Transverse Reinforcement with Beam-Tip Deflection for (a) Specimen 2 and (b) Specimen 5

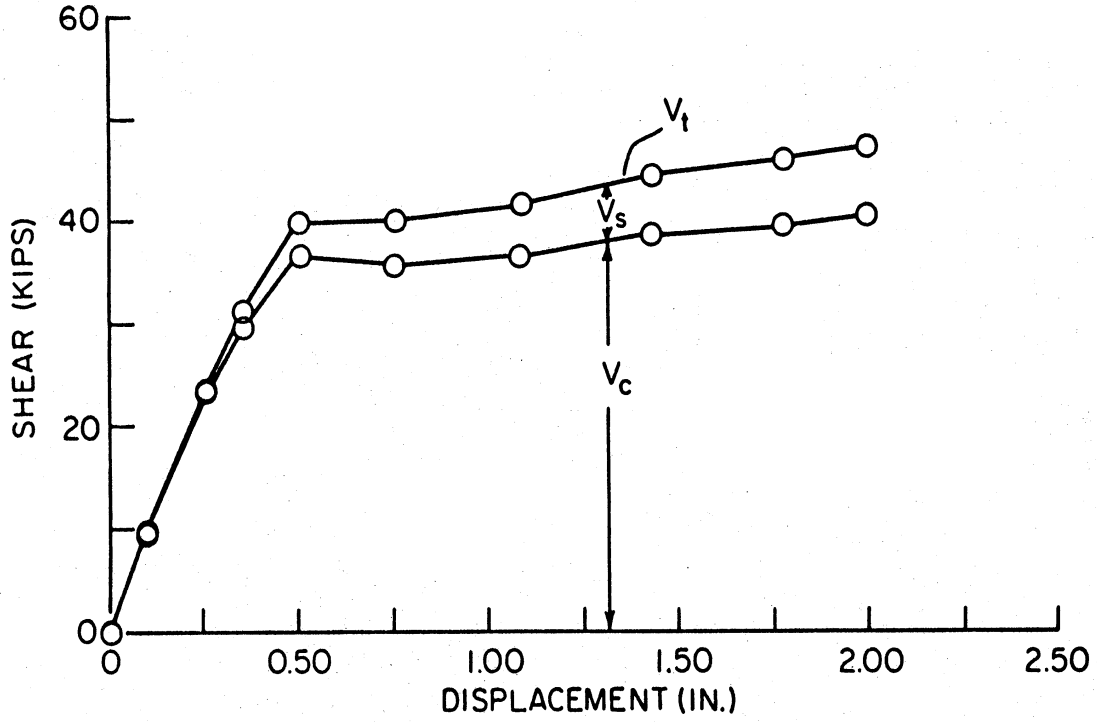

Fig. 3.32(c) Plot of Joint Shear Resisted by Concrete and Transverse Reinforcement with Beam-Tip Deflection, Specimen 6

Fig. 3.32(a) showed that the hoops resisted approximately 46 percent of the shear force at the end of the first quarter cycle of loading. Similar calculations were made for Specimens 5 and 6 with zero column axial load and the results are shown in Figs. 3.32(b) and 3.32(c) respectively. For Specimen 6, the calculation was based on the averaged strains obtained from Gages 7 and 8. The results indicated that the transverse reinforcement resisted 38 percent and 15 percent of the joint shear at the end of the first quarter cycle of loading for Specimen 5 (Type II Design) and Specimen 6 (Type I Design) respectively. This finding is not as expected and as observed for the beam

in Fig. 3.28. It was expected that the shear force resisted by the transverse reinforcement would be the same for each specimen, independent of the amount of reinforcement.

The shear in the joint at peak positive beam deflection for the second and subsequent cycles along with the first cycle of loading for Specimens 2, 3, 5, and 6 are shown in Figs. 3.33(a) through 3.33(d) respectively. For the second and subsequent cycles of loading, the force applied by the beam top reinforcement was calculated by dividing the beam moment at the beam-column interface by the distance between the top and bottom reinforcement. The results indicated that the shear force in the joint decreased with each successive cycle at the same displacement level. This decrease is due primarily to the cracking and spalling of the concrete in the beam. The shear resisted by the transverse reinforcement and the concrete in the joint are also shown in Figs. 3.33(a) through 3.33(d). The shear force resisted by the concrete was greater for Specimens 3 and 6 with Type I Design than for Specimens 2 and 5 with Type II Design.

The ACI-ASCE Joint Committee 352 (63) suggests that the following equation should be used to determine the maximum shear to be resisted by the concrete in the joint.

$$v_c \leq 3.5\ \beta\ \gamma \sqrt{f'_c \left(1 + 0.002\ \frac{N_u}{A_g}\right)} \qquad (3.6)$$

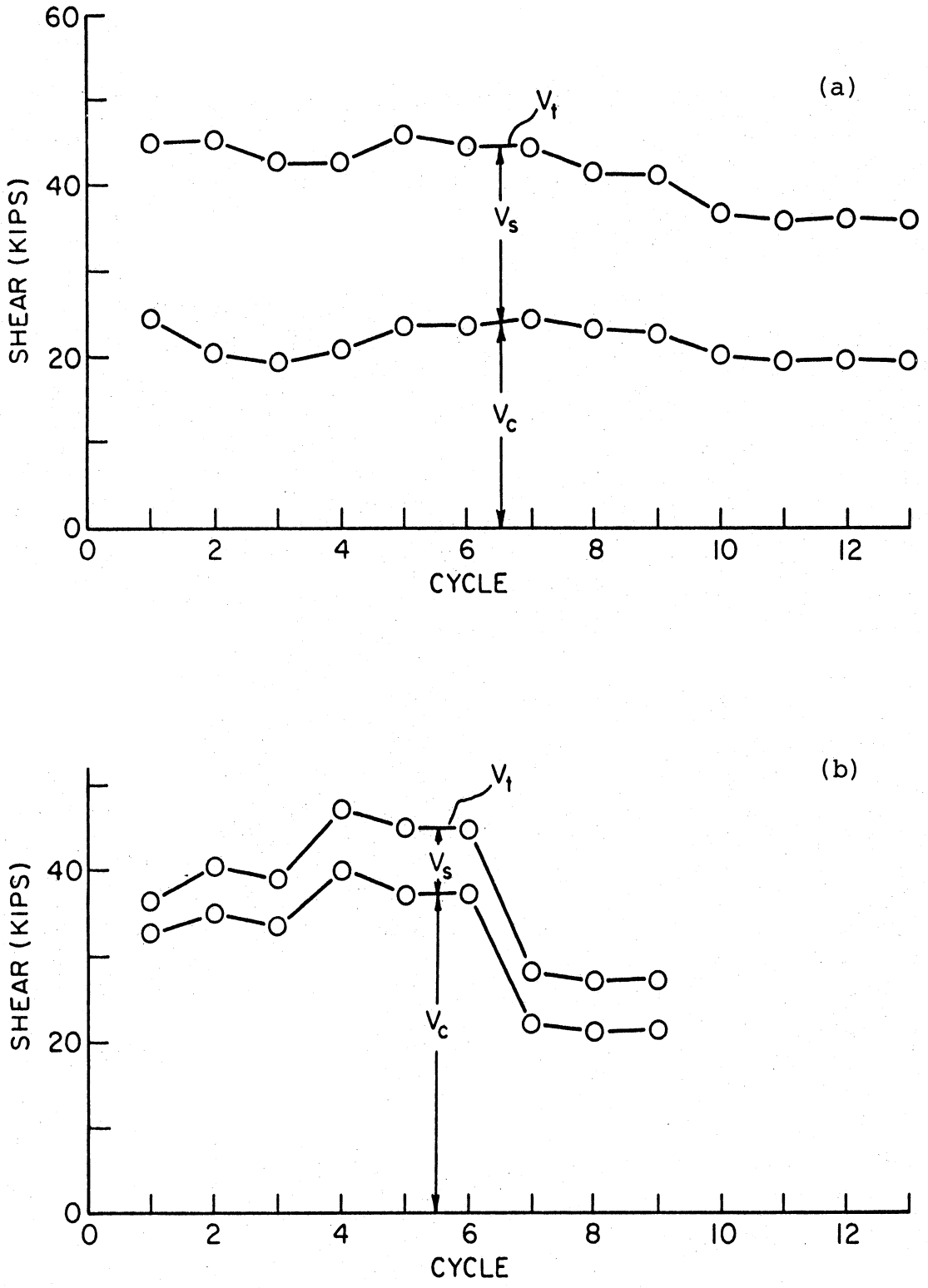

Fig. 3.33 Plot of Joint Shear Resisted by Concrete and Transverse Reinforcement at Peak Positive Beam-Tip Deflection with Cycle for (a) Specimen 2 and (b) Specimen 3

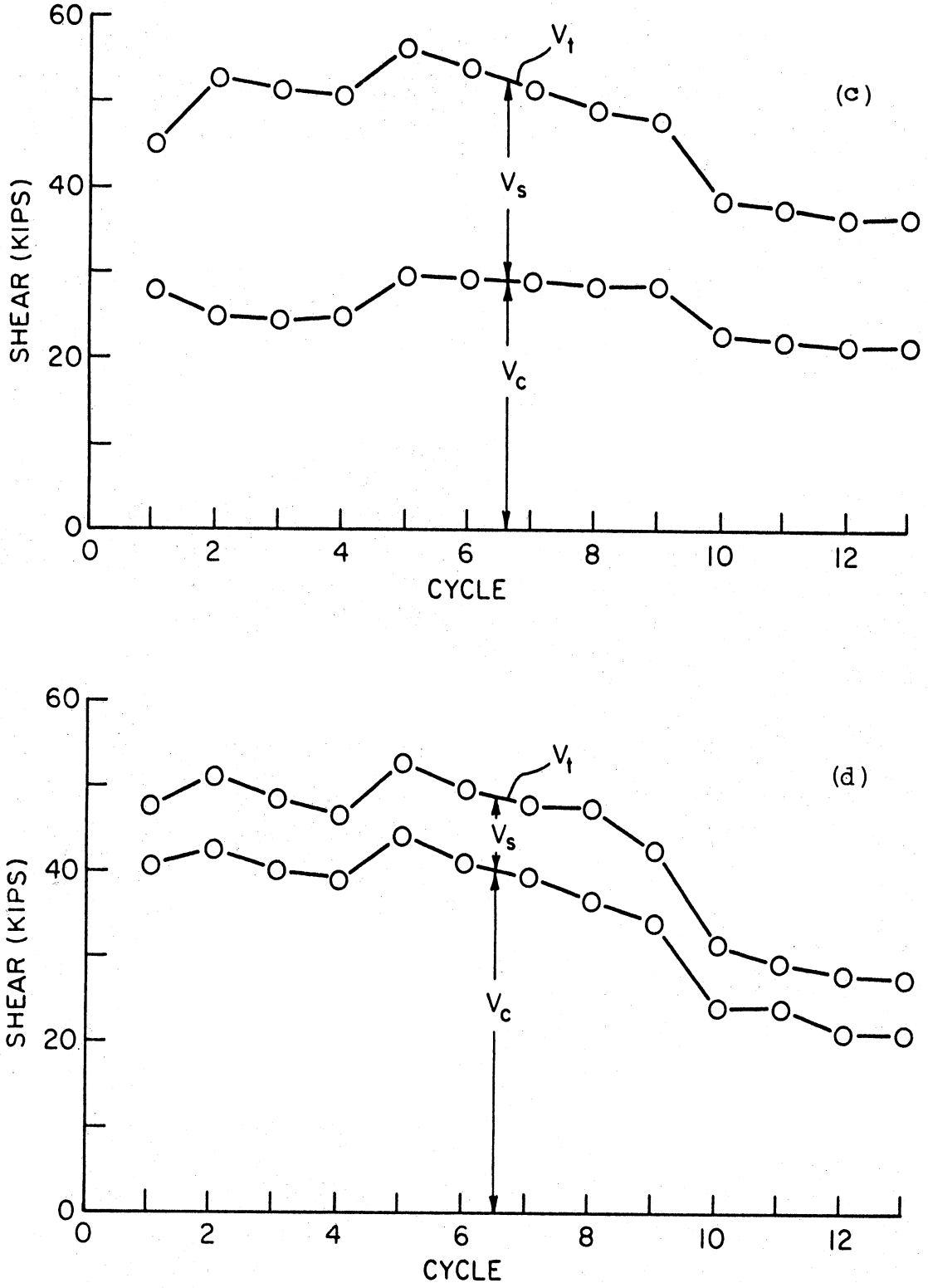

Fig. 3.33 (cont.) Plot of Joint Shear Resisted by Concrete and Transverse Reinforcement at Peak Positive Beam-Tip Deflection with Cycle for (c) Specimen 5 and (d) Specimen 6

where β = 1.4 for joints where strength is desired, and 1.0 for joints where both strength and ductility are desired,

γ = 1.4 for joints confined by members framing perpendicular to the direction of the shear force considered, and 1.0 for joints without such framing members,

f'_c = compressive strength of concrete,

N_u = axial load in the column occurring simultaneously with V_t,

and A_g = gross cross sectional area of the joint.

For this investigation, the measured shear force resisted by the concrete, V_c, was divided by b_w, the width of the joint, and d, the distance from the beam-column interface to the far column longitudinal reinforcement, to obtain the concrete shear stress for each cycle at maximum positive beam deflection. This shear stress was divided by the value of $\beta\gamma\sqrt{f'_c\left(1+0.002\frac{N_u}{A_g}\right)}$ to achieve the form given in Eq. 3.6. These results, which are plotted in Figs. 3.34(a) through 3.34(d) for Specimens 2, 3, 5, and 6 respectively, indicate that the coefficient of 3.5 used in Eq. 3.6 is too conservative and could be increased to 7. The results from Specimen 6 indicated that constant was as high as 10.2. However, as discussed later in Chapter 5, Specimen 6 gave evidence that the joint had been damaged during the original testing.

3.6.5 Beam Deflection

The beam-tip deflections measured at the load application point at first yielding of the beam top reinforcing

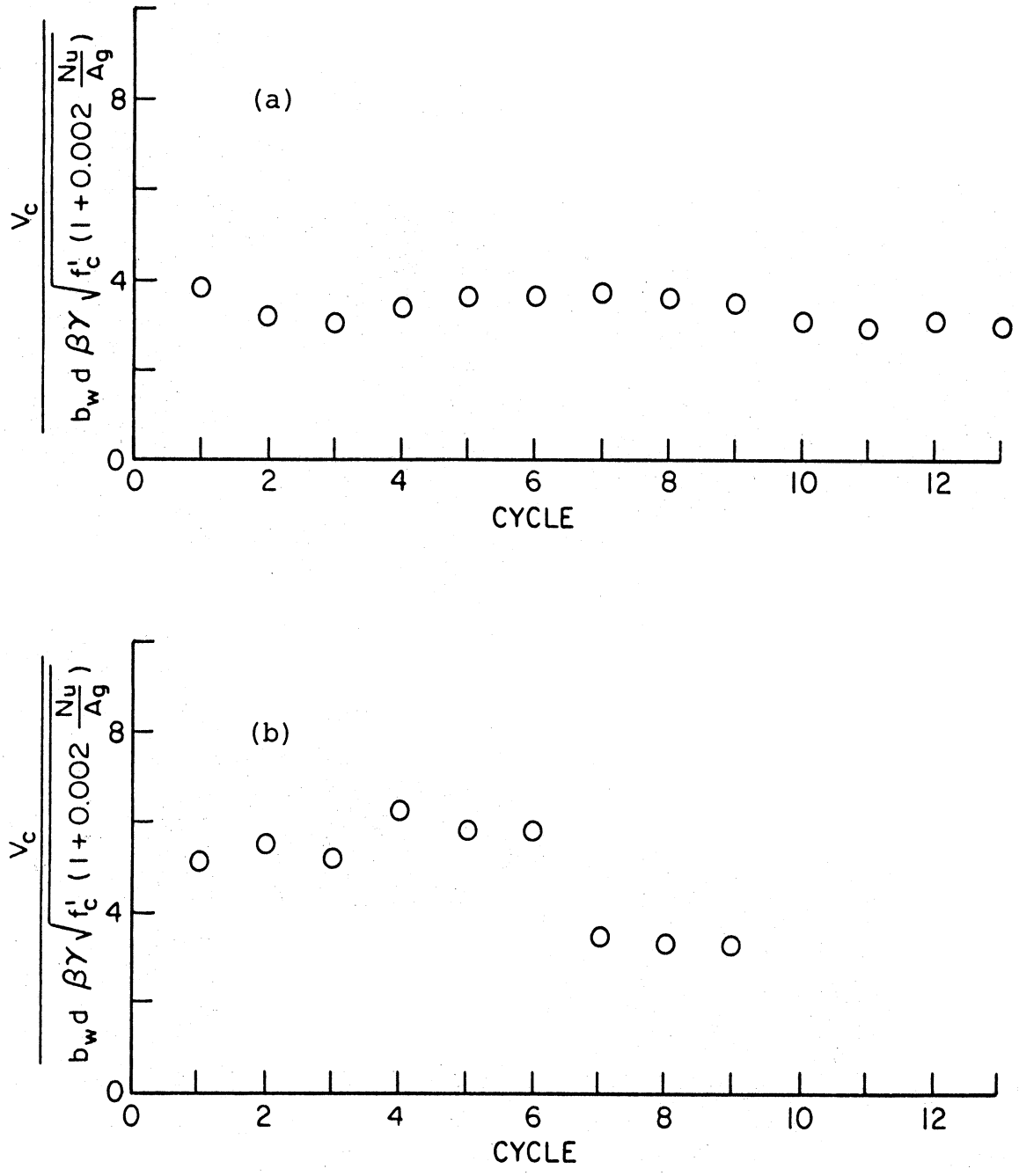

Fig. 3.34 Normalized Joint Shear Resisted by the Concrete at Peak Positive Beam-Tip Deflection for each Cycle for (a) Specimen 2 and (b) Specimen 3 for β=1.0 and γ=1.0

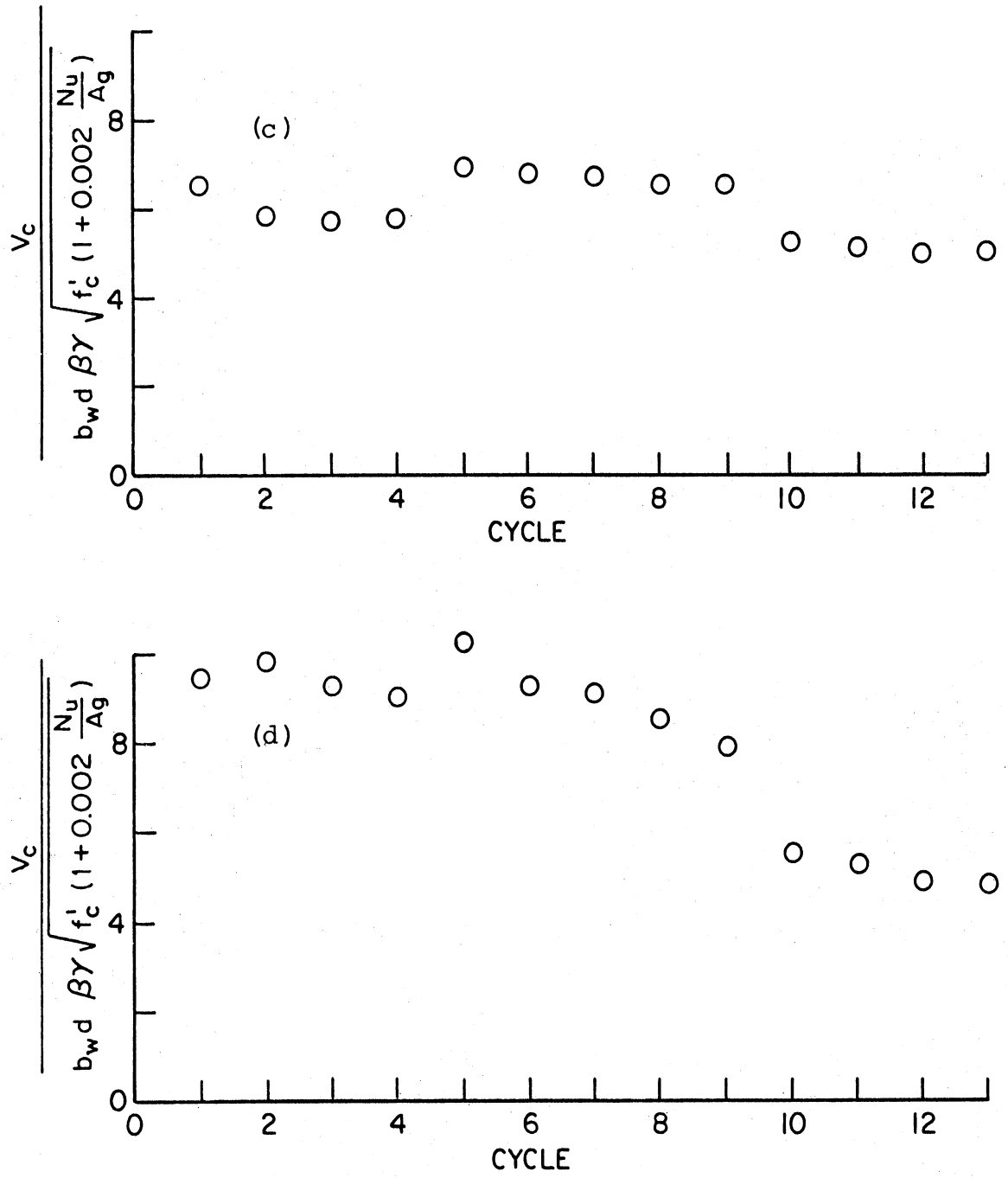

Fig. 3.34 (cont.) Normalized Joint Shear Resisted by Concrete at Peak Positive Beam-Tip Deflection for each Cycle for (c) Specimen 5 and (d) Specimen 6 for β=1.0 and γ=1.0

bars are given for all the specimens in Table 3.2. These

Table 3.2 Measured Beam-Tip Deflection at First Yielding of Top Reinforcement

Specimen	Deflection (in.)
1	0.54
2	0.56
3	0.53
4	0.53
5	0.52
6	0.50
7	0.47
8	0.46

deflections were taken from the force-deflection curves shown in Figs. 3.5(a) through 3.5(h). For Specimens 5 through 8, the yield deflections are smaller because the force was applied and the deflection was measured 41.25 in. from the inside column face rather than the 46.5 in. for Specimens 1 through 4.

Specific forces and the corresponding deflections measured during the first quarter cycle of loading for Specimen 2 are compared in Table 3.3 with computed deflections which were obtained as the sum of various deflection components which can be expressed as follows

$$\Delta_t = \Delta_1 + \Delta_2 + \Delta_3 + \Delta_4 + \Delta_5 + \Delta_6 \qquad (3.7)$$

Table 3.3 Comparison Between Calculated and Measured Beam-Tip Deflection, Specimen 2

Calculated Deflection Components						Total Calculated Deflection (in.)	Measured Deflection (in.)	Measured Force (kips)
Δ_1 (in.)	Δ_2 (in.)	Δ_3 (in.)	Δ_4 (in.)	Δ_5 (in.)	Δ_6 (in.)			
0	0	0	0	0	0	0	0	0
0.014	0.004	0.002	0.133	0.020	0.085	0.257	0.33	4.24
0.021	0.017	0.004	0.232	0.036	0.124	0.434	0.56	6.20
0.022	0.021	0.004	0.528	0.088	0.132	0.795	0.97	6.61
0.023	0.026	0.004	0.859	0.145	0.138	1.205	1.48	6.92
0.024	0.031	0.004	1.331	0.230	0.145	1.765	1.96	7.25
0.024	0.031	0.004	1.542	0.267	0.143	2.011	2.26	7.17

where Δ_t = total calculated beam deflection,

Δ_1 = deflection due to the rotation of the column at the beam-column joint,

Δ_2 = deflection due to shear distortion in the joint,

Δ_3 = deflection due to the shear distortion in the beam,

Δ_4 = deflection due to the rotation of the beam over a 10 in. length beginning from the inside column face,

Δ_5 = flexural deflection of the beam 10 in. from the inside column face relative to the column,

and Δ_6 = flexural deflection of the beam between the section 10 in. from the inside column face and the point of load application.

These components of the total beam deflection are illustrated in Fig. 3.35. When calculating Δ_6, the rotation

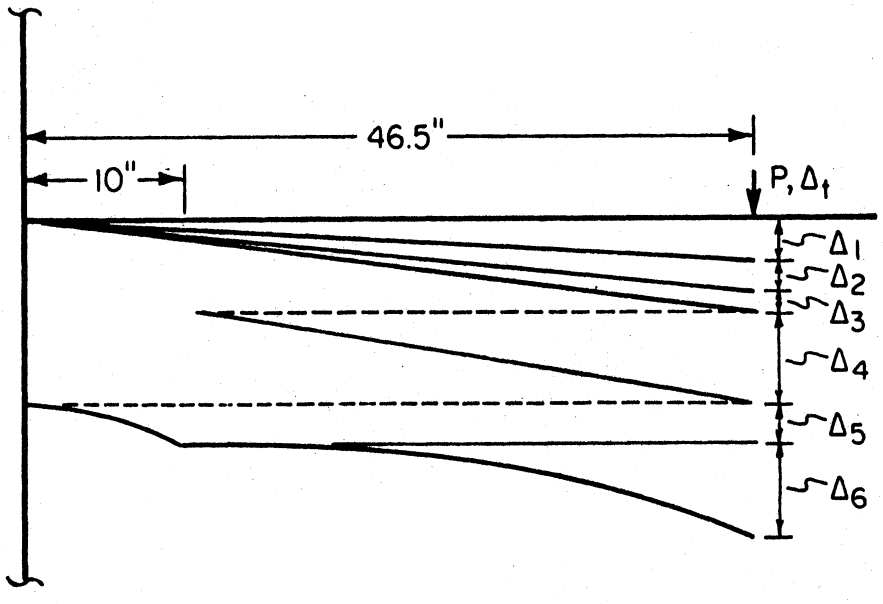

Fig. 3.35 Components of Total Calculated Beam-Tip Deflection

at the left end of the beam at a distance 10 in. from the inside column face was set equal to zero. The conjugate beam method was used to determine Δ_1, Δ_5, and Δ_6. For Δ_1, and Δ_6, the deflection was based on a uncracked column section with zero column axial load and a cracked beam section. The moduli of elasticity for the reinforcement and the concrete were based on measured values given in Appendix B. For Δ_5, the deflection was based on the total curvature obtained from the relative beam rotation shown in Fig. 3.26(b). This total curvature was linearly distributed over the 10 in. span length. The deflection due to the shear distortion in the joint Δ_2 was calculated by multiplying the joint distortion indicated in Fig. 3.23(a) by the beam length. The deflection due to the shear distortion in the beam Δ_3 was calculated by multiplying the shear distortion γ by the beam length. This shear distortion was calculated with the following expression

$$\gamma = \frac{\tau}{G} = \frac{V_t}{b_w\ d\ G} = \frac{V_t}{b_w\ d\ (0.4\ E_c)} \qquad (3.8)$$

where τ = shear stress in the beam,

G = shear modulus for the concrete,

and E_c = modulus of elasticity for the concrete.

The Δ_4 deflection was calculated by multiplying the relative beam rotation at the section 10 in. from the inside column face by the distance from this section to the point

of load application. The total calculated beam deflection was less than the measured deflection as seen in Table 3.3.

The components of the calculated deflection given in Table 3.3 were normalized by dividing each of the corresponding total measured deflection and these normalized results are given in Fig. 3.36. The deflection due to

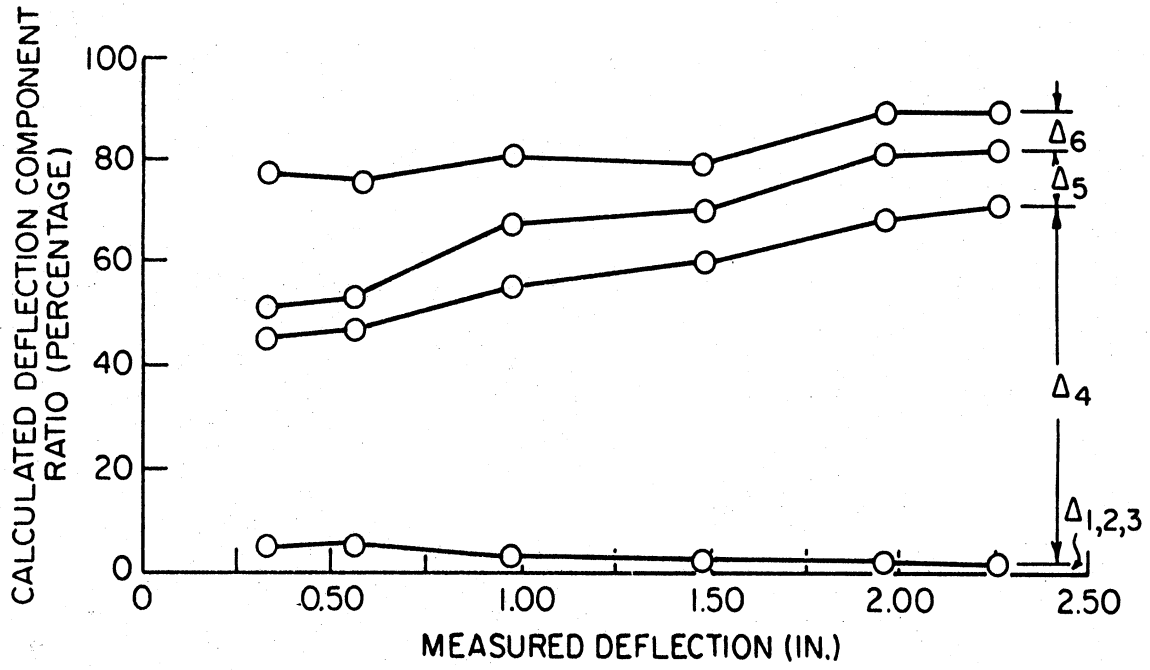

Fig. 3.36 Plot of Calculated Beam-Tip Deflection Component Ratio with Measured Deflection, Specimen 2

bending in the beam (sum of Δ_4, Δ_5 and Δ_6) represent about 86 percent of the measured deflection at the end of the first quarter cycle of loading with Δ_4 and Δ_5 representing

about 80 percent. This indicated that most of the deflection was attributed to the first 10 in. of the beam from the inside column face at the end of the first quarter cycle of loading.

3.7 Concluding Remarks and Design Recommendations

The behavior of the beam-column subassemblages during original testing indicated that the specimens with Type II Design behaved better than those of Type I Design. This is especially true for specimens subjected to the severe earthquake loading. The added transverse reinforcement in the Type II designed specimens provided a better confinement for the beam core which in turn reduced the shear slippage and buckling of the longitudinal reinforcement. The added transverse reinforcement enabled the beam to have less strength degradation, and more energy dissipation during deflection reversals. Also, for the specimens used in this investigation the damage occurred in the beam as expected because the ratio of the strength of the columns with zero and 40 kip axial load to that of the beam was respectively, three and four as discussed in Appendix A

The design recommendations made below are based on the findings made during this investigation.

Transverse Reinforcement in Beam

The transverse reinforcement should be designed and spaced to resist the total beam shear near locations where

the maximum moments are expected during seismic loading. However, the maximum stirrup-tie spacing should still be d/4 for a distance of 4d from the column as recommended by the ACI 318-71.

Shear in Joint

The allowable shear stress which the concrete in the joint can carry should be increased to that given by the following expression.

$$v_c = 7 \beta \gamma \sqrt{f'_c \left(1 + 0.002 \frac{N_u}{A_g}\right)} \qquad (3.9)$$

The remaining shear stress should be resisted by the transverse reinforcement as indicated by the following expression

$$v_s = \frac{V_t}{A_{cv}} - v_c \qquad (3.10)$$

where v_s = shear stress to be resisted by the transverse reinforcement,

and A_{cv} = effective area of the cross-section. For confinement provided by other members framing into the joint, $A_{cv} = b_w d$. For no confinement provided by other members, A_{cv} equals the width taken to the outside of the hoop multiplied by d.

For the design of the transverse reinforcement in the joint (between the beam top and bottom longitudinal reinforcement), the number of hoops can be calculated by the following expression

$$n = \frac{v_s A_{cv}}{A_v f_y} \qquad (3.11)$$

where n = number of hoops required in the joint,

A_v = area of transverse reinforcement,

and f_y = yield stress of transverse reinforcement.

The spacing of the hoops in the joint can then be made in accordance with the recommendation from ACI-ASCE Joint Committee 352 which suggests that the hoops be spaced a given distance from the beam longitudinal reinforcement anchored in the joint.

CHAPTER 4

REPAIR TECHNIQUES AND REPAIR MATERIALS

4.1 Introduction

In practice, structures that have survived an earthquake with only minor damage will usually be repaired by epoxy injection. More extensive damage will necessitate complete removal of the loose concrete at which time the reinforcement can be inspected for either necking or fracture. The resulting void can then be filled with a repair material. It is desirable to use a repair material with high early strength so the structure can be reoccupied in the shortest possible time. Regardless of which technique is used, minor cracks are usually not repaired.

Although the epoxy injection type of repair has been used extensively in the past for economical reasons, the removal and replacement method of repair is the most reliable way of repairing a damaged structural member. For the epoxy injection, the amount of penetration of the epoxy into the cracks is an unknown factor unless core samples can be taken. However, for critical locations in the structure, such as the beam-to-column joint where the penetration information is most needed, cores cannot be taken because it would remove portions of the reinforcement which cannot be replaced. Therefore, unless a nondestructive method of evaluation can be developed, the amount of epoxy penetration into cracks remains unknown.

For the removal and replacement type of repair, proper selection of a repair material to replace the damaged concrete is important if the repaired area is to dissipate the energy during subsequent earthquakes. The selection of the material should be based on the following mechanical properties which are considered ideal for a repair material: 1) compressive strength equal to or greater than that in adjacent regions, 2) stiffness comparable to that of adjacent regions, and 3) high ultimate strain capacity.

For frame structures that have been designed before the adoption of a current seismic code and have sustained damage from an earthquake, the repair of the damage should satisfy the current code requirements. Before repairs, considerations should be given to strengthening the structure for the purposes of reducing damage and even preventing collapse during subsequent earthquakes. For structures designed to a current seismic code which showed poor behavior during an earthquake, strengthening should also be considered. Strengthening of the structure can be accomplished by either erecting shear walls or enlarging beams and columns.

4.2 Repair Techniques

In this study, two techniques were used to repair the beam-column subassemblages. They are epoxy injection

and the removal and replacement of local damaged material. The procedure for both techniques is given below.

Epoxy Injection

Epoxy injection is a technique where low viscosity epoxy is injected into cracks for the purposes of restoring continuity in the concrete and bond between the concrete and reinforcing steel. A procedure used by a representative of Sika Chemical Corporation, Lyndhurst, New Jersey, using their products for the beam repairs made during this investigation was as follows. For cracks penetrating the entire width of the member, polyethylene check valve nipples, in which reverse flow in the nipples are permitted if the stopper in the valve is depressed, were located along the crack (Fig. 4.1) on both sides of

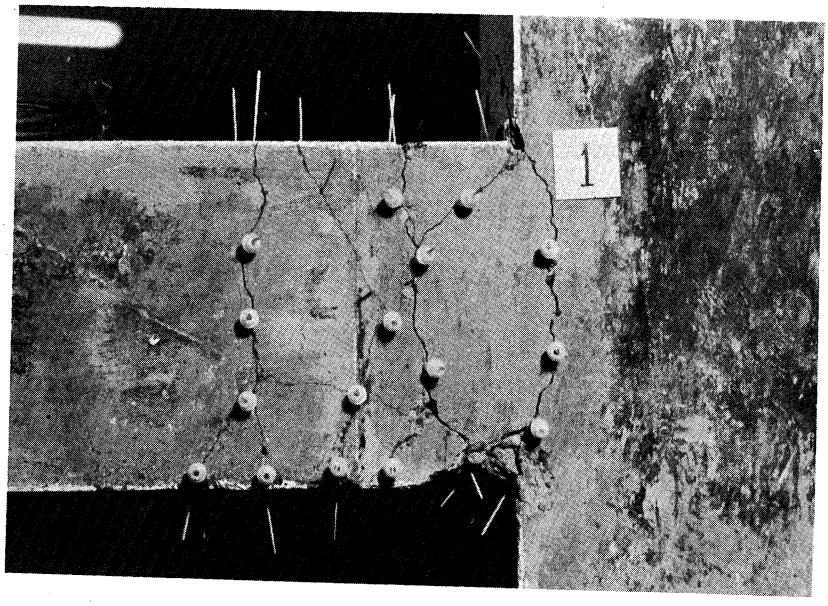

Fig. 4.1 Nipples Located Along Cracks

the member. For narrow cracks, the nipples were spaced closer together. High viscosity Colma Dur Gel epoxy was used to seal over the cracks and around the base of the nipples to prevent escape of the injected epoxy material as shown in Fig. 4.2. After the sealant cured, a

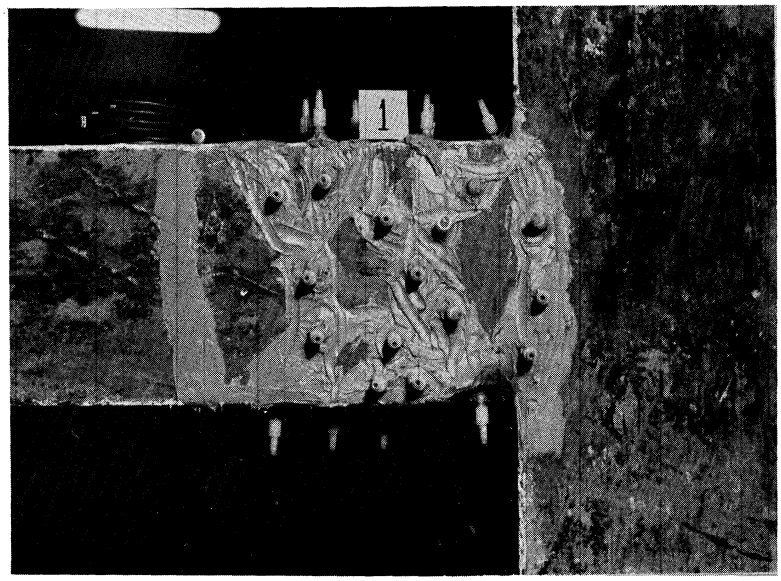

Fig. 4.2 Epoxy Used to Seal Over Cracks and Around Base of Nipples

caulking gun loaded with a cardboard cartridge was used to inject the low viscosity Sikadur Hi-Mod epoxy into the nipple at the lowest elevation while the valve stopper in the nipple at the next higher elevation along the crack was depressed to bleed off air and witness epoxy overflow. When overflow was evident in the nipples at the next higher elevation on both sides of the specimen, the crack between the injected and overflowing nipples was assumed to be saturated with epoxy. The injected nipple was closed and

the process was shifted to the overflowing nipples. This process was repeated until the entire crack had been saturated. If leakage of epoxy had occurred in the sealed cracks or around the base of the nipples during the injection process, a bar of soap was rubbed over the area of leakage to provide a temporary seal. If this method had failed, the epoxy injection process would have been delayed until the sealant could be reapplied. Figure 4.3 shows

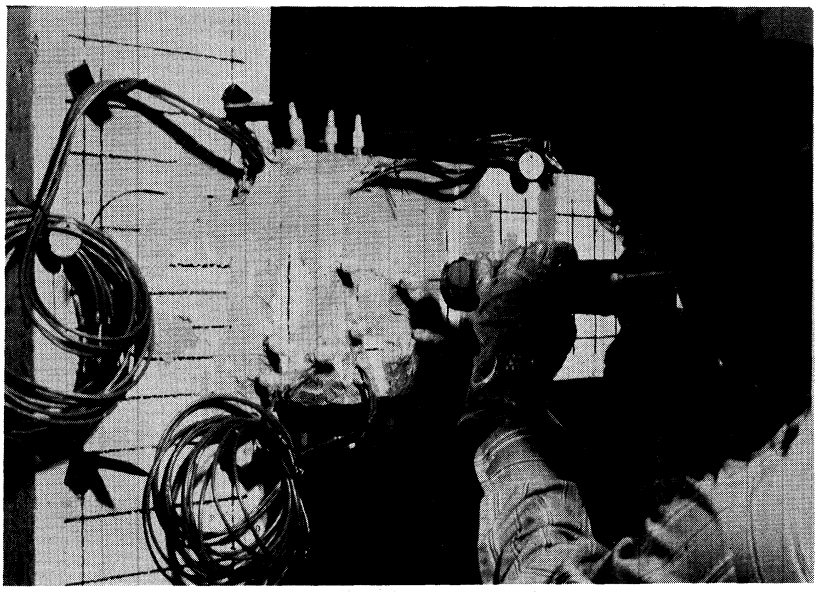

Fig. 4.3 Epoxy Injection in Progress

the injection in progress. After repair, the sealant could have been heated and scraped off to return the member to its original smooth surface.

Other epoxy manufacturers and concrete repair companies may use different methods of injecting epoxy into cracks. Their methods would be considered adequate if

complete penetration of the epoxy into the cracks can be accomplished.

Removal and Replacement

The only effective method of repairing severely damaged structural members is to remove the damaged material and replace it with a repair material. In this process, the repair of the damage should satisfy the current seismic code requirements.

The procedure for the removal and replacement repair was as follows. Loose concrete in the beam was removed with a hammer and chisel. Buckled bars were straightened as much as possible by hitting them with a hammer. None of the reinforcement was fractured during original testing. For specimens with Type I Design, No. 2 stirrup-ties were added in the void area to reduce the spacing of the transverse reinforcement from d/2 to d/4 (Fig. 4.4). This

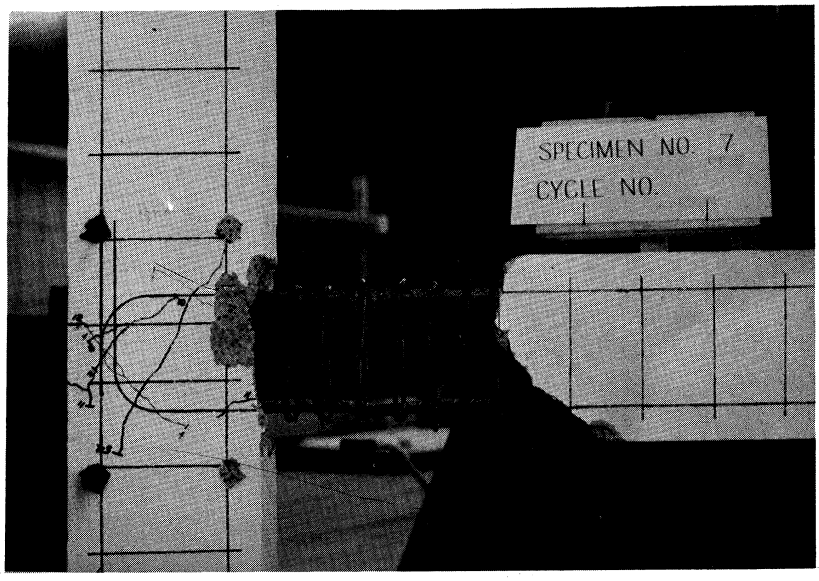

Fig. 4.4 Added Transversement Reinforcement in Void Area

latter spacing now satisfied ACI 318-71 requirements for shear and confinement. The reinforcement and existing concrete surfaces in the void were sandblasted if epoxy was used to improve the bond between the original and repair material. Wood forms, covered with polyethylene, were erected to enclose the existing void. This polyethylene was used to protect the forms from the epoxy. If epoxy was used, the Sikadur Hi-Mod epoxy was painted on the existing surfaces before placing the repair material. For the repair materials with a setup time of less than 15 min. (Duracal cement concrete and high strength quick setting concrete as described in Sec. 4.3), the aggregates were dry mixed in a wheel barrow with a hoe before adding the appropriate liquids. For the high early strength concrete repair material which has a longer setup time, the aggregates and water were combined in a portable concrete mixer. After thorough mixing, these repair materials were placed in the void and vibrated to eliminate air pockets. For specimens repaired with high early strength concrete, the repaired region was moist cured with damp burlap for three days. Other materials were air cured.

The prepack method of placement as suggested by Schutz (65) was utilized for the epoxy-sand mortar repair material. For this procedure, the sandblasted surfaces of the concrete and reinforcement were painted with Sikadur Hi-Mod

epoxy. Tightly fitted forms were erected and caulked with molding clay to prevent leakage of epoxy. A one inch layer of sand was placed in the void and then saturated with the low viscosity Sikadur Hi-Mod epoxy. Additional one inch layers of sand were placed and saturated until a total thickness of five inches was attained. A delay of several hours was taken before starting the next five inch accumulation to allow the heat generated by the chemical reaction during curing of the epoxy to dissipate. This method of placement maximizes the strength of the material by minimizing air bubbles in the mortar which are created by agitation. After placement, the epoxy-sand mortar was air cured.

4.3 Properties of Repair Material

The materials used to repair the beam-column sub-assemblages were selected primarily because of their high early strength. They are: Sikadur Hi-Mod, a low viscosity epoxy manufactured by Sika Chemical Corporation, Lyndhurst, New Jersey, which was used with the epoxy injection technique; Epoxy-Sand Mortar, consisting of Sikadur Hi-Mod epoxy and sand with a uniformity coefficient of 1.33 and a D_{50} of 1.55 mm; Duracal Cement Concrete, consisting of one part Duracal cement (produced by United States Gypsum Company, Chicago, Illinois, from gypsum and Portland cement), one part well graded sand, and 0.25 part water by weight as described in Reference

(37); High Strength Quick Setting Concrete (developed by Republic Steel Corporation, Cleveland, Ohio), consisting of one part fine, dry aggregate mixed in conjunction with powered magnesia and 0.25 part activator solution by weight as suggested by Best (10); High Early Strength Concrete consisting of three parts 1/4 in. pea gravel, four parts well graded sand, two parts Type III cement and 0.90 part water by weight. The epoxy-sand mortar, the Duracal cement concrete, and the high strength quick setting concrete are relative new materials in the construction field and their properties are not well known. Therefore, the short term and long term loading properties were investigated using standard 4 in. by 8 in. cylinders. The procedure for obtaining these standard cylinders was as follows. The cylinder molds were coated on the inside with automobile wax to act as a debonding agent. The materials were mixed and placed in the cylinders in the same manner as used in repairing the beam-column subassemblages. The cylinder molds were stripped six hours after casting. The specimens were then stored in the laboratory with no special curing conditions. For the cylinders loaded longitudinally, the top and bottom of the cylinders were capped with a high strength sulfur compound to distribute the stresses uniformly during loading.

4.3.1 Short Term Loading

The stiffness and strength properties for the epoxy-sand mortar, the Duracal cement concrete, and the high

strength quick setting concrete were investigated at ages 3, 7, 13, and 27 days. To determine the stiffness and compressive strength, the cylinders were loaded at a rate of 30 psi per sec., as suggested by ASTM C39 (72) for regular (Type I) concrete. To determine stiffness, the longitudinal deformation was measured by a 6 in. gage length compressometer which contained a dial gage that can be read to the nearest 0.0005 in. The stiffness was then taken to be the secant modulus from zero to 45 percent of the ultimate load. Typical stress-strain curves for these three materials are shown in Figs. 4.5(a) and 4.5(b) for age 3 days and 27 days respectively. The modulus of elasticity and compressive strengths obtained from these stress-strain curves are plotted in Figs. 4.6, 4.7, and 4.8 for each of these three materials. The average values also are given in Table 4.1 for age 3 days and 27 days. Table 4.1 shows that the modulus of elasticity of the epoxy-sand mortar, the Duracal cement concrete, and the high strength quick setting concrete increased 11 percent, 25 percent and 16 percent respectively from age 3 days to 27 days. For the compressive strength, the epoxy-sand mortar, Duracal cement concrete, and high strength quick setting concrete had increases of 18 percent, 50 percent, and 58 percent respectively from age 3 days to 27 days.

To obtain a measure of the tensile strength of the repair materials, the standard splitting test was utilized

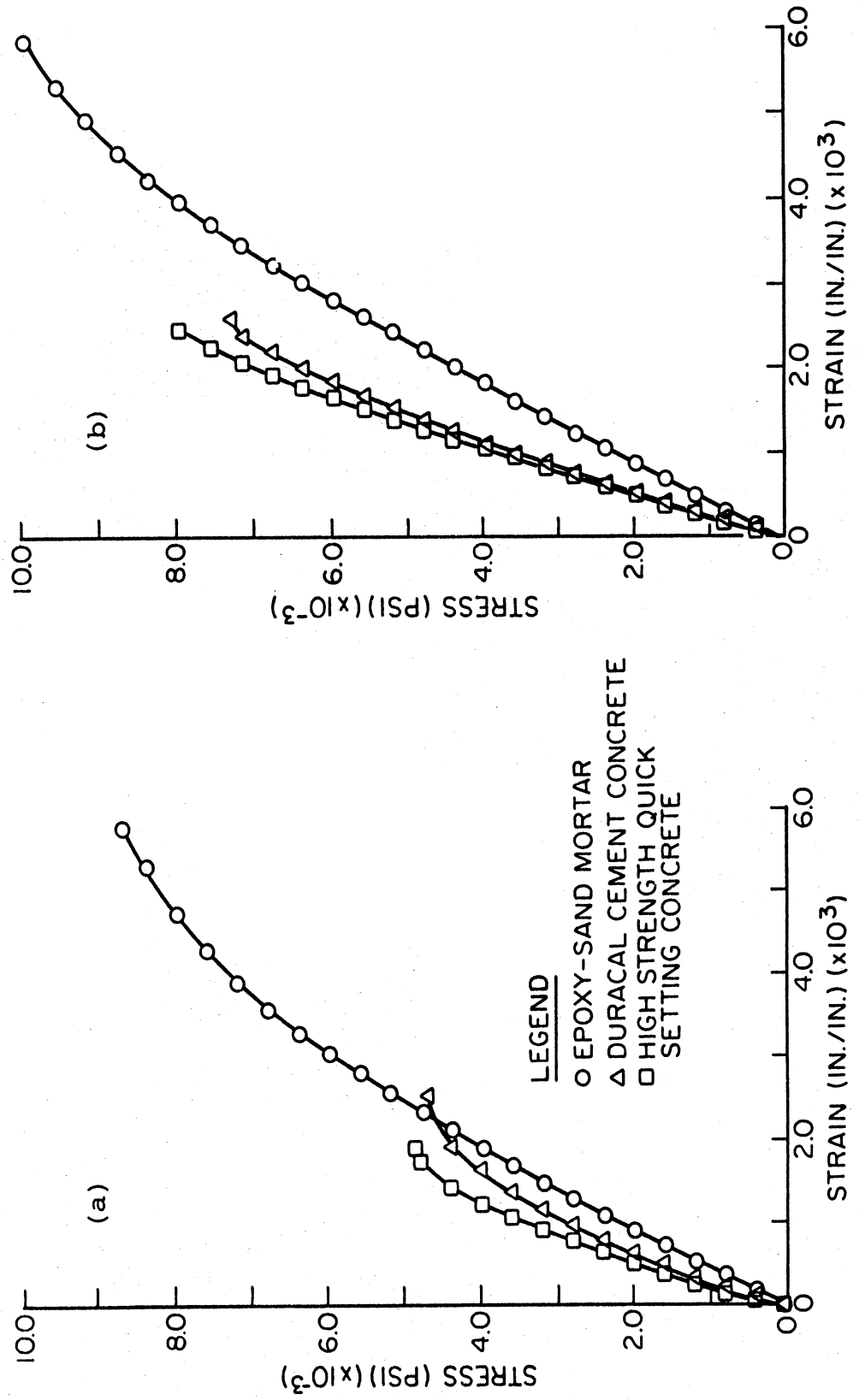

Fig. 4.5 Typical Stress-Strain Relationship for Repair Materials at Age (a) 3 Days and (b) 27 Days

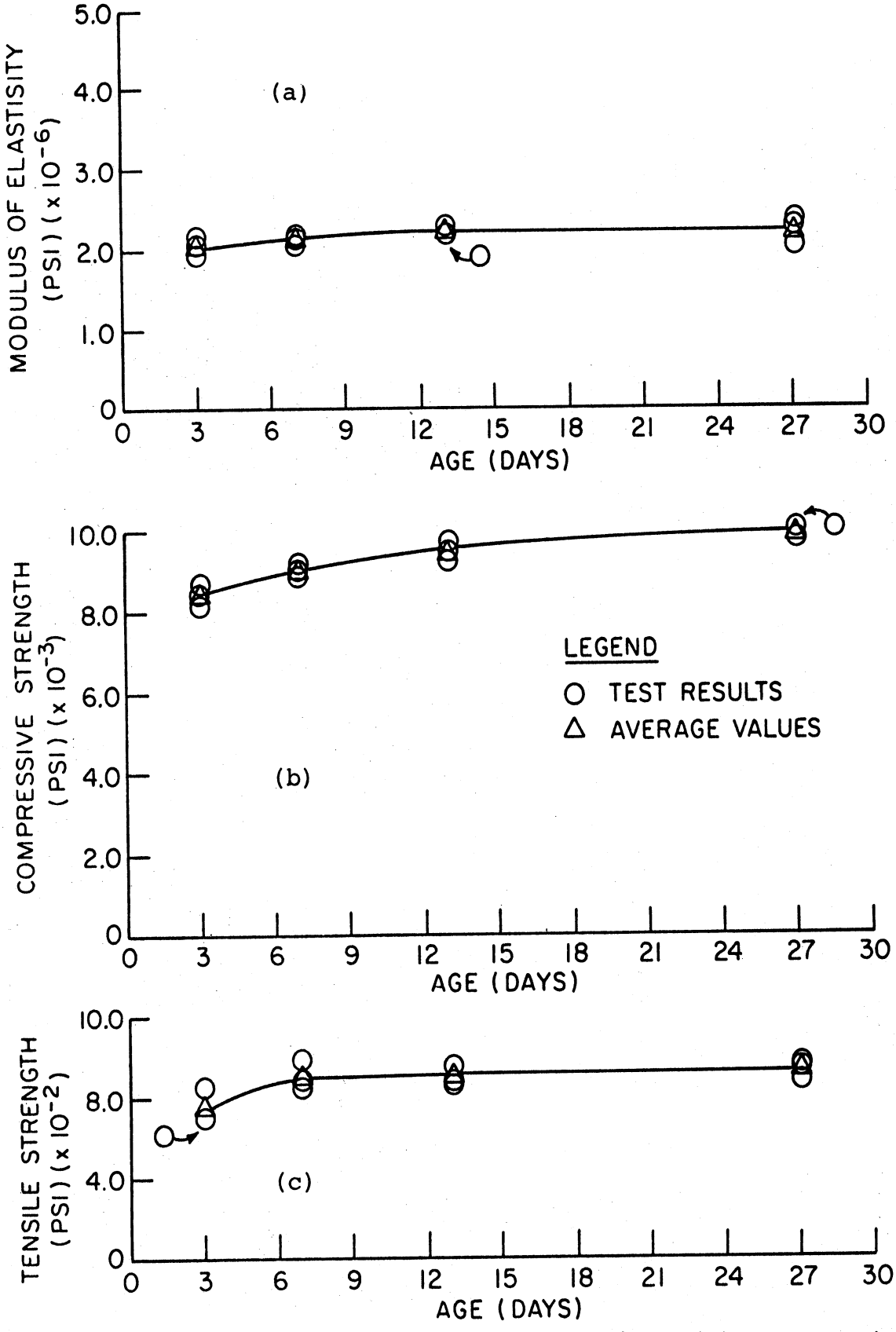

Fig. 4.6 Plot of (a) Modulus of Elasticity, (b) Compressive Strength, and (c) Tensile Strength with Age, Epoxy-Sand Mortar

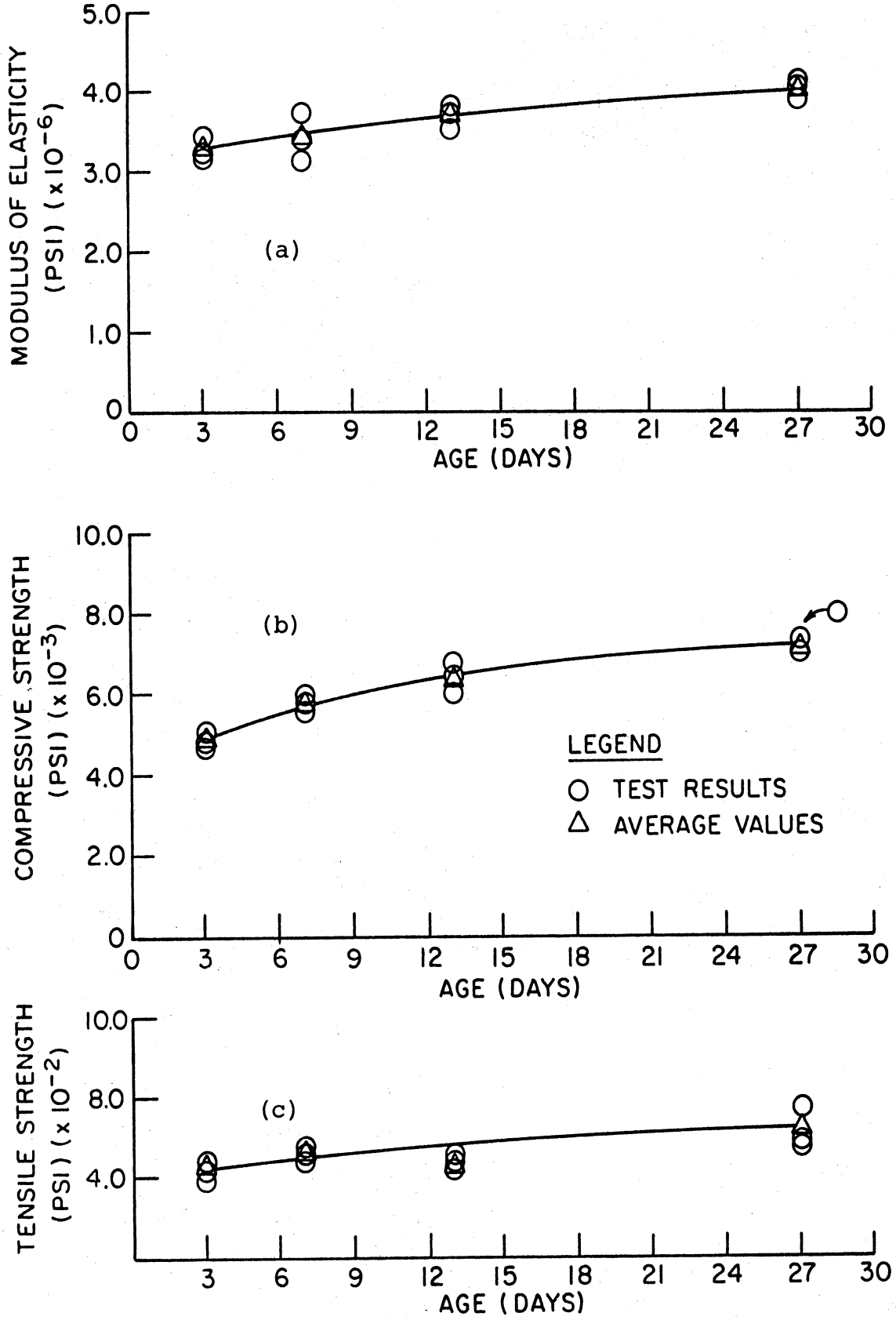

Fig. 4.7 Plot of (a) Modulus of Elasticity, (b) Compressive Strength, and (c) Tensile Strength with Age, Duracal Cement Concrete

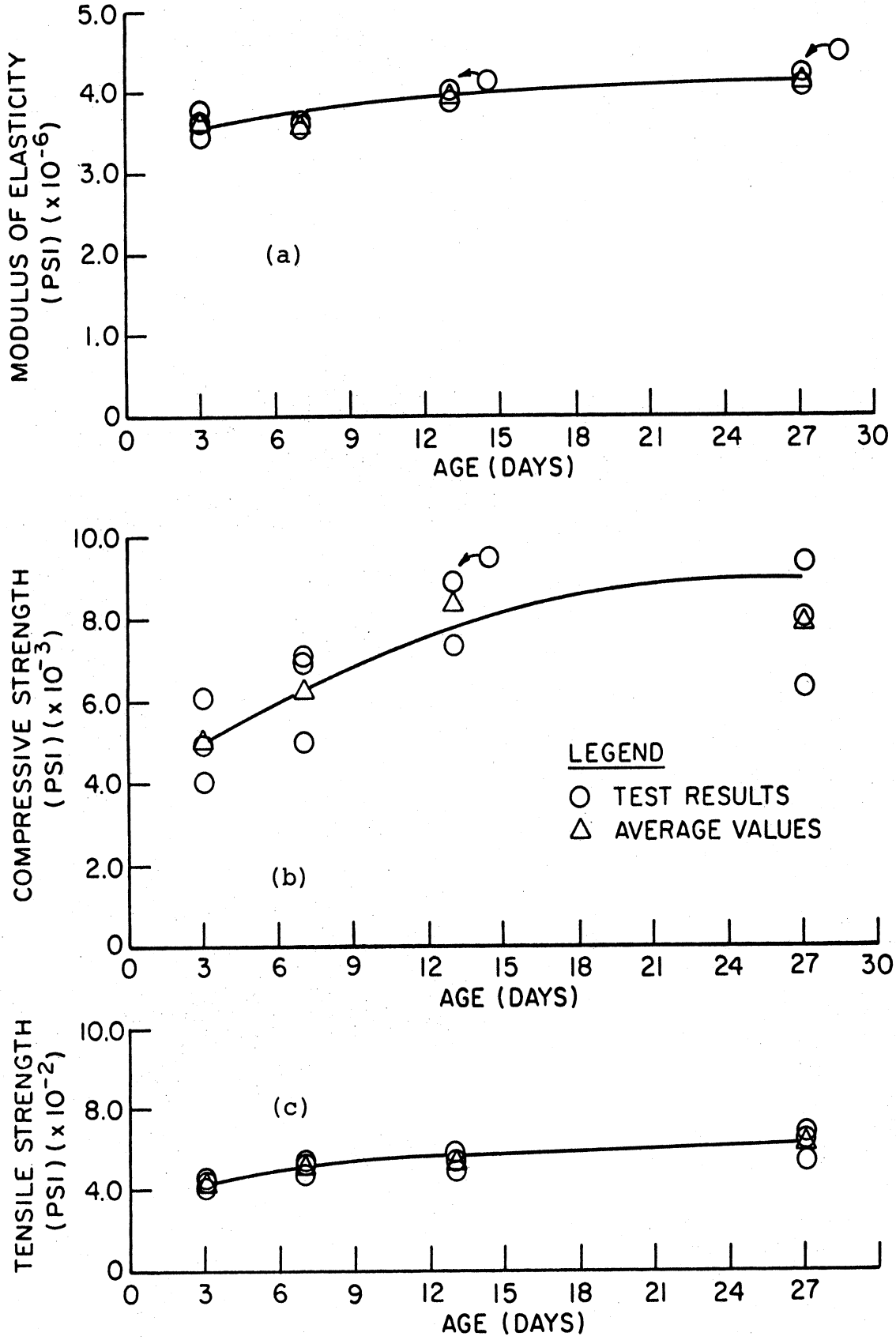

Fig. 4.8 Plot (a) Modulus of Elasticity, (b) Compressive Strength, and (c) Tensile Strength with Age, High Strength Quick Setting Concrete

Table 4.1 Average Stiffness and Strength Properties for Repair Materials

Material	3 Day Modulus of Elasticity (ksi)	27 Day Modulus of Elasticity (ksi)	3 Day Compressive Strength (psi)	27 Day Compressive Strength (psi)	3 Day Tensile Strength (psi)	27 Day Tensile Strength (psi)
Epoxy-Sand Mortar	2,000	2,200	8,400	9,900	740	920
Duracal Cement Concrete	3,200	4,000	4,800	7,200	430	630
High Strength Quick Setting Concrete	3,600	4,200	5,000	7,900	420	610
Sikadur Hi-Mod Epoxy	260 (i)	485 (i)	10,400 (i)	12,000 (i)	--	4,900 (ii)
High Early Strength Concrete	--	4,300 (iii)	--	7,000 (iii)	--	--

(i) Source: Sika Chemical Corporation (67).
(ii) From Sika Chemical Corporation (66), and was based on age 14 days.
(iii) Based on age 18 days.

with the cylinders being loaded at 2.5 psi per sec. as suggested by ASTM C496 (73) for regular concrete. The results of the splitting test are given in Figs. 4.6(c), 4.7(c), and 4.8(c) for the three materials. The average values are summarized in Table 4.1 for age 3 days and 27 days. The tensile strength for the epoxy-sand mortar, Duracal cement concrete, and high strength quick setting concrete increased 24 percent, 46 percent, and 45 percent respectively from age 3 days to 27 days.

The Sikadur Hi-Mod epoxy and the high early strength concrete were not investigated in this study at different ages for stiffness and strength. However, investigations by Sika Chemical Corporation (67) on the Sikadur Hi-Mod have shown that the stiffness and compressive strength increase about 86 percent and 15 percent respectively from age 3 days to 27 days as shown in Figs. 4.9(a) and 4.9(b) and indicated in Table 4.1. The results were based prism type specimens as suggested by ASTM D695 (71). Sika Chemical Corporation (66) also indicated the Sikadur Hi-Mod had a 14 day tensile strength of 4,900 psi which was based on coupon specimens loaded in direct tension as suggested by ASTM D638 (74). For the high early strength concrete, a compressive strength of 5,000 psi can be attained at age 7 days and the stiffness and tensile strength are similar to regular concrete.

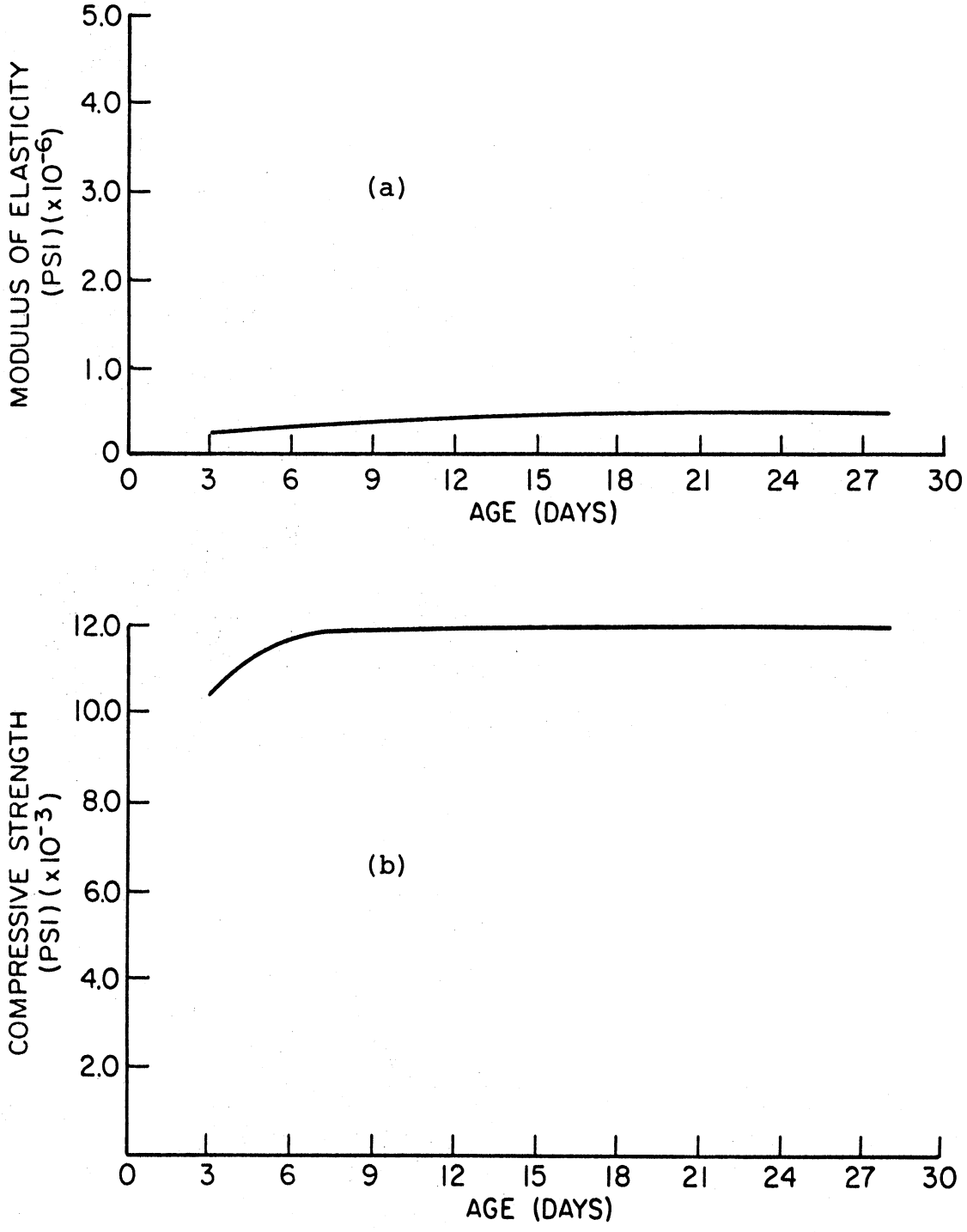

Fig. 4.9 Plot of (a) Modulus of Elasticity and (b) Compressive Strength with Age, Sikadur Hi-Mod Epoxy [From Sika Chemical Corporation (67)]

4.3.2 Long Term Loading

Standard 4 in. by 8 in. cylinders were used to investigate the long term (creep) behavior of the epoxy-sand mortar, the Duracal cement concrete and the high strength quick setting concrete. To measure the longitudinal deformation of the cylinder, gage points were located six in. apart on the side of the cylinders. A second set of gage points were located diametrically opposite to the first set. Each gage point consisted of a brass insert cast with the specimen and a center punched stainless steel screw. The gage points were manufactured by Soiltest, Inc., Evanston, Illinois.

At age three days, three sets of creep specimens were loaded to different stress levels. For the Duracal cement concrete and the high strength quick setting concrete, stress levels of 1,000 psi, 2,000 psi, and 3,000 psi were selected to represent 20 percent, 40 percent, and 60 percent of the three day compressive strength. For the epoxy-sand mortar, higher stress levels of 1,000 psi, 2,500 psi and 4,000 psi were used to represent corresponding loading levels for higher three day compressive strength. To determine shrinkage and environmental effects, a total of four control cylinders for each material were stored with the creep specimens.

The creep specimens were loaded in the stress racks shown in Fig. 4.10. During initial loading and reloading

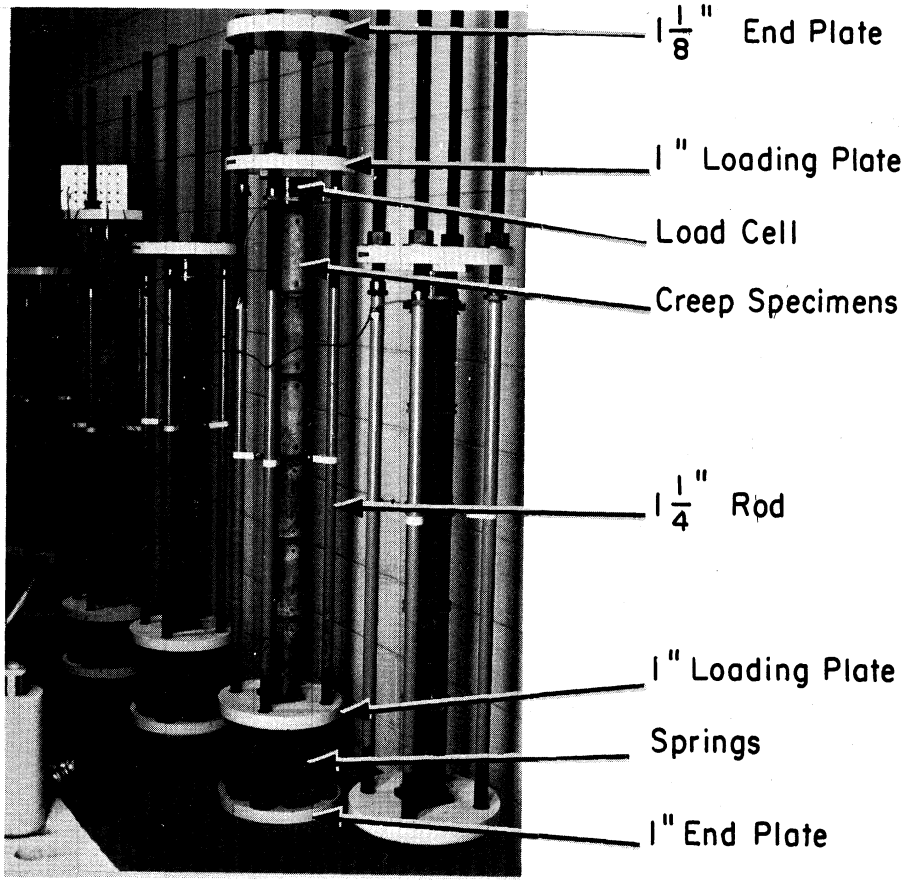

Fig. 4.10 Creep Specimens Loaded in Stress Racks

of the specimens, a 30 ton capacity hydraulic ram was placed between the one inch loading plate and the 1 1/8 in. end plate. The applied force was measured with a load cell and was checked by the pressure gage on the hydraulic pump. After reaching the desired load, the loading plate was fixed to serve as an end plate.

The relative movement of the gage points on the side of the cylinders were measured with a mechanical multi-position strain indicator capable of measuring movement to the nearest 0.0001 in. The indicator was manufactured

by Soiltest, Inc. Before measurements were made on the cylinders, the strain indicator was "zeroed" against an invar bar to eliminate the effects of the temperature on the indicator.

The schedule for measuring load and deformation of the cylinders are given in Table 4.2 and was similar to

Table 4.2 Data Acquisition Schedule for Creep Study

1. Before loading
2. After loading
3. Several hours after loading
4. Every day for the next week
5. Every fourth day for the next two weeks
6. Every week for the next month
7. Every two weeks for the next month
8. Once a month up to a year
9. Once every two months thereafter

to that suggested by ASTM C512 (75) to investigate the creep and shrinkage of concrete. Temperature and humidity measurements were continuously recorded during the first year of loading.

The initial and time dependent strains for the stressed specimens are shown in Figs. 4.11(a), 4.12(a) and 4.13(a) for each of the three materials. Each figure contains the data from three cylinders for each of the three different stress levels and each data point represents the average of the two sets of gage point readings from one cylinder. For the Duracal cement concrete and the high

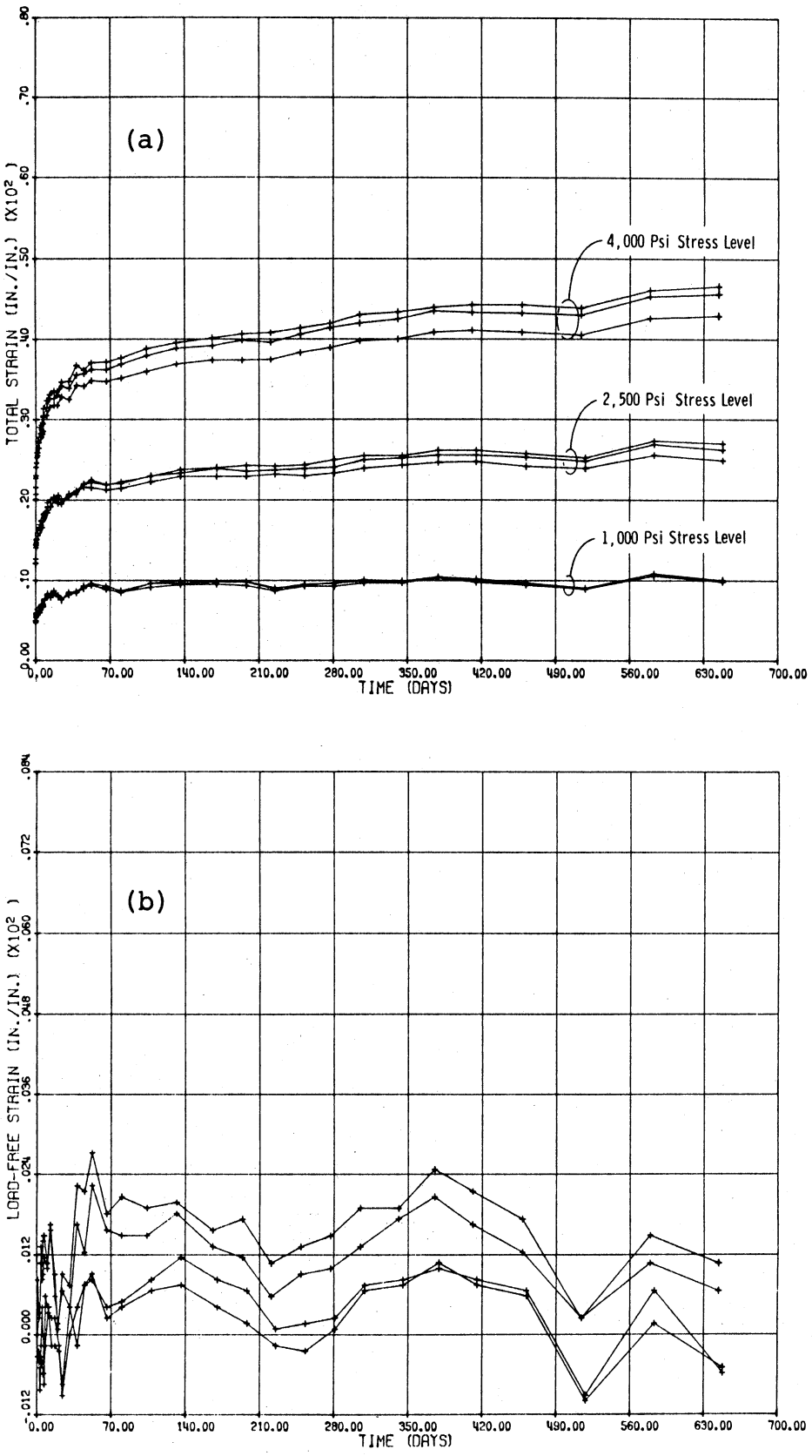

Fig. 4.11 Creep Test of Epoxy Sand Mortar (a) Total Strain and (b) Load-Free Strain with Time

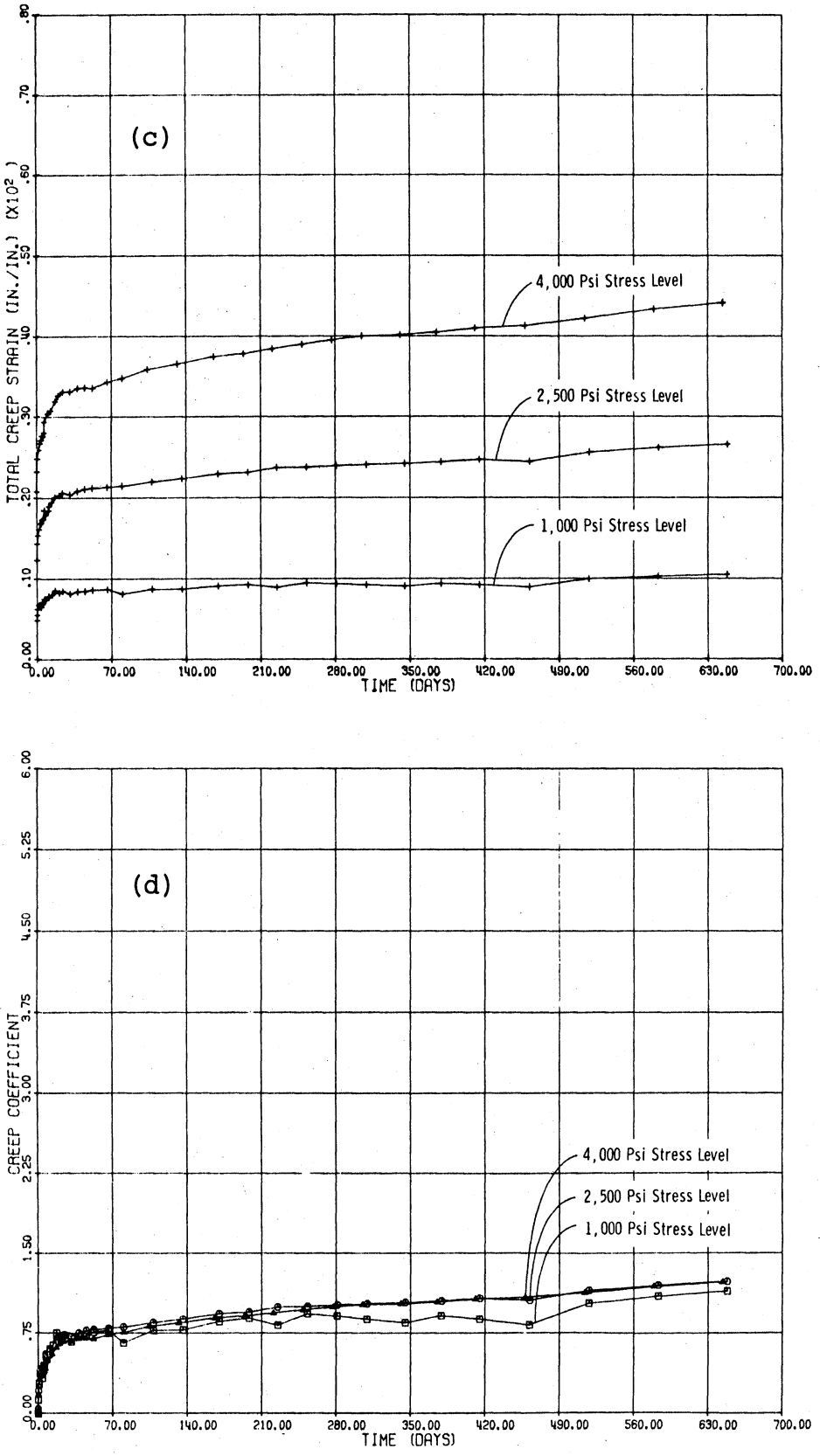

Fig. 4.11 (cont.) Creep Test of Epoxy-Sand Mortar (c) Total Creep Strain and (d) Creep Coefficient with Time

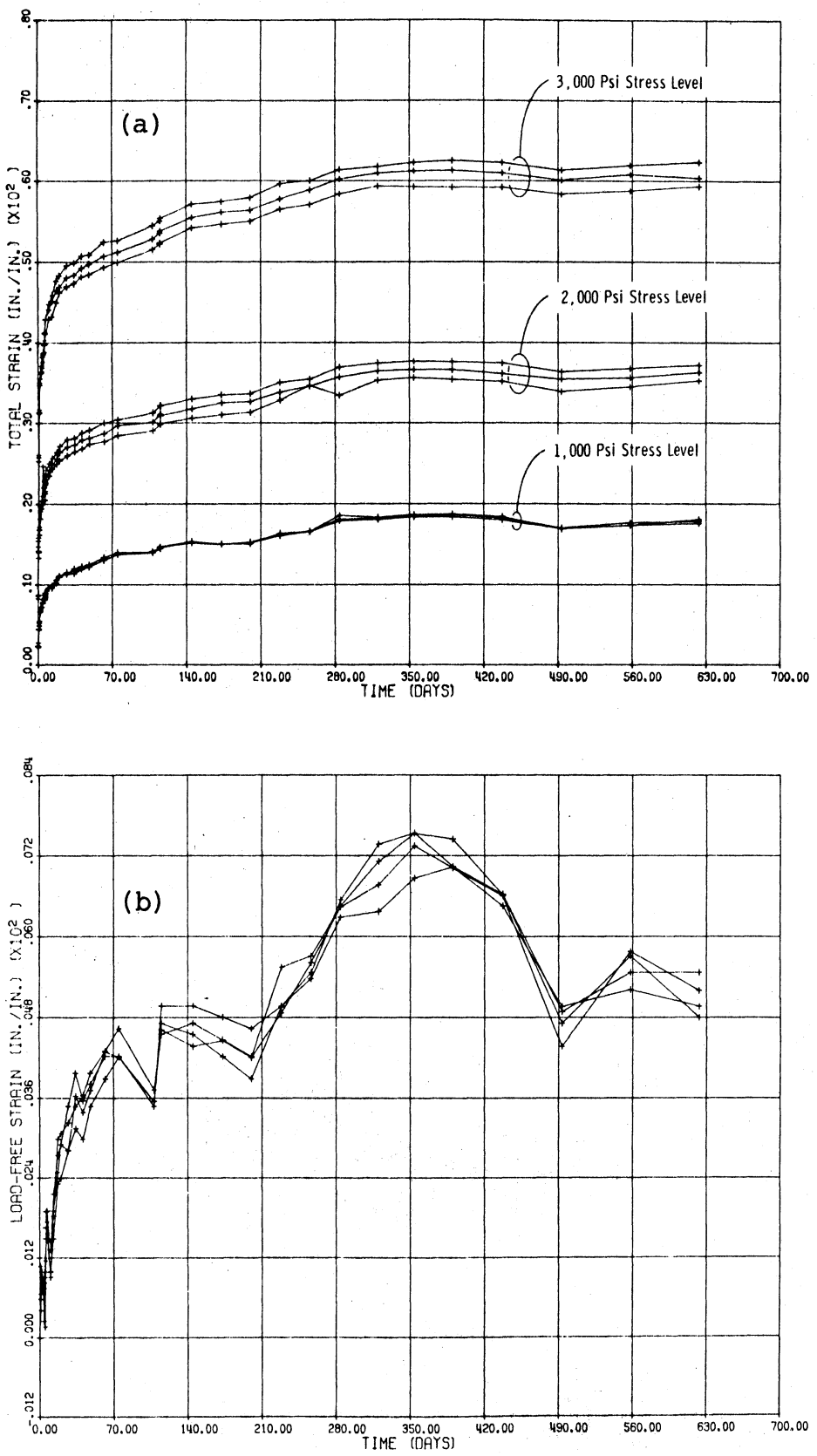

Fig. 4.12 Creep Test of Duracal Cement Concrete (a) Total Strain and (b) Load-Free Strain with Time

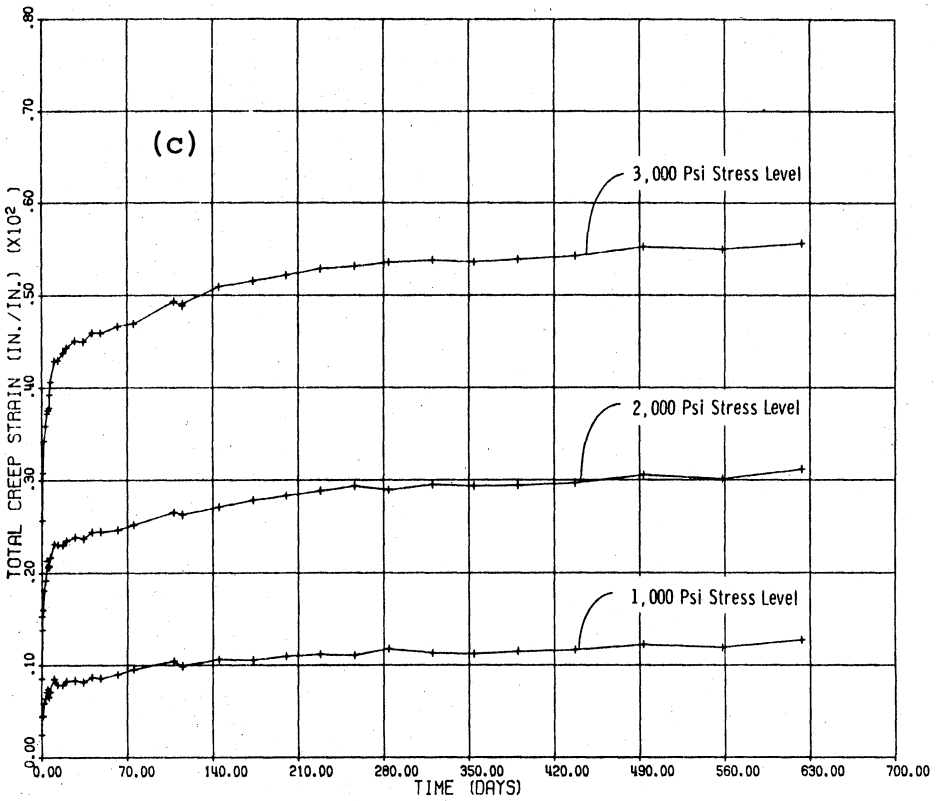

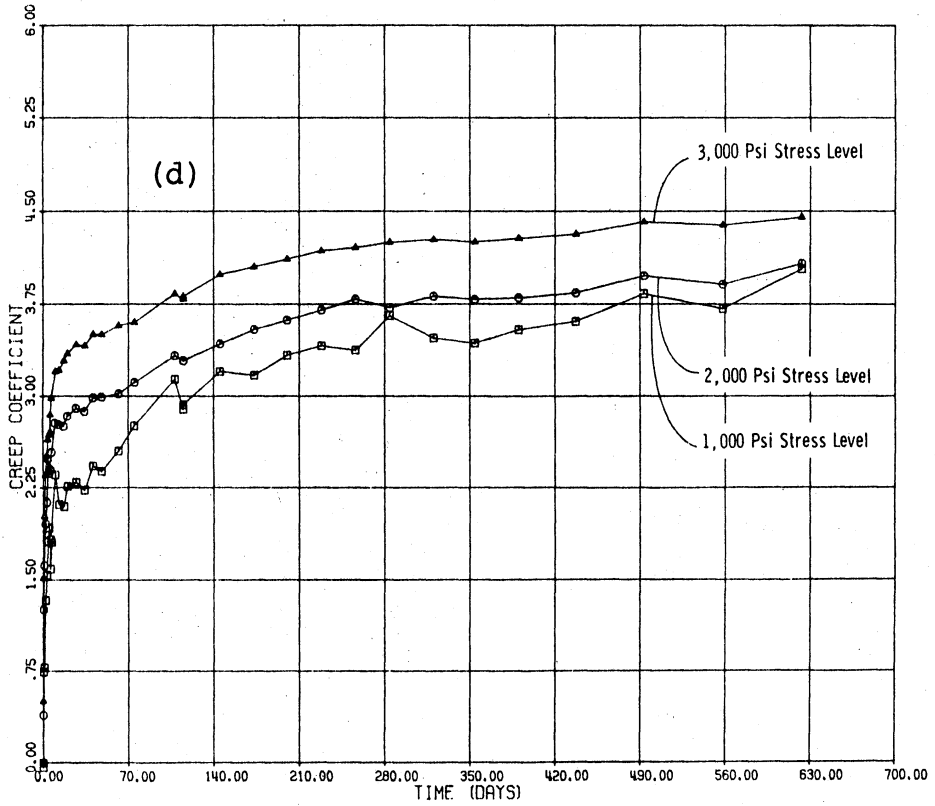

Table 4.12 (cont.) Creep Test of Duracal Cement Concrete (c) Total Creep Strain and (d) Creep Coefficient with Time

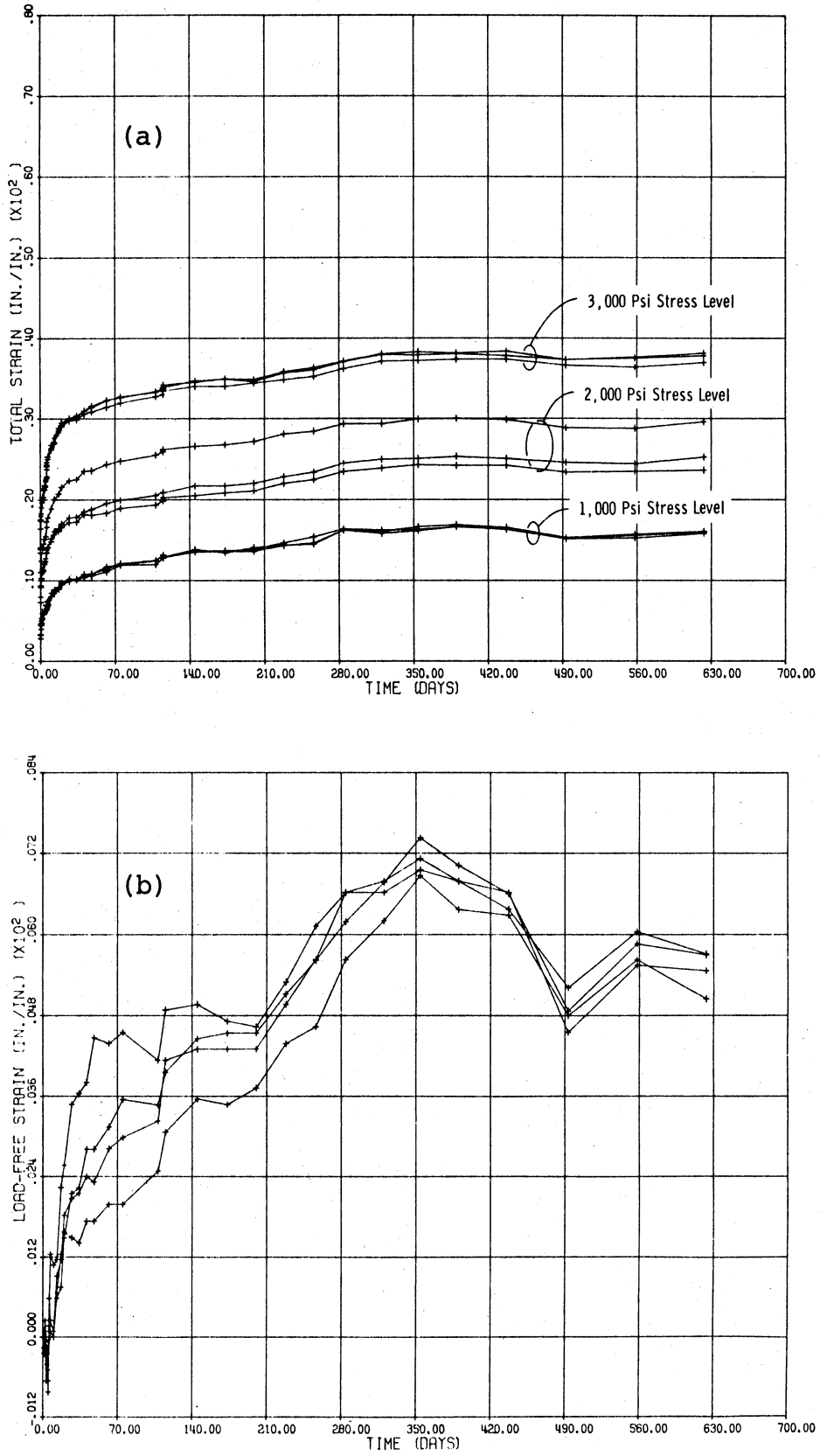

Fig. 4.13 Creep Test of High Strength Quick Setting Concrete (a) Total Strain and (b) Load-Free Strain with Time

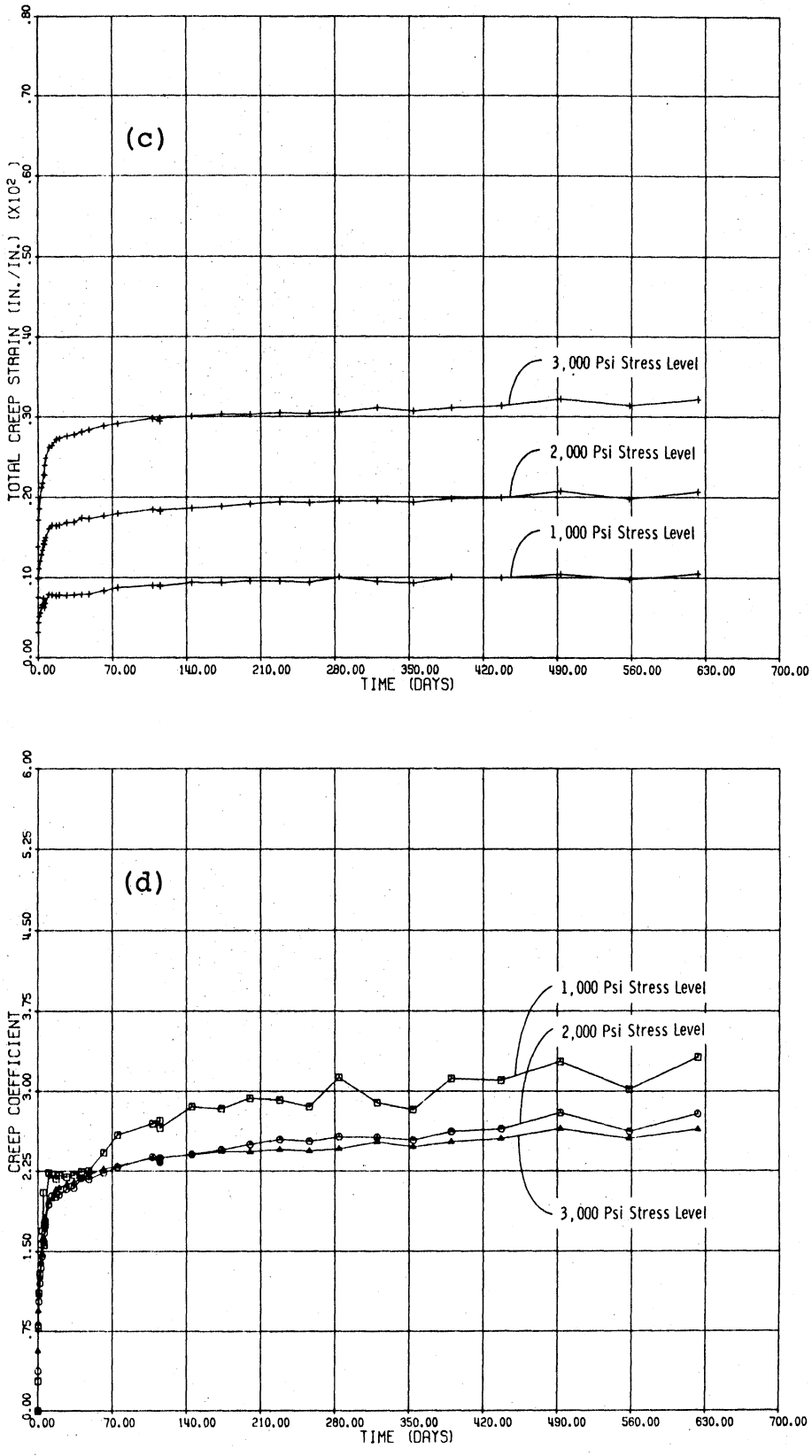

Fig. 4.13 (cont.) Creep Test of High Strength Quick Setting Concrete (c) Total Creep Strain and (d) Creep Coefficient with Time

strength quick setting concrete, the load was adjusted at 6 days and 115 days. The load was adjusted at 11 days for the two lowest stress levels and at 7 days for the highest stress level for the epoxy-sand mortar. The reduction in load before adjustment represented less than a 10 percent drop for all the materials.

The time dependent strains measured from the load-free specimens after age three days are shown in Figs. 4.11(b), 4.12(b), and 4.13(b) for each material. Each data point represented the average of the two sets of gage point readings from one cylinder. These strains include the shrinkage of the material as well as strains due to temperature and humidity effects. For the Duracal cement concrete and the high strength quick setting concrete, the maximum average strain based on four cylinders are given in Table 4.3. For the epoxy-sand mortar, the maximum

Table 4.3 Measured Maximum Load-Free Strains for Repair Material

Material	Load-Free Strain ($X10^{-6}$ in./in.)
Epoxy-Sand Mortar	247
Duracal Cement Concrete	732
High Strength Quick Setting Concrete	709
High Early Strength Concrete	415-1,000 (i)
Regular (Type I) Concrete	415-1,000 (i)

(i) Suggested by Meyers (55), and are ultimate shrinkage values starting from age 7 days.

average strain in Table 4.3 was based on two cylinders cast with the 4,000 psi creep specimens. (The other two cylinders were cast simultaneously with the 1,000 psi and 2,500 psi creep specimens.) These values may be used in calculations requiring an ultimate shrinkage strain.

The averaged strains from the load-free specimens were subtracted from the averaged strain for each stress level to obtain the initial and time dependent creep strains shown in Figs. 4.11(c), 4.12(c), and 4.13(c) for each of the materials. The epoxy-sand mortar exhibited linear visco-elastic behavior with respect to scaling as seen in Fig. 4.11(c). Scaling implies that if a stress is changed by factor α, the time dependent strains are also changed by the factor α.

To calculate the initial and time dependent creep coefficients, the initial strain was subtracted from the creep strain and the quantity divided by the initial strain. The initial strain values were obtained from the average of stress-strain curves from Sec. 4.3.1, one of which is shown in Fig. 4.5(a) for each material. The time dependent creep coefficient for each stress level are shown in Figs. 4.11(d), 4.12(d), and 4.13(d) for each of the materials. The creep coefficient at about 600 days for different stress levels are given in Table 4.4 for each of the materials investigated.

The Sikadur Hi-Mod epoxy and the high early strength concrete were not investigated for long term behavior.

Table 4.4 Experimental Creep Coefficients for Repair Material

Material	Stress Level (psi)	Time (Days)	Creep Coefficient
Epoxy-Sand Mortar	1,000	648	1.14
	2,500	648	1.23
	4,000	644	1.23
Duracal Cement Concrete	1,000	623	4.04
	2,000	623	4.08
	3,000	623	4.45
High Strength Quick Setting Cement	1,000	623	3.32
	2,000	623	2.79
	3,000	623	2.64
High Early Strength Concrete		ultimate	1.98-4.07 (i)
Regular (Type I) Concrete		ultimate	1.98-4.07 (i)

(i) Suggested by Meyers (55), and was based on loading at age 7 days.

For the Sikadur Hi-Mod epoxy, the amount of material used in repair applications such as epoxy injection is usually small. Therefore creep of the material does not seem to be an important factor in determining deflections. For the high early strength concrete, investigators (30) have found the ultimate creep coefficient based on loading at age of seven days is bounded by values of two and four.

4.3.3 Discussion of Material Behavior

The materials which were investigated and later used to repair the beam-column subassemblages showed high three

days compressive strength, especially the epoxy type materials. For the Duracal cement concrete and the high strength quick setting concrete, the stiffness and tensile strength were comparable to that of regular concrete. The epoxy-sand mortar had about half the stiffness of regular concrete and about twice the tensile strength. For the Sikadur Hi-Mod epoxy, which had high strengths, the low stiffness may not be critical if only small amounts of the material are used as in the injection technique.

From age 3 days to 27 days, the Duracal cement concrete and the high strength quick setting concrete did show an appreciable gain in stiffness and strength whereas the epoxy-sand mortar showed only a small increase as indicated in Table 4.1. The small increase in stiffness and strength implies that full loads can be applied to the epoxy-sand mortar earlier than for the other two materials.

The long term creep coefficients are given in Table 4.4 for the repair materials. For the Duracal cement concrete, the creep coefficient at age 623 days is somewhat higher than for regular concrete. However, it was felt that the creep coefficient can be reduced by delaying the age of loading to sometime later than three days. For the epoxy-sand mortar and high strength quick setting concrete, the creep coefficients are reasonable and are quite acceptable compared to regular concrete.

CHAPTER 5

BEHAVIOR OF REPAIRED SPECIMENS

5.1 Introductory Remarks

The beam-column specimens had been subjected to the loading parameters summarized in Table 2.1 to obtain different degrees of damage. After that original testing, the specimens were repaired in a upright position to simulate actual repair situations.

Specimens 1 and 3 after being damaged by the displacement pattern representing moderate earthquake loading [(Fig. 2.4(a)], were repaired by the epoxy injection technique. The details on this repair procedure were given in Sec. 4.2. Cracks smaller than about 0.01 in. in width, such as those in the joint, were not injected. Specimens 2, 4, and 6 through 8 were more severely damaged and were repaired by the removal and replacement technique described in Sec. 4.2. During repairs, additional stirrup-ties were added in the void area of the beam for Specimens 4, and 6 through 8, which had Type I Design. The additional stirrup-ties reduced the spacing from d/2 to d/4. This latter spacing satisfied ACI 318-71 requirements for shear and confinement. For Specimen 4, which was repaired with high strength quick setting concrete, sides of the void and the exposed reinforcement in the void were not sandblasted and painted with epoxy because of the good bonding characteristics of the repair material. However,

the sides of the void and the reinforcement were painted with activator solution just before placing the high strength quick setting concrete as suggested by Best (10). For Specimens 2, and 6 through 8, the void was sandblasted and then painted with Sikadur Hi-Mod epoxy before placing the new material. After repairs, the specimens were stored in the laboratory without special curing conditions, except for the high early strength concrete which was moist cured for three days. Specimen 5 was not repaired.

The repaired subassemblages were subjected to the same loading as summarized in the Table 2.1 for the retest so that a direct comparison with the original behavior could be made.

The material used in the repair of each specimen and their stiffness and compressive strength at the time of retest of the subassemblages are summarized in Table 5.1. These stiffness and compressive strengths are based on the average of two or more tests of 4 in. by 8 in. cylinders which were stored with the subassemblages. The compressive strengths of the repair materials were higher than for the original material which had a nominal strength of 4,000 psi.

5.2 Visual Observations

Observations made during the retest for each specimen are briefly described here.

Table 5.1 Repair Parameters and Strength Properties of Repair Material

Specimen	Repair Technique	Material	Age	Stiffness (ksi)	Compressive Strength (psi)
1	Epoxy Injection	Sikadur Hi-Mod	49	490 (i)	12,000 (i)
2	Removal and Replacement	High Early Strength Concrete	12	4,180	7,100
3	Epoxy Injection	Sikadur Hi-Mod	43	490 (i)	12,000 (i)
4	Removal and Replacement	High Strength Quick Setting Concrete	38	5,050	8,000
5	(Not Repaired)				
6	Removal and Replacement	High Early Strength Concrete	18	4,350	7,000
7	Removal and Replacement	Duracal Cement Concrete	15	3,470	6,000
8	Removal and Replacement	Epoxy-Sand Mortar	17	2,180	9,000

(i) Source: Sika Chemical Corporation (67).

Specimens 1 and 3. The epoxy injected cracks remained closed during the first cycle of loading. Unrepaired cracks opened and new cracks formed in the beam both within and adjacent to the repaired region. Little additional cracking occurred during subsequent cycles of loading. At the higher displacement level, the cracks became wider. No spalling occurred in the beam. The joint sustained no additional cracking during retest and no cracks were seen in the column.

Specimen 2. During the first quarter cycle of loading, cracking and spalling in the compression zone occurred in the region repaired with the high early strength concrete. Unrepaired cracks opened and new cracks were formed in the beam adjacent to the repaired region. After the first cycle, little additional cracking and spalling occurred during subsequent cycles of loading. The joint sustained no additional cracking during retest and no cracks were observed in the column. Figure 5.1 shows Specimen 2 after retest.

Specimen 4. During the first quarter cycle of loading, cracking and a sudden spalling in the compression zone occurred in the region repaired with the high strength quick setting concrete. Unrepaired cracks opened and new cracks were formed in the beam adjacent to the repaired region. After the first cycle, little additional cracking and spalling occurred during subsequent cycles of loading at

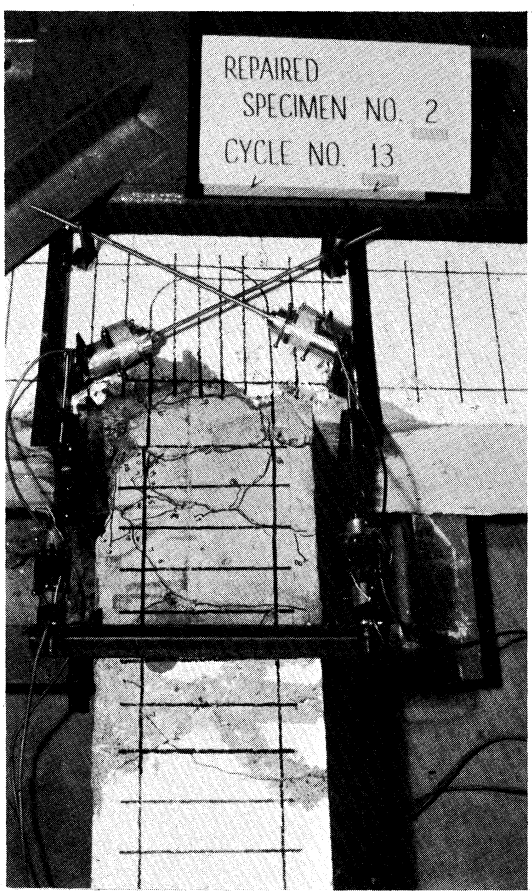

Fig. 5.1 Repaired Specimen 2 after Retest

the same displacement level. For cycles at the higher displacement level, shear slippage along vertical cracks in the repaired region was observed. Due to this slippage, additional cover was spalled off. For the remaining cycles at the lower displacement level, slipping and spalling continued in the beam. The joint sustained little additional cracking during retest and no cracks were seen in the column. Figure 5.2 shows Specimen 4 after retest.

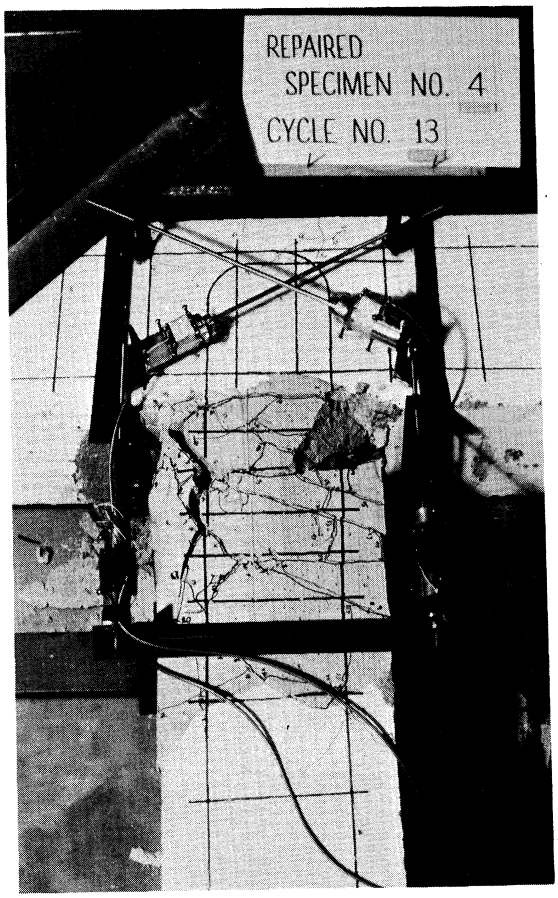

Fig. 5.2 Repaired Specimen 4 after Retest

Specimen 6. The region of the beam repaired with high early strength concrete sustained only minor cracking. A considerable amount of cracking occurred in the joint during retest as illustrated by comparing Figs. 5.3(a) and 5.3(b) after original testing and retest respectively. Slippage of the reinforcement anchored in the joint was observed during the cycles at the high displacement level and the slippage continued at the low displacement level. Cracks were observed in the column.

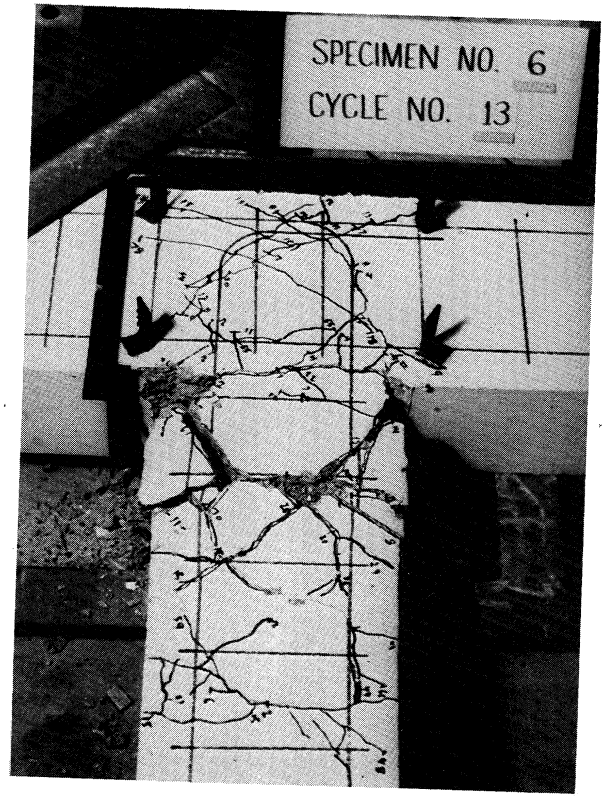

(a) Specimen 6 after Original Testing

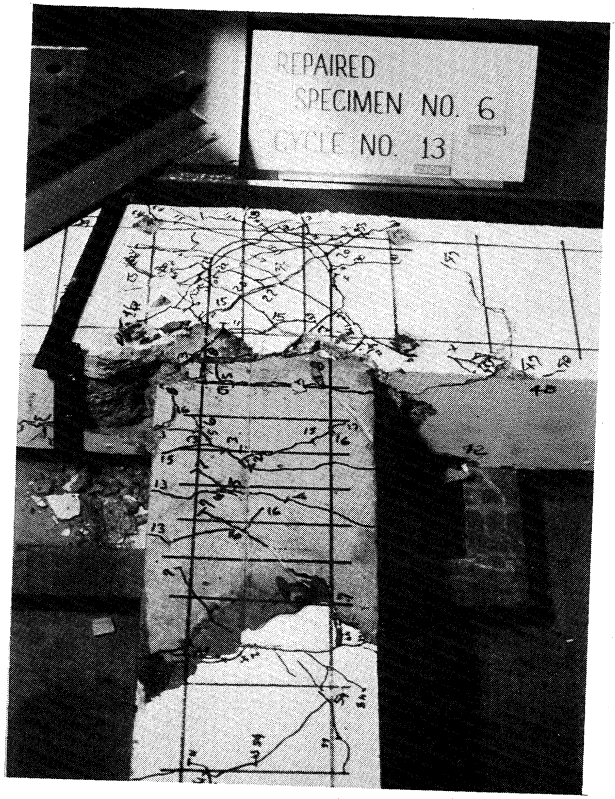

(b) Repaired Specimen 6 after Retest

Fig. 5.3 Comparison of Damage for Original and Repaired Specimen 6

Specimen 7. The beam was repaired with Duracal cement concrete in two lifts with the second lift being the top one in. of the beam. Cracking and spalling in the compression zone occurred in the repaired region during the first quarter cycle of loading. Unrepaired cracks opened and new cracks were formed in the beam adjacent to the repaired region. After the first cycle, little additional cracking and spalling occurred during subsequent cycles of loading at the same displacement level. At the higher displacement level, the first and second lifts of the repair material separated at the construction interface where Sikadur Hi-Mod epoxy was used to improve the bond. Further examination showed that the epoxy bonded only to the second lift. Shear slippage was observed along vertical cracks in the repaired region. Due to this slippage, additional cover was spalled off. For the cycles at the lower displacement level, the slipping and spalling continued in the beam. The joint sustained additional cracking during retest as seen by comparing Fig. 5.4 with Fig. 3.2(b) obtained after original testing. No cracks were observed in the column.

Specimen 8. The region in the beam repaired with epoxy-sand mortar sustained only cracking. Cracks were concentrated at the beam-to-column interface adjacent to the repaired region as seen in Fig. 5.5. Shear slippage was observed along these cracks during load reversals. The joint sustained additional cracking during retest. A longitudinal crack was observed in the column.

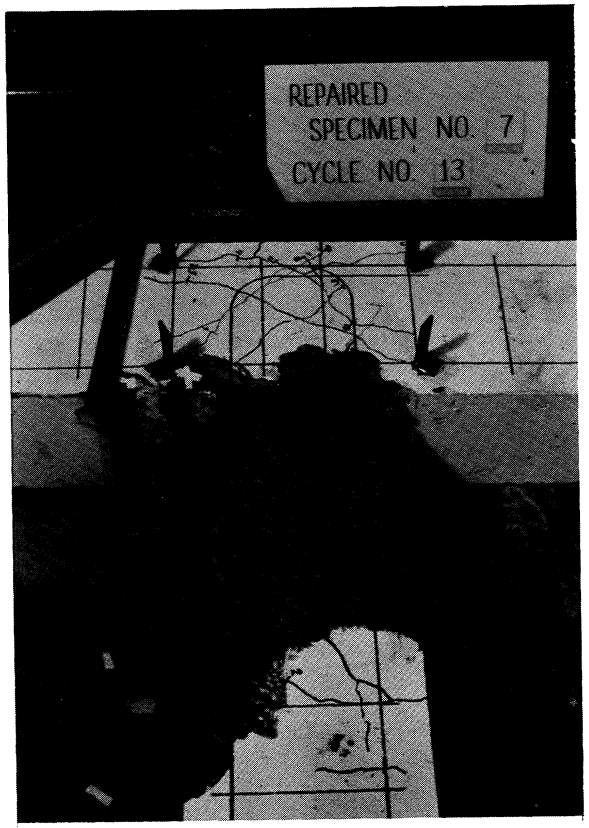

Fig. 5.4 Repaired Specimen 7 after Retest

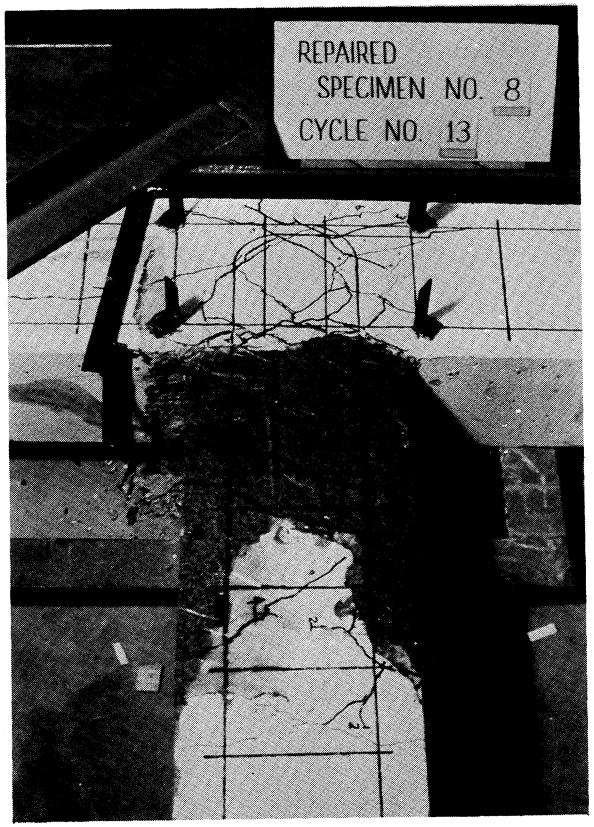

Fig. 5.5 Repaired Specimen 8 after Retest

For specimens where Sikadur Hi-Mod epoxy was used during repairs to improve the bond between the existing surfaces and the new material, no concrete was found bonded to the exposed reinforcement after retest. Instead, the longitudinal and transverse reinforcement were smooth. This observation questions the effectiveness of the epoxy to improve the bond when the bonded materials are subjected to large strain reversals.

None of the longitudinal or transverse reinforcement fractured during retesting of the subassemblages.

5.3 Measured Force and Deflection

The beam-tip force vs deflection curves are given in Figs. 5.6(a) through 5.6(g) for repaired Specimens 1 through 4, and 6 through 8. During the first quarter cycle of loading, the specimens initially exhibited almost linear behavior followed by a reduction in stiffness which was attributed primarily to the yielding of the beam top reinforcement. Specimens 2, 4, and 7 showed a decrease in load during the first quarter cycle of loading as a result of the concrete crushing in the beam compression zone. For the remainder of the first cycle and for subsequent cycles of loading, the force-deflection curves were similar in shape to those obtained during original testing after the first cycle.

The force-deflection curves demonstrated behavior ranging from that of flexural distress in the beam for Specimen

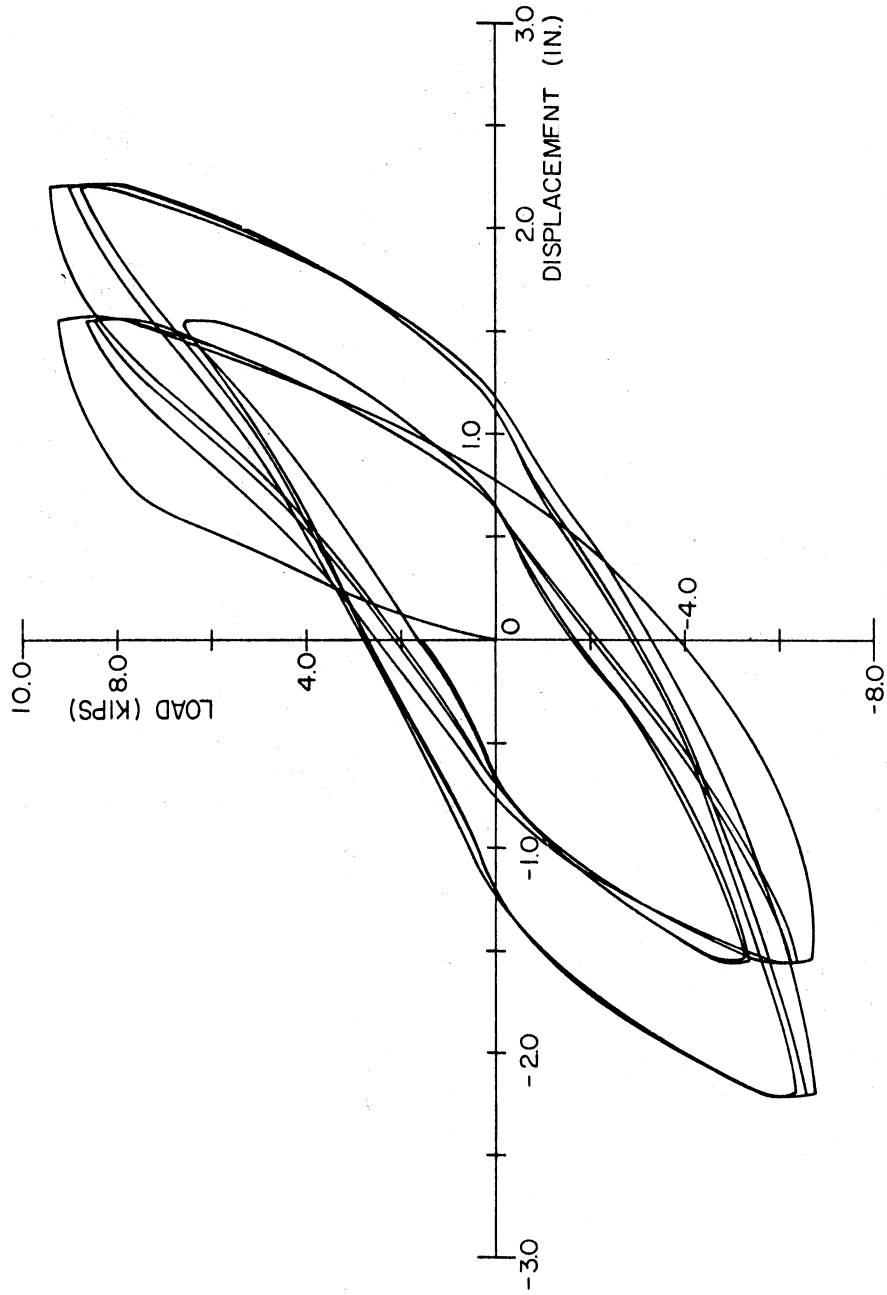

Fig. 5.6(a) Beam-Tip Force-Deflection Curves, Repaired Specimen 1

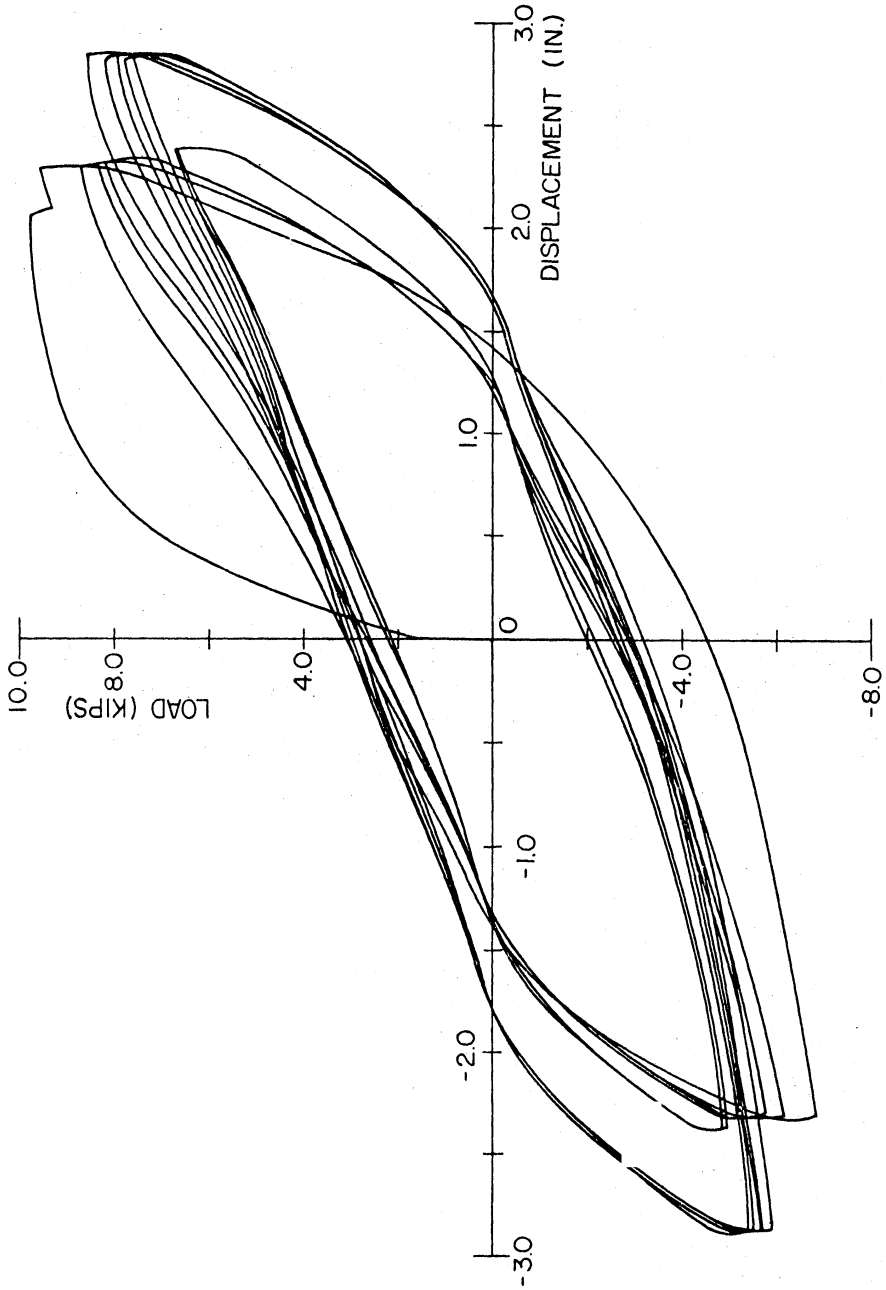

Fig. 5.6(b) Beam-Tip Force-Deflection Curves, Repaired Specimen 2

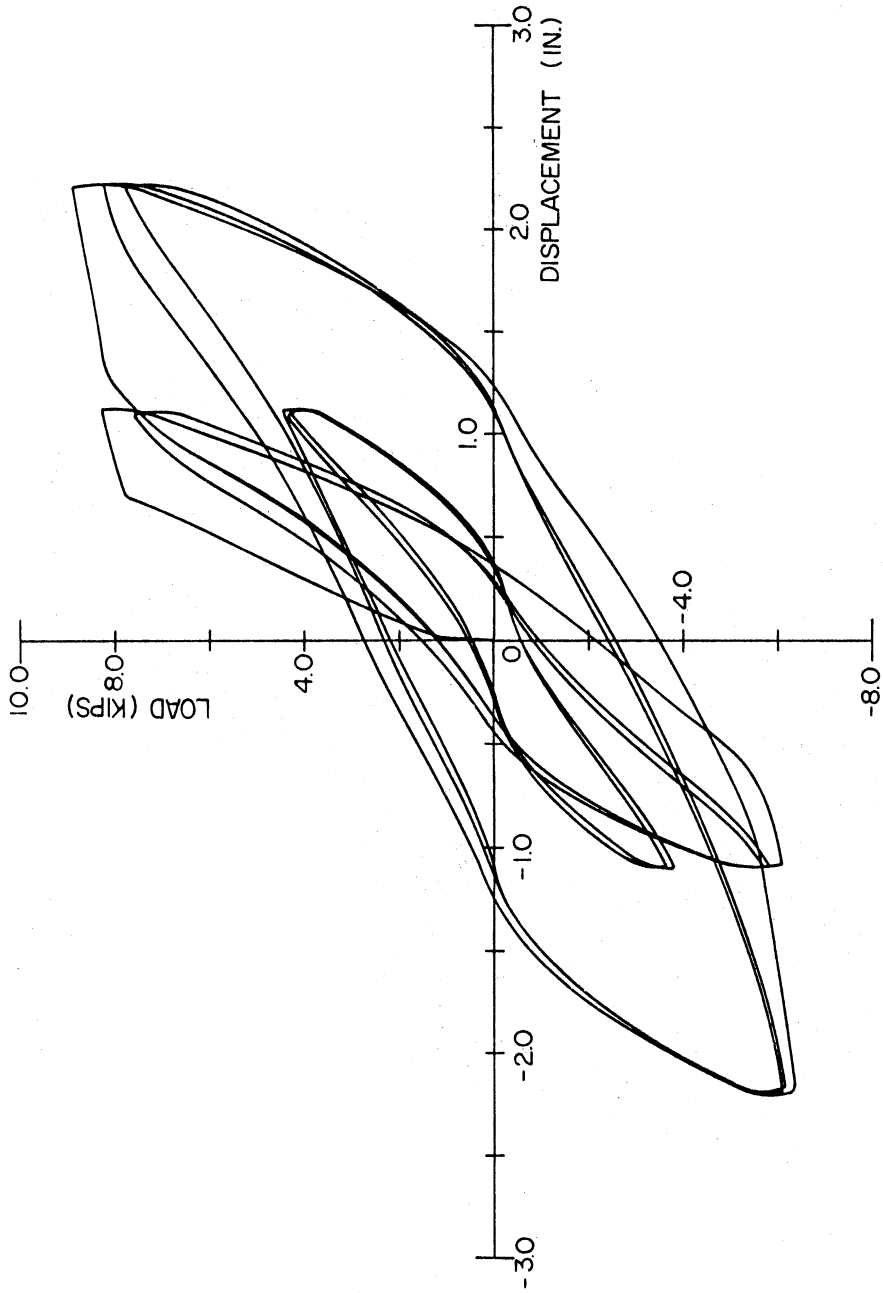

Fig. 5.6(c) Beam-Tip Force-Deflection Curves, Repaired Specimen 3

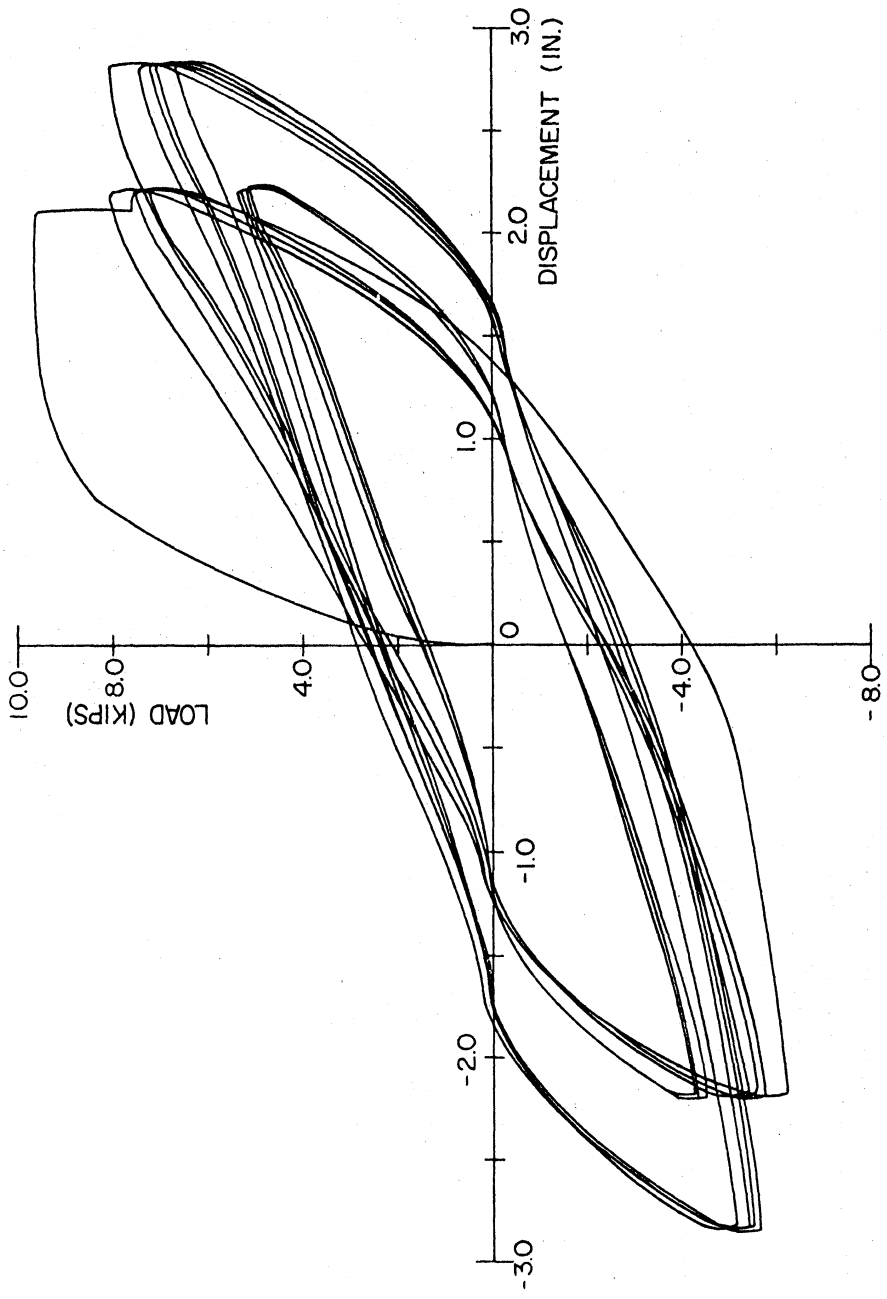

Fig. 5.6(d) Beam-Tip Force-Deflection Curves, Repaired Specimen 4

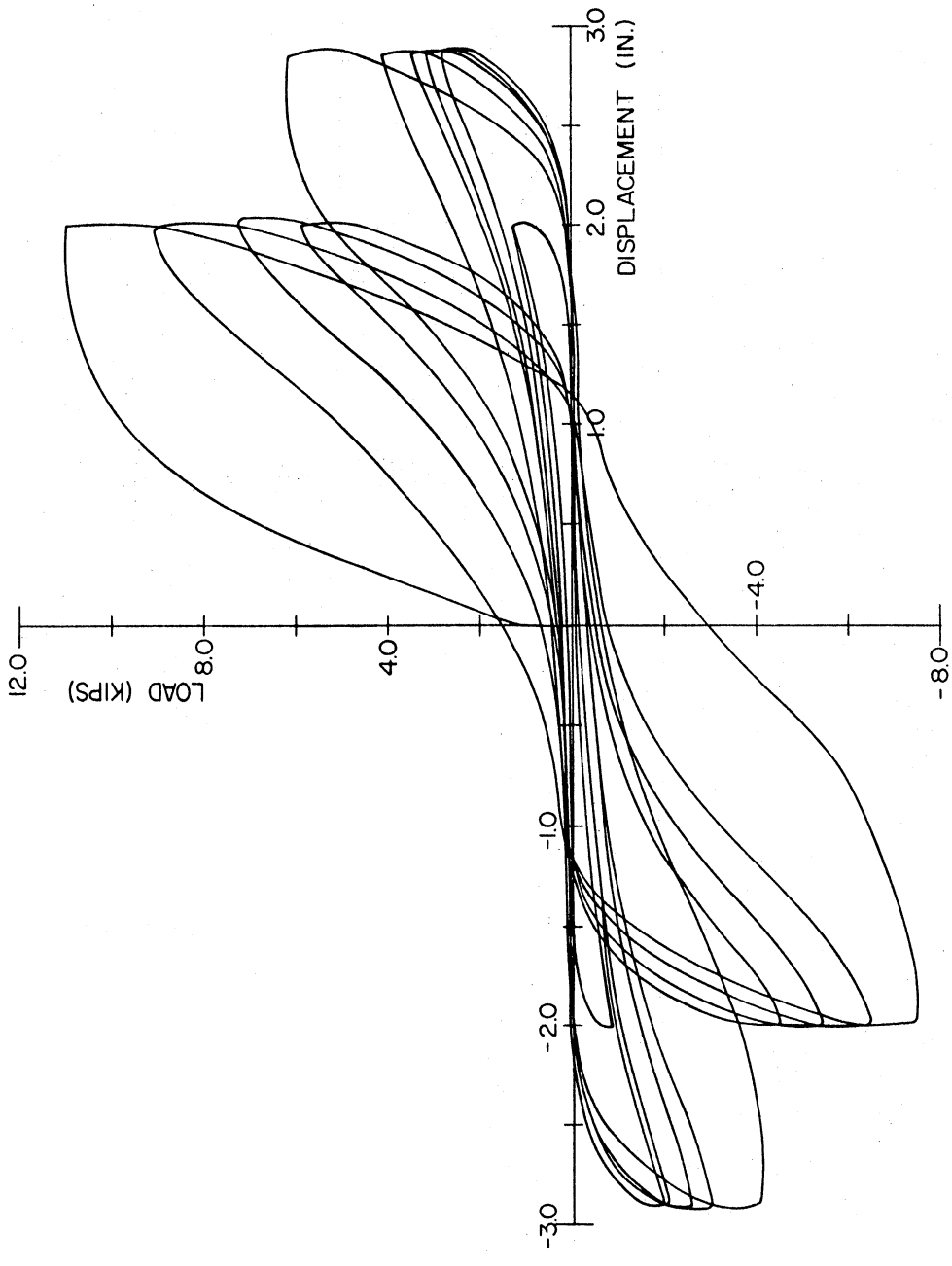

Fig. 5.6(e) Beam-Tip Force-Deflection Curves, Repaired Specimen 6

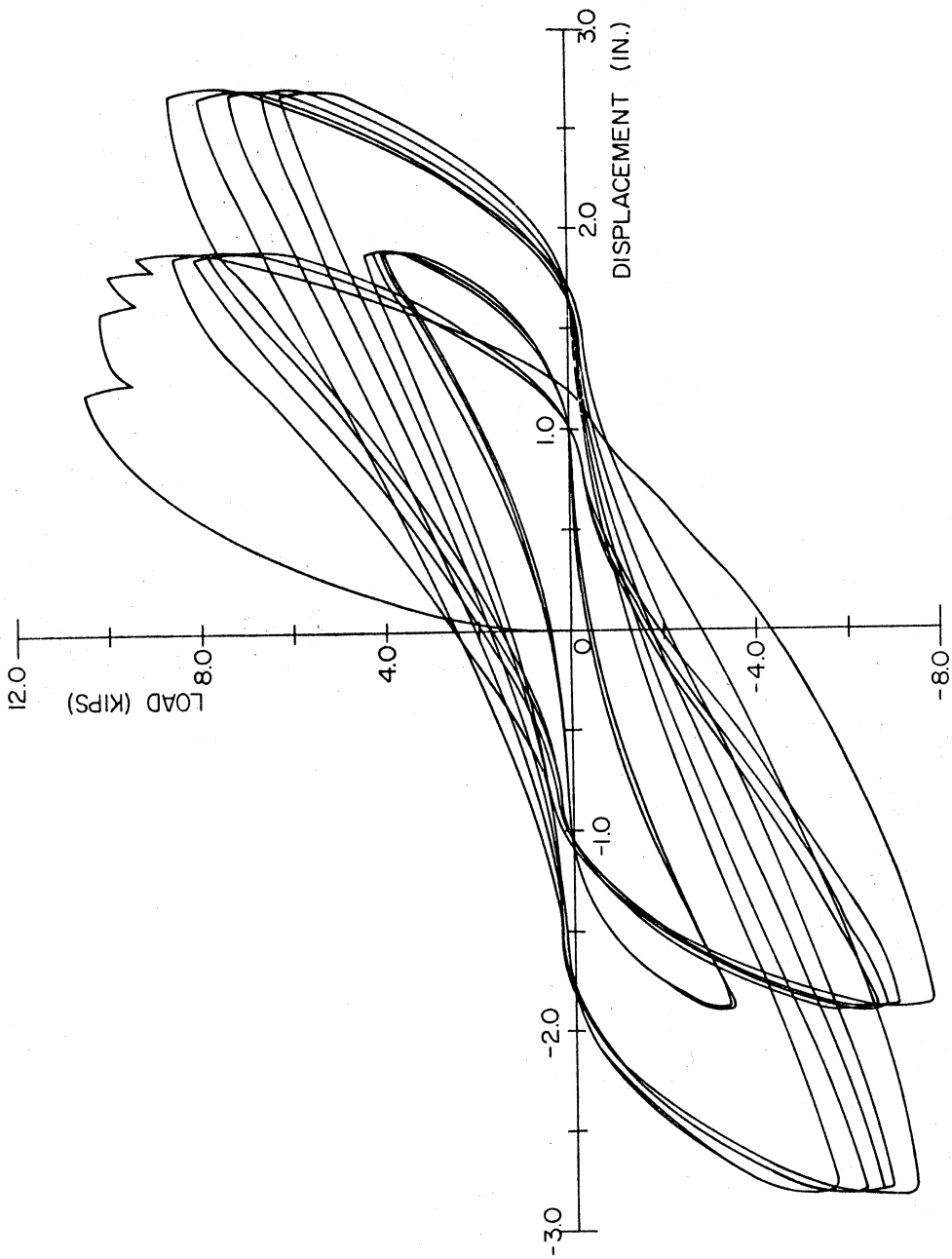

Fig. 5.6(f) Beam-Tip Force-Deflection Curves, Repaired Specimen 7

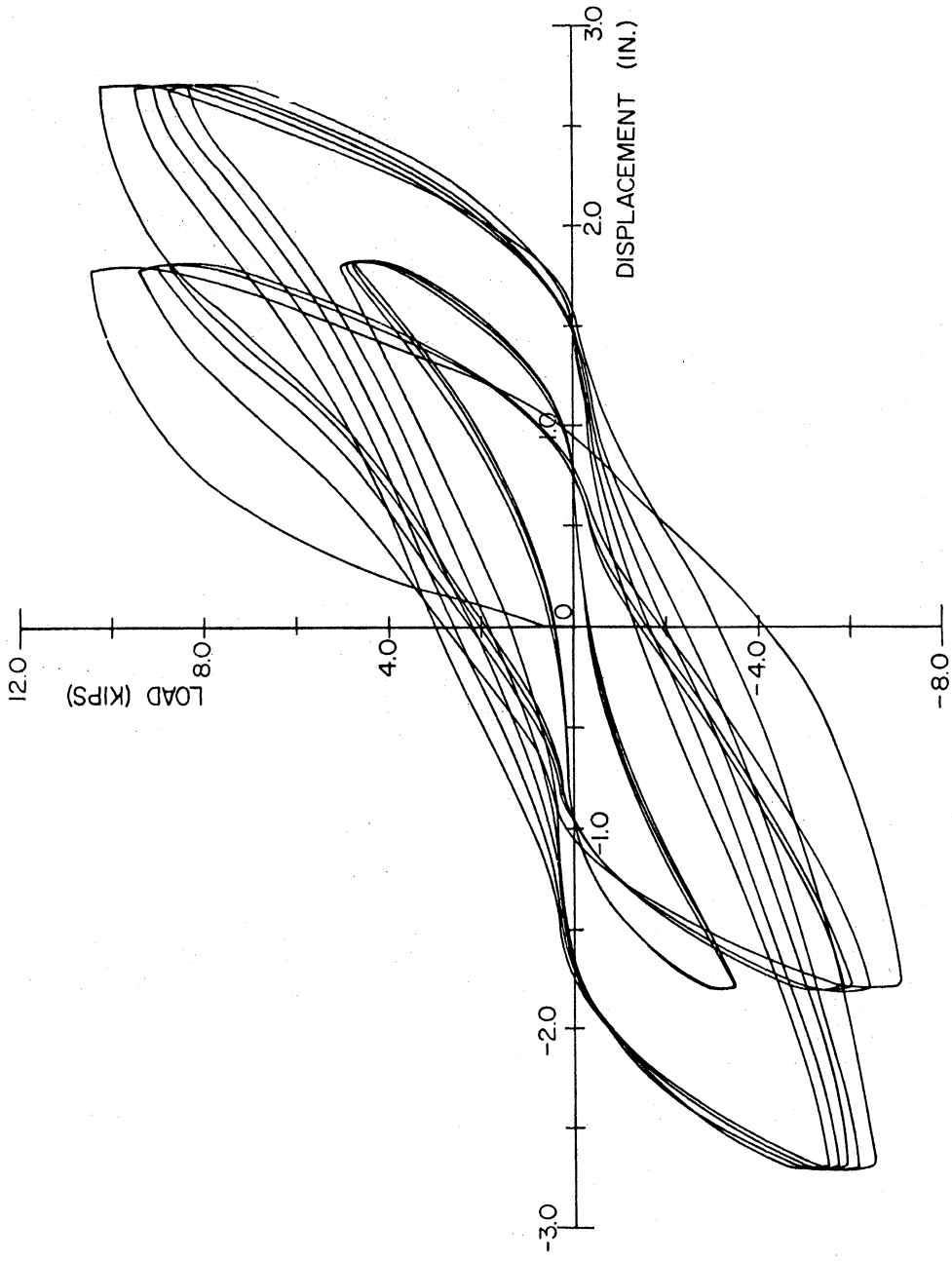

Fig. 5.6(g) Beam-Tip Force-Deflection Curves, Repaired Specimen 8

2 as in Fig. 5.6(b) to shear and anchorage distress in the joint for Specimen 6 as in Fig. 4.6(e). The flexural type behavior in the beam was more stable from cycle to cycle.

The initial stiffness from the first quarter cycle on the force-deflection curve is given in Table 5.2 for all

Table 5.2 Secant Stiffness Modulus of Subassemblages During First Loading

Specimen	Stiffness (kip/in.)	
	Original	Repaired
1	11.3	10.3
2	10.3	11.3
3	9.5	9.8
4	10.4	10.5
5	12.6	--
6	13.2	11.3
7	13.0	11.7
8	12.0	12.3

the repaired specimens. The stiffness was based on the secant modulus between beam-tip deflections of 0.10 in. and 0.40 in. The initial stiffness of the repaired specimen was almost the same as that for the original specimen.

The peak-to-peak loads at the maximum beam deflections, the energy dissipated, and the cumulative energy dissipated are compared with the original behavior for each cycle of loading in Figs. 3.6(a) through 3.6(d) and Figs. 3.6(f) through 3.6(h) respectively for Specimens 1 through 4 and 6 through 8. The peak-to-peak loads were consistantly higher for the repaired specimens as compared

to the original specimens, except for Specimen 6. The higher peak-to-peak loads were attributed to higher stresses in the beam longitudinal reinforcement during retest. The higher stresses occurred because the longitudinal reinforcement was strained further into the strain hardening range. Figure 3.6 shows that repaired Specimens 1 through 4 dissipated just as much energy as the original specimens. However, repaired Specimen 6 through 8 dissipated less energy than the original specimens with Specimen 6 being the extreme case.

The peak-to-peak loads and the energy dissipated were less for repaired Specimen 6 because the primary damage occurred in the joint during retest. Damage in the joint enabled the reinforcement anchored in the joint to slip during cyclic type loading. For Specimens 7 and 8 which sustained less cracking in the joint after original testing as compared to Specimen 6, the lower energy dissipated during retest was attributed to both the shear slippage in the beam and the increase in slippage of the reinforcement anchored in the joint.

5.3 Measured Distortion in Joint

The joint distortion is plotted with beam deflection in Figs. 5.7(a) and 5.7(b) for repaired Specimens 2 and 6 respectively. The peak-to-peak distortions at maximum beam deflection for each cycle of loading are plotted in Figs. 5.8(a) and 5.8(b) for Specimens 2 and 6 respectively.

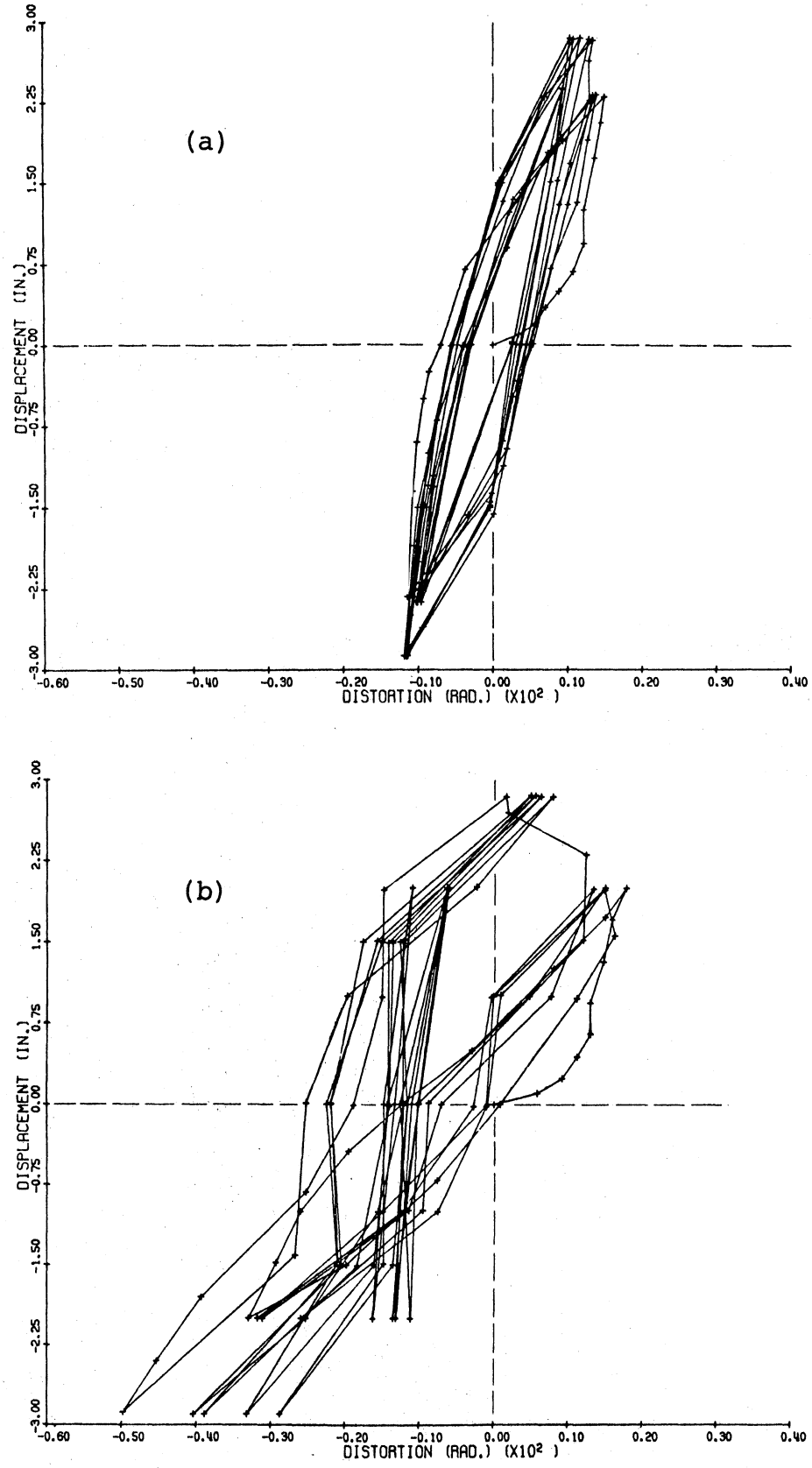

Fig. 5.7 Plot of Joint Distortion with Beam-Tip Deflection for (a) Repaired Specimen 2 and (b) Repaired Specimen 6

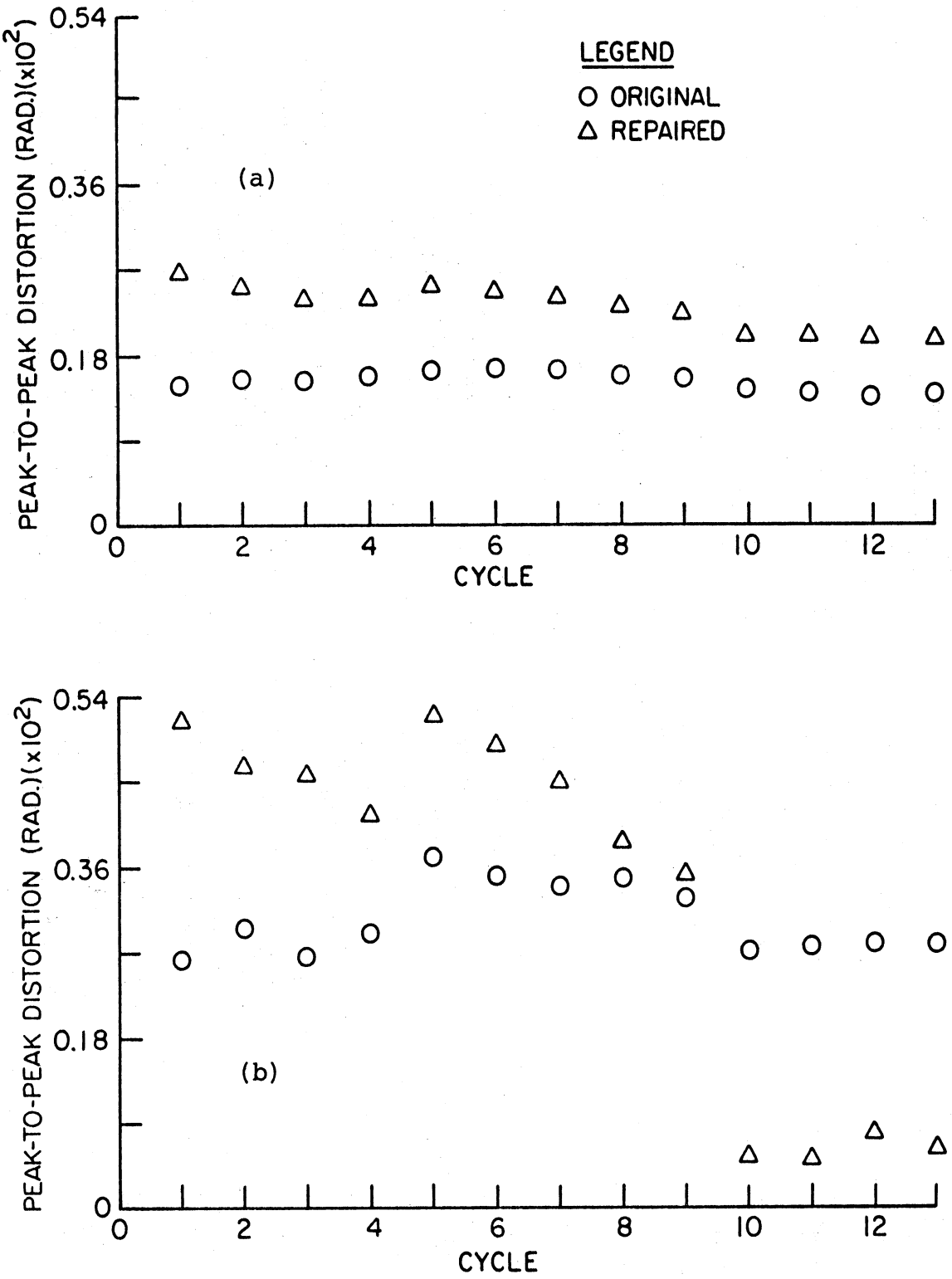

Fig. 5.8 Comparison of Peak-to-Peak Joint Distortion for (a) Specimen 2 and (b) Specimen 6

Compared with the original tests, the repaired specimens show more joint distortion except for the last four cycles for Specimen 6, at which time the joint had been severely cracked and the beam reinforcement anchored in the joint slipped. Specimens 1, 3, 4, 7, and 8 also had more distortion in the joint during retest as compared to original testing. This increase in distortion for the repaired specimens was attributed to the increase in shear in the joint resulting from the higher peak-to-peak applied beam force.

5.4 Measured Rotation in Beam

The beam rotation at a section 10 in. from the inside column face, measured relative to the column face, is plotted with beam force and deflection for repaired Specimens 1 and 2 in Figs. 5.9(a), 5.9(b), 5.10(a) and 5.10(b). As in the force vs deflection curves for the repaired specimens, distinct yield rotation is not observed during the first quarter cycle of loading in Figs. 5.9(a) and 5.10(a).

The peak-to-peak relative beam rotations for repaired Specimens 1 and 2 are plotted for each cycle of loading in Figs. 5.11(a) and 5.11(b) respectively and are compared with the rotations from the original tests. The rotations are less for the repaired specimens. The decrease in relative beam rotation is primarily attributed to the absence of the yielding plateau on the stress-strain curve

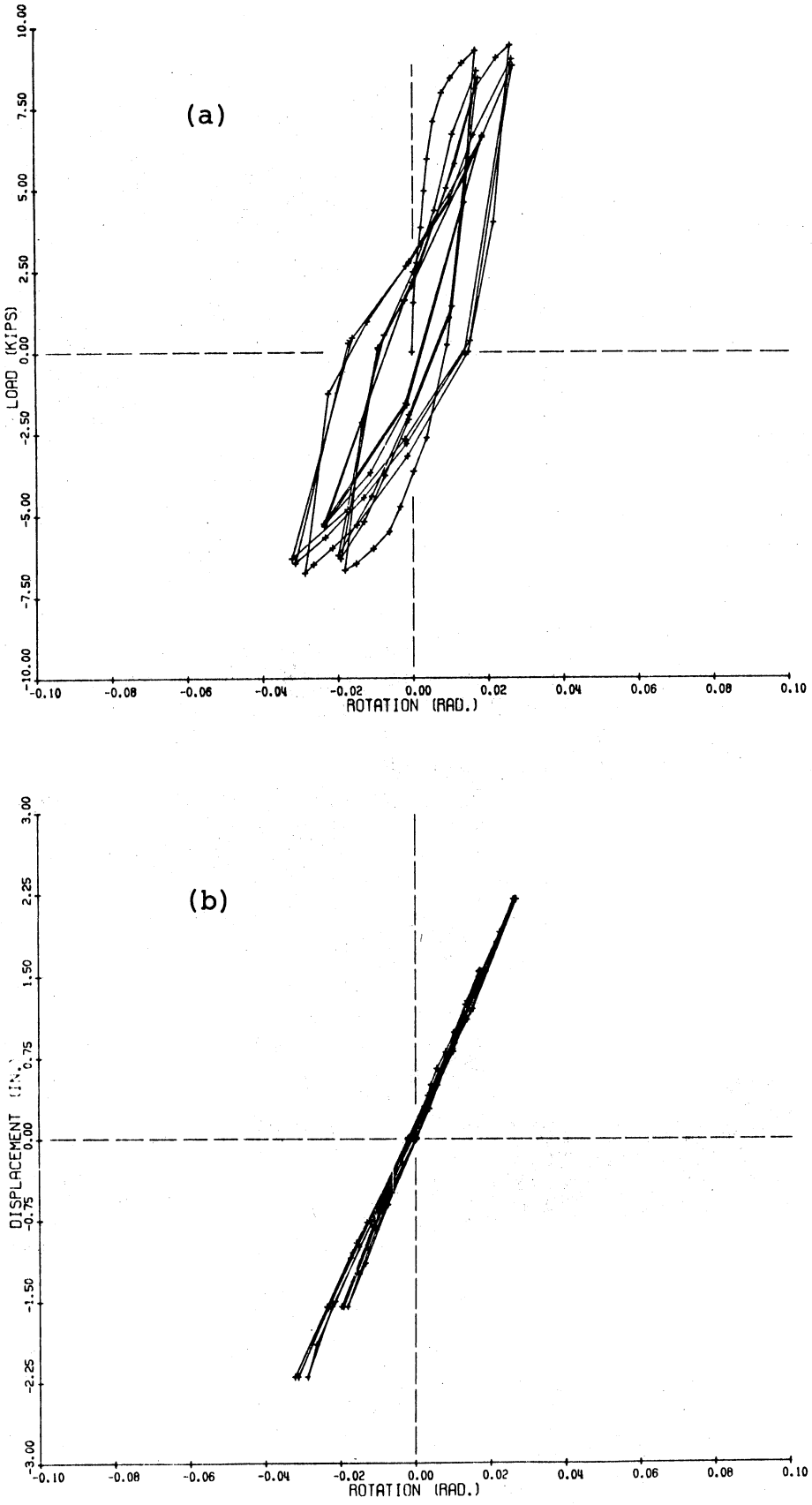

Fig. 5.9 Plot of Relative Beam Rotation with (a) Beam-Tip Force and (b) Beam-Tip Deflection, Repaired Specimen 1

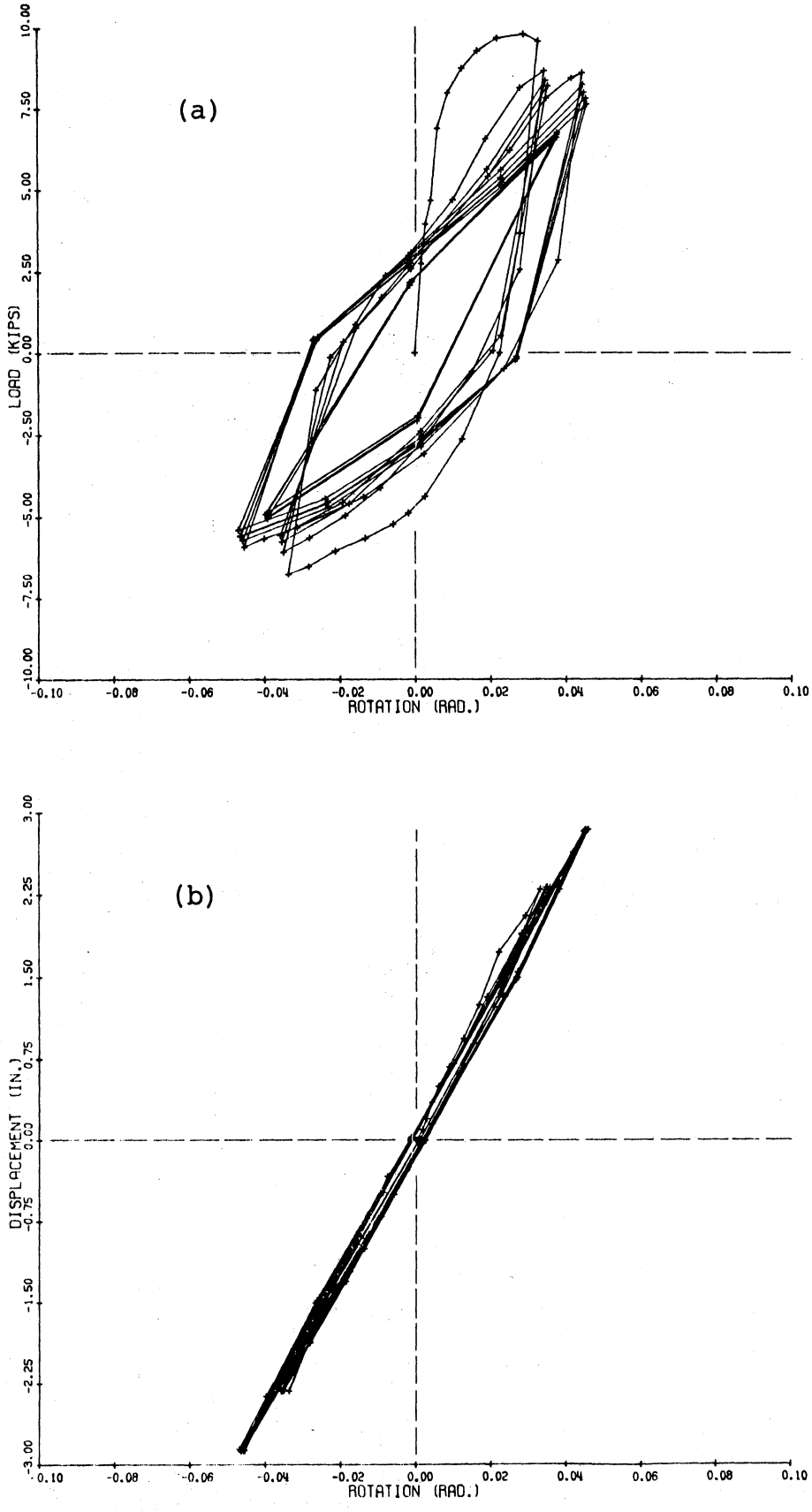

Fig. 5.10 Plot of Relative Beam Rotation with (a) Beam-Tip Force and (b) Beam-Tip Deflection, Repaired Specimen 2

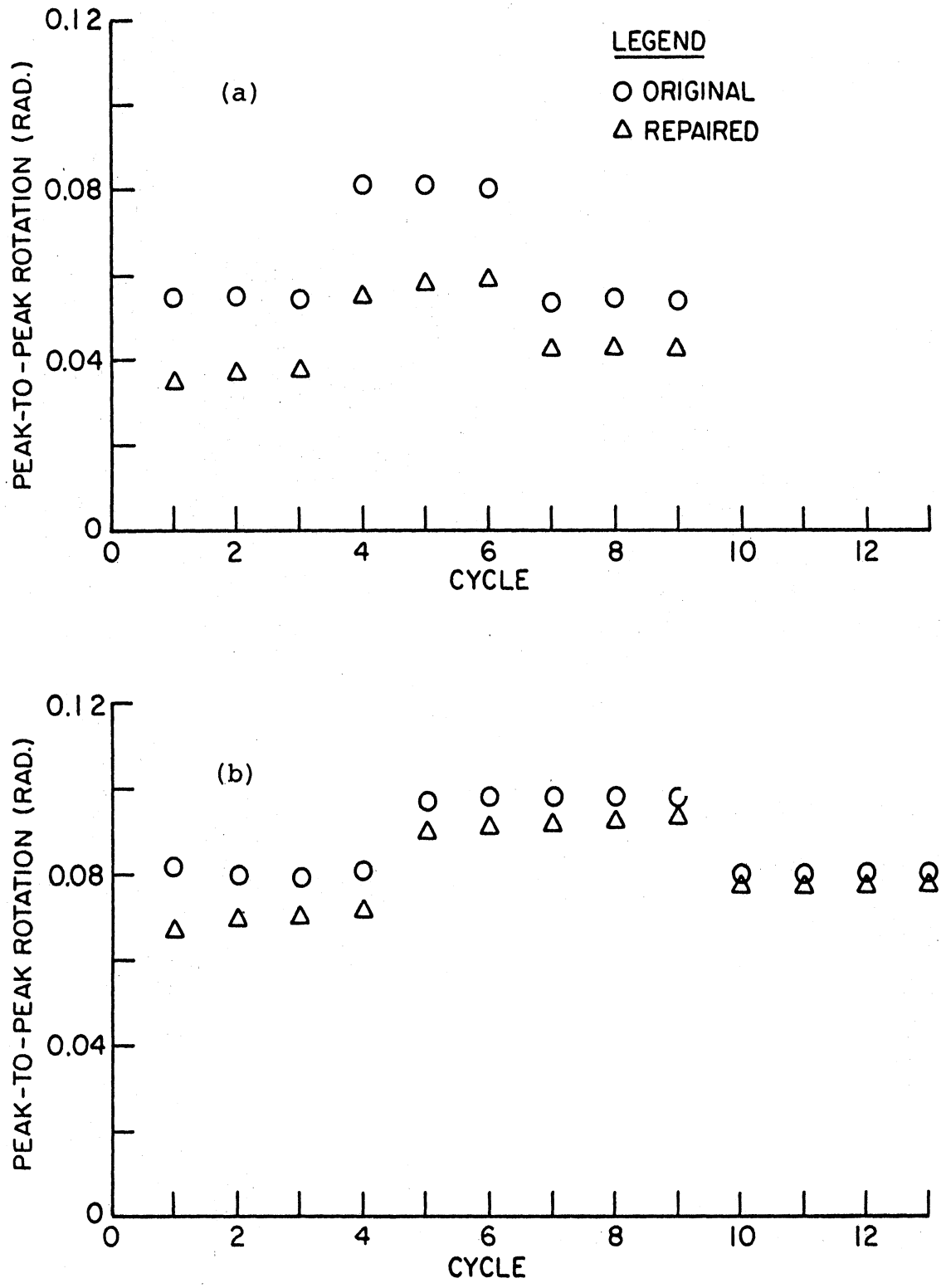

Fig. 5.11 Comparison of Peak-to-Peak Relative Beam Rotation for (a) Specimen 1 and (b) Specimen 2

for the tension reinforcement after original testing. Specimens 3, 4, 6 and 8 also had less relative beam rotation during retest. For repaired Specimen 7, which sustained severe spalling in the beam compression zone during the first quarter cycle of loading, the relative beam rotation was greater.

5.5 Beam Deflection

The measured and calculated beam-tip deflections during the first quarter cycle of loading are summarized in Table 5.3 for repaired Specimen 2. The beam deflections were calculated using Eq. 3.7 as described in Sec. 3.6.4. For Δ_5, the deflection was based on the total curvature being distributed uniformly over the 10 in. span length. When the moment exceeded the yield moment capacity of the original section, the deflection component Δ_6 was based on the experimental moment-curvature relationship (Fig. 5.12) obtained at the beam-column interface during the first quarter cycle of original testing. The curvature was calculated by taking the difference in strains between the top and bottom longitudinal reinforcement and dividing it by the distance between the reinforcement. The calculated total beam deflection was less than the measured deflection as was the case during original testing (Table 3.3).

The components of the calculated beam deflection given in Table 5.3 are normalized by dividing the corresponding

Table 5.3 Comparison Between Calculated and Measured Beam-Tip Deflection, Repaired Specimen 2

Calculated Deflection Components						Total Calculated Deflection (in.)	Measured Deflection (in.)	Measured Force (kips)
Δ_1 (in.)	Δ_2 (in.)	Δ_3 (in.)	Δ_4 (in.)	Δ_5 (in.)	Δ_6 (in.)			
0	0	0	0	0	0	0	0	0
0.014	0.031	0.002	0.155	0.021	0.082	0.305	0.35	4.66
0.021	0.040	0.004	0.219	0.030	0.122	0.436	0.50	6.88
0.027	0.056	0.005	0.459	0.063	0.276	0.886	0.94	8.74
0.030	0.062	0.005	0.801	0.110	0.536	1.544	1.73	9.68
0.030	0.070	0.005	1.201	0.164	0.536	2.006	2.30	9.58

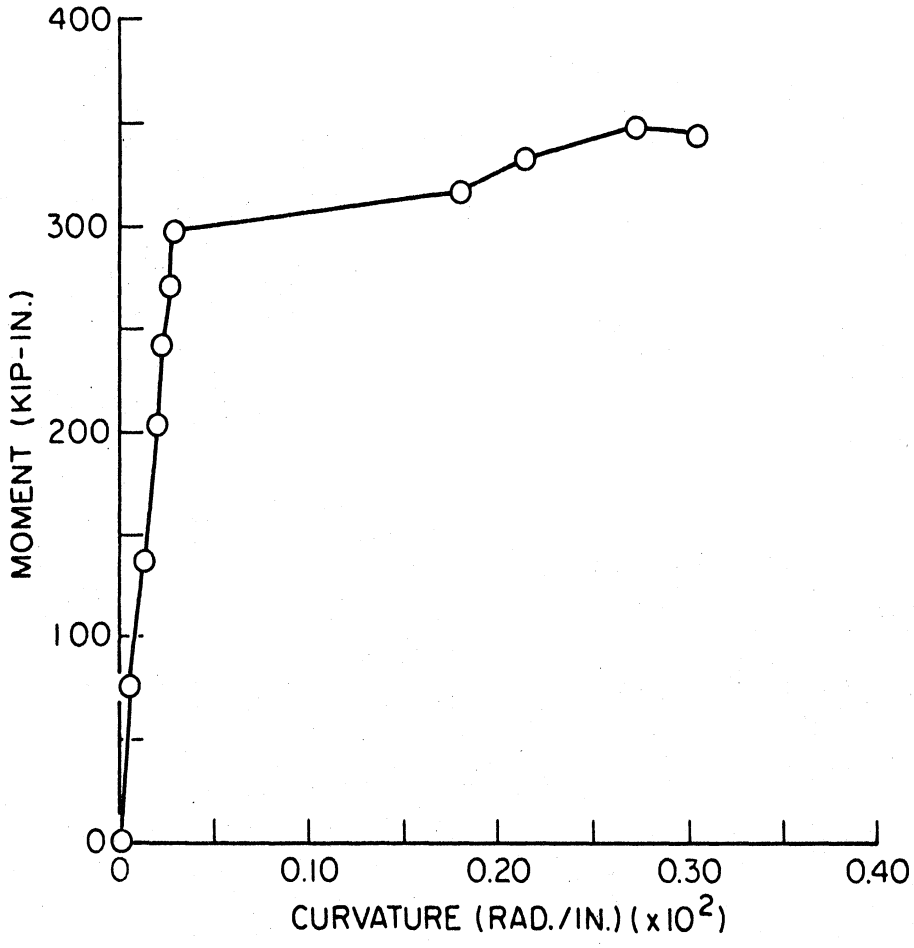

Fig. 5.12 Moment-Curvature Relationship, Specimen 2

measured deflections and the cumulative results are illustrated in Fig. 5.13 for repaired Specimen 2. The deflection due to bending in the beam (sum of Δ_4, Δ_5, and Δ_6) represents about the same percentage (84) of the total as during original tests. The contributions of deflections Δ_4, Δ_5, and Δ_6 to the total deflection were in different proportions for the repaired specimen than for the original specimen. Deflections Δ_4 and Δ_5 providing less and Δ_6 providing greater contributions. The increase in Δ_6 is

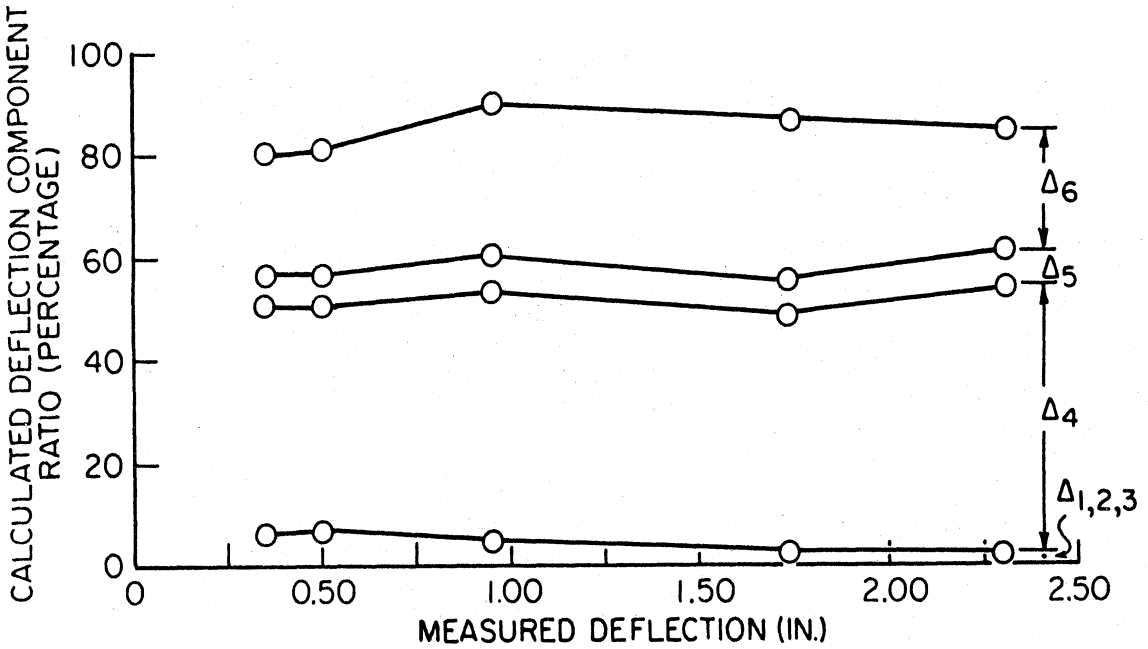

Fig. 5.13 Plot of Calculated Beam-Tip Deflection Component Ratio with Measured Deflection, Repaired Specimen 2

due to the higher applied moments which caused the beam top reinforcement to yield beyond the 10 in. region of the beam next to the column during retesting.

5.6 Discussion of Results and Recommendations

Retests of the repaired beam-column subassemblages made in this investigation indicated that the epoxy injection and the removal and replacement techniques of repair were both effective in restoring structural integrity to the beam. The beam-tip force vs deflection curves shown in Figs. 5.6(a) through 5.6(d) for Specimens 1 through 4, indicate that the stiffness, strength, and energy dissipation capacity have been restored.

The repaired beams were stronger during retest due to the use of high strength replacement materials and the previous strain hardening of the reinforcement during original testing. Because of the increase in strength, the joint and column were usually stressed to a higher level, thereby creating the possibility that the damage during retest could move from the beam to the joint and/or column as seen by Specimen 6. Because damage in the joint can produce a rapid loss of structural integrity, it is recommended that exterior joints be reevaluated before repairs for conformance with the current seismic code to determine if the joint is adequate to resist a future earthquake.

The addition of stirrup-ties to the beam for the purpose of confinement during repair seems beneficial, especially to resist large displacement reversals. Visual observations of Specimen 7 indicated that the beam core held together better during retesting than during original testing. It is recommended that whenever necessary, stirrup-ties should be added in the beam during repair to satisfy the current seismic code for confinement.

Brittle materials with low ultimate strains should be avoided in repair. These materials will usually crush during early stages of bending action and cause a sudden loss of the cover in the compression zone, thus reducing the beam cross section. Also, after these materials are

cracked in tension, smooth crystalline planes are formed that offer little resistance to shear slippage during load reversals. This is especially true for materials containing only fine aggregates which provide little interlocking resistance. Of the materials used in the repairs described herein, the high early strength concrete seems to be the most practical. The high early strength concrete is compatible with the original concrete; it is the most economical of these materials, and it does not require new material handling techniques.

Epoxy used as a bonding agent needs further investigation. Observations of the damaged specimens after retesting showed no traces of epoxy bonded concrete on the exposed reinforcement in the repaired region. Where epoxy was used to bond the first lift of Duracal cement concrete to the second lift in Specimen 7, the material separated at this construction interface after a few cycles of inelastic loading. Therefore, it is recommended that before epoxy is used in new applications with different materials, it should be laboratory tested in a manner similar to the expected field conditions.

CHAPTER 6

SUMMARY AND CONCLUSIONS

6.1 Introduction

The principal objectives of this investigation were (1) to experimentally investigate the behavior of exterior reinforced concrete beam-column subassemblages designed according to the most recent earthquake resistant design recommendations, (2) to use these test results to suggest improved recommendations for design of the subassemblages, (3) to evaluate two repair techniques currently used in practice, (4) to investigate the short term loading stiffness and strength properties and long term loading creep properties of different materials which may be used for structural repairs, and (5) to investigate the behavior of repaired beam-column subassemblages.

6.2 Experimental Investigation

Eight exterior beam-column subassemblages were designed using either of two design criteria. The ACI 318-71 Building Code for nonseismic areas was used for the first design to represent existing structures which were designed without seismic considerations. The second design used the ACI 318-71 Building Code with seismic considerations along with recommendations from ACI-ASCE Joint Committee 352 for the design of beam-column joints in monolithic reinforced concrete structures. The primary difference between the two designs was the amount of transverse reinforcement in the subassemblages.

The specimens were tested with the ends of the column being simply supported. A constant axial load of either zero or 40 kips was applied to the column before slowly deflecting the beam tip.

Two beam displacement patterns were used to obtain different degrees of damage during original testing. The patterns were meant to represent subassemblage response to either a moderate or severe earthquake loading.

After original testing, the specimens were repaired using one of two repair techniques. For the subassemblages that sustained moderate damage, the epoxy injection technique was used. The removal and replacement technique, which utilized different high early strength replacement materials, was used to repair more severely damaged members. After repairs, the specimens were retested with the same loading parameters as for the original tests in order to provide a direct comparison of results.

The force and deflection at the beam loading point were continuously recorded during original testing and retesting. For original testing, strains in the reinforcing steel in and near the joint were measured. Joint distortion and relative beam rotation were also measured during original testing and retesting.

6.3 Original Behavior of Specimens

For all the specimens the primary damage occurred in the portion of the beam adjacent to the beam-column

interface. Most of this damage was attributed to flexural action. Some hairline cracks were observed in the joint. Specimens with 40 kip column axial load sustained fewer cracks in the joint. No cracks were observed in the column.

The measured beam-tip force and deflection indicated that the strength and energy dissipation capacity degraded after every cycle of loading at the same displacement level. This degradation was less for specimens containing more transverse reinforcement.

The measured strains in the reinforcing steel in and near the joint indicated that

(1) the transverse reinforcement in the beam resisted almost all of the shear at the end of the first quarter cycle of loading,

(2) the beam longitudinal steel anchored in the joint yielded at a location just before the hook during the first cycle of severe earthquake loading, and

(3) the increase in transverse reinforcement in the joint resulted in a decrease in shear resisted by the concrete which shows that the truss analogy was not applicable in the joint.

The measured joint distortion indicated that the joint was stiffer for specimens with the 40 kip column axial load than for the specimens without axial load. Also, the distortion showed less variation for cycles at the same displacement level.

The measured relative beam rotation was used in the calculations for the deflection of the beam at the loading point. These calculations indicated that about 80 percent of the measured deflection at the end of the first quarter cycle of loading was attributed to flexure of the first 10 in. of the beam from the inside column face.

6.4 Repair Techniques and Repair Materials

The procedure for the epoxy injection and the removal and replacement technique was described in Sec. 4.2.

Epoxy-sand mortar, Duracal cement concrete, and high strength quick setting concrete were used as replacement materials and were investigated for short term and long term loading properties. A description of these materials and their properties were given in Sec. 4.3.

6.5 Behavior of Repaired Specimens

For the specimens repaired with the epoxy injection technique, the epoxy injected cracks remained closed during retest. Unrepaired cracks opened and new cracks formed in the beam both within and adjacent to the repaired region. For some of the specimens repaired with the removal and replacement technique, severe spalling of the beam compression zone in the repaired region was observed during the first quarter cycle of loading. This was caused by the low ultimate strain capacity of the repair material. Cracking occurred in and adjacent to the

repaired region for all the specimens. Few new cracks were observed in the joint and no cracks were observed in the column for specimens with the 40 kip column axial load. For the specimens with zero column axial load, new cracks were observed in the joint. Also, cracks were observed in the column for Specimens 6 and 8 during retest.

The measured beam-tip force and deflection indicated that the strength capacity was higher for the repaired specimens. This increase in strength can be attributed to the stressing of the beam longitudinal reinforcement further into the strain hardening range during retest.

The measured joint distortions were greater for the repaired specimens. This was due to the increase in shear in the joint resulting from the higher beam strength. The measured relative beam rotation over the first 10 in. of the beam was less for the repaired specimens. This reduction was due to the absence of the yielding plateau on the stress-strain curve for the tensioned reinforcement after original testing.

6.6 Conclusions

Based on this investigation, the following conclusion are made.

(1) Epoxy injection, and removal and replacement techniques of repair can effectively restore the stiffness, strength and energy dissipation

capacity of a reinforced concrete member when the damage was primarily caused by flexural action.

(2) The shear stress resisted by the concrete in a reinforced concrete beam-column joint should be

$$v_c = 7\sqrt{f'_c}\left(1 + 0.002\,\frac{N_u}{A_g}\right)$$

This value is twice as large as the current value given in ACI 318-71, Eq. (11-7).

(3) The transverse reinforcement in a reinforced concrete beam should be designed to resist the entire shear force at locations of maximum moment caused by gravity plus seismic loading. Also, the maximum stirrup-tie spacing in these regions should be less than or equal to d/4.

(4) For the design of the transverse reinforcement in the beam-column joint, the number of hoops should be calculated by the following expression given earlier in Sec. 3.7, Eq. 3.11.

$$n = \frac{v_s\, A_{cv}}{A_v\, f_y}$$

These hoops should be equally spaced in the region between the top and bottom beam bars in the joint.

(5) High early strength (Type III) concrete should be used as the replacement material in the removal and replacement repair technique. This material was compatible with the original concrete, it was the most economical, and it did not require new material handling techniques. Brittle materials with low ultimate strain capacity are less suitable for many repair situations. These materials will crush sooner during bending action and reduce the effective cross section of the member.

(6) Epoxy was not effective in improving the bond between the concrete and the reinforcement when the repaired regions were subjected to large strain reversals.

(7) The specimens with stirrup-tie spacing of d/4 had less degradation in strength and dissipated more energy than the specimens with a d/2 stirrup-tie spacing. The primary reason for this improved behavior was the additional confinement of the beam core provided by the closer spaced stirrup-ties.

(8) The repaired beams were stronger than the original beams at the same maximum beam deflections. This additional strength was attributed to the strain hardened reinforcement and the higher strength repair materials.

(9) Exterior joints should be reevaluated before repairs are made to determine if the joint is adequate to resist a future earthquake. Severe damage in the joint can result in the structure behaving poorly during an earthquake.

During the execution of this investigation, it was seen that additional research is needed in the following areas: (1) The influence of the column axial load and the amount of transverse reinforcement on the behavior of the exterior beam-column joints. The effect of the strength ratio between the beam and column on the behavior of the joint should also be investigated. (2) The effectiveness of epoxy used as a bonding agent when the bonded materials are subjected to large strain reversals.

APPENDIX A

DESIGN OF SPECIMENS

Two types of subassemblages were designed. The first type was designed using the American Concrete Institute Building Code (ACI 318-71) (17) for nonseismic areas and it is designated as "Type I Design". The second type of subassemblage was designed using ACI 318-71 including its special provisions for seismic design along with recent recommendations from ACI-ASCE Joint Committee 352 (63). It is designated as "Type II Design". Both designs assumed a nominal concrete strength of 4,000 psi, and steel yield strength of 40,000 psi for all the reinforcement except 60,000 psi for column longitudinal bars. The construction details shown in Figs. 2.1(a) and 2.1(b) for the two types of design resulted from the analysis which will now be presented.

A.1 Analysis of Flexural Strength for Subassemblage

The ultimate positive and negative bending moment capacity for the beam was calculated to be 279 kip-in. and 219 kip-in. respectively. The calculations were based on a) a linear strain distribution through the section, b) the concrete having no tensile strength, c) the concrete having a strain at the extreme compression fiber of 0.003, and d) the concrete having a Whitney rectangular compressive stress distribution. For the column, the

interaction between the axial load and moment at ultimate conditions is plotted in Fig. A.1. The values in the

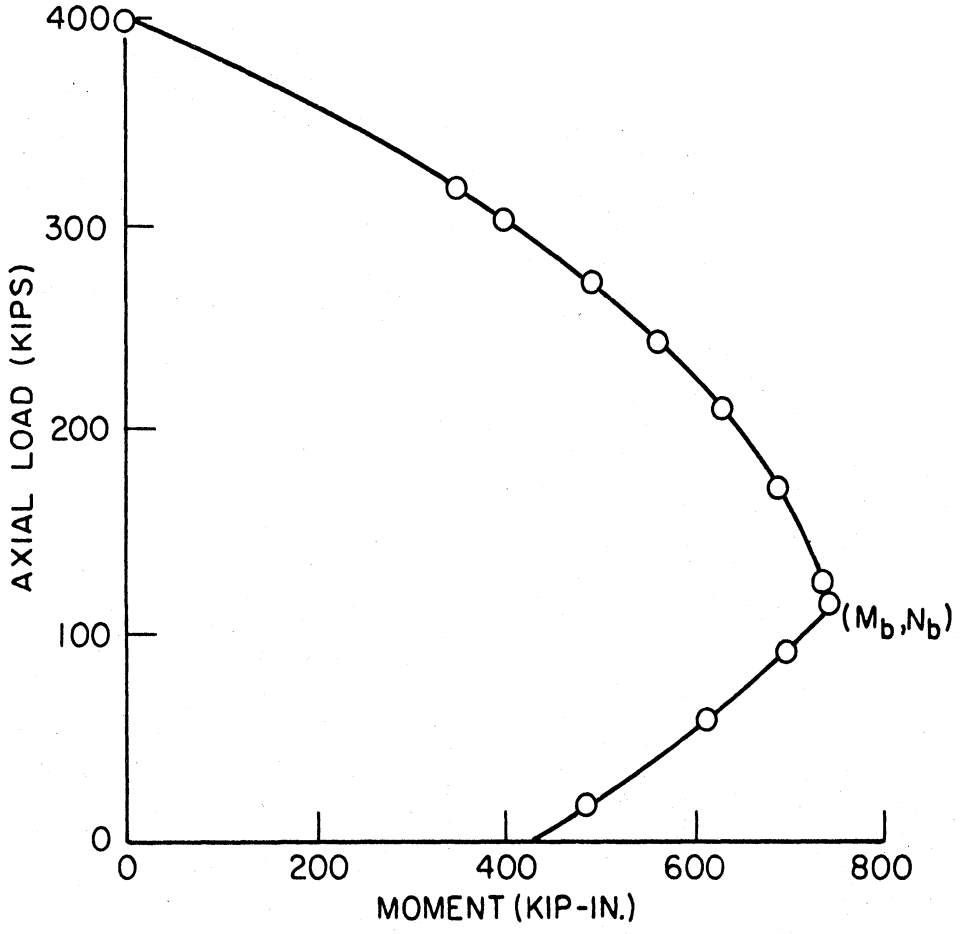

Fig. A.1 Interaction Diagram for Column Section

diagram were based on the same assumption as for the beam. The procedure used to calculate the load and moment was first to assume different locations of the neutral axis in the column cross section. For each location, a resultant axial load and moment were calculated using static equilibrium. The interaction diagram indicated that the

balanced axial load and moment were 115 kips and 740 kip-in respectively. At the balance condition, the concrete reaches a compressive strain of 0.003 in the extreme fiber simultaneously with the commencement of yield of the tension reinforcement.

The two axial loads used in this investigation were zero and 40 kips. The moment corresponding to zero and 40 kip axial load are 432 kip-in. and 562 kip-in. respectively (Fig. A.1). Twice the ultimate moment capacity of the column at zero and 40 kip axial load is about three and four times greater than the ultimate moment of the beam respectively which indicates a "strong column - weak beam" subassemblage.

A.2 Analysis of Shear in Beam and Column

Based on a ultimate beam moment of 276 kip-in. and a loading arm of 46.5 in. as shown in Fig. A.2, the ultimate shear force in the beam was calculated to be 5.9 kips. For the column, the shear force was calculated by static equilibrium to be 4.6 kips.

A.2.1 Type I Design

The following equations in this section were obtained from Chapter 11 of ACI 318-71.

Beam. The ultimate shear stress v_u in the beam was calculated to be 108 psi using the following expression

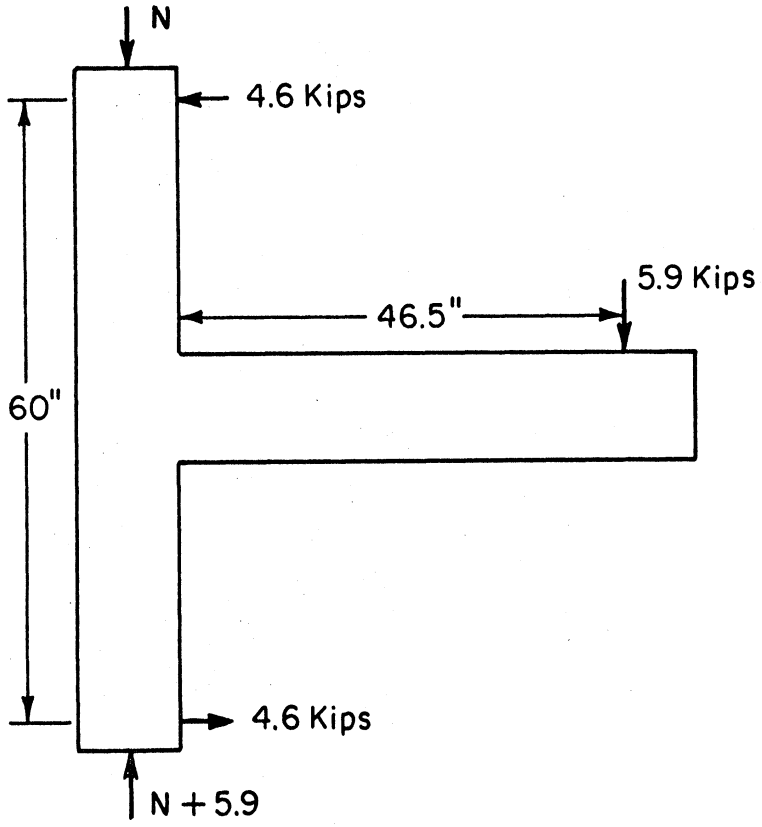

Fig. A.2 Ultimate Shear Forces for Beam and Column

$$v_u = \frac{V_u}{\phi\ b_w\ d} \qquad (A.1)$$

where V_u = total applied shear force at the section,

b_w = width of the cross section,

d = distance from the extreme compression fiber to the tension reinforcement,

and ϕ = capacity reduction factor. For shear ϕ = 0.85.

The shear stress resisted by the concrete v_c was taken to be 126 psi using the following expression

$$v_c = 2\sqrt{f'_c} \qquad (A.2)$$

where f'_c = compressive strength of the concrete.

Because v_u is less than v_c, only minimum transverse reinforcement was required. The maximum spacing, s that satisfies the minimum area required for a No. 2 stirrup-tie can be calculated by using the following expression

$$s = \frac{A_v f_y}{50 b_w} \qquad (A.3)$$

where A_v = area of the transverse reinforcement within a distance s,

and f_y = yield strength of the reinforcement.

This spacing calculated using Eq. A.3 was equal to 10 in. which is greater than the maximum allowable spacing of d/2 (4.0 in.). Therefore, a 4.0 in. spacing was used throughout the beam length.

Column. The ultimate shear stress in the column was calculated to be 75 psi using Eq. A.1. The shear stress resisted by the concrete was calculated using the following expression

$$v_c = 2\left(1 + 0.0005 \frac{N_u}{A_g}\right)\sqrt{f'_c} \qquad (A.4)$$

where N_u = axial load in the column occurring simultaneously with V_u,

and A_g = gross area of the cross section.

The result was equal to 126 psi for zero axial load. For the 40 kip axial load, v_c was greater than 126 psi. Because v_u is less than v_c, only minimum transverse reinforcement was required. The maximum spacing that satisfies the minimum area requirement for a No. 2 hoop was calculated using Eq. A.3 to be 10 in. which was greater than the maximum allowable spacing of d/2 (4.5 in.). Therefore, a 4.5 in. spacing was used in the column.

A.2.2 Type II Design

In addition to the requirements for specimens with Type I Deisgn, the Type II Design specimens satisfied the following requirements.

Beam. To provide confinement the seismic provision of ACI 318-71 requires a maximum spacing for the transverse reinforcement over a distance of 4d (32 in.) from the inside column face as indicated by the following expression

$$s = \frac{A_v\, d}{0.15\, A_s} \qquad (A.5)$$

where A_s = area of the tension reinforcement.

For a No. 2 stirrup-tie, the calculated spacing was 6 in. which is greater than the more stringent maximum allowable spacing of d/4 (2.0 in.).

ACI-ASCE Joint Committee 352 suggests that the transverse reinforcement be designed to resist all of the shear developed out to be section 2d (16 in.) from the

inside column face. Also, the ultimate shear calculation should be based on an increase in the nominal yield stress of the beam longitudinal reinforcement. For joints where ductility and strength are required, as opposed to just strength, the Committee suggests that the increase factor α should be greater than or equal to 1.25. The purpose of this factor is to account for strain hardening of the flexural reinforcement during inelastic action. Therefore, the ultimate shear stress based on the flexural reinforcement having a yield stress of αf_y can be approximated by the following expression.

$$v_u = \frac{\alpha V_u}{\phi b_w d} \tag{A.6}$$

The shear stress calculated from the above expression was 135 psi for α equal to 1.25. The maximum spacing for a No. 2 stirrup-tie was found to be 3.7 in. using the following expression.

$$s = \frac{A_v f_y}{v_u b_w} \tag{A.7}$$

This spacing was still greater than the maximum allowable spacing of 2.0 in. indicated earlier. Therefore, a 2.0 in. spacing was used over a distance of 32 in. from the inside column face.

Column. To provide confinement, the seismic provisions require that for a column axial load less than or equal to 40 percent of the balance load, the maximum spacing for a No. 2 hoop over a distance of 4d (36 in.)

above and below the beam was found to be 6.8 in. using Eq. A.5. This spacing was greater than the maximum allowable spacing of d/4 (2.25 in.).

ACI-ASCE Joint Committee 352 suggests that the transverse reinforcement be designed to resist all of the shear within the regions from the beam faces to 2d (18 in.) above and below the beam. As before, using αf_y with α equal to 1.25 to represent the maximum stress expected in the beam longitudinal reinforcement, the ultimate shear stress was calculated to be 94 psi. The resulting maximum spacing for a No. 2 hoop, calculated with Eq. A.7, was 5.3 in. This spacing is greater than the allowable spacing of 2.25 in. indicated earlier. Therefore, a 2.25 in. spacing was used in the column above and below the beam except the first d (9 in.) distance which was govern by the spacing in the joint as described below.

A.3 Analysis of Shear in Joint

A.3.1 Type I Design

For nonseismic design, ACI 318-71 does not provide additional design requirements for joints, except to consider them as part of the column.

A.3.2 Type II Design

The ultimate shear force in the joint can be calculated by taking the difference between the shear

produced by the beam longitudinal reinforcement anchored in the column and the column shear as indicated in Fig. A.3. The following expression was suggested by

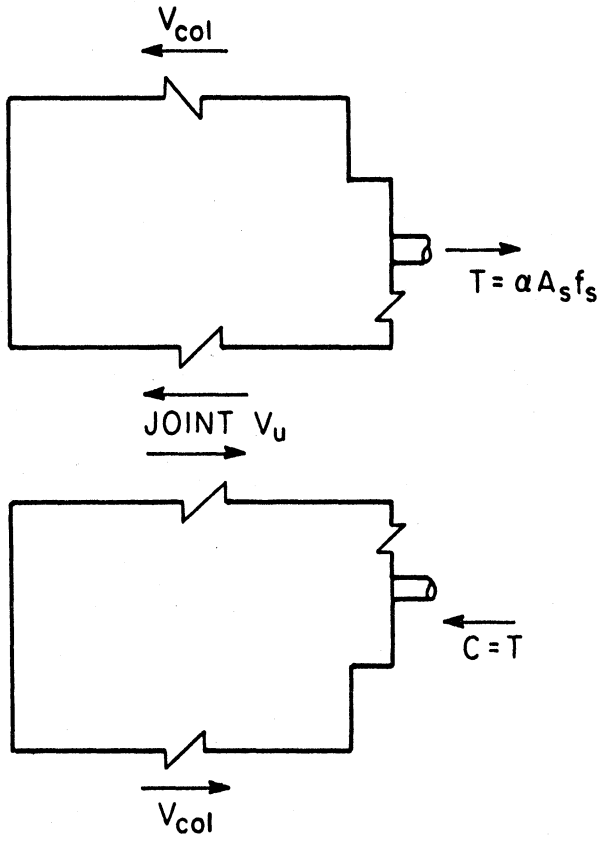

Fig. A.3 Forces Contributing to Shear in Joint

ACI-ASCE Joint Committee 352

$$V_u = \alpha\ A_s\ f_y - V_{col} \qquad (A.8)$$

where V_{col} = shear force in the column.

As mentioned earlier in Sec. A.2.2, the factor α takes into account the increase in stress caused by strain hardening of the reinforcement during inelastic action.

For α equal to 1.25, the ultimate shear force was calculated to be 39.4 kips. The ultimate shear stress in the joint core was found to be 896 psi using the following expression

$$v_u = \frac{V_u}{\phi A_{cv}} \qquad (A.9)$$

where A_{cv} = effective area of the cross section.
With no confinement provided by other members framing into the joint, A_{cv} was equal to the width taken to the outside of the hoop multiplied by d. The shear stress resisted by the concrete in the joint was calculated by the following expression

$$v_c = 3.5\ \beta\ \gamma \sqrt{f'_c}\left(1 + 0.002\ \frac{N_u}{A_g}\right) \qquad (A.10)$$

where γ = constant dependent upon the confinement provided by other members framing into the joint,

and β = constant dependent upon whether both ductility and strength or just strength is required.

For this design, β and γ were taken to be 1.0 because both the strength and ductility were desired and because confinement was not provided by other members. The shear stress resisted by the concrete was calculated to be 221 psi for zero axial load. The resultant shear stress to be resisted by the transverse reinforcement v_s was 675 psi. Instead of calculating the spacing, the number, n, of transverse reinforcement required in the joint between

the beam top and bottom reinforcement was calculated using the following expression.

$$n = \frac{v_s \, A_{cv}}{A_v \, f_y} \tag{A.11}$$

For No. 3 hoops, four were required. ACI-ASCE Joint Committee 352 also suggest the spacing of the transverse reinforcement in the joint be continued for a distance d (9 in.) above and below the beam. For the No. 3 hoop, the spacing was calculated to be 2.25 in. using the following expression.

$$s = \frac{A_v \, f_y \, d}{v_s \, A_{cv}} \tag{A.12}$$

This spacing was equal to the maximum allowable spacing of d/4 indicated earlier in Sec. A.2.2. Therefore, No.3 hoops were continued above and below the beam at a spacing of 2.25 in. for a distance of 9 in.

A.4 Analysis of Anchorage for Beam Reinforcement

A.4.1 Type I Deisgn

From Chapter 12 of ACI 318-71, the straight anchorage length l_d required for a No. 6 bar anchored in the column was calculated to be 12.0 in. using the expression

$$l_d = 0.0004 \, d_b \, f_y \tag{A.13}$$

where d_b = nominal diameter of the bar.

A standard 90 deg. hook, defined as a 90 deg. turn plus an extension of 12 bar diameters at the free end, is

capable of developing a tensile stress f_h in a No. 6 bar of 22,700 psi as calculated by the following expression

$$f_h = \xi\sqrt{f'_c} \tag{A.14}$$

where ξ = constant and equal to 360 for No. 6, Grade 40 bars.

The equivalent straight embedment length l_e provided by the hook was calculated to be 6.33 in. using the following expression

$$l_e = \frac{0.04 \quad A_b \; f_h}{\sqrt{f'_c}} \tag{A.15}$$

where A_b = area of the bar.

Therefore, a straight lead embedment length of 5.67 in. was required which was less than the 6.37 in. provided between the inside column face and the beginning of the hook (Fig. A.4). A similar type of analysis was made for the beam No. 5 bar. This analysis indicated that the anchorage was adequate.

A.4.2 Type II Design

The ACI-ASCE Joint Committee 352 suggest the following expression for calculating the tensile stress developed by a 90 deg. standard hook

$$f_h = 700 \;\; \psi \, (1 - 0.3 \; d_b) \sqrt{f'_c} \tag{A.16}$$

where ψ = constant dependent upon the straight embedment length, the concrete cover normal to the plane of the hook and over the tail extension, and the confinement provided by transverse reinforcement in the joint.

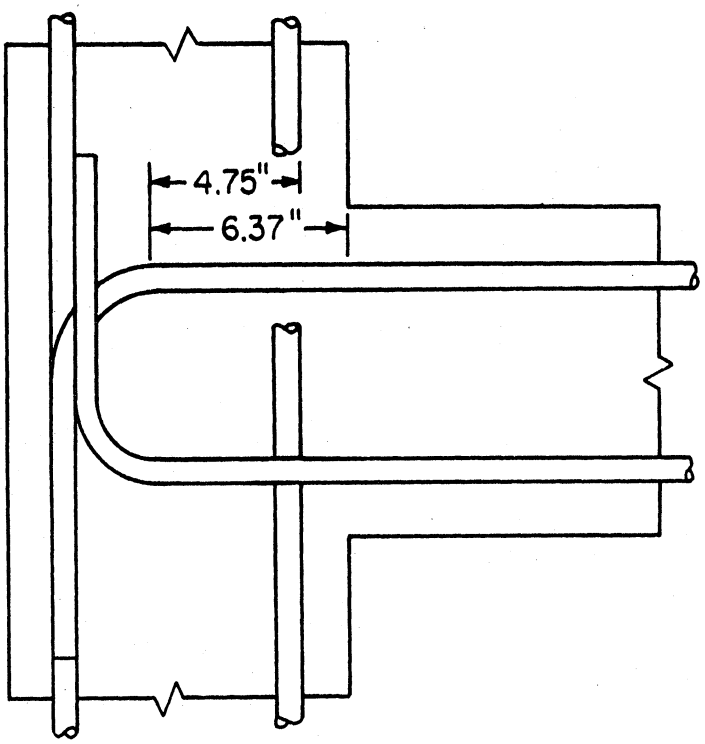

Fig. A.4 Straight Embedment Length Provided Before Hook

For a No. 6 bar, the stress resisted by the hook was calculated to be 34,300 psi for ψ equal to 1.0. The required straight embedment length l_s between the start of the column core and the beginning of the hook was calculated using the expression

$$l_s = \frac{0.04\ A_b\ (\alpha f_y - f_h)}{\psi \sqrt{f'_c}} \qquad (A.17)$$

For α = 1.25 and ψ = 1.0, the required straight embedment length was 4.40 in. which was less than the 4.75 in. provided in the column core (Fig. A.4). A similar type of analysis was made for the beam No. 5 bar. The analysis indicated that the anchorage was adequate.

A.5 Summary

The above analysis showed that the beam-column subassemblages satisfied the respective design criteria for shear and anchorage. The design was based on a concrete strength of 4,000 psi and a steel yield stress of 40,000 psi for all the reinforcement except the column longitudinal bars which had a nominal yield stress of 60,000 psi.

The above calculation for shear in the beam was based on a beam force being applied 46.5 in. from the inside column face as indicated in Fig. 4.2. For Specimens 5 through 8, the shear span was reduced to 41.25 in. causing the shear forces in the beam and column to be increased by about 10 percent. However, the spacing of the transverse reinforcement in the beam and column was still adequate since it resulted from maximum allowable spacing requirements.

APPENDIX B

MEASURED PROPERTIES FOR REINFORCING STEEL AND CONCRETE

Reinforcing Steel. A 1 1/2 ft. long coupon specimen was taken from each bar used for the beam and column longitudinal reinforcement. The specimens were tested uniaxially in tension to obtain the yield and ultimate strength, and ultimate elongation over a gage length of 8 in. The 8 in. gage length represented a standard recommended by the American Society for Testing and Materials (ASTM) A615 (76). The measured reinforcing steel properties for each of the beam-column subassemblages are given in Table B.1. The average yield strength for the beam No. 6 and No. 5 bars, and the column No. 6 bars was 1.24, 1.26, and 1.30 times greater than the nominal yield respectively. The results given in Table B.1 indicate the average ultimate elongation for the Grade 40 reinforcement in the beam was about two times greater than the Grade 60 reinforcement in the column. The difference between the actual and nominal yield strength, and the difference in ultimate elongation between Grade 40 and Grade 60 reinforcement is typical and should be expected.

For the transverse reinforcement, three 1 1/2 ft. long coupon samples were taken from both the No. 2 and No. 3 bars and tested in tension. The results showed the No. 2 and No.3 bars had an average yield strength of

Table B.1 Reinforcing Steel Strength Properties

Specimen	Beam						Column (No. 6)		
	Top Bar (No. 6)			Bottom Bar (No. 5)					
	Yield (psi)	Ultimate (psi)	Elongation (percent)	Yield (psi)	Ultimate (psi)	Elongation (percent)	Yield (psi)	Ultimate (psi)	Elongation (percent)
1	52,500	88,200	17	54,500	91,000	18	77,700	124,500	10
2	48,600	81,800	20	54,500	89,700	18	78,000	123,900	9
3	48,700	82,000	18	49,400	76,100	20	78,200	124,300	10
4	48,900	82,000	20	48,100	75,500	20	78,900	126,400	10
5	50,900	87,300	18	46,800	77,100	23	--	132,000	9
6	51,600	87,300	18	49,000	79,700	22	77,000	123,900	11
7	47,500	80,900	19	53,900	88,400	18	--	126,100	11
8	48,200	81,400	22	48,100	75,500	24	77,700	123,900	10
Avg.	49,600	83,900	19	50,500	81,600	20	77,900	125,600	10

39,600 psi and 56,400 psi, an average ultimate strength of 52,900 psi and 77,300 psi, and an average ultimate elongation (based on a 8 in. gage length) of 22 percent and 18 percent respectively.

Measured stress-strain curves for different diameter reinforcing bars used as reinforcement in the beam-column subassemblages are given in Figs. B.1(a) through B.1(e). The test specimens were 1 1/2 foot long bar "turned down" on a lathe at the center to a specified diameter to obtain yielding at that location. The stress was applied uniaxially in tension and the strains were measured at the location of the reduced diameter using a high elongation strain gage. For information on the strain gage and its application, see Appendix E. The stress-strain curves showed typical behavior for Grade 40 and Grade 60 reinforcing steel. Note from Figs. B.1(d) and B.1(e) for the No. 6 bar that the Grade 40 reinforcement has a longer yield plateau than the Grade 60 reinforcement.

Concrete. Standard 4 in. by 8 in. test cylinders which were cast and cured with the beam-column subassemblages were used to determine the stiffness, compressive strength, and tensile strength of the concrete. To obtain the stiffness and compressive strength, the cylinders were loaded at a rate of 30 psi per sec. as recommended by the ASTM C39 (72). Axial deformation of the cylinders was measured with a 6 in. gage length compressometer. A

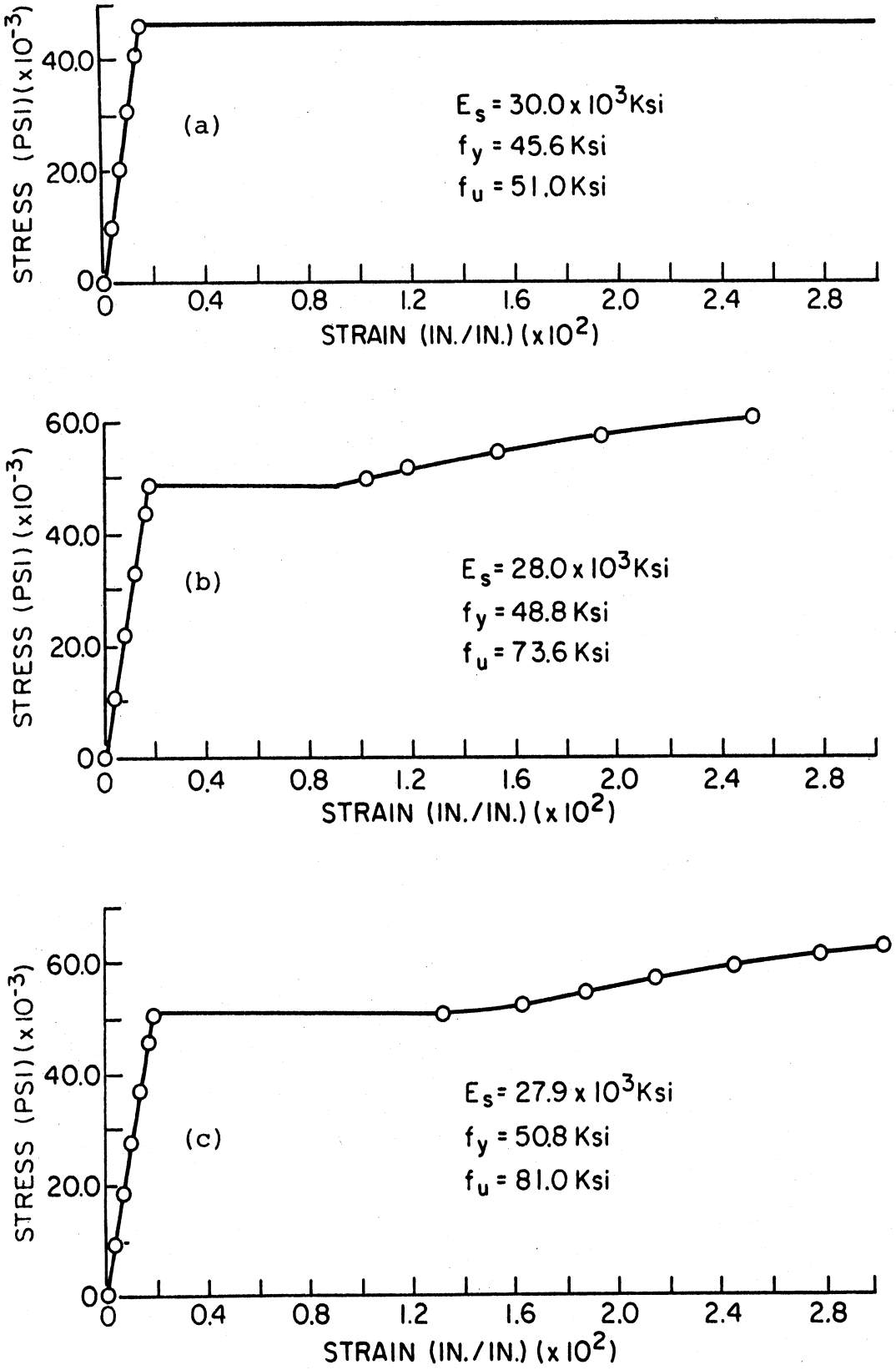

Fig. B.1 Measured Stress-Strain Relationships for Grade 40 Bars (a) No. 2, (b) No. 3, and (c) No. 5

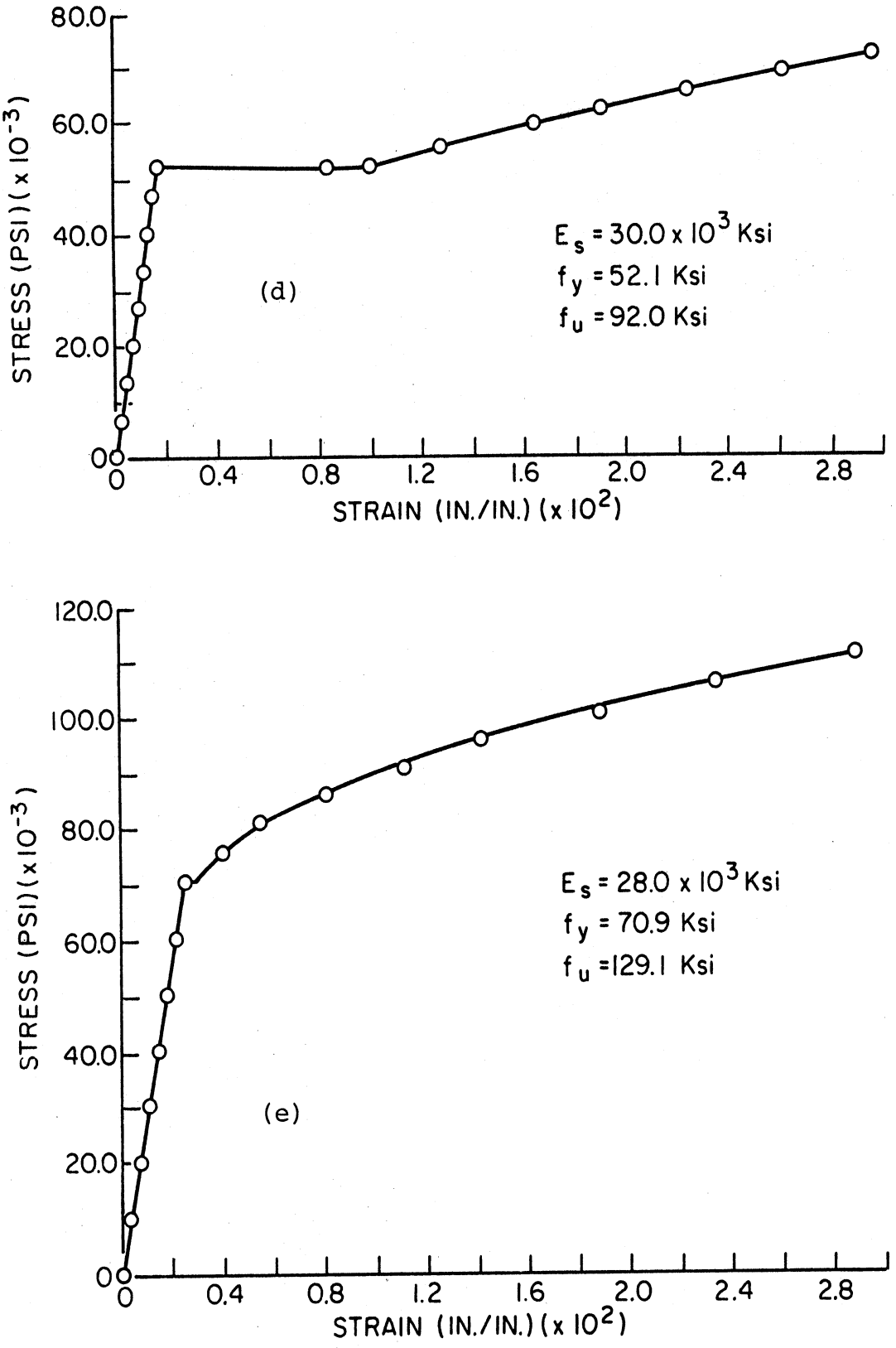

Fig. B.1 (continued) Measured Stress-Strain Relationships for No. 6 Bars (d) Grade 40 and (e) Grade 60

measure of the tensile strength was obtained utilizing the standard splitting test with a loading rate recommended by ASTM C496 (73) of 2.5 psi per sec.

For each of the two sets of beam column subassemblages cast (one set consisted of Specimens 1 through 4 and the other set consisted of Specimens 5 through 8), a typical stress-strain curve at age 28 days is shown in Figs. B.2(a) and B.2(b). From figures like these the

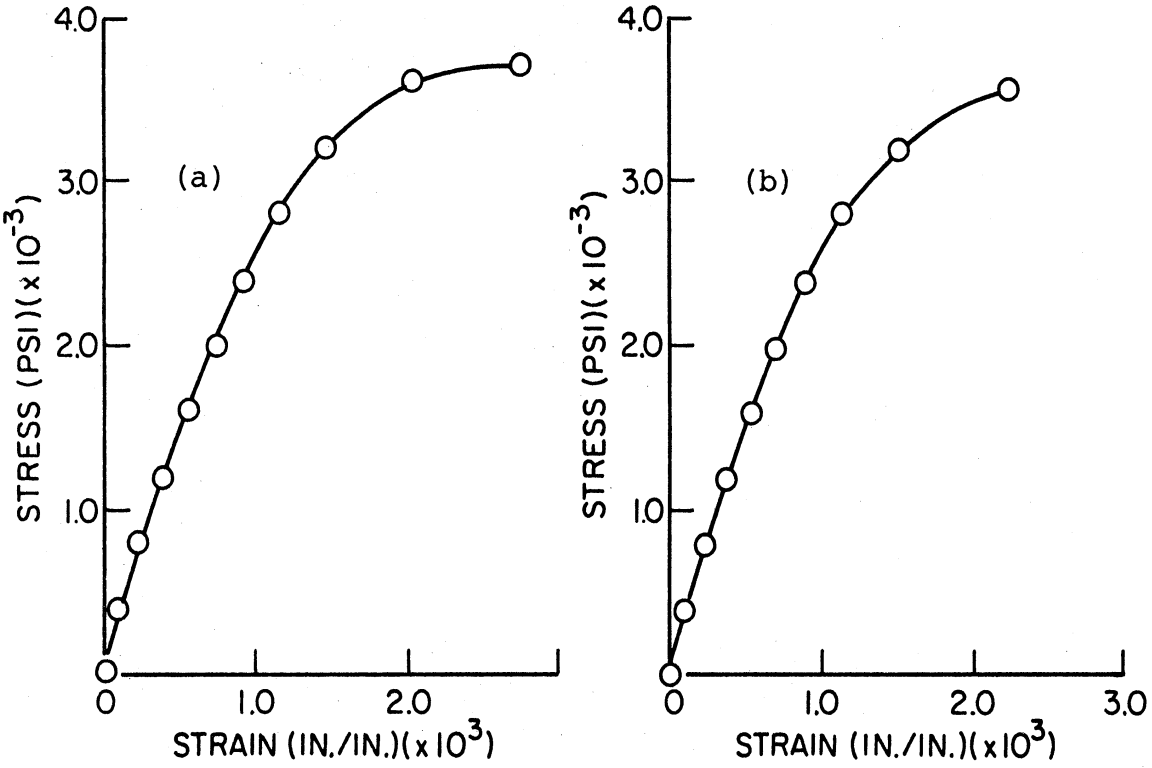

Fig. B.2 Typical Measured Stress-Strain Relationships for Concrete Used for (a) Specimens 1 through 4 and (b) Specimens 5 through 8

stiffness was obtained by taking the secant modulus from 0 to 0.45 of the ultimate load. The 28 day stiffness and compressive strength along with the tensile strength are given in Table B.2 for the two sets of beam-column specimens. The compressive strength values at age 28 days

were in good agreement with the design value of 4,000 psi. At the time of original testing of the subassemblages, which was sometime after 28 days, the beam-column specimens had concrete stiffness and compressive strength given in Table B.2. All the values in Table B.2 were based on the average of three test cylinders.

Table B.2 Concrete Strength Properties

Specimen	Age 28 Days			Original Testing	
	Stiffness (ksi)	Compressive (psi)	Tensile (psi)	Stiffness (ksi)	Compressive (psi)
1	3,180	3,700	470	3,320	4,200
2	3,180	3,700	470	3,320	4,200
3	3,180	3,700	470	3,230	4,100
4	3,180	3,700	470	3,060	4,000
5	2,880	4,200	490	2,880	3,600
6	2,880	4,200	490	2,880	3,600
7	2,880	4,200	490	3,110	3,700
8	2,880	4,200	490	3,240	4,200

APPENDIX C

FABRICATION OF SPECIMENS

The beam-column subassemblages were fabricated in a horizontal position. Four sets of wood forms were constructed for easy assembly and disassembly after casting. The bottom and the sides of the forms consisted of 3/4 in. plywood with the latter stiffened with a 1 1/2 in. square border. One-quarter in. bolts were used to hold the sides and bottom pieces together. The forms were painted with shellac to reduce the absorption of moisture from the concrete. Figure C.1 shows one of the

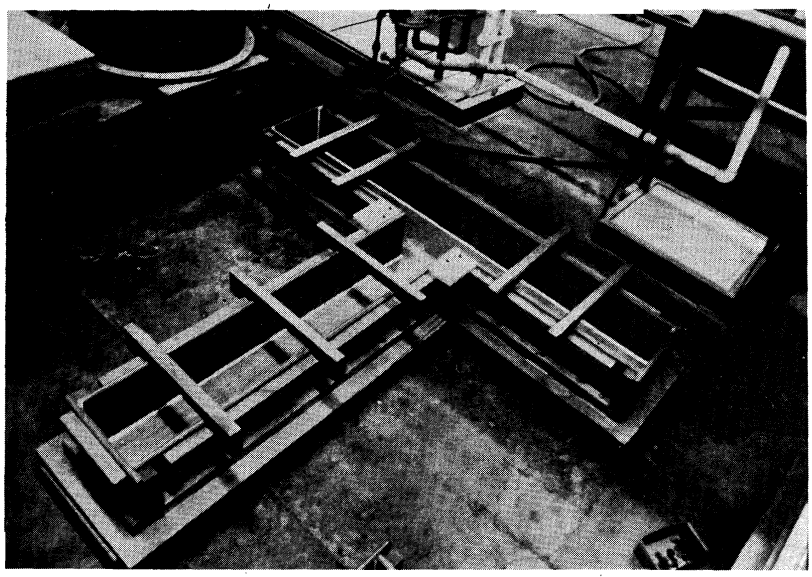

Fig. C.1 Wood Form Used to Cast Specimens

forms assembled.

For the assembly of the reinforcing steel, a 1/2 in. steel plate containing 3/4 in. dia. holes was used as a jig to position one end of the column longitudinal bars.

All the column hoops were slid in from the other end before locating the other 1/2 in. plate. Both ends of the column bars were later fillet welded to the plate to provide a permanent connection. Besides positioning the longitudinal bars, the steel plate provided a bearing surface for the column axial load.

The beam top and bottom reinforcement was positioned perpendicular to the column longitudinal bars before sliding in the stirrup-ties from the far end of the beam. The column and beam transverse reinforcement was then positioned and tied to the longitudinal reinforcement with a flexible steel wire. Figure C.2 shows the

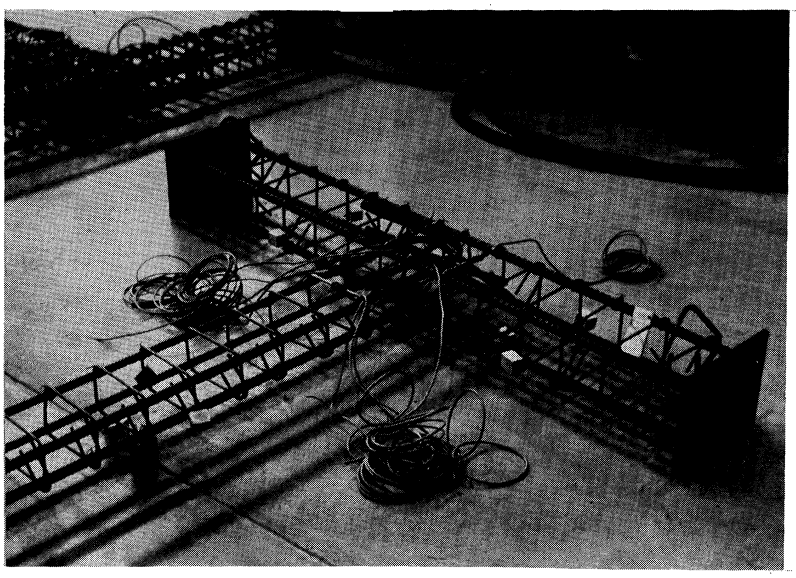

Fig. C.2 Reinforcement Cage for Beam-Column Specimen

reinforcement cage for the subassemblage.

The edges of the forms were caulked with molding clay to make them water tight. The forms were then

coated with a thin film of oil to reduce the bond between the concrete and the wood before placing the fabricated reinforcement cage in the forms. Chairs made from cement mortar were used to maintain the proper cover distance between the form and the reinforcement.

The concrete mix design was specified as follows for one cubic yard of material.

Type I Cement--470 lbs.

Well Graded Sand--1785 lbs.

3/8 in. Pea Gravel--1225 lbs.

Water--240 lbs.

The concrete was delivered to the laboratory by ready-mix truck at which time additional water was added to obtain a slump of about 4 in. The concrete was then shoveled into the forms and vibrated to eliminate voids. The excess concrete was struck off and the surface troweled to obtain a smooth finish. Several hours after casting, the specimens were covered with damp burlap to provide a moist curing condition. Polyethylene sheets were used over the burlap to help retain moisture. The burlap was kept damp by wetting it twice a day. After three days, the forms were stripped. The specimens were moist cured for another four days and then air cured in the laboratory until the time of testing which was always more than 28 days after casting.

Before testing, the subassemblages were painted with a flat white paint to aid in locating the cracks. Black lines were drawn over the white paint surface at the locations of the reinforcement.

APPENDIX D

LOADING AND DATA ACQUISITION SYSTEM

Loading. The loading frame used to test the specimens is shown in Fig. 2.2. Two 30 ton capacity hydraulic rams connected to one manual hydraulic pump was used to apply the column axial load. The rams and pump were manufactured by Templeton-Kenly and Company. A 20 kip capacity hydraulic actuator with a stroke of $\pm$ 3.0 in. was used to displace the end of the beam. This actuator and the associated control console and hydraulic pumping system were manufactured by Gilmore Industries.

Data Acquisition. The displacement of the beam and the resulting load were recorded simultaneously on a Honeywell 530 XY Recorder. The strains in the longitudinal and transverse reinforcement in and near the joint were measured with EP-08-250BG-120Ω-E electrical resistance strain gages, manufactured by Micro-Measurements Company. Identification and location of the high elongation, post yield gages for both Type I and Type II Designs are shown in Fig. 2.5. The strain gage output was indicated on a Autodata 5404 Digital Data Acquisition System, manufactured by Vidar Corporation. The system consisted of a 644 System Controller, a 502B-01 Integrating Digital Voltmeter, a 606-03 Master Scanner, and Visig 611 Signal Conditioners. The data were recorded during the test on paper tape using a 3320-5JE Teletype. The Vidar unit

was used to read ten strain gages and all additional gages, if any, were read with a BLH 20 Strain Indicator with a switch box.

The joint distortion was measured with two LVDTs; one a Schaevitz 300HR and the other a Sanborn 858DT-250. The locations of these displacement transducers are shown in Fig. 2.6. The output from the LVDTs was recorded on a Sanborn system consisting of a 8805A Carrier Preamplifier, a 7714-04A Power Supply, and a 7700 Series Recorder.

The beam rotation at a section 10 in. from and relative to the inside column face was measured by a Schaevitz 500HR and a Sanborn 585DT-500 displacement transducer. The locations of the transducers are shown in Fig. 2.7. The output from the transducers was recorded on a Hewlett Packard 7702B Recorder.

The data from the strain gages and the displacement transducers were later transferred to computer cards. A computer program was used to reduce the data and plot the results.

APPENDIX E

APPLICATION OF STRAIN GAGES

High elongation strain gages were applied to the reinforcing steel for some of the beam-column specimens tested during this investigation. The procedure for applying the gages was as follows: The bars were milled (except for the No. 2 plain bars), at the location of the gages to obtain a flat surface 1/4 in. by 1 1/2 in. Sandpaper was used to improve the finish of the surface which was then treated with a metal conditioner and a neutralizer.

The gages (EP-08-250BG-120Ω-E) were laid out on the reinforcing bars at prescribed gage locations. Cellophane tape was used to hold the gages in place. Peeling back one end of the cellophane tape, AE-10 adhesive was applied under the gage before applying pressure to the gage.

Tabs were used as connection points between gage wires and lead wires to the strain indicator. The lead wires were Belden #22 AWG stranded three conductor wires. For a quarter bridge hook-up, one of the wires went to one terminal on the tab and two wires to the other terminal which compensated for cable length. The three conductor wire was fastened to the reinforcing bar with flexible steel wire to avoid pulling off the tab and gage during specimen fabrication and testing.

M-Coat D and then M-Coat B were painted over the gages and wire leads to provide insulation and moisture proofing respectively. Protective coating Barrier E, manufactured by BLH, was used to cover the gages and pro tect them during handling of the bars and placement of the concrete.

Unless otherwise noted, the above products were manufactured by Micro-Measurements Company.

LIST OF REFERENCES

1. Agrawal, G.L., L.G. Tulin, and K.H. Gerstle, "Reponse of Double Reinforced Concrete Beams to Cyclic Loading," ACI Journal, Proceedings, Vol. 62, No. 7, July 1965, pp. 823-835.

2. Aktan, A.E., B.I. Karlsson, and M.A. Sozen, "Stress-Strain Relationships of Reinforcing Bars Subjected to Large Strain Reversals," Civil Engineering Studies, Structural Research Series No. 397, University of Illinois, Urbana, June 1973.

3. Atchley, B.L. and H.L. Furr, "Strength and Energy Adsorption Capabilities of Plain Concrete under Dynamic and Static Loading," ACI Journal, Proceedings, Vol. 64, No. 11, November 1967, pp. 745-756.

4. Barda, F., J.M. Hanson, and W.G. Corley, "An Investigation of the Design and Repair of Low-Rise Shear Walls," Proceedings, Fifth World Conference on Earthquake Engineering, Paper 104, Rome, Italy, June 1973, pp. 872-881.

5. Beaufait, F. and R.R. Williams, "Experimental Study of Reinforced Concrete Frames Subjected to Alternating Sway Forces," ACI Journal, Proceedings, Vol. 65, No. 11, November 1968, pp. 980-984.

6. Bertero, V.V., "Experimental Studies Concerning Reinforced, Prestressed Concrete Structures and Their Elements," Introductory Report of the International Association for Bridge and Structural Engineering Symposium on Resistance and Ultimate Deformability of Structures Acted on by Well-Defined Repeated Loads, Lisboa, Portugal, 1973, pp. 67-100.

7. Bertero, V.V. and E.P. Popov, "Hysteretic Behavior of Ductile Moment-Resisting Reinforced Concrete Frame Components," Earthquake Engineering Research Center, University of California, Berkeley, Report No. EERC 75-16, April 1975.

8. Bertero, V.V., E.P. Popov, and T.Y. Tang, "Hysteretic Behavior of Reinforced Concrete Flexural Members with Special Web Reinforcement," Earthquake Engineering Research Center, University of California, Berkeley, Report No. EERC 74-9, 1974.

9. Bertero, V.V. and G. McClure, "Behavior of Reinforced Concrete Frames Subjected to Repeated Reversible Loads," ACI Journal, Proceedings, Vol. 61, No. 10, October 1964, pp. 1305-1330.

10. Best, R.C., Private Communication, Market Development Representative, Republic Steel Corporation, Cleveland, OH.

11. Blume, J.A., "Design of Earthquake-Resistant Poured-in-Place Concrete Structures," Earthquake Engineering, R.L. Wiegel, ed., Prentice-Hall, Inc., Englewood Cliffs, N.Y., 1970.

12. Blume, J.A., N.M. Newmark, and L.H. Corning, Design of Multistory Reinforced Concrete Buildings for Earthquake Motions, Portland Cement Association, Chicago, Ill., 1961.

13. Bresler, B. and J.G. MacGregor, "Review of Concrete Beams Failing in Shear," Journal of the Structural Division, ASCE, Vol. 93, No. ST1, February 1967, pp. 343-372.

14. Bresler, B. and V. Bertero, "Behavior of a Reinforced Concrete under Repeated Load," Journal of the Structural Division, ASCE, Vol. 94, No. ST6, June 1968, pp. 1567-1589.

15. Broms, B.B., "Shear Strength of Reinforced Concrete Beams," Journal of the Structural Division, ASCE, Vol. 95, No. ST6, June 1969, pp. 1339-1358.

16. Brown, R.H. and J.O. Jirsa, "Reinforced Concrete Beams under Load Reversals," ACI Journal, Proceedings, Vol. 68, No. 5, May 1971, pp. 380-390.

17. "Building Code Requirements for Reinforced Concrete (ACI 318-71)," ACI Committee 318, American Concrete Institute, Detroit, Mich., 1971.

18. Burnett, E.F.P. and R.J. Trenberth, "Column Load Influence on Reinforced Concrete Beam-Column Connection," ACI Journal, Proceedings, Vol. 69, No. 2, February 1972, pp. 101-109.

19. Burnett, E.F.P. and R.P. Jajoo, "Reinforced Concrete Beam-Column Connection," Journal of the Structural Division, ASCE, Vol. 97, No. ST9, September 1971, pp. 2315-2335.

20. Burns, N.H. and C.P. Siess, "Plastic Hinging in Reinforced Concrete," Journal of the Structural Division, ASCE, Vol. 92, No. ST5, October 1966, pp. 45-64.

21. Burns, N.H. and C.P. Siess, "Repeated and Reversed Loading in Reinforced Concrete," Journal of the Structural Division, ASCE, Vol. 92, No. ST5, October 1966, pp. 65-76.

22. Celebi, M. and Penzien, "Hysteretic Behavior of Epoxy-Repaired Reinforced Concrete Beams," Earthquake Engineering Research Center, University of California, Berkeley, Report No. EERC 73-5, February 1973.

23. Chung, H.W., "Epoxy-Repaired Reinforced Concrete Beams," ACI Journal, Proceedings, Vol. 72, No. 5, May 1975, pp. 233-234.

24. Clough, R.W., "Effect of Stiffness Degradation on Earthquake Ductility Requirements," Structural Engineering Laboratory, University of California, Berkeley, Report No. 66-16, October 1966.

25. Ernst, G.C., "Plastic Hinging at the Intersection of Beams and Columns," ACI Journal, Proceedings, Vol. 53, No. 6, June 1957, pp. 1119-1144.

26. Ferguson, P.M., R.D. Turpin, and J.M. Thompson, "Minimum Bar Spacing as a Function of Bond and Shear Strength," ACI Journal, Proceedings, Vol. 50, No. 6, June 1954, pp. 869-887.

27. Frazier, G.A., J.W. Wood, and G.W. Housner, "Earthquake Damage to Buildings," Engineering Features of the San Fernando Earthquake, February 9, 1971, P.C. Jennings, ed., Earthquake Research Laboratory, California Institute of Technology, Pasadena, June 1971.

28. Gulkan, P. and M.A. Sozen, "Inelastic Response of Reinforced Concrete Structures to Earthquake Motions," ACI Journal, Proceedings, Vol. 71, No. 12, December 1974, pp. 604-610.

29. Hansen, R.J. and A.A. Liepins, "Behavior of Bond under Dyanmic Loading," ACI Journal, Proceedings, Vol. 59, No. 4, April 1962, pp. 563-583.

30. Hansen, T.C. and A.H. Mattock, "The Influence of Size and Shape of Member on the Shrinkage and Creep of Concrete," Portland Cement Association, R and D Series 1176, 1965.

31. Hanson, N.W., "Seismic Resistance of Concrete Frames with Grade 60 Reinforcement," Journal of the Structural Division, ASCE, Vol. 97, No. ST6, June 1971, pp. 1685-1700.

32. Hanson, N.W. and H.W. Connor, "Seismic Resistance of Reinforced Concrete Beam-Column Joints," Journal of the Structural Division, ASCE, Vol. 93, No. ST5, October 1967, pp. 533-560.

33. Hanson, R.D. and H.J. Degenkolb, The Venezuela Earthquake, July 29, 1967, American Iron and Steel Institute, New York, N.Y., 1969.

34. Hidalgo, P. and R.W. Clough, "Earthquake Simulator Study of a Reinforced Concrete Frame," Earthquake Engineering Research Center, University of California, Berkeley, Report No. EERC 74-13, December 1974.

35. Ismail, M.A.F. and J.O. Jirsa, "Bond Deterioration in Reinforced Concrete Subjected to Low Cycle Loads," ACI Journal, Proceedings, Vol. 69, No. 6, June 1972, pp. 334-343.

36. Jirsa, J.O., "Factors Influencing the Hinging Behavior of Reinforced Concrete Members under Cyclic Overloads," Proceedings, Fifth World Conference on Earthquake Engineering, Paper 147, Rome, Italy, June 1973, pp. 1198-1204.

37. Johnson, J.E., D.O. Baehr, and R.J. Wenk, "Research on an Extremely Rapid Setting High Strength Concrete," ASCE Annal and National Environmental Engineering Meeting, Preprint No. 2097, New York, N.Y., October 1973.

38. Johnston, D.W. and P. Zia, "Analysis of Dowel Action," Journal of the Structural Division, ASCE, Vol. 97, No. ST5, May 1971, pp. 1611-1630.

39. Karsan, I.D. and J.O. Jirsa, "Behavior of Concrete under Varying Strain Gradients," Journal of the Structural Division, ASCE, Vol. 96, No. ST8, August 1969, pp. 2543-2563.

40. Karsan, I.D. and J.O. Jirsa, "Behavior of Concrete under Compressive Loadings," Journal of the Structural Division, ASCE, Vol. 95, No. ST12, December 1969, pp. 1675-1696.

41. Kent, D.C., "Inelastic Behavior of Reinforced Concrete Members with Cyclic Loading," Ph.D. Thesis, University of Canterbury, Christchurch, New Zealand, 1969.

42. Kent, D.C. and R. Park, "Flexural Members with Confined Concrete," Journal of the Structural Division, ASCE, Vol. 97, No. ST7, July 1971, pp. 1969-1990.

43. Kinney, J.S., Indeterminate Structural Analysis, Addison-Wesley, Inc., Reading, Mass., 1957.

44. Krawinkler, H. and E.P. Popov, "Hysteretic Behavior of Reinforced Concrete Rectangular and T-Beams," Proceedings, Fifth World Conference on Earthquake Engineering, Paper 28, Rome, Italy, June 1973, pp. 249-258.

45. Lee, D.L.N. and R.D. Hanson, "Inelastic Behavior of Repaired Beam-Column Connections," Presented at U.S.-Japan Seminar on Earthquake Engineering, Berkeley, Calif., September 1973.

46. Lutz, L.A., "Information on the Bond of Deformed Bars from Special Pullout Tests," ACI Journal, Proceedings, Vol. 67, No. 11, November 1970, pp. 885-887.

47. Lutz, L.A. and P. Gergely, "Mechanics of Bond and Slip of Deformed Bars in Concrete," ACI Journal, Proceedings, Vol. 64, No. 11, November 1967, pp. 711-721.

48. Meehan, J.F., H.J. Degenkolb, D.F. Moran, and K.V. Steinbrugge, "Engineering Aspects," Managua, Nicaragua Earthquake of December 23, 1972, Earthquake Engineering Research Institute Reconnaissance Report, Oakland, Calif., May 1973.

49. Mahin, S., V.V. Bertero, M.B. Atalay, and D. Rea, "Rate of Loading Effects on Uncracked and Repaired Reinforced Concrete Members," Earthquake Engineering Research Center, University of California, Berkeley, Report No. EERC 72-9, December 1972.

50. Marques, J.L.G. and J.O. Jirsa, "A Study of Hooked Bar Anchorages in Beam-Column Joints," ACI Journal, Proceedings, Vol. 72, No. 5, May 1975, pp. 198-209.

51. McCafferty, R.M. and M.L. Moody, "An Example of Epoxy Mortar Repair of a Reinforced Concrete Beam-Column Joint," Proceedings, Fifth World Conference on Earthquake Engineering, Paper 103, Rome, Italy, June 1973, pp. 868-871.

52. McClure, G.S., K.H. Gerstle, and L.G. Tulin, "Sustained and Cyclic Loading of Concrete Beams," Journal of the Structural Division, ASCE, Vol. 99, No. ST2, February 1973, pp. 243-257.

53. Medearis, K. and D.H. Young, "Energy Absorption of Structures under Cyclic Loading," Journal of the Structural Division, ASCE, Vol. 90, No. ST1, February 1964, pp. 61-91.

54. Megget, L.M., "Exterior Reinforced Concrete Joints with and without Intersecting Beams under Seismic Loading," Bulletin of the International Institute of Seismology and Earthquake Engineering, Vol. 11, Tokyo, Japan, 1973, pp. 115-167.

55. Meyers, B.L., D.E. Branson, C.G. Schumann, and M.L. Christiason, "The Prediction of Creep and Shrinkage Properties of Concrete," Department of Civil Engineering, University of Iowa, Iowa City, Report No. 70-5, August 1970.

56. Minor, J. and J.O. Jirsa, "Behavior of Bent Bar Anchorages," ACI Journal, Proceedings, Vol. 72, No. 4, April 1975, pp. 141-149.

57. Nielsen, N.N. and K. Nakagawa, "The Tokachi-Oki Earthquake, Japan, May 16, 1968," International Institute of Seismology and Earthquake Engineering, Tokyo, Japan, IISEE Earthquake Report No. 2, June 1968.

58. Otani, S. and M.A. Sozen, "Simulated Earthquake Tests of R/C Frames," Journal of the Structural Division, ASCE, Vol. 100, No. ST3, March 1974, pp. 687-701.

59. Park, R., D.C. Kent, and R.A. Sampson, "Reinforced Concrete Members with Cyclic Loading," Journal of the Structural Division, ASCE, Vol. 98, No. ST7, July 1972, pp. 1341-1360.

60. Park, R. and T. Paulay, "Behavior of Reinforced Concrete External Beam-Column Joints under Cyclic Loading," Proceedings, Fifth World Conference on Earthquake Engineering, Paper 88, Rome, Italy, June 1973, pp. 772-781.

61. Popov, E.P., V.V. Bertero, and H. Krawinkler, "Cyclic Behavior of Three R.C. Flexural Members with High Shear," Earthquake Engineering Research Center, University of California, Berkeley, Report No. EERC 72-5, October 1972.

62. Rajagopalan, K.S. and P.M. Ferguson, "Exploratory Shear Tests Emphasizing Percentage of Longitudinal Steel," ACI Journal, Proceedings, Vol. 65, No. 8, August 1968, pp. 634-638.

63. "Recommendations for Design of Beam-Column Joints in Monolithic Reinforced Concrete Structures," ACI-ASCE Joint Committee 352, American Concrete Institute, Detroit, Mich., (in preparation).

64. Ruiz, W.M. and G. Winter, "Reinforced Concrete Beams under Repeated Loads," Journal of the Structural Division, ASCE, Vol. 95, No. ST6, June 1969, pp. 1189-1211.

65. Schutz, R.J., Private Communication, Vice President, Research and Development, Sika Chemical Corporation, Lyndhurst, N.J.

66. Sikastix Technical Bulletin 73/6, Sika Chemical Corporation, Lyndhurst, N.J.

67. "Sikastix Test Results," Sika Chemical Corporation, Lyndhurst, N.J., January 1973.

68. Singh, A., K.H. Gerstle, and L.G. Tulin, "The Behavior of Reinforcing Steel under Reversal Loading," ASTM Journal, Materials Research and Standards, Vol. 5, No. 1, January 1965, pp. 12-17.

69. Sinha, B.P., K.H. Gerstle, and L.G. Tulin, "Response of Singly Reinforced Beams to Cyclic Loading," ACI Journal, Proceedings, Vol. 61, No. 8, August 1964, pp. 1021-1038.

70. Sinha, B.P., K.H. Gerstle, and L.G. Tulin, "Stress-Strain Relations for Concrete under Cyclic Loading," ACI Journal, Proceedings, Vol. 61, No. 2, February 1964, pp. 195-211.

71. "Standard Method of Test for Compressive Properties of Rigid Plastics," 1975 Annual Book of ASTM Standards, Part 35, American Society for Testing and Materials, Philadelphia, Pa., pp. 236.

72. "Standard Method of Test for Compressive Strength of Cylindrical Concrete Specimens," 1975 Annual Book of ASTM Standards, Part 14, American Society for Testing and Materials, Philadelphia, Pa. pp. 25.

73. "Standard Method of Test for Splitting Tensile Strength of Cylindrical Concrete Specimens," 1975 Annual Book of ASTM Standards, Part 14, American Society for Testing and Materials, Philadelphia, Pa., pp. 308.

74. "Standard Method of Test for Tensile Properties of Plastics," 1975 Annual Book of ASTM Standards, Part 35, American Society for Testing Materials, Philadelphia, Pa., pp. 192.

75. "Standard Method of Testing for Creep of Concrete in Compression," 1975 Annual Book of ASTM Standards, Part 14, American Society for Testing and Materials, Philadelphia, Pa., pp. 315.

76. "Standard Specifications for Deformed and Plain Billet-Steel Bars for Concrete Reinforcement," 1975 Annual Book of ASTM Standards, Part 4, American Society for Testing and Materials, Philadelphia, Pa., pp. 522.

77. Takeda, T., M.A. Sozen, and N.N. Nielsen, "Reinforced Concrete Response to Simulated Earthquakes," Journal of the Structural Division, ASCE, Vol. 96, No. ST12, December 1970, pp. 2557-2573.

78. Thompson, C.J., "Repair of Buildings Damaged by the 1969 Boland Earthquake," Proceedings, Fifth World Conference on Earthquake Engineering, Paper 106, Rome, Italy, June 1973, pp. 886-893.

79. Timoshenko, S.P., Strength of Materials, Part 2, Van Nostrand, N.Y., 1956, pp. 413.

80. Townsend, W.H., "The Inelastic Behavior of Reinforced Concrete Beam-Column Connections," Ph.D. Dissertation, University of Michigan, Ann Arbor, May 1972.

81. Untrauer, R.E. and R.L. Henry, "Influence of Normal Pressure on Bond Strength," ACI Journal, Proceedings, Vol. 62, No. 5, May 1965, pp. 577-586.

82. Uzumeri, S.M. and M. Seckin, "Behavior of Reinforced Concrete Beam-Column Joints Subjected to Slow Load Reversals," Department of Civil Engineering, University of Toronto, Canada, Publication No. 74-5, March 1974.

83. Wang, C.K. and C.G. Salmon, Reinforced Concrete Design, International Textbook Company, Scranton, Pa., 1969.

84. Warner, J., "Restoration of Earthquake Damaged Concrete and Masonry," Proceedings, Fifth World Conference on Earthquake Engineering, Paper 105, Rome, Italy, June 1973, pp. 882-885.

85. Wight, J.K. and M.A. Sozen, "Strength Decay of RC Columns under Shear Reversals," Journal of the Structural Division, ASCE, Vol. 101, No. ST5, May 1975, pp. 1053-1065.

86. Wyllie, L.A. and R.G. Dean, "Seismic Failures and Subsequent Performance after Repair," ASCE National Structural Engineering Convention, Preprint 2489, New Orleans, La., April 1975.